INJURY BIOMECHANICS (4J610)

w5-pp3-4.3

(third printing, 2000)

Authors:
Prof.dr.ir. J.S.H.M. Wismans
Ir. E.G. Janssen
Ir. M. Beusenberg
Dr.ir. W.P. Koppens
Dr.Ir. R. Happee
Dr.Ir. P.H.M. Bovendeerd

Eindhoven University of Technology
Division of Dynamics and Control
P.O. Box 513
5600 MB Eindhoven, The Netherlands

TNO Crash-Safety Centre
Schoemakerstraat 97
P.O. Box 6033
2600 JA Delft, The Netherlands

PREFACE

Injuries due to motor vehicle crashes are one of the leading causes of death and disability in our motorized society. The problem can be reduced considerable if adequate attention is given to accident and injury prevention strategies. Injury prevention (or injury control) measures are based on the recognition that death and injuries can be reduced in number and severity if the actual conditions operating during the crash phase are modified. Injury biomechanics, which is the subject of this course, can be considered as the basic science of "injury prevention".

The contents of this course is not only relevant for an engineer seeking a career as a scientist in the field of injury biomechanics but also for design engineers in the automotive and aircraft industry where injury control constitutes a mayor design condition, for accident experts within insurance companies involved with the analysis of real accidents, for researchers in the field of home and leisure accidents or for engineers working within governmental agencies on safety regulation developments. Also for engineers specializing in general biomechanics or biomedical engineering this course may be of interest since research methods developed in injury biomechanics are closely related to, and often directly applicable within, these disciplines.

Subjects to be covered in this report include the epidemiology of accidents, research methods in injury biomechanics, the use of human body models for injury biomechanics research, injury scaling and injury risk functions. For three body parts, namely the head, neck and thorax, injury types and mechanisms, biomechanical impact response, injury criteria and tolerance levels will be presented. Furthermore the modelling of the human body by means of mechanical and computer models will be treated in detail. Research issues for the future will be identified.

Computer modelling of the human brains and the cervical spine is the main research item for the coming years within the injury biomechanics research programme at the Faculty of Mechanical Engineering of the Eindhoven University of Technology. Separate course material will be developed dealing in more detail with these topics as would be possible within the scope of the current report.

Preparation of this course material would not have been possible without the support of the TNO Road-Vehicles Research Institute. Among others, a number of their key staff members were made available for preparation of important parts of this report. Furthermore I would like to express my gratitude to Fons Sauren for carefully proofreading the first versions of the course notes.

CONTENTS

CHAPTER 1

GENERAL INTRODUCTION

1.1 Course objectives

Injuries are the leading cause of death and disability of children and young adults in our industrialised society [1]. Motor vehicle crashes cause about half a million road deaths annually throughout the world [2], which is about 30-50% of all injury related fatalities. Furthermore about 15 million are injured yearly as a result of a traffic accident [2]. But injury is a problem that can be controlled considerably if adequate attention is given to accident and injury prevention strategies.

Injury of the human body occurs by deformation of anatomical structures beyond their failure limits resulting in damage of tissue or alterations in the normal function. The subject of this course is "injury biomechanics" which uses the principles of mechanics to study the behaviour of biological material under extreme loading conditions. Knowledge of this behaviour is essential in order to be able to develop adequate measures for protection of the human body under extreme mechanical loading conditions. The capability to design a less injurious environment, like for example safer motor vehicles, will depend partly on our understanding of injury mechanisms and injury treshholds.

The mayor objectives of this course in injury biomechanics are:

- To offer an insight in the trauma problem and the methods used to quantify and to reduce this problem.
- Discuss the research methods used in the discipline of injury biomechanics and their limitations.
- Provide a basic understanding on injury mechanisms and injury tolerances for the most vulnerable body parts.
- Present background, capabilities and limitations of experimental and numerical tools for safety assessment and design.

In the next Section first a brief introduction in biomechanics is presented followed by a discussion on accidents and prevention. A summary of the contents of this course is given in Section 1.4.

1.2 Biomechanics

Biomechanics is the science which applies the principles of mechanics to biological systems. It extends classical applied mechanics to living materials with peculiar constitutive equations, large deformations and complex geometries and boundary conditions. The field of biomechanics exists already for a long time. It is closely related to physiology, i.e. the science dealing with the normal functions of living subjects and their organs. Famous scientists known for their contributions to biomechanics (and physiology) are for example [3]:

Galilei (1564-1642): measurement techniques in biology
Harvey (1578-1658): discovery of blood circulation
Borelli (1608-1679): muscular movements
Boyle (1627-1691): fish respiration
Euler (1707-1783): waves in arteries
Poiseuille (1799-1869): blood pressure measurement
Helmholtz (1821-1894): mechanisms of the eye and hearing

Within the biomechanical discipline often a distinction is made between more fundamental oriented research and practical or application directed work. Fundamental research aims to increase our basic knowledge for example on the structure of living materials, the constitutive equations, growth and repair of living material and tissue strength. This basic understanding is an essential condition to achieve significant advances in various fields of bioengineering. Typical application fields where biomechanics is involved are for example medical diagnosis and treatment, rehabilitation, sports, safety and health, medical instruments and prosthetic devices, comfort and ergonomics and agriculture.

This course deals with a special area within biomechanics namely "biomechanics of trauma" also called "injury biomechanics" or "impact biomechanics". Injury biomechanics studies the behaviour of the human body under extreme injury producing loading conditions like they occur for example in traffic accidents. Injury biomechanics as such can be considered as the basic science of "injury control" which will be introduced in the next Section.

Research in injury biomechanics involves a number of disciplines including engineering, epidemiology, traumatology, anatomy, biology, physiology. It is still a relatively young science which came to grows after the second world war due to the many accidents that happened in military aviation. However also before this time some rather interesting work took place, which still is of importance for our present knowledge on injury biomechanics. One example of this earlier research will be given here as a conclusion of this Section.

It concerns the experimental work of Messerer [4] conducted more than a century ago. His work can be considered as an excellent illustration of the complexity of experimental injury biomechanics research. The subject of Messerer's research was the determination of the

elasticity and fracture strength of human bones including the skull and the pelvis. For this purpose a large number of static tension, compression and bending tests were conducted at specially designed manually-operated test devices. Fig. 1.1 illustrates the set-up for the torsion tests.

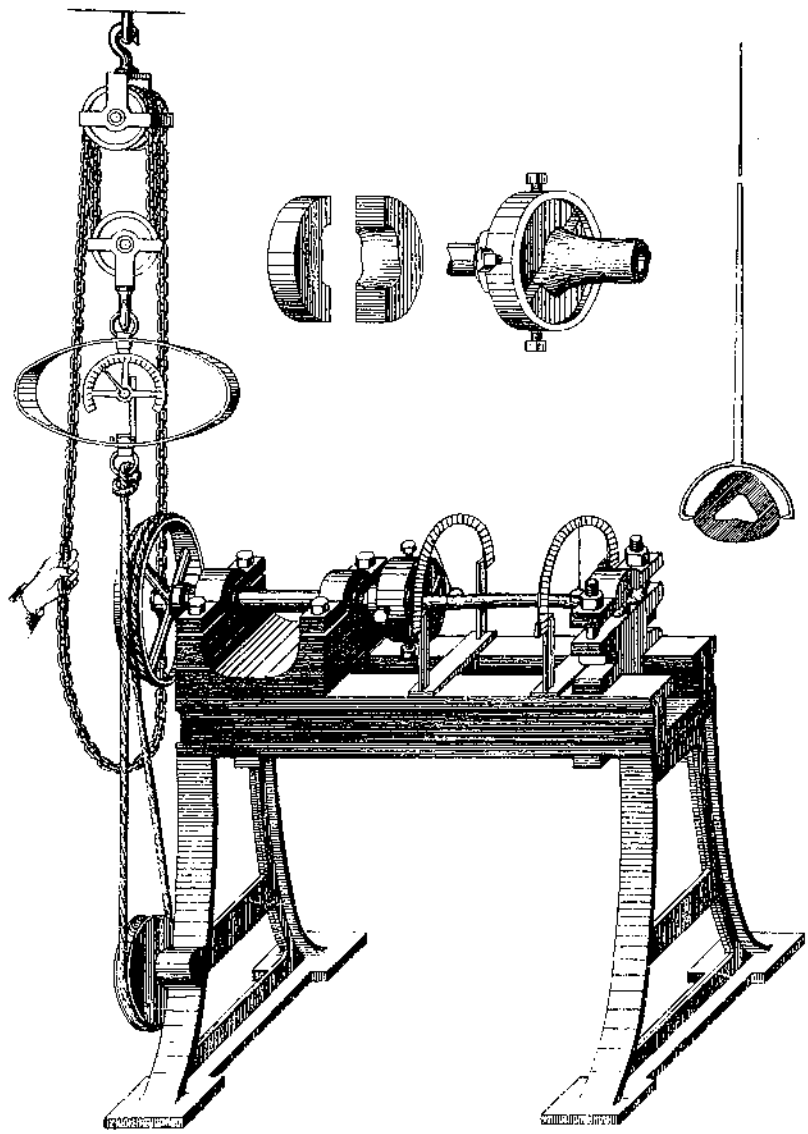

Fig. 1.1 Torsion test device for the determination of the elasticity and fracture strength of human bones [4].

Messerer's special concern was the selection of human test material and the variability between specimens. The thoroughness of his approach can be illustrated by means of the following citations (translated from German):

"The influence of age, bodyside and sex should be considered". "When I realized that this type of research, in which calculations are not practical, only will be of value if it is based on a large sample, I tried to conduct the tests on as much bone specimens as possible and

by the kindness of my respected principal Professor Von Nussbaum it was made possible for me to test 500 bones and bone combinations (skull, thorax and pelvis counted as one) from 90 cadavers in this way". "My bone specimens always were completely fresh, cut from the cadaver shortly before the experiment, and tested without soft tissue". "If an option was possible only persons with a short sickness period were selected in which the bones seem to be completely normal and healthy and not affected by earlier bone diseases".

1.3 Accidents and prevention

1.3.1 History

Travel always has been one of the basic needs of the human race. Ancient man walked perhaps 20 or 30 km a day to meet other people or to find food. His hazards of travel were rather small since his speed was limited to 5-10 km/hr. His risk of being injured existed more in case of an accident during hunting or in conflicts with other tribes than due to collisions. Many weapons found from ancient time illustrate this risk. Especially the head was vulnerable. Since the beginning of civilization man has attempted to minimize the effects of violence on his body. A well-known example is the helmet. Fig. 1.2 shows a Corinthian helmet of the 4th century B.C. weighing about 1.5 kg [5].

Fig. 1.2 Corinthian helmet of the 4th. century B.C. [5]

Travel hazards changed completely after the invention of the automobile in the second part of the 19th Century. On July 3rd 1886 Carl Benz in Mannheim was the first person driving in public in a vehicle powered by a one-cylinder engine. The maximum velocity of this 3-wheel vehicle was 15 km/hr. Twenty years later the maximum vehicle speed increased already to close to 100 km/hr. Due to the higher vehicle speeds, but more important due to the larger speed differences between various means of transport, the first traffic accidents occurred. The increasing motorization generated mobility and consequently more people were exposed to risk.

In the beginning of the 20th Century the Frenchman M. Gustave-Désiré Leveau was the first person who suggested to protect vehicle occupants by means of a system of seat belts (Fig. 1.3). On his invention a patent was granted in 1903 [6]. Except for car races seat belts however were hardly used until 1955 when Ford Motor Cie and Chrysler Corporation both decided to offer seat belts as an option in their automobiles. At present in most countries in Europe wearing of seat belts is obligatory on front seats.

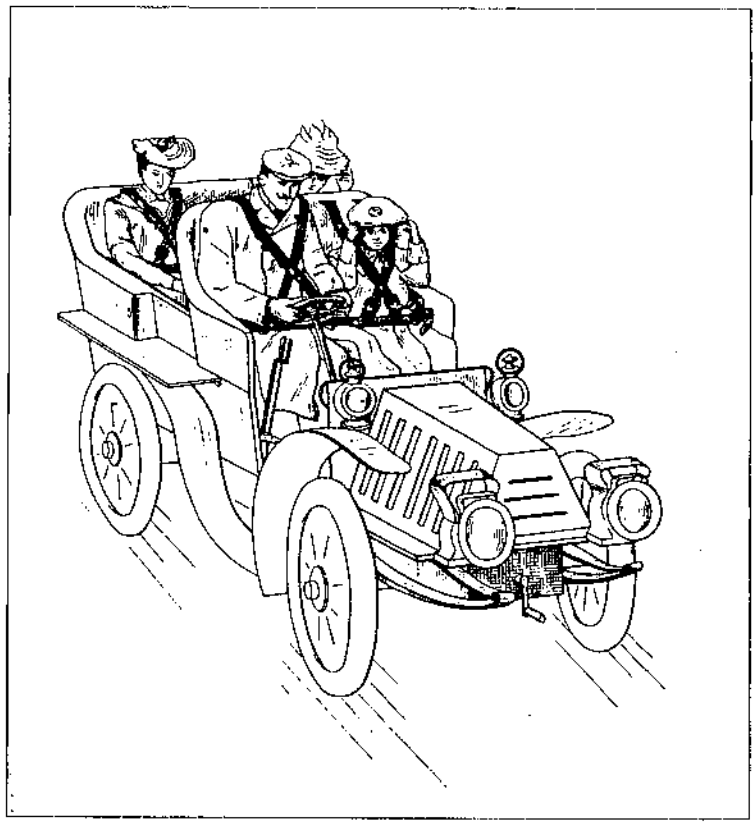

Fig. 1.3 *Seat belt patent of Gustave-Désiré Leveau in 1903 [6].*

1.3.2 The traffic trauma problem

In the Netherlands the number of passenger cars now is more than 5 million which is an increase by a factor 2 since 1970 [7]. Worldwide the number of motor vehicles is estimated

to be 500 million [2]. The consequences of this motorisation are dramatic. Some data to illustrate this:

- In 1989 in the Netherlands 1460 people died as a direct result of traffic accidents [8], while 13.650 traffic victims had to be treated in a hospital (in-patients). In addition yearly more than 200.000 people sustain injuries in a traffic accident requiring medical treatment by a general practitioner or as out-patient in a hospital [9].

- In the Netherlands traffic injury is the main cause of death in the age groups between 5 and 25 years. This is illustrated in Fig. 1.4 which presents the causes of death for various diseases in the Netherlands in percentages by age [10]. Traffic accidents and other accident types are shown as separate categories.

- Motor vehicle crashes cause about half a million road deaths annually throughout the world [2].

- The economic costs of traffic accidents are very high. A minimum estimate for the Netherlands in the mid-eighties was fl 6.000.000.000 a year and this is excluding the costs of prevention, for instance [11].

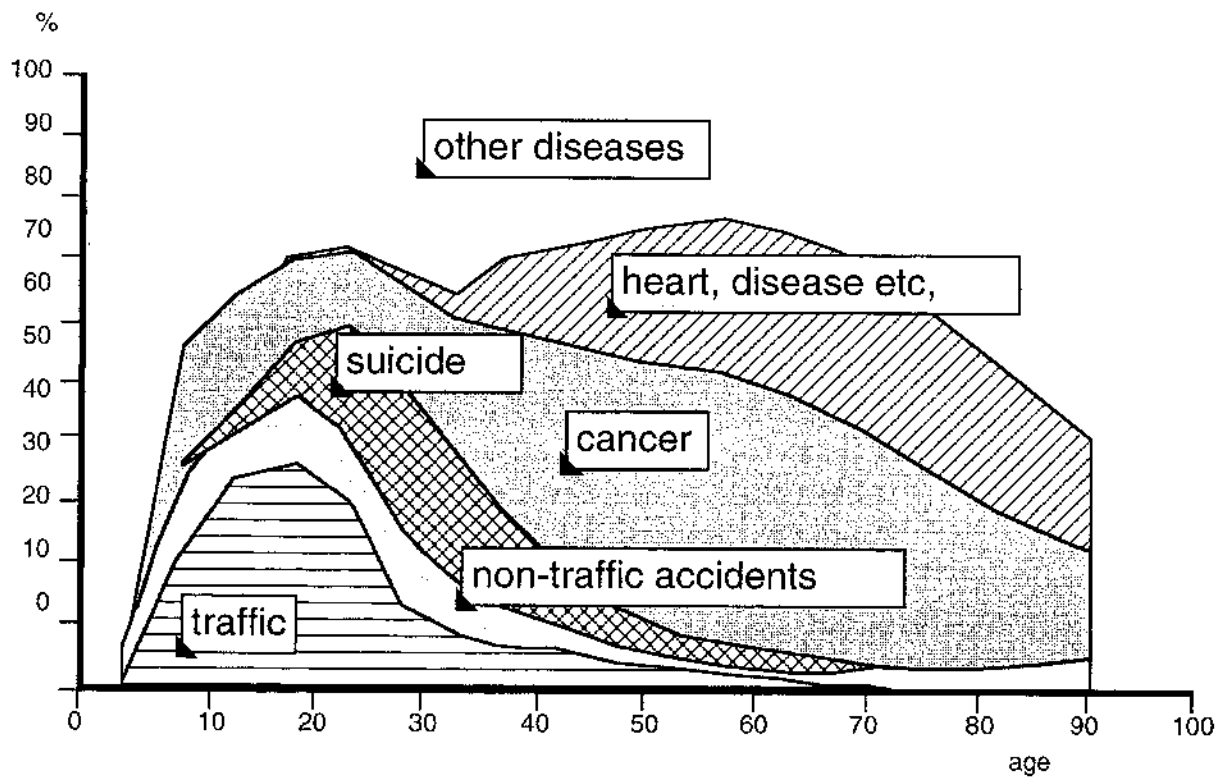

Fig. 1.4 *Percentage of death from injury and other causes by age in 1987. Source: CBS data in [10].*

1.3.3 Injury reduction strategies

The seat belt and helmet are typical examples of measures to reduce the number and severity of injuries but many other methods are available to reduce the trauma problem. Often five basic strategies are distinguished [2]:

Exposure control
This approach tries to reduce the amount of travel or to substitute less safe forms of travel by safer forms. Exposure control includes legislation, licensing procedures and fiscal policies. One should realize that this type of measures will be in conflict with other values important in a society, like the choice where to work and live and the freedom of movement.

Crash prevention
This strategy concerns measures usually of a technical nature aimed to reduce the risk of getting involved in an accident. Important aspects are adequate road design and maintenance (road engineering) and active safety aspects of a vehicle like anti-lock brakes, good visibility etc. (vehicle engineering). Separate road systems for various categories of road users are also part of this strategy.

Injury control (or injury prevention)
The objective of this strategy is to reduce the number and severity of injuries in case an accident occurs. This approach is based on the recognition that death and injuries can be reduced in number and severity if the actual conditions operating during the crash phase are modified. Typical examples are passive restraint systems in a vehicle, vehicle crush zones and energy absorbing structures at the roadside. Such measures are often referred to as "passive safety measures". Injury biomechanics as such can be considered as the basic science of "injury control". In Section 1.3.4 the various principles of injury control will be discussed.

Behaviour modification
This strategy aims to modify the behaviour of the road users by means of, for instance, education, incentive and adequate traffic laws in order to reduce the risk of being involved in an accident or the risk of being injured in case of an accident. As such this approach is closely related to the strategies of "crash prevention" and "injury control". Examples of this approach are promotion campaigns to use seat belts or programs to change alcohol and drug related behaviour in traffic.

Post injury management
As accidents and injuries during a crash cannot be prevented entirely, efficient emergency, medical treatment and rehabilitation services are needed for the injured. Special trauma centres with experienced teams are essential in this respect [12].

1.3.4 Injury control

Injury control measures have been proven to be a very effective method for the reduction of the trauma problem [1,2,13,14]. This can be illustrated with German accident data, for instance. In the period from 1970-1987 the number of accidents on German roads increased by about 40 %. In this same period however the number or traffic injuries decreased by 20% and the number of fatalities even by about 50%. It was concluded that this decrease to a large extent was due to injury prevention measures like significant improvements of the vehicle crashworthiness and the introduction of the seat belt [13].

The injury reduction capability of safety devices like the helmet or the seat belt are based on different mechanical principles. Basically four methods for injury control can be distinguished:

- Control of the *accident conditions* by changing the environment of the crashing vehicle. A well-known example of such a measure is a deformable guard rail.

- Improvement of the *crashworthiness* of the vehicle by means of the design of the vehicle construction. Examples are crush zones and energy absorbing steering columns.

- Control of the *occupant motion* during the crash. The seat belt is based on this principle. The primary function of the seat belt is to connect the motion of the occupant to the vehicle motion in order to use the built-in deceleration properties of the vehicle (crashworthiness) and to control the motion of the passenger within the free space between occupant and vehicle interior.

- Control of the *impact contact* between the body and environment. A safety helmet is based on this principle. The function of a safety helmet is the reduction of the impact load (energy absorption) as well as the distribution of the load over a larger contact area (pressure distribution). In addition the hard outer shell of a helmet prevents penetration of sharp objects.

For a specific accident situation often a combination of above principles will offer the optimal protection. In a lateral collision for instance the *accident conditions* can be influenced by specification of requirements for the vehicle weight and vehicle front stiffness of the potential crash partner (compatibility issues). Of course this is a rather radical measure. The deformations of the vehicle side structure can be influenced by the stiffness of this structure (*crashworthiness*). By introduction of energy absorbing padding at the inside the *impact contact* can be influenced. Finally also the *occupant motion* can be influenced for example by a special airbag system located in the door. Such an airbag will affect the *impact contact* as well.

1.4 Course contents

As a conclusion of this Chapter a brief summary of the remaining part of this course will be given.

The next Chapter deals with the epidemiology of accidents i.e. the science which studies real world accident data. For an engineer working in the field of injury biomechanics and injury control a detailed knowledge and understanding of real world accident data is essential and he clearly should be aware of the potential and limitations of these data. Topics to be presented include injury surveillance systems, accident data bases in the Netherlands and the United States, accident statistics and restraint system effectiveness.

Chapter 3 provides an introduction to injury biomechanics. Attention is given to research methods in injury biomechanics, the use of human body models in injury biomechanics research, injury mechanisms and injury scaling, injury risk functions, injury tolerances etc...

Chapters 4, 5 and 6 present an overview of injury biomechanics for 3 important body parts, namely the head, neck and thorax, respectively. Subjects to be covered include anatomy, injury types, injury mechanisms, biomechanical impact response, injury criteria and tolerance levels. Research issues for the future will be identified.

Chapters 7 and 8 relate to modelling of the human body, where Chapter 7 specifically concerns mechanical models, the so-called crash dummies. Attention will be given to: biofidelity aspects of dummies, reproducibility, repeatability and durability, effective mass, anthropometry, scaling methods, injury recording and calibration. Furthermore an overview of current crash dummies will be given.

Chapter 8 deals with mathematical models. Types of crash simulations, capabilities and limitations of computer simulations and model verification will be discussed. Beside simulation of the human body also some aspects of modelling of the vehicle structure and safety devices will be presented.

REFERENCES

1. Committee on Trauma Research, Commission on Life Sciences, National Research Council and the Institute of Medicine: "Injury in America. A continuing Public Health Problem". National Academy Press, Washington, 1985.

2. Trinca, G. et. al.: "Reducing Traffic Injury". A Global Challenge, A.H. Massina & Co., Melbourne, 1988.

3. Fung, Y.C.: "Biomechanics; Mechanical properties of living tissues", Springer Verlag, New York, Heidelberg, Berlin, ISBN 0-387-90472-7, 1981.

4. Messerer, O.: "Uber Elasticitat und Festigkeit der Menschlichen Knochen". Stuttgart, Verlag der J.G. Cotta'schen Buchhandlung, 1980.

5. Gurdjian, E.S.: "Head Impact Injury". Mechanistic, Clinical and Preventive Correlations, Charles C. Thomas Publisher, Springfield, Illinois, USA.

6. Brevet d'Invention. No. 331.926. Republique Francaise. Office National de la Propriete Industrielle, 1903.

7. Wegman, F.C.M.: Mathijsen, M.P.M. en Koornstra, M.J.: "Voor alle Veiligheid". SDU Uitgeverij, 's-Gravenhage, 1989.

8. J. Wismans: "Over Mechanica, Letsels en Preventie", Rede uitgesproken bij de aanvaarding van het ambt van bijzonder hoogleraar in de letselbiomechanica aan de faculteit Werktuigbouwkunde van de Technische Universiteit Eindhoven op 6 april 1990.

9. Montfoort, G.L.M. van, Galen, W.C.C. and S. Harris: "Ongevallen in Nederland". Report (in Dutch), Consumers Safety Institute, The Netherlands, 1988.

10. Blokpoel, A.: "De verkeersonveiligheid in 1988" (in Dutch). Report R-89-34, Institute for Road Safety Research, SWOV, The Netherlands, 1989.

11. "Naar een veiliger Verkeer". Uitgave Ministerie van Verkeer en Waterstaat, Directie Verkeersveiligheid, 's-Gravenhage, 1986.

12. Goris, R.J.A.: "Ongevalsdalen: 25% minder in het jaar 2000?", MC nr. 20, 1989.

13. "Verletzungsfolgekosten nach Strassenverkehrsunfallen". Schriftenreihe des Hauptverbandes der gewerblichen Berufsgenossenschaften e.V. A. Sutter Druckerei GmbH, Essen, 1988.

14. Stuurgroep Toekomstscenario's Gezondheidszorg: "Ongevallen in het jaar 2000". Scenario's over Ongevallen en Traumatologie 1985-2000, Bohn, Scheltema & Holkema, Utrecht/Antwerpen, 1988.

CHAPTER 2

EPIDEMIOLOGY OF INJURIES

2.1 Introduction

Epidemiology is the fundamental science for studying the occurrence, causes, and prevention of disease [1]. Objectives of injury epidemiology include the development of epidemiologic tools to identify the injury problem, the determination of causative factors that amenable to intervention and the develop of methods to determine the effectiveness of countermeasures. For an engineer working in the field of injury biomechanics and prevention a detailed knowledge and understanding of real world accident data is essential and he clearly should be aware of the potential and limitations of these data. The purpose of this Chapter is to provide some of the essential background information.

A prerequisite for the study of the epidemiology of injuries is the collection, classification and interpretation of accident data on which to base priorities for research and interventions. Accident data are stored in accident data bases, often referred to as injury surveillance systems. Deciding what injury to collect and ensuring its reliability over time is essential to establish a useful data base.

Large differences can exist in definitions and type of data between two injury surveillance systems within the same country and sometimes even larger differences between data collection systems of different countries. For example some countries define a traffic accident fatality only if it occurs at the scene of the accident while others use a 30 day or even one year period after the crash if the death is attributed to the injuries sustained. The difference in traffic fatalities in a country due to these different interpretations can be 30 or more per cent [2].

In this Chapter first, different categories of injury surveillance systems will be introduced with some of their characteristics and limitations. Then a brief description of accident data bases available in the Netherlands is given, followed by an illustration of typical injury data which can be obtained from the various sources available in the Netherlands.

For engineers in traffic safety or policymakers it is very important to get information on the performance and effectiveness of restraint systems in real live conditions. If an injury surveillance system contains sufficient detailed data on the accident and if proper analysis techniques are employed it is possible to generate this type of information. At the end of this Chapter an example is given where the so-called "double paired comparison method" was applied on United States data in order to get information on restraint system effectiveness.

2.2 Injury surveillance systems

Accident data bases can be subdivided into two main categories: general or global accident files which contain for a large number of accidents relatively limited information per accident and data bases on the basis of "in-depth", on the spot studies, with detailed accident data on a relatively small number of accidents.

Examples of general accident files are the traffic accident registration by the police, medical registration by hospitals and data collected by insurance companies. Data collected by the police is in most countries the basis for the official national road accident statistics. The data usually collected, is information on place and time of the accident, the type of accident, persons involved and who is guilty in terms of traffic legislation and information on injuries and damage.

It will be clear that the amount and type of information police can collect from an accident is limited. The accident forms they are using allow only certain specific information to be included. Police officers usually do not have the expertise to make a complete, detailed and correct judgement of all the parameters involved in an accident and it is normally not their task. The resulting information available for researchers who study this type of accident data only can be of a general nature and so will be the findings from these studies.

Therefore many countries have established special accident investigation teams which perform on the spot of the accident so-called "in-depth" analyses. Such teams are usually multidisciplinary with 2-3 team members having engineering, medical and/or social behaviour expertise. They use special equipment to record the accident scene in as much detail as possible. Accident investigation teams are rather expensive and can investigate usually not more than 250 accident per year. They are restricted to a certain geographical area. Collecting relevant data for a representative sample off all accidents (or specific accidents like those involving pedestrians) requires a thorough planning of the research protocol. A detailed analysis of the accident data is required in order to get maximum benefit from the work carried out.

For the field of injury biomechanics in-depth studies are particularly useful if accident reconstruction techniques (e.g. computer simulations) are employed to support the analysis and to estimate afterwards the loading conditions for the accident victim so that correlations with the sustained injuries can be made.

The best known example of above set-up is the Crashworthiness Data system (CDS) in the United States which is part of the National Accident Sampling System (NASS). It is a data collection system operated since 1979 using accident investigation teams at 24 sites (status 1991). Each team performs on the spot analyses of a sample of the crashes occurring in that region. Data are collected on crashes involving passenger cars, light trucks and vans, but

(since 1991) not on motorcycles, heavy trucks or pedestrians. Currently about 7000 crashes are investigated per year in this way. An essential characteristic of CDS is its sample design which is considered to be representative for the accident situation in the United States. Data are available in electronic form and individual detailed cases are also available for analysis.

As mentioned before the detail of the data in police accident data bases is rather limited. The usefulness of the data can be improved considerably if they are linked with information available in other data bases like insurance and hospital based data bases. Also by linking with files containing information on the vehicle characteristics useful additional information can be achieved.

Finally also by interviewing the accident victim and other parties involved and by detailed analysis of the damage of the vehicle(s) within a shorter and/or longer period after the accident, very useful additional information on the accident, the injuries and the long term effects of the injuries, the vehicle damage etc. can be obtained. The amount of data and details obtained for an accident in this way lies somewhere between results from general/global injury surveillance systems and data available through "in-depth" on the spot studies. This type of accident research therefore sometimes is defined by the term "intermediate level" accident analyses. Accident investigations conducted by car companies concerning accidents involving a vehicle produced by this company, can be considered as part of this category.

2.3 Accident data bases in the Netherlands

2.3.1 Introduction

The most important general accident surveillance systems in the Netherlands are:

- VOR (police traffic accident data)
- LMR/SIG (in-patient hospital data)
- PORS (hospital home and leisure accident data)

These surveillance systems will be briefly described in the next Sections. Furthermore attention will be given to the data base of the Dutch insurance companies, a traffic accident data base in Groningen (RVG) and the SWOV accident data base. Finally the completeness of data bases will be discussed.

2.3.2 VOR

The police accident registration forms in the Netherlands are sent to the Road Accident Registration Office in Heerlen (Verkeersongevallenregistratie: VOR). The data is published by the Central Bureau of Statistics (CBS). Data collected by the Dutch police include:

- date and time
- location, road and weather conditions etc.
- vehicle type, registration number and damage
- brief description of the accident, accident type
- data on driver(s) and victim(s)
- hospital and place and date of death

2.3.3 LMR/SIG

The Centre for Health Care Information (Stichting Informatiecentrum voor de Gezondheidszorg (SIG), formally the Medical Records Foundation SMR) records all hospital admissions (in-patients) in the Netherlands. As far as trauma patients are concerned data like the injury sustained, the means of transport, treatment and length of stay are collected. The information on injuries is limited to a classification according to the ICD (International Classification of Diseases), version ICD-9-CM, which lacks information concerning the severity of the injury (see also Chapter 3 - Injury scaling). The hospital data are particularly of interest if they can be linked to the police accident data in order to study for instance the long term effects of injuries. A trial linkage of this type has been realised in 1986 and the results and problems encountered are expected to be reported soon.

2.3.4 PORS

Reliable and detailed accident surveillance systems in the world appear to be usually limited and specifically developed for traffic accidents. One of the few exceptions is PORS, the Dutch Home and Leisure Accident Surveillance System [3]. This system was set up in 1983 by the Consumer Safety Institute (SCV: Stichting Consument en Veiligheid in Amsterdam). It is a continuous data collection system of all accidents, other than road and industrial accidents, treated in fourteen Accident and Emergency hospital departments. The fourteen hospitals in which both the in- and outpatients are recorded constitute a representative sample taken from a population of about 140 general and university teaching hospitals in the Netherlands which have an Accident and Emergency department with 24 hour service. The data collection is much more detailed than the general hospital data base LMR/SMG. Among the information collected is the type of accident (fall from height, poisoning, etc.), a description of how the accident occurred, products/utensils involved in the accident, type of injury, treatment, etc. It is a two-phase registration system. In the first phase the brief epidemiological information indicated above is collected. For specific accidents the accident victims can be contacted in a second phase to obtain more detailed information.

2.3.5 Other sources

In addition to above national surveillance systems the data bases of the Dutch insurance companies should be mentioned here. They developed a centralized computer file of accident claims covering the great majority of insurance companies [4]. In countries like Germany, Sweden and the United States research teams founded and supported by insurance companies are continuously involved in analyzing insurance based accident data and many relevant findings have been reported. In the Netherlands the insurance data are closed for all, except the participating insurance companies themselves. No significant scientific findings concerning the epidemiology of traffic accidents in the Netherlands have been reported thus far on the basis of this data.

Another source of information in the Netherlands is the traffic accident registration system in the town of Groningen (RVG). Here a rather promising linkage between medical and accident data has been realised. Since 1978 data from the traumatology department of the Groningen University hospital have been coupled with police data as well as with data from the ambulance services. Analysis of these data is an ongoing activity and some interesting findings have been reported already e.g. concerning the long term effects of bicyclist accidents [5].

Finally the SWOV accident investigation data base is of interest although the information contained in this data base is already more than 15 years old. In the Netherlands as opposed to many other countries no in-depth, on the spot accident investigations have been carried out in the past, neither are they planned for the near future. A large scale intermediate level accident analysis was carried out in the period 1976-1977 by the Dutch Institute for Road Safety Research SWOV. In this study 3 successive steps could be distinguished [6]:

- observation of damaged vehicles in vehicle repair shops.
- if damage exceeds a certain level, the vehicle owner and occupants(s) were interviewed shortly after the accident.
- a second interview after 1 year in order to collect data on long-term effects.

The resulting data base contained more than 8000 vehicles and almost 14000 car occupants of which 4476 persons were injured. An estimate for the injury severity is included in this data base. This sample represents about 10 % of all accidents (with comparable severity) in the Netherlands in this period. Rather interesting results were obtained from this study, for instance concerning the effect of restraint systems [7] and injury patterns in specific collision types [8]. Since the traffic situation changes continuously e.g. by new protection systems which become available, a repeat of a study of this type at regular intervals is highly recommended.

2.3.6 Completeness of the data

The completeness of the VOR data as far as fatal accidents are concerned is 100 %. In other words it can be assumed that the police records every road accident with fatalities [9]. As far as the injured accident victims is concerned, the completeness of the police data appears to be much less however. Between august 1986 and july 1987 an extensive survey was conducted in the Netherlands in order to determine the number of injured persons in traffic as well as other type of accidents and to evaluate the completeness of the national injury surveillance systems [10, 11]. During the survey period almost 25.000 households were interviewed by telephone. Table 2.1 presents estimates for the annual number of injuries in the Netherlands by type of accident (excluding occupational injuries) and medical treatment (hospital admissions, hospital out-patients, general practitioner and others) based on this telephone survey.

Table 2.1 *Estimation of the annual number of injuries by accident type (excluding occupational injuries) and medical treatment in 1986,1987. Source: telephone survey in [11].*

	Hospital Admitted	Out-patient	General Practitioner	Others
Traffic	18.000	116.000	106.000	19.000
Sports	17.000	297.000	750.000	90.000
Others[1)]	17.000	570.000	570.000	290.000

[1)] Home and leisure accidents excluding sports

It can be seen that yearly about 3 million people sustain injuries that need medical treatment. About 30 % are treated in a hospital either as in-patient or out-patient. Home and leisure accidents constitute the most important cause of injuries with a large contribution from sport injuries.

It was found that the police accident data only contain 70 % of the patients admitted to the hospital (in-patients). In case of traffic accident victims treated as out-patients in the hospital this Fig. was even much less: 25 %. In other words only 1 out of 4 injured persons needing medical treatment in the hospital are included in the official dutch accident statistics. From the injured persons treated by a doctor without needing hospital treatment only 12 % appeared to be included in the police accident data. Such Figs indicate that the traffic injury problem is much larger than indicated by the official statistics.

2.4 Injury distribution

In this Section results of analyses of some of the aforementioned accident data bases will be presented with respect to the body parts injured and the type of injuries sustained. First traffic injuries will be considered followed by sport injuries.

The distribution of injured body regions for various road user categories admitted in the hospital is presented in Fig. 2.1 (Source: LMR/SIG data [12]). In the category "all" the total of all road traffic injuries is presented including public transport and other means of road transport. Head injuries appear to be the largest group in accidents involving pedal cyclists and motor vehicle occupants. Lower extremity injuries are the most frequent injuries in accidents involving moped drivers and motorcyclists. For pedestrians the frequency of head and lower extremity injuries is about the same.

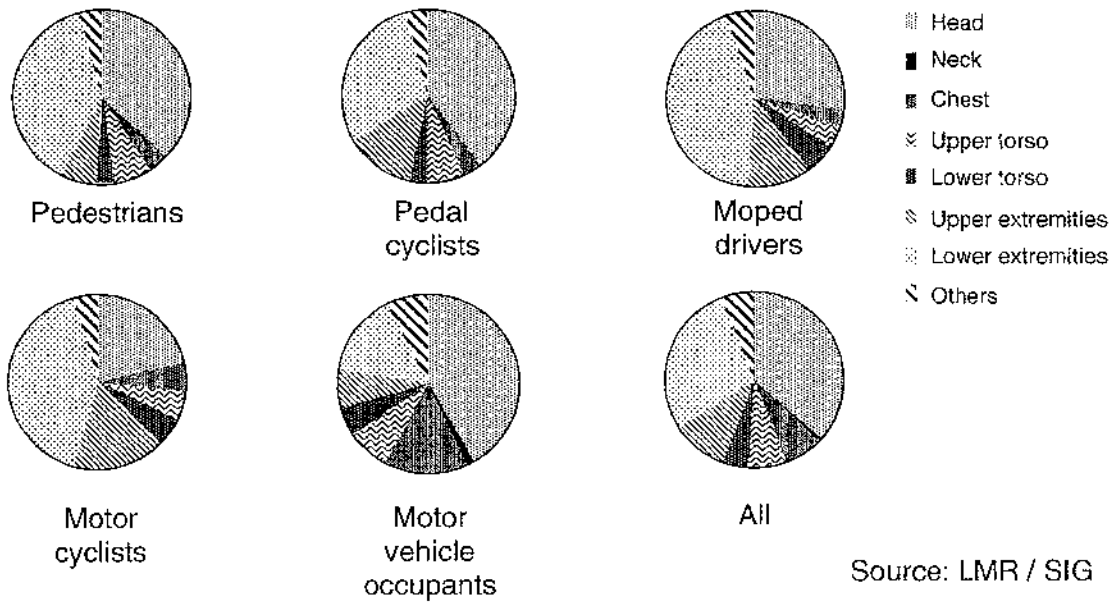

Fig. 2.1 *Body region injured in traffic accidents treated in hospitals (admissions) by type of road user in 1987. Source: LMR/SIG data in [12].*

From the SWOV accident investigation discussed earlier the distribution of injuries by body region and by collision type is available (Table 2.2). The most significant differences in injuries between the various collision types are less facial and more pelvis injuries in lateral than in frontal collisions and much more neck injuries in rear end collisions than in the other collision types. Also the number of leg injuries appears to be less for lateral than for frontal collisions while on the other hand arm injuries are slightly more frequent.

Sport injuries constitute a significant proportion of the total number of injuries (Table 2.1). Injury control strategies like, for example, the use of protective materials are considered to be a rather effective means of reducing the total number and severity of sports injuries. First Table 2.3 presents the distribution of injury types, treated in the hospital in 1986 based on PORS data [13]. The most frequent injuries are sprains, particularly in the ankle. Striking is also the high number of fractures.

Table 2.2 *Distribution of injuries by body region for several collision types, drivers only. Source: SWOV accident investigation in [7].*

Main group	Lateral collisions	Front to front	Rear collisions	Total (incl. other types)
1 Skull & brain	23.7	20.0	14.4	22.2
2 Face	11.2	21.1	7.2	16.1
3 Neck	4.4	3.7	51.6	6.9
4 Thorax	20.2	16.9	6.8	16.5
5 Abdomen	2.6	2.3	0.4	2.3
6 Back	2.4	1.3	4.0	2.4
7 Pelvis	5.0	1.3	0.4	2.0
8 Arms	16.0	13.6	7.2	14.2
9 Legs	14.5	19.8	8.0	17.3
Total	100%	100%	100%	100%

Table 2.3 *Type of injuries in sport accidents in 1986. Source: PORS data in [13].*

Type	%
sprain	32.7
bruising	26.7
fracture	21.4
cuts	6.4
dislocation	2.9
open wound	1.7
grazes	1.4
damage to nervous system	0.6
other	3.7
no injury	1.4
unknown	1.1

The location of injuries in sport accidents by body region, expressed as a percentage of the total number of injuries, is indicated in Fig. 2.2 [13]. Note that the frequency of head and neck injuries due to sports accidents is much less than in traffic accidents (compare with Fig. 2.1) while the number of lower leg injuries is higher.

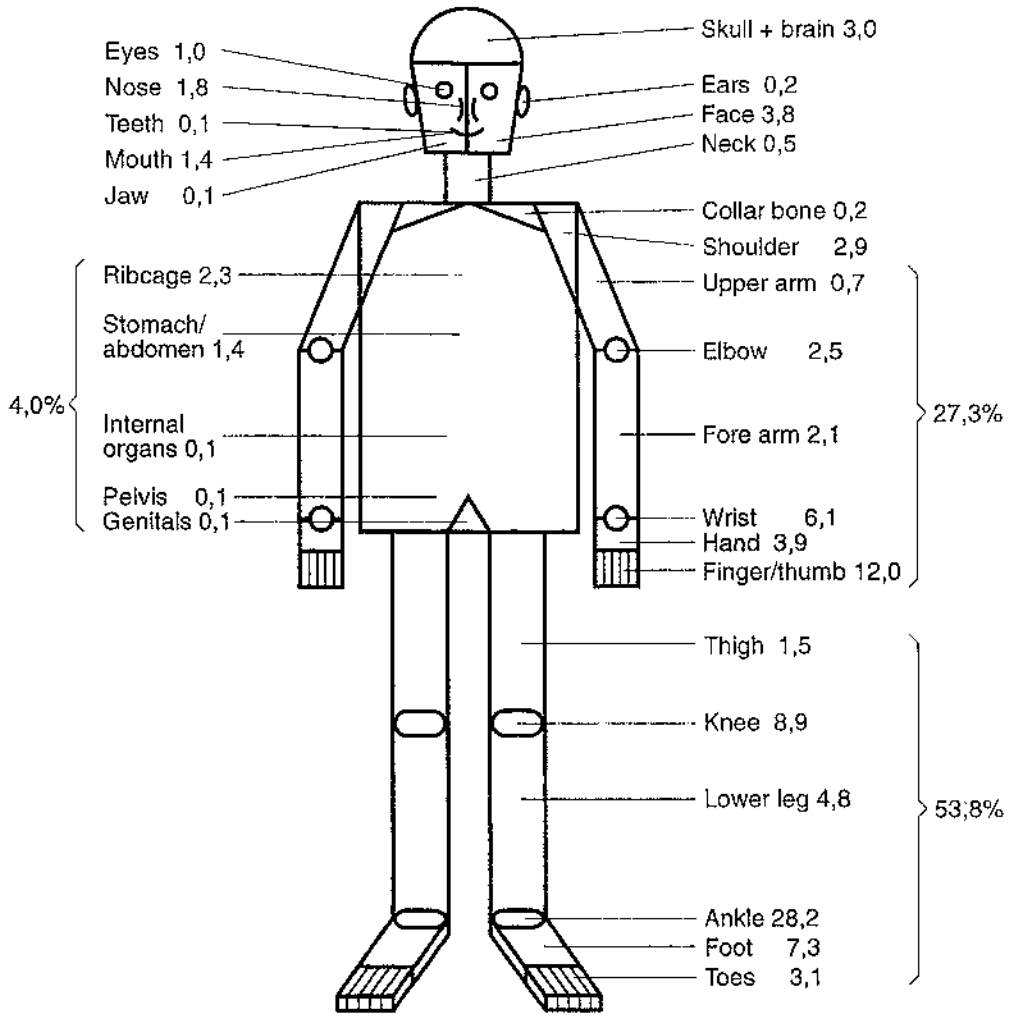

Fig. 2.2 *Sport injuries treated in the hospital by body region in 1984/1985. Source: PORS data in [13].*

The sport which accounts for the largest number of injuries is soccer: 33.3% of all injuries recorded by PORS in 1986 [13]. Other sports that score high within PORS are school physical education, volleyball, hockey, tennis and ice skating.

2.5 Restraint system effectiveness

The effectiveness of restraint systems can be determined from analyses of data in injury surveillance systems, provided that reliable information on restraint system usage is available. A statistical method developed in the mid-eighties for this type of analysis is the so-called double paired comparison method. A detailed treatment here of this method would be out of the scope of this biomechanics course. An interested reader is referred to Evans [15].

The method compares the number of fatalities between two occupants: a "subject" occupant and an "other" occupant, where the other occupant serves a normalizing, or exposure estimating role. In order to determine the effectiveness of a restraint system, let's say a safety belt, two sets of fatal crashes are selected from the data base. Let us assume here that the unbelted passenger of the car is the "other" occupant. The first set of crashes contains belted drivers and unbelted passengers, at least one of whom is killed. From this set a belted driver to unbelted passenger fatality ratio is calculated. From a second set of crashes involving cars with unbelted drivers and unbelted passengers, an unbelted driver to unbelted passenger fatality ratio is calculated in a similar way. When the first fatality ratio is divided by the second it gives the probability that a restrained driver is killed compared to an unrestrained driver. The resulting ratio is denoted as R by Evans. The restraint system effectiveness in case of belt effectiveness, is usually defined as the percentage reduction in fatalities an unbelted population of occupants would obtain by conversion to universal belt use, all other factors remaining unchanged, in other words as (1-R)*100.

An important data base in the United States is FARS (Fatal Accident Reporting System). This data base describes all fatal crashes since 1975 on the basis of information collected in each state [14]. The sources for FARS include police accident data, vehicle registration files, vital statistics, coroner reports, etc. On the basis of this data base, Evans [16] studied the effectiveness of lap/shoulder belts in various collision types and the fraction of the effectiveness related to preventing ejection from the vehicle. Results are shown in Fig. 2.3 as far as the driver is concerned. Lap/shoulder belts appear to reduce fatalities in all impact directions and not only in frontal direction as is often assumed. Much of this effectiveness is due to ejection prevention particularly in case of rollovers (non-collisions). The overall effectiveness of lap/shoulder belts, i.e. all impact directions combined is 42% which compares well with other estimates given in literature.

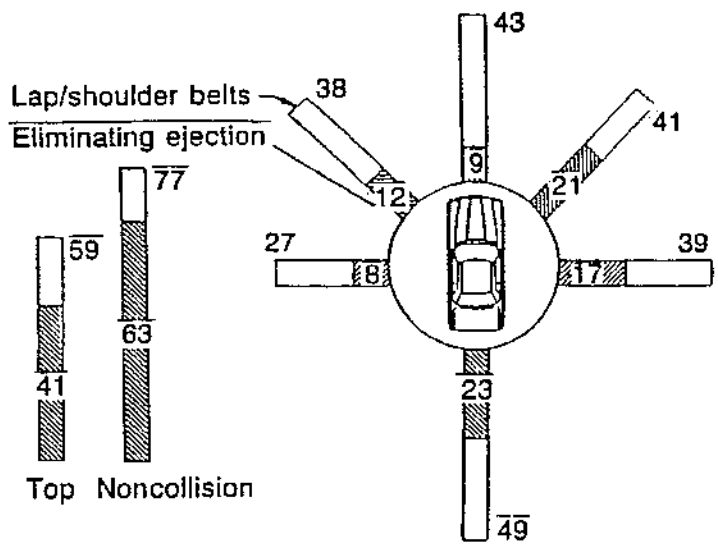

Fig. 2.3 *Effectiveness of lap/shoulder belts in preventing driver fatalities by impact direction and the contribution of preventing ejection [10].*

Note that such restraint system effectiveness estimates only have been carried out so far for fatality reduction estimates. The effect on reducing the severity of injuries is much more difficult to determine from accident data bases. Furthermore the method of doubled pair comparisons is based on a number of assumptions, which if violated, could introduce serious errors into the method (see [15] for a discussion on possible error sources).

REFERENCES

1. Committee on Trauma Research, Commission on Life Sciences, National Research Council and the Institute of Medicine: "Injury in America. A continuing Public Health Problem". National Academy Press, Washington, 1985.

2. Trinca, G. et. al.: "Reducing Traffic Injury". A Global Challenge, A.H. Massina & Co., Melbourne, 1988.

3. "PORS 1988-89". Report Consumer Safety Institute, Amsterdam.

4. Harris, S.: "Linking road accident data to other files". Report R-86-20, Institute for Road Safety Research, SWOV, The Netherlands, 1986.

5. Passies, G.: "Langdurige gevolgen van ongevalsletsels bij fietsers" (in Dutch). Rapport RVG, Sectie Traumatologie, Academisch Ziekenhuis Groningen, 1990.

6. Clay, W.: "Letselgevolgen van auto-inzittenden na een auto-ongeval" (in Dutch). Thesis, University of Groningen, 1986.

7. Van Kampen, L.T.B.: "Hoofdsteunen in personenauto's" (in Dutch). Report R-82-33, Institute for Road Safety Research, SWOV, The Netherlands, 1982.

8. "Lateral Car Collisions": Report R-79-48, Institute for Road Safety Research, SWOV, The Netherlands, 1979.

9. Maas, M.W. and Harris, S.: "Police Recording of Road Accident In-Patients". Accident Analysis and Prevention 16-3, pp. 167-184, 1984.

10. Harris, S.: "Verkeersgewonden geteld en gemeten" (in Dutch). Report R-89-13, Institute for Road Safety Research, SWOV, The Netherlands, 1989.

11. Montfoort, G.L.M. van, Galen, W.C.C. and S. Harris: "Ongevallen in Nederland". Report (in Dutch), Consumers Safety Institute, The Netherlands, 1988.

12. Blokpoel, A.: "De verkeersonveiligheid in 1988" (in Dutch). Report R-89-34, Institute for Road Safety Research, SWOV, The Netherlands, 1989.

13. De Vent, T.G.M.: "Sports injuries prevention by information and education". Report no. 51, Consumer safety institute (SVC), Amsterdam, 1988.

14. "Fatal Accident Reporting System 1988". Report DOT HS 807 507, US Dept. of Transportation, National Highway Traffic Safety Administration (NHTSA), 1989.

15. Evans, L.: "Double pair comparison - a new method to determine how occupant characteristics affect fatality risk in traffic crashes". Accid. Anal. & Prev. Vol. 18. No. 3. pp. 217-227, 1986.

16. Evans, L.: "Restraint effectiveness, occupant ejection from cars, and fatality reductions". Accid. Anal. & Prev. Vol. 22. No. 2. pp. 167-175, 1990.

CHAPTER 3

INTRODUCTION IN INJURY BIOMECHANICS

3.1 Introduction

Injury of the human body can be caused by different loading situations including mechanical, chemical, thermic and electric load. The field of injury biomechanics deals with the effect on the human body of mechanical loads, in particularly impact loads. Therefore also often the term "impact biomechanics" is used instead of "injury biomechanics". Viano [1] defines the objectives and research methods of injury biomechanics as follows:

"The broad goal of injury biomechanics research is to understand the injury process and to develop ways to reduce or eliminate the structural and functional damage that can occur in an impact environment". "To achieve this goal, researchers must identify and define the mechanisms of impact injury, quantify the responses of body tissues and systems to a range of impact conditions, determine the level of response at which the tissues or systems will fail to recover, develop protective materials and structures that reduce the level of impact energy and force delivered to the body, and develop test devices and computer models that respond to impact in a human like manner, so that protective systems can be accurately evaluated"

Note that above description relates to impact type of loading conditions. But usually the response of biological tissue under *static* injury producing loading conditions is considered to be subject of injury biomechanics research as well.

In this Chapter first a short discussion on the use of human body models in injury biomechanics research will be presented (Section 3.2). Human body models are used to study the dynamical response of the human body under extreme loading conditions and more specifically, to determine injury mechanisms and injury tolerances. Furthermore human body models are applied for the assessment of the protection offered by safety provisions. Five types of models will be distinguished: human volunteers, human cadavers, living and dead animals, mechanical models (crash dummies) and mathematical models.

In Section 3.3. the load/injury model will be introduced, which can be of help in understanding and interpreting the methodology and terminology used in the field of injury biomechanics research. Some basic relevant anatomy and injury terminology used in this course is summarized in Appendix A.

An important aspect of injury biomechanics and trauma research is the classification of the injury severity. Section 3.4 deals with this subject, where various methods to assess the

severity of injury will be introduced, including the Abbreviated Injury Scale (AIS) and scales which prescribe the severity of an injury in terms of societal costs.

Assessment of the (statistical) relationship between injury severity and injury criteria will be discussed in Section 3.5. The so-called injury risk function will be introduced which describes the probability of a certain injury or a fatality as function of the loading in an accident or a laboratory experiment.

The last Section of this Chapter discusses the tolerance of the whole human body in an impact environment. Injury mechanisms and tolerances of individual body segments will be presented in separate Chapters. Attention will be given to injury biomechanics of the head (Chapter 4), the spine (Chapter 5) and the thorax (Chapter 6).

3.2 Models in injury biomechanics

3.2.1 Introduction

In order to protect the human body against injuries in case of extreme loading conditions, a clear insight in the ways injuries arise and into loads at which they occur is needed. Accident analysis studies and biomechanical research are carried out for this purpose. In injury biomechanics research several types of models for the human being are used to study biomechanical response of the human body and to study injury mechanisms and tolerances. Also for the assessment of the protection offered by safety provisions, like seat belts and crushable vehicle structures, models for the human being are needed. In fact five types of human models can be distinguished: human volunteers, human cadavers, animals, mechanical models and mathematical models. In the next Sections the capabilities and limitations of the various models will be discussed.

3.2.2 Human volunteers

For obvious reasons it is impossible to experiment with human beings fitted with instrumentation under injury producing conditions. Only in low severity tests, i.e. below the pain thresholds, sometimes human volunteers are used. Such tests, which are limited by rigid regulations and guidelines, can contribute to general knowledge on the human body non-injurious response. The results are very important for the development of mechanical or mathematical models. The human subjects are mostly young, well-trained, military volunteers (Fig. 3.1). Their pain tolerance is usually much higher than that of the general population. Therefore the test results are not representative of females, children and elderly people.

An advantage of the use of human volunteers is that the effect of muscle tone and pre-bracing on the dynamical response can be studied. But this influence, which might be relatively large at low impact levels, cannot be simply extrapolated to higher impact levels.

The first well-documented human volunteer test was conducted in 1954 in the dessert of New Mexico at Holloman Air Force Base. Test subject was Colonel John Paul Stapp who sustained, without serious complaints, a velocity change of 1000 km/h during 1.4 sec on a rocket propelled sled device. The maximum deceleration was 40g, in other words 40 times the deceleration of gravity. For comparison: the average deceleration during a 50 km/h vehicle crash test against a brick wall is about 25g. And this deceleration usually doesn't take longer than 0.1 sec.

Well-known for its research using human volunteers is the Naval Biodynamics Laboratory in New Orleans. One of the objectives of their tests is the analysis of head-neck motions. In Chapter 5 some of the Naval Biodynamics work will be presented.

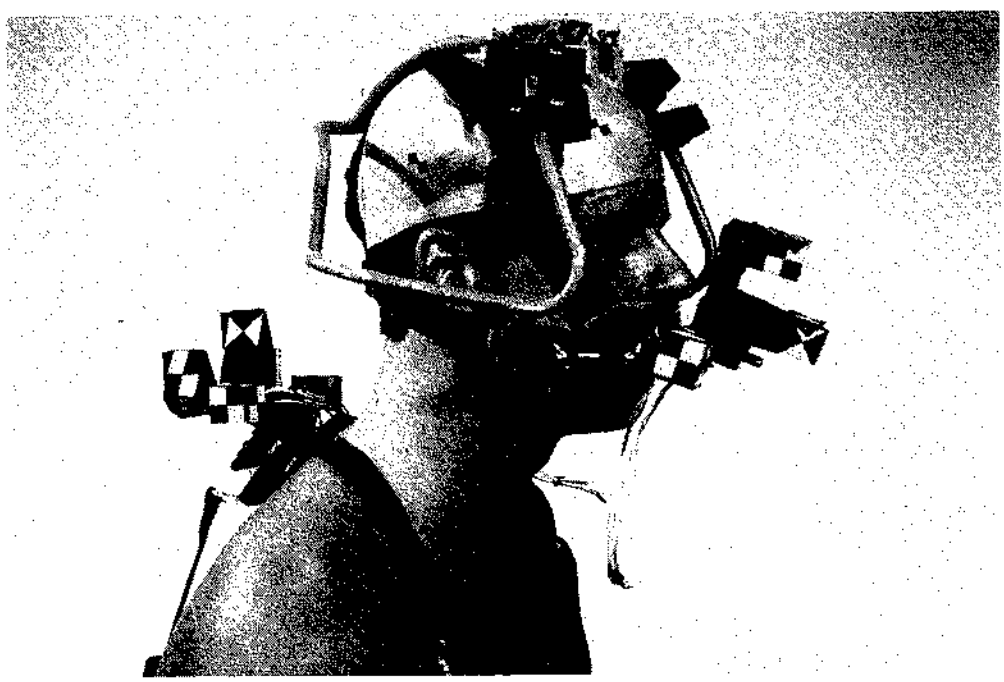

Fig. 3.1 *Human volunteer test at the Naval Biodynamics Laboratory in New Orleans*

3.2.3 Human cadavers

The primary research tool to evaluate injurious biomechanical response is a human cadaver (sometimes referred to as PMHS: post-mortem human subject). The anthropometry of a human cadaver is almost identical to the living human and material properties are often close to living tissue. This latter aspect however is strongly dependent on the preparation

techniques applied and the time duration since death. Very often the lungs of the cadavers are inflated during the test and the blood pressure is partly restored by infusion. Disadvantages of the use of human cadavers are the absence of muscle tone and that physiologic responses cannot be determined. Furthermore the age of cadavers is often high and since the mechanical strength of most tissues in the human body tends to decrease with age, the data obtained are not necessarily representative of the general population.

3.2.4 Animals

Research using anaesthetized animals as human surrogates, is vital to obtain information on physiologic responses, in injury producing loading conditions, for specific body areas like the brains and the spinal cord. Furthermore tests with animals can provide insight in the differences between dead and living surrogates and as such provide the information for correct interpretation of human cadaver testing. Due to differences in size, shape and also structural differences between humans and animals, quantitative scaling and extrapolation of results of animal testing to the human is very difficult.

3.2.5 Mechanical models

Mechanical models or crash dummies (sometimes also referred to as anthropomorphic test devices) normally consist of a metal or plastic skeleton, including joints, covered by a flesh-simulating plastic or foam. They are constructed such that dimensions, masses and mass-distribution, and therefore the kinematics in a crash are human like. The dummy is fitted with instrumentation to measure accelerations, forces and deflections during the tests, that correlate with injury criteria for human beings. Dummies are often used in approval tests on vehicles or safety devices, in which the measured values should remain below certain (human tolerance) levels. Very important in this respect is a repeatable response of the dummy in identical tests. Furthermore crash dummies sometimes are used for the reconstruction of real accidents in order to study the correlation between real world injuries and actual loading conditions. Chapter 7 specifically deals with mechanical models.

3.2.6 Mathematical models

The behaviour of human beings in crashes can also be simulated by mathematical models. Together with a mathematical description of the environment (e.g. steering-wheel, dashboard, seat and belts) and the impact conditions (e.g. vehicle deceleration), the model provides a numerical description of the crash event. Like mechanical surrogates, mathematical models can be used to study the protection offered by safety devices and for accident reconstructions. Furthermore they can be used to analyze biomechanical experiments and to

quantify mechanical parameters in the experiment which cannot be assessed experimentally. Another potential of computer models is the use in the design of vehicles and restraint systems as a computer aided design tool. They offer a very economical means of system optimisation. Finally mathematical models can be used to scale results of animal tests.

An important limitation of a computer model is that the accuracy and reliability of the model strongly depends on the (biomechanical) information available on the system(s) to be modeled as well as the assumptions made in the model formulation. Therefore detailed experimental verification is often a necessity. Chapter 8 deals with mathematical models.

3.3 The load-injury model

3.3.1 Introduction

Fig. 3.2 schematically presents the accident/injury process in case of mechanical (over)-loading and the various parameters affecting the outcome of this process. This schematic representation will be called the load/injury model. The model will be used here to define and explain some of the terminology used in injury biomechanics research.

The load/injury model shows that, as a consequence of an accident, the human body is exposed to a mechanical load condition. Through *injury control measures*, as discussed in Chapter 1, the magnitude of the load acting on the body can be reduced.

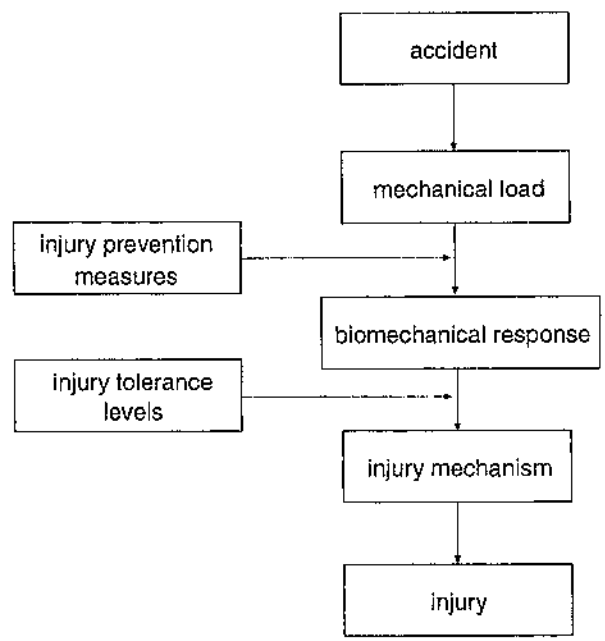

Fig. 3.2 *The load/injury model.*

In the following Sections the reaction of the human body to the mechanical load will be discussed. First the so-called biomechanical response will be described, then the injury mechanisms and finally definitions like injury severity, injury criteria and injury tolerances will be introduced.

3.3.2 Biomechanical response

Due to the mechanical load a body region will experience mechanical and physiological changes: the so-called *biomechanical response*. Biomechanical response will be defined here as any change in time of the position and shape (due to deformation) of the human body, a body region or tissue and any physiological changes related to these mechanical changes. Examples of biomechanical response are the motion of the head-neck system in an accident, the brain motions and deformations in case of a head impact or thorax deformation in case of an impact with the steering wheel.

Examples of physiological changes are changes in reflexes, dizziness and headache. It is important to realize here that biomechanical response not necessarily has to result in injury. Human volunteers e.g. are tested in impact biomechanics research below pain levels as was discussed in Section 3.2.2. The information of such tests can be very important to develop mechanical or mathematical models of the human body.

3.3.3 Injury mechanisms

Injury will take place if the biomechanical response is of such a nature that the biological system deforms beyond a recoverable limit, resulting in damage to anatomical structures and alteration in normal function. The mechanism involved is called *injury mechanism*. Identification and understanding of injury mechanisms is one of the main objectives of research in the field of injury biomechanics.

Usually a distinction is made between penetrating and non-penetrating injuries. Penetrating injuries are caused by high-speed projectiles, such as bullets, or by sharp objects moving with a lower velocity such as knives. In this type of injury the (impact) energy is concentrated on a small area and injury will occur if local stresses exceed failure levels.

Non-penetrating injuries are more complicated and the corresponding injury mechanisms are not always easy to understand. Loads are usually acting on a larger contact area caused by contacts with blunt objects. Inertia, elastic and visco-elastic aspects will effect the load distribution within the body region involved. Bones like the ribs and the skull protect vital organs by absorbing some of the impact energy. Damage of an anatomical structure will occur if tensile, compressive or shear stresses exceed a tolerable level.

Three principal injury mechanisms are usually distinguished, as is illustrated in Fig. 3.3 [2]:

- Compression of the body causing injury if elastic tolerances are exceeded. Injury can occur in case of slow deformation of the body (crushing) as well as due to high velocity impacts.

- Impulsive (shock) type of loading causing shock waves in the body, which results in internal injuries if so-called viscous tolerances are exceeded. Even without significant outside deformation of the body this type of injury is possible, for example in the chest cavity in case of an impact on the sternum.

- Acceleration type of loading causing tearing of internal structures due to inertia effects. In case of brain injuries, for example, this mechanism plays an important role.

Above mechanisms also can occur in combination with each other depending on the loading situation. Increase of the load levels often will lead to more severe injuries while the same injury mechanism takes place. However higher loads may also result in different mechanisms and as a consequence will show a different injury outcome.

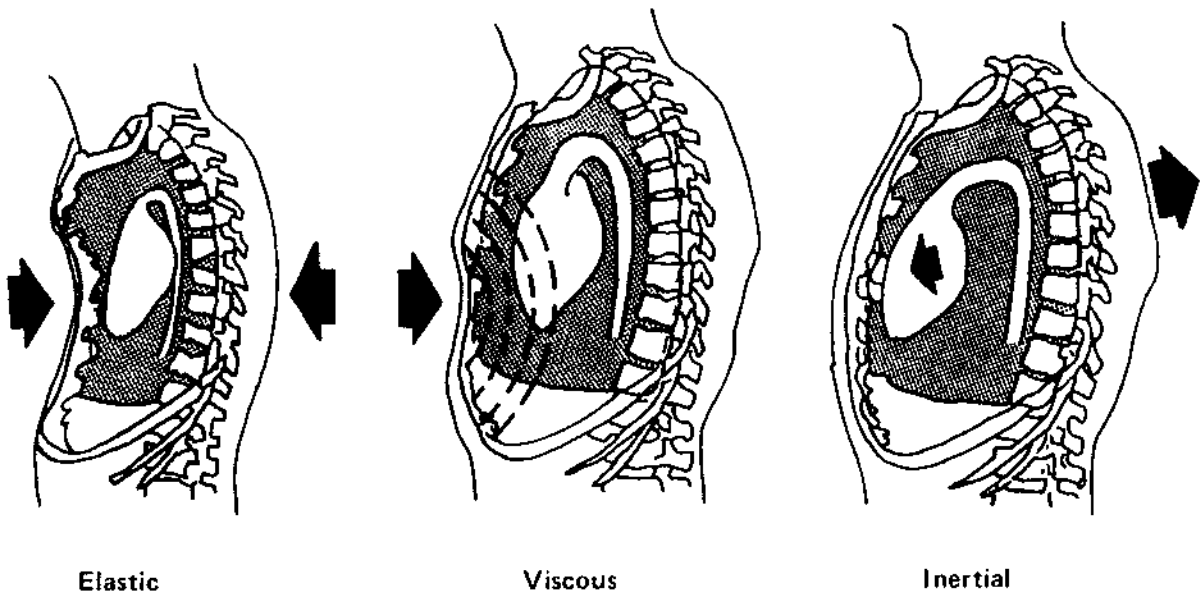

Fig. 3.3 Three principle injury mechanisms [2].

3.3.4 Injury severity, criteria and tolerances

The severity of the resulting injury is indicated by the expression *injury severity*. It is defined as the magnitude of changes, in terms of physiological alterations and/or structural

failure, which occur in a living body as a consequence of mechanical violence [3]. Section 3.4 will deal in detail with injury severity and various methods to assess the injury severity level including the widely used Abbreviated Injury Scale (AIS).

The next term that will be introduced here is the *injury criterion*, which is defined as a physical parameter or a function of several physical parameters which correlates well with the injury severity of the body region under consideration. Frequently used parameters are those quantities that relatively easy can be determined in tests with human substitutes like the linear acceleration experienced by a body part, global forces or moments acting on the body or deflection of structures. Later in this course several examples of injury criteria will be given.

In conjunction with the injury criterion the term *tolerance level* (or injury criterion level) will be defined here as the magnitude of loading indicated by the threshold of the injury criterion which produces a specific type of injury severity. It should be noted that there are large variations in tolerance levels between individuals. Tolerance levels for populations can therefore only be determined statistically. Section 3.5 deals with this subject.

Above terminology refers here to the living human body as well as to biological substitutes like human cadavers or animals. In some literature (e.g. Ref. [3]) above terminology is solely reserved for the living human body since the injury mechanisms in substitutes might differ from those in the living human body. For the injury process in human substitutes a corresponding terminology is proposed like damage severity instead of injury severity and damage criteria instead of injury criteria. In this course we will not adopt this terminology since it is seldom applied in practice up to now.

3.3.5 Protection criteria and biofidelity

Also for non-biological substitutes, i.e. the mechanical and mathematical models the terms injury severity, injury criterion and tolerance level are applied although these substitutes are not actually injured. For mechanical models (dummies) rather than the term injury criterion however also sometimes the term *performance or protection criterion* is used. In these models, levels of biomechanical response are determined and judged as if the model were a living human body.

The correct interpretation of injury criteria determined at models and the "translation" into injury in the living human body is one of the challenges in injury biomechanics research. Important here is whether the model responds to impact in a human like manner, the so-called *biofidelity* of the model. The biofidelity of a model can be judged by comparing the response (i.e. motions, displacements etc..) with average data generated in test with human

volunteers or cadavers. Response data from tests with biological substitutes used for the purpose of biofidelity judgement are often defined as *biofidelity performance requirements*.

3.4 Injury scaling

3.4.1 Introduction

Injury scaling is defined here as the numerical classification of the type and severity of an injury. Many schemes have been proposed for ranking and quantifying injuries. They can be grouped into three main types:

- *Anatomic scales* which describe the injury in terms of its anatomical location, the type of injury and its relative severity. These scales rate the injuries itself rather than the consequences of injuries. The most well-known scale, which is accepted worldwide, is the Abbreviated Injury Scale (AIS). Section 3.4.2 deals with anatomic scales.

- *Physiologic scales* which describe the physiological status of the patient based on the functional change due to injury. This status and consequently its numerical assignment, may change over the duration of the injury's treatment period, in contrast to anatomical scales where a single numerical value is assigned to a certain injury. A well-known example is the Glasgow Coma Scale (GCS) which was specifically developed for head injuries. It is a way of quickly assessing the nature and severity of brain injuries on the basis of three indicators: eye opening, verbal response and motor response. Physiological scales are particularly important in a clinical environment; they will not be further discussed here.

- *Impairment, disability and societal loss scales.* Here not the injury itself or the functional changes due to the injury are rated, but the long term consequences and in relation to this the "quality of life". Examples are the Injury Cost Scale ICS, the Injury Priority Rating, IPR and the HARM concept, which all are attempts to assign an economic value to the various injuries. These scales are discussed in 3.4.3.

Note that above types of injury scales basically relate to injuries in the living human body. Anatomical scales like the AIS however also can be applied to rate the injury severity in human cadavers after dissection of the body.

In the Netherlands none of the above injury scales are applied, except for the AIS which was used in the SWOV accident investigation mentioned earlier in this course (see 2.3.5). In the LMR/SIG hospital data base (see 2.3.3) the ICD (International Classification of Diseases) is used, however this classification only codes the location and nature of the injury and not its severity.

3.4.2 Anatomical scales

3.4.2.1 The Abbreviated Injury Scale (AIS)

The need for a standardized system for injury severity rating arose in the mid nineteen-sixties in the USA with the first generation of multidisciplinary motor vehicle crash investigation teams. In 1971 the first Abbreviated Injury Scale (AIS) was published and has since then been revised four times (1976, 1980, 1985 and recently in 1990). This last update [4] will be referred to as "AIS 90". Although originally intended for impact injuries in motor vehicle accidents, the several updates of the AIS allow its application now also for other injuries like burns and penetrating injuries (gun shots). The AIS distinguishes between the following severities of injury:

Table 3.1 The Abbreviated Injury Score (AIS) [4].

AIS	Severity code
0	no injury
1	minor
2	moderate
3	serious
4	severe
5	critical
6	maximum injury (virtually unsurvivable)
9	unknown

The information for AIS scaling is contained in the AIS manual, which is organized into nine Sections dealing with several body regions (head, face, neck, thorax, abdomen and pelvic contents, spine, upper extremity, lower extremity, external and other). Within each Section, injury descriptions are provided by specific anatomical part. In case of the lower extremities for instance, these anatomical parts are: the whole area, vessels, nerves, skeletal-bones, skeletal-joints and muscles-tendons-ligaments. For each specific injury the manual provides a 7-digit coding, where the digit right of the decimal point is the AIS score. The other digits are used to specify body region, anatomic structure, type of injury etc. Table 3.2 illustrates examples of injuries in the AIS manual for several body regions.

The AIS is a so-called "threat to life" ranking. Higher AIS levels indicate an increased threat to life. The numerical values have no significance other than to designate order. They do not indicate relative magnitudes, in other words an AIS 2 level is not twice as severe as an AIS 1 level. Several attempts have been made to establish a quantitative relationship between the various AIS levels. One attempt is the calculation of a fatality rate for each AIS value. Table 3.3 summarizes the range of results of several studies [5]. Another attempt is the HARM concept [6], which assigns an average economic value to each of the AIS injuries. See Table 3.3 and Section 3.4.3 for more details.

Table 3.2 *AIS examples by body region [5].*

AIS	Head	Thorax	Abdomen and pelvic contents	Spinre	Extremeties and bony pelvis
1	headache or dizziness	single rib fracture	abdominal wall: superficial laceration	acute strain (no fracture or disl.)	toe fracture
2	unconscious less than 1 hour; linear fracture	2-3 rib fracture; sternum fracture	spleen kidney or liver: laceration or contusion	minor fracture without any cord involvement	tibia, pelvis or patella: simple fracture
3	unconscious 1-6 hours; depressed fracture	≥4 rib fracture; 2-3 rib fracture with hemoth. or pneumoth.	spleen or kidney: major laceration	ruptured disc with nerve root damage	knee dislocation; femur fracture
4	unconscious 6-24 hours: open fracture	≥4 rib fracture with hemoth. or pneumoth.; flail chest	liver: major laceration	incomplete cord syndrome	amputation or crush above knee; pelvis crush (closed)
5	unconscious more than 24 hours; large hematoma (100 cc)	aorta laceration (partial transection)	kidney, liver or colon rupture	quadriplegia	pelvis crush (open)

Table 3.3 *AIS vs. fatality rate and vs. Economic Costs (HARM) [5].*

Injury Severity AIS	Fatality rate (range %)	Costs (HARM) ($1000)
1	0.0	0.4
2	0.1-0.4	2.7
3	0.8-2.1	7.1
4	7.9-10.6	38.8
5	53.1-58.4	186.6
6	...	165.0

3.4.2.2 Multiple injury scales

The AIS does not assess the effect of multiple injuries in patients. One possibility is to take the highest AIS score for a certain body region as a measure for the overall injury severity: the M(aximum)AIS. The value of the MAIS in trauma research is considered limited due to its nonlinear relationship with the probability of death.

As mentioned before the AIS is not applied in the Netherlands. The only exception is the SWOV accident investigation conducted in the mid-seventies (see Chapter 2). As a measure for the injury severity of the complete body the O(verall)AIS was used which is comparable with the MAIS. Results of the AIS findings in this SWOV study for various accident configurations are summarized in Table 3.4.

A more general accepted approach for rating multiple injuries is the ISS or Injury Severity Score [4]. The ISS distinguishes 6 body regions: Head or Neck, Face, Chest, Abdominal or Pelvic contents, Extremities or Pelvic girdle and External, where external injuries include lacerations, abrasions, contusions and burns, independent of their location on the body surface. For each of these regions the most severe injury on the basis of the AIS code is determined. The ISS is the sum of the squares of the three largest AIS values. The maximum value for the ISS is 75 (three AIS 5 injuries). An AIS 6 automatically becomes an ISS 75 score according to the ISS specifications. The ISS has been shown to correlate quite well with the probability of death as is illustrated in Fig. 3.4.

Table 3.4 Severity of injuries in SWOV accident investigation for some collision types, drivers only [7].

OAIS	Lateral (%)	Front (%)	Rear (%)	Rollovers (%)	Total (%)
1	18.0	22.4	21.4	18.0	18.6
2	10.9	16.1	3.0	14.1	11.2
3	4.1	4.4	0.7	5.3	3.1
4	1.0	0.7	0.4	0.3	0.5
5	0.3	0.2	-	-	0.2
6	2.2	2.7	-	1.9	1.5
Total	100% (2044 cases)	100% (2138 cases)	100% (743 cases)	100% (640 cases)	100% (8173 cases)

3.4.3 Injury cost scales

In case of injury severity scales which rate the long term consequences of injuries, numerical values are much more difficult to determine and the status of the accident victim has to be monitored during a long period. The interest in, and importance of these scales is growing since they provide a much better means of establishing priorities for injury prevention measures than the anatomical based scales since much more factors are taken into account and since injury severities usually are expressed in term of economic costs. Examples of these scales are the Injury Priority Rating, IPR, the HARM concept and the Injury Cost Scale ICS, which all are attempts to assign an economic value to the various injuries.

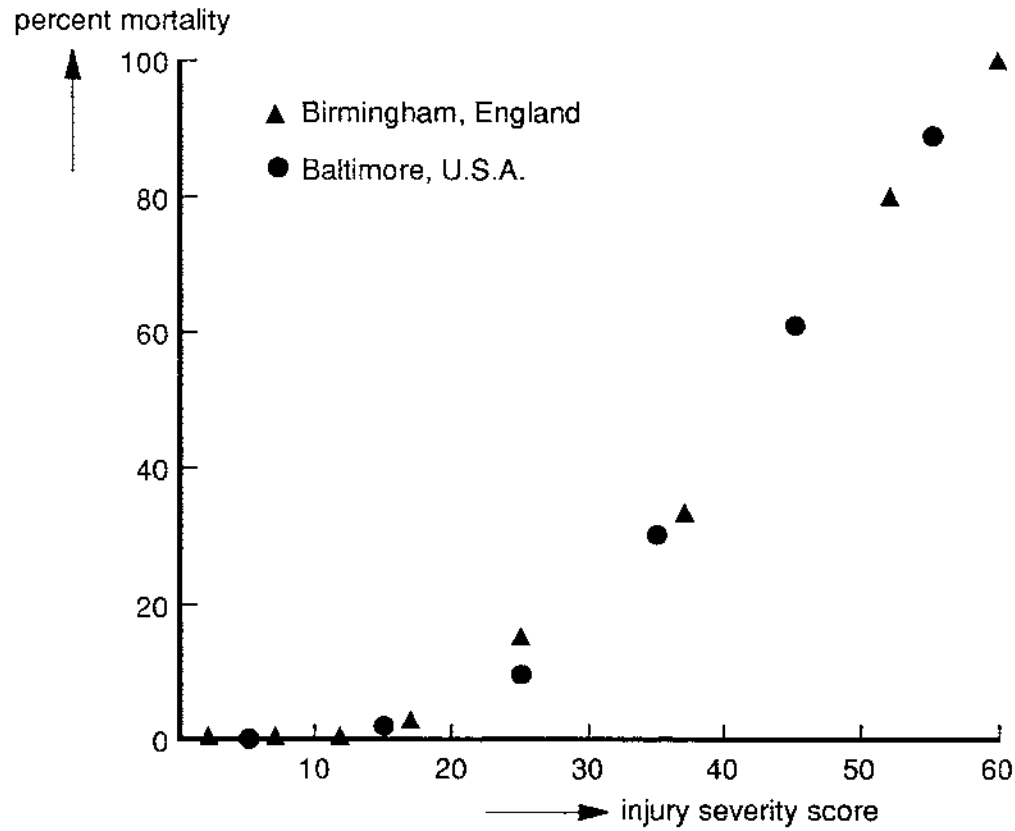

Fig. 3.4 *ISS as function of mortality rate [8].*

The HARM concept is an attempt to assign an average economic cost to an AIS value [6]. Table 3.3 illustrates this relationship. Since the AIS rates the injury severity itself and not the long term consequences a large variation in actual economic costs per injury within an AIS level will exist and therefore useful application of the average costs for each AIS level as rated by HARM is rather limited. The US government applies the HARM score for instance to calculate the effect of various governmental interventions in the field of vehicle safety.

A more reliable and detailed effort to weigh the various injuries in terms of economic costs, is the IPR [9]. The analysis, resulting in the IPR, was based on the NASS files discussed in Chapter 2. The information in the NASS files was first augmented with estimates for the impairment of the accident victims. Then the loss of expected lifetime earnings were estimated, had the victim not been injured. In this way for the various injuries within NASS "costs" values became available, the so-called Injury Priority Rating (IPR). The analysis presented in Ref. [9] dealt with the NASS data for 1980 and 1981. IPR's per injury were summed per body region. Results for each body region were expressed as a percentage of the total "costs" for all body regions (Table 3.5). Clearly the importance of head, face and neck injuries is illustrated: together more than 60%.

Table 3.5 IPR Distribution by body region [9].

Body Region	Distribution (%)
Head	44.6
Face	10.5
Neck	5.1
Shoulder	0.3
Chest	18.9
Back	1.6
Abdomen	7.5
Pelvis	1.1
Thigh	2.1
Knee	1.6
Lower leg	1.0
Ankle/Foot	0.6
Lower Limb	0.0
Upper Arm	1.3
Elbow	0.5
Forearm	1.3
Wrist/Hand	0.4
Upper Limb	0.3
Whole Body	0.9
Unknown	0.2
TOTAL	100.0

Since the NASS injury surveillance system only takes into account tow away motor vehicle accidents the IPR information only applies to occupants of motor vehicles. So lower leg injuries e.g. are underrepresented compared to the all over traffic accident situation. The last scale to be discussed here, i.e. the Injury Cost Scale (ICS) [10], is more general in this respect since it also considers other road user categories. Moreover the ICS is based on actual cost figures rather than estimates like the IPR.

The ICS is based on an analysis of data on road accidents of the working population in Germany, available in a data base of the German Workman's Compensation (an insurance type of data base). The analysis concerns accidents in 1985 with 1026 traffic fatalities and 15.407 injured persons. For each type of injury the average costs were determined taking into account costs of medical treatment and rehabilitation, loss of income, disability benefits etc. Also the societal costs due to a fatality were estimated. This analysis resulted in two injury cost scales: the ICS and the ICSL. The difference between both scales is that the

ICS only considers injured persons while the ICSL (Injury Cost Scale Lethal) also takes fatalities into account. For example: the costs of a Contusio Cerebri are 129.000 DM according to the ICS scale and 288.000 DM according to the ICSL scale. For a cervical spine fracture these numbers are 217.000 DM (ICS) and 464.000 DM (ICSL), respectively.

Apart from the costs per injury type in this study also the frequency of injuries was taken into account. An "expensive" injury type with a very low frequency is, from the societal point of view, less relevant than an injury with lower costs and a high frequency. By multiplication of frequency and costs a ranking of the various injuries in the data base was obtained. Table 3.6 shows the 10 most cost-intensive injuries according to the ICSL scale. The most expensive injury is the contusio cerebri followed by a closed fracture of the upper leg/hip joint/pelvis.

Table 3.6 *Most cost-intensive injuries arranged according to the resultant social costs of the sample (ICSL) [10].*

Injuries	Resultant social costs in million $
1. contusion cerebri	225
2. closed fracture of hip joint, pelvis or femur	120
3. spine fracture	98
4. closed tibia/fibula fracture	79
5. closed foot fracture	48
6. closed glenohumeral fracture	45
7. open tibia/fibula fracture	45
8. commotio cerebri	39
9. closed ulna/radius fracture	34
10. knee laceration	19

3.5 Injury risk function

This Section deals with probably the most important problem in injury biomechanics research: assessment of the correct relationship between injury severity and a mechanical load which causes this injury. It is a statistical problem which usually cannot be solved directly by analyzing accident data since the load parameters which are assumed to cause, or to correlate well with, the injury can not be measured during the accident. A few attempts varying from simple methods to assess the belt elongation in a crash to complicated crash recorders have not been introduced yet on a large scale. Moreover the information obtained from these methods is limited to parameters like the vehicle acceleration or the belt load.

Therefore laboratory experiments have to be conducted using human substitutes which allow extensive measurements to be made. For a number of reasons the transformation of the findings from these laboratory experiments to the real world however is not trivial, like:

- differences in biomechanical response between surrogates, (e.g. human cadavers, animals) and the living human body.
- the small number of tests and differences between the population of test subjects and the real world population of risk.
- large spread in test results due to, for instance, variations in test conditions and variations in anthropometry, age and sex of the subjects.
- the problem of finding the appropriate parameter(s), i.e. injury criteria which cause or correlate well with the injury sustained.
- the large number of injury mechanisms and resulting injuries that can occur etc.

Moreover injury biomechanical tests often are, what statisticians call, "censored". This means that the actual parameter (load) measured in the test is usually not the magnitude that exactly causes the injury. It is either too small if no injury occurs or too large in case of injury.

Let us consider a hypothetical experiment dealing with bone fractures. Fig. 3.5 illustrates the results of a set of n experiments. The outcome of the experiments are either a fracture or a non-fracture. For small loads all tests appear to result in a non-fracture. For medium level loads there is a transition zone where both fractures and non-fractures can be observed. In this zone clearly some randomness can be observed. Finally for high loads only fractures occur.

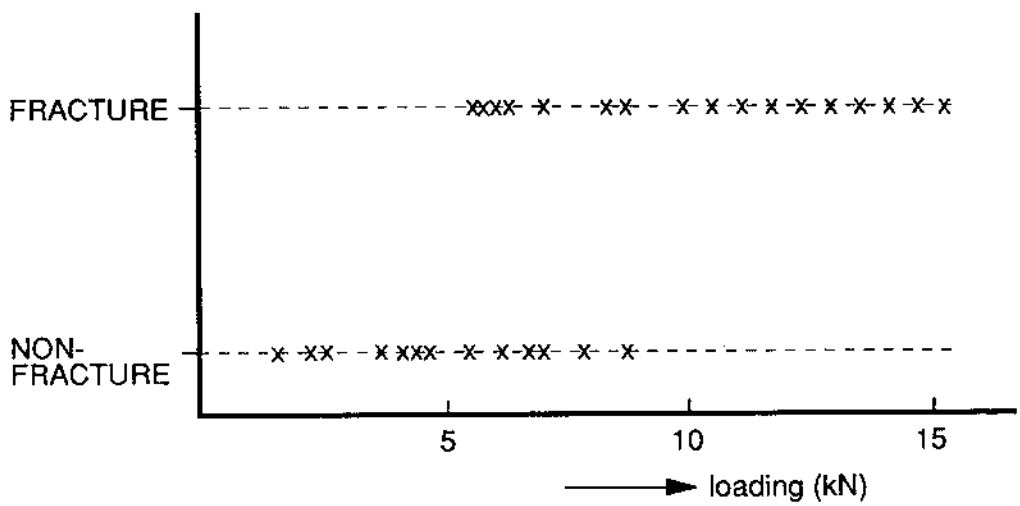

Fig. 3.5 A hypothetical example of a bone fracture experiment.

Statistical methods are available which can deal with this type of observations. One of the methods which has been recommended for this purpose is the so-called "Maximum Likeli-

hood Method", developed already in the twenties. Another method is "Probit analysis". Detailed treatment of such methods here would be out of the scope of this course, however some background information is considered useful for an engineer working in this field. For more details it is suggested to study Ref [11] and statistical handbooks dealing with probability and reliability analysis. We will concentrate here on the Maximum Likelihood Method.

Let us first introduce for the above example the so-called "cumulative frequency distribution" F(z), illustrated in Fig. 3.6. It can be interpreted as the probability, or risk, that a loading of the magnitude z would cause a fracture. It rises from zero to 100 % over the range of loadings. The objective of the statistical method is to find the best possible representation for F(z), i.e. to find a curve which best fits the experimental test series.

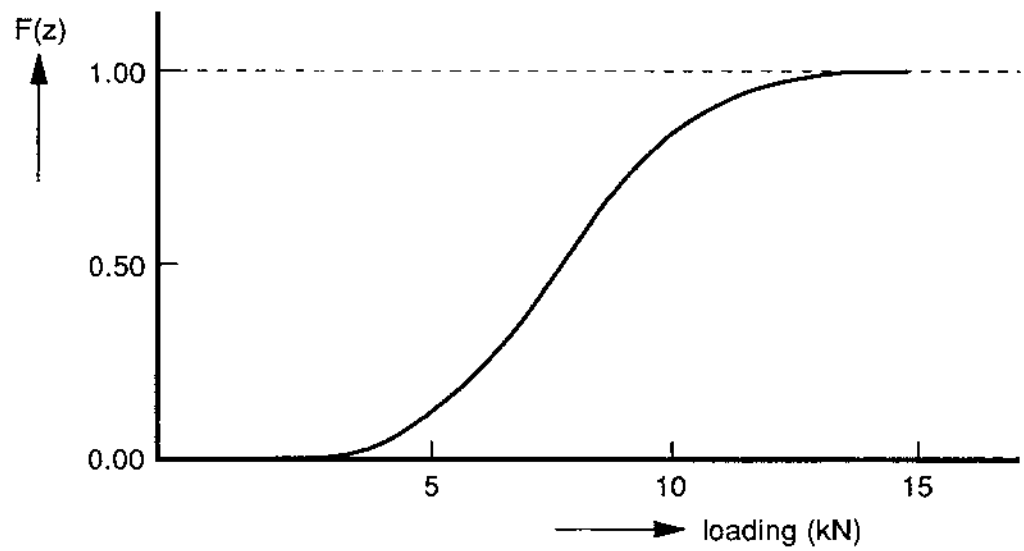

Fig. 3.6 *Cumulative frequency distribution: Risk for fracture as function of loading.*

The probability that, complementary, a non-fracture would occur at a given loading z is identical to (1 - F(z)). We will index now the non-fractures by i = 1, 2, ...p, where p is the total number of non-fractures, and the fractures by j = 1, 2,.....q, where q is the total number of fractures. Each test in our test series has had an occurrence probability which is $F(z_j)$ for a fracture and $1 - F(z_i)$ for a non-fracture. The likelihood, denoted by L, for all observations in this test series to occur is:

$$L = \prod_{j=1}^{q} F(z_j) \times \prod_{i=1}^{p} (1 - F(z_i)) \qquad (3.1)$$

where Π is the product sign. The Maximum Likelihood Method tries to find a distribution F(z) such that L gets a maximum value. The resulting F(z) is assumed to be the best model for the recorded observations. The candidate distributions F(z) should be selected from the

many S-shaped (sigmoid) functions that are available. Such distributions have a value close to 0 % for low values of z and close to 100 % for high values. A function that successfully has been applied in injury biomechanics research for this purpose is the Weibull cumulative distribution function, which has the form:

$$W(z, \alpha, \beta, \gamma) = 1 - e^{-((z-\gamma/\alpha)^{\beta}} \tag{3.2}$$

where:

α is the scale parameter (α>1)
β is the shape parameter (β > 1)
γ is the location parameter.

α, β and γ are parameters yet to be determined. Standard optimization routines can be applied, like available for instance in the software library NAG, to solve this optimization problem. Such routines allow additional constraints to be added in the search for a maximum of L, e.g. based on physical reasoning. Application of the Weibull function has shown to result often in higher likelihood values than other candidate distributions.

Assuming that the test sample is representative for the population of risk (which is however often not the case) and that the loading parameter is considered suitable to be used as an injury criterion, one might propose a tolerance level (or injury criteria level) from the resulting distribution for instance at the 25 or 50% risk level. In Chapter 4 an example of application of the Maximum Likelihood Method with a Weibull cumulative distribution function will be presented.

3.6 Whole body tolerance to impact

The term "whole body tolerance" originates from the earliest laboratory studies with human substitutes, in which the complete body was exposed to acceleration or impact type of loading. Results of such tests, together with information obtained from analysis of real accidents, like falls have contributed to a great extent to our present knowledge on the tolerance of the human body. The term "whole body response" was used, since in these tests the physiological response, which concerns the complete body, is evaluated. If injury occurred like in a rare accidental case with human volunteer tests or in tests with animals, actually one or more specific body parts like the head will be injured, rather than the "whole body".

In order to specify the direction of the load acting on the body first an orthogonal body fixed axis system (x,y,z) will be introduced. In most injury biomechanics literature the axis system shown in Fig. 3.7 is employed, although there are a few exceptions like the axis system recommended by a Committee of the Society of Automotive Engineers (SAE) for use in mechanical human substitutes [12]. Throughout this course we will adopt the axis

system in Fig. 3.7. The positive x-axis is forward (anterior direction), the z-axis upwards (superior) and the y-axis to the left. The axis system proposed by SAE is rotated 180 degrees about the y-axis, in other words the positive z-axis is directed downward.

The direction of a load vector acting on the human body is usually denoted as plus (+) or minus (-) G_i, where the subscript i refers to the coordinate axis. For example in a $-G_X$ impact, the load vector acts from front to back on the body, causing the body to accelerate in backward direction. In air force crash-safety literature often the motion of the eyeballs relative to the human body is used to define the impact direction. A $-G_X$ impact is defined in this literature as "eyeballs out", a $+G_X$ as "eyeball in", a $+G_Z$ as "eyeball down" etc. According to these definitions, a normal seated occupant (i.e. forward facing), which is exposed to a pure frontal impact in a motor vehicle will experience the equivalent of a $-G_X$ impact.

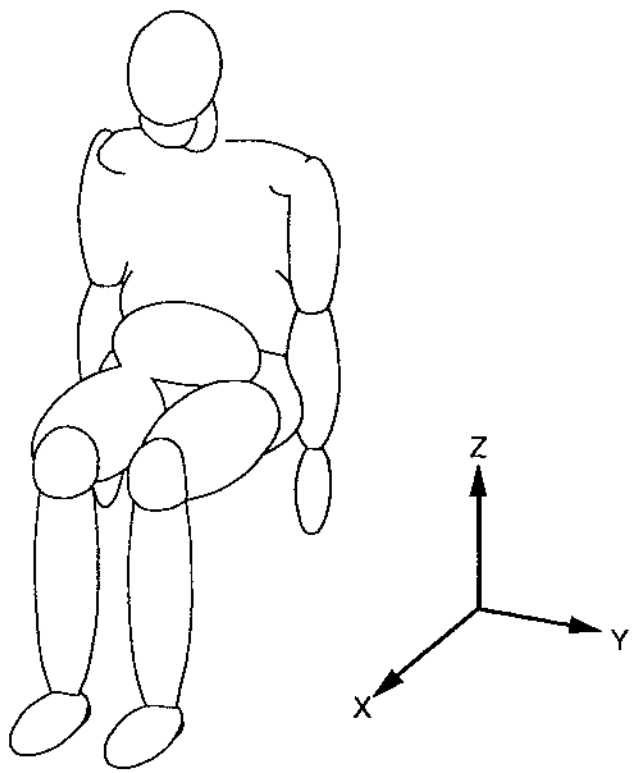

Fig. 3.7 *Human body with coordinate system.*

The earliest studies of the effects of impact loads on the human body are primarily from the field of aviation and aerospace medical impact research. They were initiated from the need to study the levels of acceleration pilots can sustain during high speed manoeuvres or in case of ejection from the aircraft in case of an emergency. Particularly the increase in aircraft accidents during the second world war stimulated the research in crash injuries. To

study tolerance against long duration accelerations, tests with human volunteers in centrifuges were widely conducted. The "injury" in such tests usually took the form of unconsciousness due to decreased blood flow to the brain [13].

For short duration impacts swing type of impact devices or deceleration sleds were used. Well known are the rocket sled test with human volunteers and animals conducted by Stapp at the Aeromedical Research Laboratory at Holloman Airforce Base in New Mexico (USA), where thousands of tests have been conducted [14].

The earlier experiments with volunteers have shown that a $+G_x$ impact, where the body is accelerated in forward direction, is the most survivable one of the principal directions, provided that the body and the head are fully supported. This is mainly due to the fact that the load on the body very well can be distributed under this condition over a large surface. The most severe impact reported for a human volunteer (with reversible injuries), occurred in such a configuration. In this test an acceleration of 82.6 G was recorded at the sternum and 40.6 g at the sled for about 40ms. The subject complained of severe lower back pain and lost consciousness 10 seconds after the test. He was hospitalized for 3 days to recover from headache and backpain [13]. It should be realized that the measurement technology in these early days was still rather primitive and consequently less accurate than what is possible today.

Numerous of above types of tests have been documented extensively in literature. Several studies have attempted to bring together these data, where the most important ones are Eiband in 1959 [15] and Snyder in the early seventies [14]. Two figures which summarize some of the findings will be presented here. Fig. 3.8 shows a graph originally developed by Roth in 1967 and adapted by Snyder [14] which summarizes human impact experience as function of deceleration distance and impact velocity. Most of the data concern free fall situations. The free fall distance is included in the graph. Assuming constant deceleration over the stopping distance, the average acceleration as well as stopping time was calculated and included in the graph.

From this data an approximated survival limit of 175-200 G was estimated. This limit should be used with much caution due to the various assumptions made. Moreover it is a survival limit which means that below this limit serious injuries can occur.

Fig. 3.9 is from Eiband [15] who summarized human and animal impact experience for various impact directions. Injury occurrence is presented as function of mean acceleration level and duration of this acceleration in case of $+G_x$ impacts. Three categories are shown: voluntary human exposure, moderate injury and severe injury.

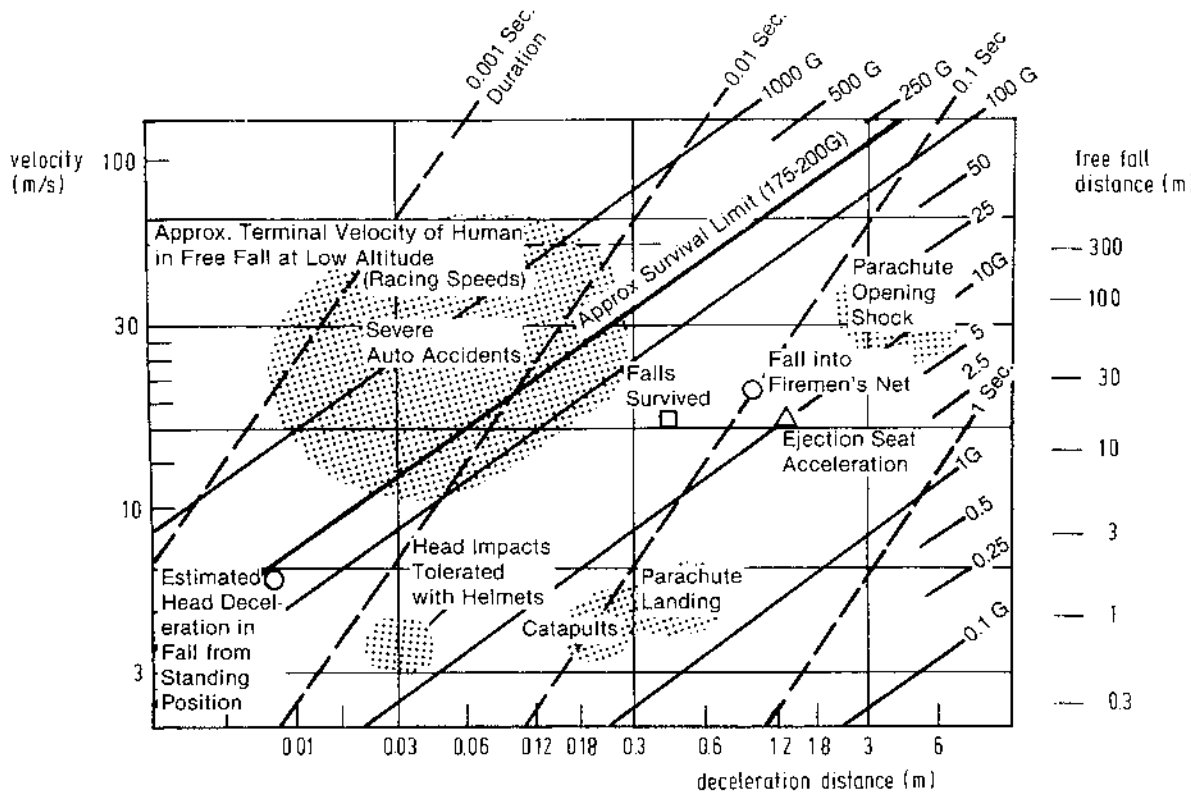

Fig. 3.8 *Impact experience from several sources [14].*

The most interesting finding from this figure is that the tolerance decreases with increasing pulse duration. The limit of voluntary exposure is about 40 G. Also such values should be handled with much caution since many factors will affect the actual tolerance like the restraint system used, the shape of the acceleration pulse applied and the individual condition of the subject.

For $-G_X$, $+G_X$ and $-G_Z$ impacts similar graphs were prepared by Eiband. The tolerance in $-G_X$ impacts was found to be from the same order of magnitude. For z-direction impacts the tolerable levels were found to be lower, in particular the level of voluntary exposure (about 15 G in case of $+G_Z$ and 10 G for $-G_Z$). Tolerance in $-G_Z$ impacts has had very limited study since the human body is hardly exposed to accidents in this loading direction.

Also in lateral direction (G_Y) much less data appear to be available. Impact tolerances in this direction are reported to be much lower than in G_X or $+G_Z$ direction [13].

The whole body response data presented here represents the basis of the current knowledge on tolerance values for thorax and head. In the next Chapters we will address in detail head injury tolerances, neck injury tolerances and thoracic injury tolerances.

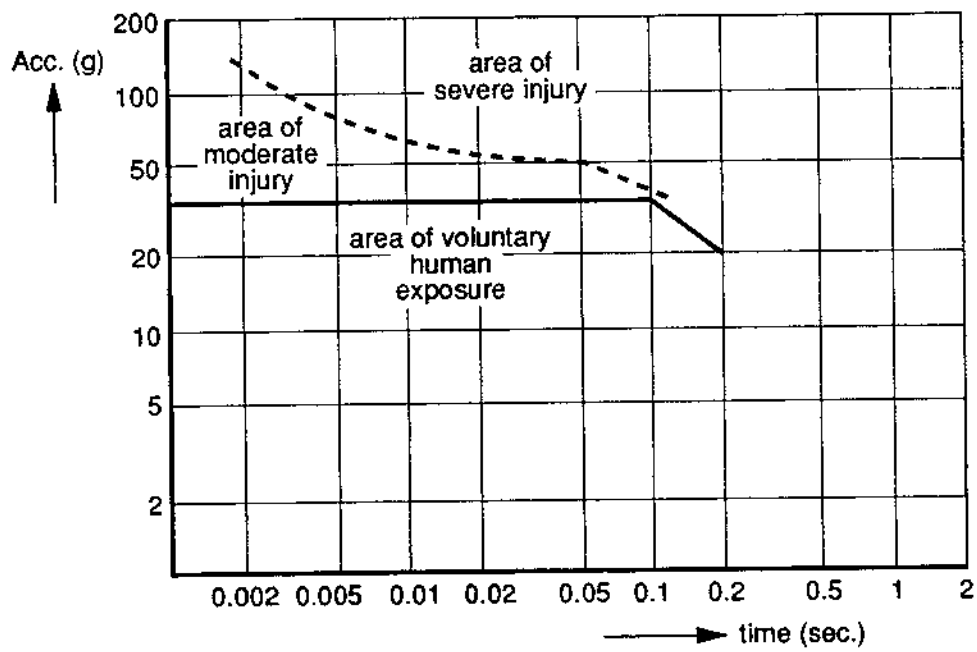

Fig. 3.9 *Summary of impact experience in $+G_x$ impacts as function of mean acceleration and pulse duration (after Eiband in [13]).*

REFERENCES

1. Viano, C., King, A.I., Melvin, J.W. and K. Weber: "Injury Biomechanics Research: an essential Element in the Prevention of Trauma". J. Biomechanics Vol. 22, No. 5, pp 403-417, 1989.

2. Committee on Trauma Research, Commission on Life Sciences, National Research Council and the Institute of Medicine: "Injury in America. A continuing Public Health Problem". National Academy Press, Washington , 1985.

3. Aldman, B., Mellander, H. and M. Mackay: "The structure of the European research into the biomechanics of impacts". Proceedings of the 27th Stapp Car Crash Conference, San Diego, SAE paper 831610, Soc. of Automotive Engineers, Inc., 1983.

4. "The Abbreviated Injury Scale - 1990 revision": Association for the Advancement of Automotive Medicine, 2340 Des Plaines River Road, Suite 106, Des Plaines, Il 60018, USA, 1990.

5. Pike, J.A.: "Automotive Safety". Society of Automotive Engineers, Inc., 400 Commonwealth Drive, Warrendale, PA 15096-0001, USA, 1990.

6. Malliaris, A.C. et. al.: "Harm Causation and ranking in car crashes". SAE paper 85090, Society of Automotive Engineers, Inc., 400 Commonwealth Drive, Warrendale, PA 15096-0001, USA, 1985.

7. "Lateral Car Collisions": Report R-79-48, Institute for Road Safety Research, SWOV, The Netherlands, 1979.

8. Baker, S.P. and B.O. O'Neill: "The injury severity score: an update". J. of Trauma 11, pp. 882-885, 1976.

9. Carsten, O. and J. Day: "Injury priority analysis". Task A in: Technical report DOT HS 807 224, February 1988, U.S. Department of Transportation National Highway Traffic Safety Administration (NHTSA) Washington, D.C. 20590.

10. Zeidler F., Pletschen B., Mattern R., Alt B., Miksch T., Eichendorf W., Reiss S., "Development of a New Injury Cost Scale", 33rd Annual Proceedings, Association for the Advancement of Automotive Medicine, 1989.

11. Ran, A., Koch, M. and H. Mellander: "Fitting injury versus exposure data into a risk function". International IRCOBI conference, Delft 1984.

12. "Instrumentation for impact test". SAE Recommended Practise, SAE J211 OCT88, 1988.

13. McElhaney, J.H., Roberts, V.L. and J.F. Hilyard: "Handbook of human tolerance". Japan Automobile Research Institute, Inc. JARI, 1976.

14. Snyder, R.G.: "Human impact tolerance". Paper 700398, In: 1970 International Automobile Safety Conference Compendium. Society of Automotive Engineers, Warrendale, PA, 1970.

15. Eiband, A.M.: "Human tolerance to rapidly applied accelerations - A summary of the literature". NASA Memo-5-19-59E, 1959.

16. "Human Tolerance to Impact Conditions as related to Motor Vehicle Design". SAE information report J885 JUL86, Society of Automotive Engineers, Warrendale, PA, 1991.

CHAPTER 4

HEAD INJURY BIOMECHANICS

4.1 Introduction

The head and spine of the human body are considered the most critical body parts injured in crash situations because of the often irreversible nature of injuries to the central nervous system. In this course, the head and spine are dealt with separately, mainly because of differences in anatomical structure and different mechanical behaviour under impact. The biomechanics of injuries to the spinal column will be discussed in chapter 5. This chapter deals with head injury biomechanics.

Despite development of injury protection measures (belt, air bag, helmet), and increase of governmental regulations, still about 40% of serious brain injury accidents is due to traffic-related causes [96]. The results of a typical study into the incidence and outcome of brain injury in traffic accidents are shown in table 4.1. In this study, about one third of the victims suffered from permanent disability. By the 1980's the average life-expectancy of these patients was 35 years [42]. These figures illustrate the consequences of traumatic brain injury, both in terms of loss of quality of life of the patient and his family, and in terms of health-care economic costs.

To quantify these economic and social costs, injury cost scales were introduced in the previous chapter. There it was shown that in terms of the Injury Priority Rating (IPR), injuries to head and face accounted for about 55% of the costs for all body regions. According to the Injury Cost Scale Lethal (ICL) the head injury 'contusion cerebri' was the most expensive injury.

In this chapter, first the anatomy of the head will be discussed in section 4.2, showing the most important parts of the head that can be injured in a crash. In the next sections, from 4.3 to 4.5, the problem of head injury will be dealt with using the load-injury model, introduced in the previous chapter. Types of head injury and their clinical relevance are presented in section 4.3. The mechanical loads, causing the injury, will be discussed in section 4.4. Current thoughts about head injury mechanisms are presented in section 4.5. Head injury criteria and tolerances are discussed in section 4.6.

Table 4.1: *Results of a study [97], evaluating incidence and outcome of brain injury in the Stockholm area (population 1.8 million). From 1981–1992, 1812 patients were hospitalized (84 per million per year), of whom 695 were injured in traffic accidents (32 per million per year). Numbers refer to percentages in the latter group.*

distribution of primary injury		level of consciousness		final outcome	
brain contusion	61.6	deep coma	25.3	brain dead	21.0
extracerebral hematoma	16.4	severe injury,		continuous care	
commotio	11.2	comatose	39.6	required	11.5
fractures	8.1	moderate		return to previous	
intracerebral hematoma	2.7	injury	35.1	occupation	67.5

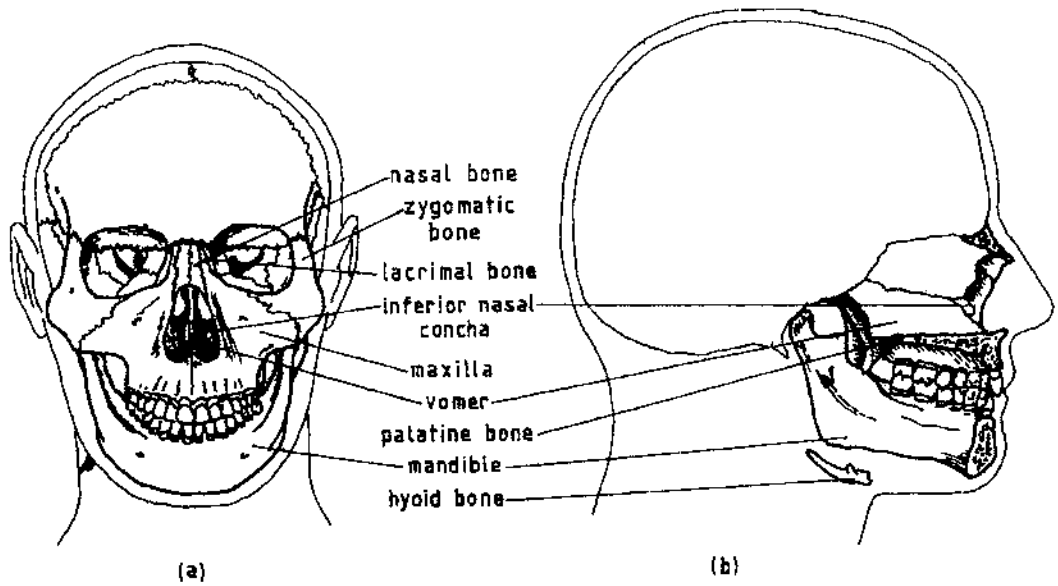

Figure 4.1: *The facial cranium in frontal (a) and medial (b) view [92].*

In the next sections, from 4.7 to 4.9, some material of the first sections is elaborated into more detail. First, in section 4.7 the failure of the intracranial contents at cellular level is discussed. The next two sections focus on assessment of local mechanical brain response, either by experiments (4.8), or by numerical models (4.9). The chapter is concluded with a discussion.

4.2 Anatomy

To facilitate the discussion on the mechanics of head injuries and for reasons of classification of these injuries, the head is divided into two parts:

- The *face*: defined as the front part of the head (from the forehead to the lower jaw, including the outer part of the ears), comprising the facial cranium, its skin, muscles (the socalled muscles of facial expression), the blood vessels to the facial structures and the facial nerves.
- The *head*: defined as the center and rear part of the head, comprising the neurocranium, its skin covering (the scalp) and its contents : the brain and meninges. This part of the body part 'head' has the same name, however, this is thought not to cause confusion here.

Clinical classification of injuries, in most cases, is based on anatomical structures and body parts [1]. Distinction is made between bony structures and soft tissues. The anatomy of the face and head is presented in sections 4.2.1 and 4.2.2 respectively, using this distinction.

4.2.1 Anatomy of the face

The *facial cranium* (facial skull/viscero-cranium) consists of 14 bones, of which 13 are relatively flat (approximately 5 mm in thickness) and fused together through complete

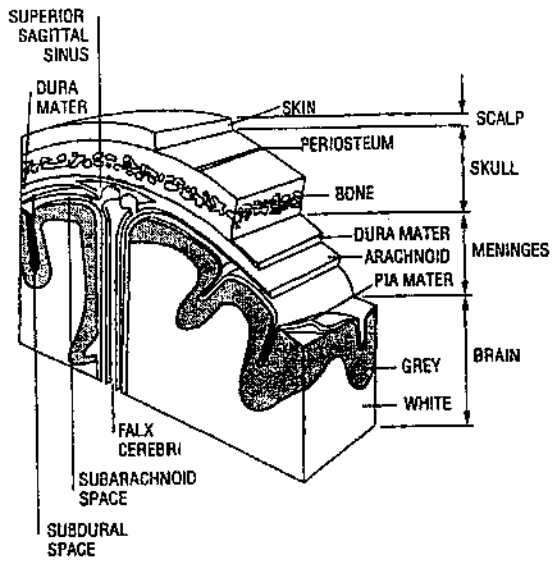

Figure 4.2: *The scalp, skull, meninges and brain [68].*

sutures. The one exception is the mandible which is a rather thick bone and, as only bone of the skull, connected to the skull (in fact to the temporal bones; see section 4.2.2) by free movable joints: the 'temporomandibular joints' at the base of the skull.

Because of the flat and irregular shape of the facial bones, the facial cranium contains vaults e.g. for the eyes, nose and mouth. The facial bones are frequently hollow and are provided with openings for vessels or nerves. Figure 4.1 shows the facial cranium in frontal and medial view.

The facial skull is covered with relatively thin *skin and muscles* that allow for movement about the nasal, orbital and mouth openings. Other soft tissues of the face are the eyes, tongue, various blood vessels (e.g. the external carotid artery), nerves (e.g. the optic nerve) and cartilages and ligaments (e.g. external parts of the ears and nose and the temporomandibular joints).

4.2.2 Anatomy of the head

The various features of the head's anatomy are described here in order from the outer surface to the internal structures. In doing this, we come across the scalp, the skull (neuro-cranium), the meninges (including cerebrospinal fluid) and the central nervous system (brain). Figure 4.2 shows these layers.

Scalp

The outer surface of the neuro-cranium is covered by the *scalp*. This structure of soft tissue, about 5 to 7 mm thick, is build up of 5 layers which, from the outside to the inside, are:

- (hair bearing) *skin* which includes the superficial epidermis and the dermis,
- *connective tissue*,

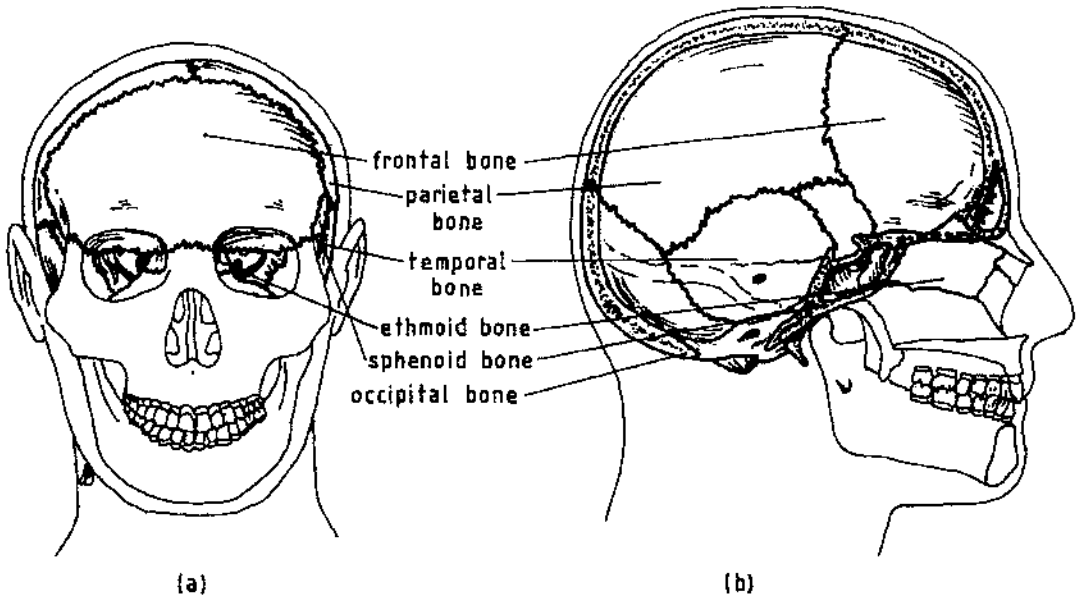

Figure 4.3: *The neuro-cranium in frontal (a) and medial (b) view [92].*

- *aponeurosis*, a strong membraneous sheath preventing superficial cuts to extend,
- *loose connective tissue*, and
- *periosteum* which contacts the bony skull.

Note that the first characters of these layers form the word *'scalp'*. In case traction force is applied to the scalp, the outer three layers move together as one. Avulsions (tearing of tissue) therefore usually take place at the level of the loose connective tissue. The periosteum, a fibrous membrane, directly covers the skull.

Skull

The neuro-cranium (that part of the skull covering the brain) consists of 8 bones (4 to 7 mm thick) and provide reinforcement of the cranial vault or calvarium. The cranial vault is thus formed by:

- the frontal bone,
- two parietal bones,
- two temporal bones,
- the occipital bone,
- the sphenoid bone, and
- the ethmoid bone.

The latter 2 bones also form the facial structure. Figure 4.3 shows the neuro-cranium in frontal and medial view.

The large cranial bones have a sandwich-like construction: dense bone at the outer and inner surface, held together by spongeous bone in the middle. The base of the cranial vault is a thick and irregular plate of bone, containing small holes for arteries, veins and nerves as well as a large hole - the *foramen magnum* - through which the spinal cord enters into the brain.

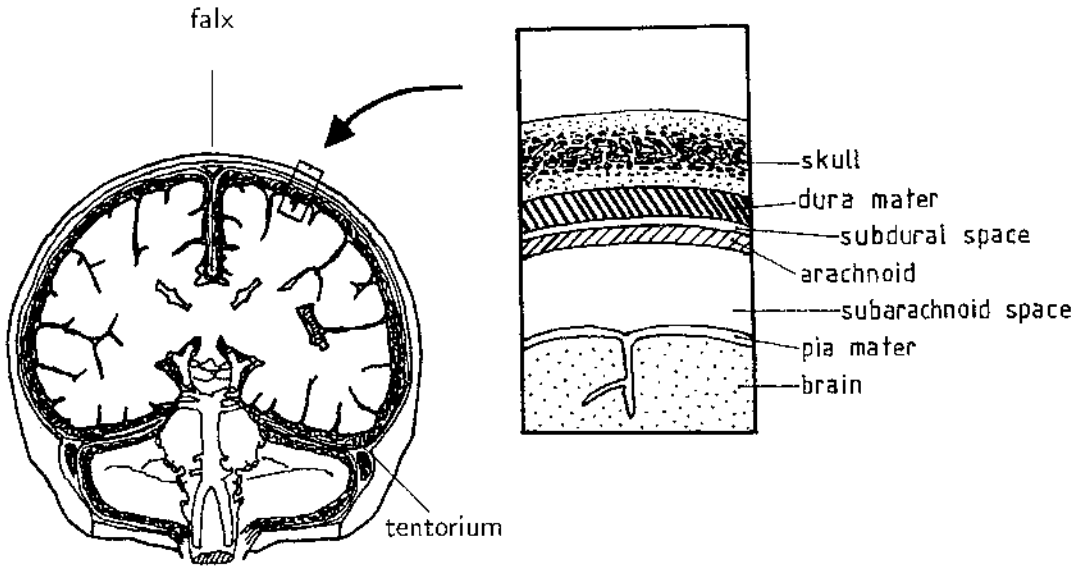

Figure 4.4: *The meninges of the brain [68].*

Meninges

Further inwards - between the neuro-cranium and the brain - we cross three membranes protecting and supporting the brain and the spinal cord: the *meninges*. These meninges separate the brain and spinal cord from the surrounding bones. From the outside to the inside we find:

- the *dura mater*: a tough fibrous membrane that surrounds the spinal cord and, in the skull, is divided into two layers: the outer cranial (periosteal) layer of dura mater lines the inner body surface of the cranial vault, while the inner (meningeal) layer covers the brain. The two layers of dura mater are fused except where they separate and form sub-structures, e.g. at the *falx cerebri*, in between the right and left cerebrum, the *falx cerebelli*, in between the right and left cerebellum, and the *tentorium*, in between the cerebri and cerebelli (see figure 4.2). These structures are thought to prevent large brain displacements.
- the *arachnoid*: a spider-web-like membrane, separated from the dura mater by a narrow subdural space. This space is filled with a thin film of watery fluid: the *cerebrospinal fluid* (CSF).
- the *pia mater*: a thin membrane of fine connective tissue invested with numerous small blood vessels. This membrane covers the surface of the brain, well into its fissures (see figure 4.2). The pia mater is separated from the arachnoid by the subarachnoid space, also filled with CSF.

Figure 4.4 shows the position of the meninges relative to the skull, brain and each other, separated by the subdural and subarachnoid spaces.

The brain (and spinal cord) is surrounded with ca. 140 ml of CSF. This fluid cushions the brain from mechanical shock and, during normal movement, shrinking and expansion of the brain is quickly balanced by an increase or decrease of CSF that

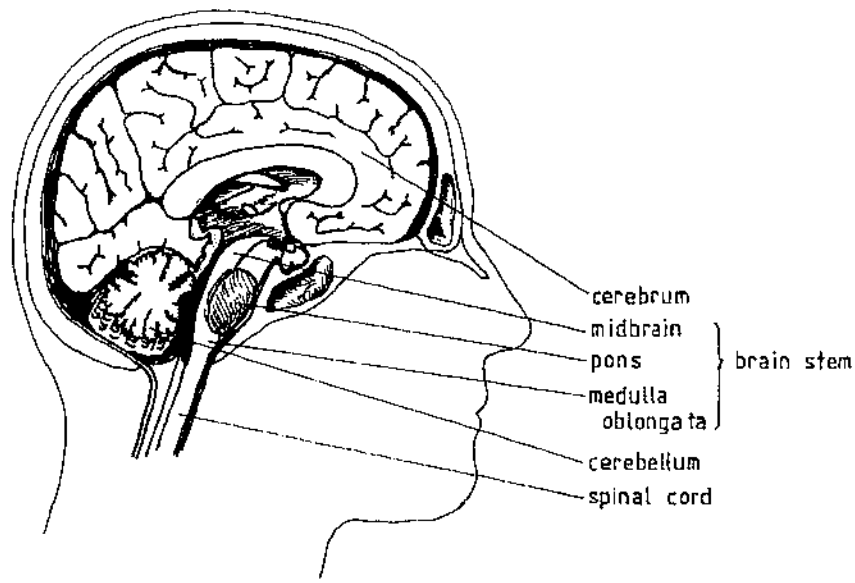

Figure 4.5: *The head in sagittal section: principal parts of the brain.*

can flow from the cranial cavity into the spinal cavity through the foramen magnum.

Brain

To the centre of the head we come to the *brain*. The brain (and spinal cord) is largely a network of neurons and supportive tissue, functionally arranged into areas that are gray or white in color and have different densities. *Gray matter* is composed primarily of nerve cell bodies, *neurons*, concentrated in locations on the surface of the brain and deep within the brain; *white matter* is composed of myelinated nerve cells processes, *axons*, that largely form tracks to connect parts of the central nervous system to each other.

Average anterior-posterior length of the brain is about 165 mm and its greatest transverse diameter is about 140 mm. The average weight is 1.36 kg for the adult male (ca. 2% of the total weight of the body) and a little less for the female [69].

The brain can be divided structurally and functionally into five parts:

- *cerebrum*: divided into right and left cerebral hemispheres which are at the centre of the head connected by a mass of white matter called *corpus callosum*. Each cerebral hemisphere has a surface layer of gray matter called the cerebral cortex (see figure 4.2). The cortex is arranged into a number of folds separated by fissures. These fissures further separate the cerebral hemispheres into four lobes, named by its association to the nearest cranial bone: frontal, parietal, temporal and occipital lobes.
- *brainstem*, consisting of the:
  - *midbrain*: connects to the cerebral hemispheres above and the pons below (mainly fibers passing to and from the cerebral hemispheres above).
  - *pons*: mostly composed of white matter nerve fibers passing to and from the

spinal cord.

- *medulla oblongata*: connects the pons above and the spinal cord below. In the lower part of the medulla oblongata (mostly white matter), motor fibers and some sensory fibers cross from one side to the other.

- *cerebellum*: lying behind the brain stem and consists of two hemispheres, joined by the vermis. The outer cortex of the cerebellar hemispheres consists of gray matter, the inner cortex is white matter. The outer surface of the cerebellum form into narrow folds separated by deep fissures.

Figure 4.5 shows the head in sagittal section, showing the principal parts of the brain.

4.3 Head injuries and their clinical relevance

As is obvious from the anatomy of the head, various types of injuries may occur to the head. Important for this course is to identify those head injuries which have clinical relevance, either by their incidence and/or by their severity. In this section, severity of head injury is chosen as starting point to discuss the most important types of head injury.

Several scales exist to quantify the severity of head injury [46, 11] caused by mechanical load. One of these is the Abbreviated Injury Scale (AIS), discussed in chapter 3. As is done in section 4.2, the AIS divides the head into a facial and a cranial part. For each of these parts, the AIS considers injuries to the 'whole area', 'vessels', 'nerves', 'internal organs' and 'skeleton', and assigns a value to injury to these structures according to the threat to life (ranging from 1 to 6). Note: various types of injuries may occur to these structures, such as abrasions, avulsions, fractures, contusions, lacerations, etc.. Table 4.2 gives the AIS classification of injuries to various structures of the head and face. The numbers between brackets indicate the range of AIS severity for injuries to that specific structure.

From this table it appears that injuries to the skull and brain are the most severe head injuries. These injuries will be discussed here for the face (only skull; section 4.3.1) and the head (section 4.3.2).

4.3.1 Facial injuries

For a long period of time, research in automotive industry on the face merely concerned the facial skull. Reason for this is that in case of contact impact to the face, brain injury may occur, depending on the response of both the brain and the face. Today, however, also attention is given to lower severity facial injuries, because of their high incidence and associated overall costs. Here, we will concentrate on higher severity injuries only (AIS 3 or above).

As shown in table 4.2 specific fractures at the maxilla are considered severe (up to AIS 4). These fractures are known as 'LeFort fractures' of which three different types are known [49]. Other serious facial injuries are open, displaced or comminuted fractures close to the orbit (AIS 3). Figure 4.6 shows the LeFort classification of maxillary fractures.

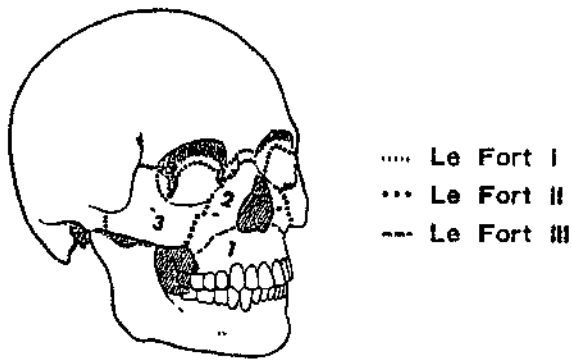

Figure 4.6: *LeFort classification of maxillary fractures [49].*

4.3.2 Head injuries

Most important injuries to the head are those to the skull (neuro-cranium) and the brain (including the meninges). Injuries to the scalp, although quite common in impact situations, are considered to be of minor importance. Severe injuries to the scalp concern avulsions of large areas of the head accompanied with heavy blood loss but these are rarely seen in impact or accompanied by other serious injuries to the head. Injuries to the scalp are not further discussed here.

Skull fractures

Fractures to the neuro-cranium are divided into basilar skull fractures and vault fractures (fractures to the non-base part of the skull). Skull fractures by themselves are not considered life threatening [1] but the type of fracture may include (severe) damage to soft tissues of the head.

- *Basilar fractures* are considered clinically significant because the dura may be torn adjacent to the fracture site and thus the probability of contamination of the central nervous system is highly increased. Problem with determining the relevance of basal fractures is that this type of injury is hard to be seen during clinical examination and difficult to visualize radio-graphically. Under-report of basilar fractures thus seems very likely.
- *Vault fractures* are divided into linear and depressed fractures:
  - *Linear fracture* (no bone displacement) is considered not severe (Maximum AIS 2) and does not have much significance on the course of brain injury, although this subject is still controversial. Examination of 434 patients showed similar incidence of linear fracture across all severities of brain injuries (AIS 1-6) [25] and this finding was supported in other studies (Cooper in [69, 12]).
  - *Depressed fracture* - fracture of the skull with bone displacement - is likely to be associated with neural injury and/or intracranial hematoma, especially when the depression is deeper than the thickness of the skull [69].

Table 4.2: *AIS classification of head injuries [1].*

	whole area	vessels	nerves	internal organs	skeletal
head	crush (6) scalp (1-3)	various (3-5)	cranial nerve I-XII (2)	brain stem (5-6) cerebellum (3-5) cerebrum (3-5)	base (3- 4) vault (2-4)
face	facial skin (1-3)	ext. carotid artery (1-3)	optic (1-2)	ear (1) eye (1-2) mouth (1) gingiva (1) tongue (1-2)	alveolar ridge (2) mandible (1-2) maxilla (1-4) nose (1-2) orbit (2-3) teeth (1) t.m. joint (1-2) zygoma (2)

Focal Brain Injury

Various types of brain injury may occur due to impact. Generally two categories are distinguished, based on their clinical appearance: *focal injury* and *diffuse injury*. Principally, the AIS classification is based on anatomical injury. But, by adding a scale based on 'loss of consciousness', a more detailed classification of brain injury is possible with the AIS. Loss of consciousness will be shown to be an important physiological parameter to assess injury severity.

Focal brain injuries are those in which a lesion has occurred large enough to be visualized without special equipment (provided an autopsy would be possible), and thus always include anatomical damage. In this case brain dysfunction occurs due to local brain damage and/or the presence of masses within the cranium, causing brain shift, herniation and possible brain stem compression. Focal brain injuries account for approximately 50% of all patients admitted to hospitals and are responsible for 2/3 of head injury deaths. Four types of focal brain injuries are distinguished:

- *Epidural hematoma* (EDH) concerns the meningal vessels directly underneath the skull. EDH is infrequently seen and the mortality rate of this type of injury merely depends on associated injuries rather than the EDH itself. Because of its low incidence, this type of brain injury is considered of minor clinical relevance.
- *Subdural hematoma* (SDH) of which the acute form (ASDH) is the most severe. The most important cause for ASDH is tearing of the bridging veins and arteries between the brain's surface and dural sinuses (thus crossing the subdural space). This type of brain injury is of high clinical relevance, especially because of the poor outcome: the mortality rate reported in most studies exceeds 35% and in some studies even 50%.
- *Cortical contusion*, the most frequently found trauma following head impact, consists of a mixture of vascular and brain damage. It occurs at the site of impact (coup contusion) or at remote sites of the impact (contre-coup contusion). Contre-coup contusions are considered more significant than coup-contusions [69]. Contu-

Table 4.3: *Important types of head injury and their clinical relevance [12].*

	skull injuries	focal injuries	diffuse brain injuries
	vault fractures	epidural hematoma	mild concussion
	linear	subdural hematoma	classical cerebral concussion
	depressed	contusion	diffuse injury
	basilar fracture	ICH	shearing injury (DAI)
hospitalization		50 %	40 %
deaths		2/3	1/3
disability		+	++

sions most often are multiple and are frequently associated with other lesions like SDH, EDH and especially skull fracture (estimated association: 60-80%). Mortality rates reported for this type of injury range from 25% to 60% with a tendency to increase with increasing age.

- *Intracerebral hematoma* (ICH) includes homogeneous collections of blood within the brain and is distinguished from contusions by a more pronounced localization of the hematoma (visualized by CT-scan). Usually ICH begins superficially and extends well into the white matter. Mortality rates reported differ a lot (6% to 72%) and survivable outcome is considerably affected by the presence or absence of loss of consciousness.

Diffuse Brain Injury

Diffuse brain injuries are associated with widespread brain damage. They account for about 40% of head injury patients admitted to hospitals and comprises about 1/3 of the deaths. We distinguish between two main types [26, 27]:

- *Cerebral concussion*, a transient neurological dysfunction, which has two subtypes:
  - *Mild concussion*, resulting in confusion, disorientation and/or minor loss of memory. This type of injury does not involve loss of consciousness, and is completely reversible.
  - *Classical cerebral concussion*, that involves temporary loss of consciousness which lasts less than 24 hours and is reversible. The clinical outcome of the patient with this trauma depends on the associated injury, such as brain contusions, basilar fracture or depressed fracture. The classification *commotio cerebri* is used in cases where loss of consciousness lasts less than 15 minutes.
- *Diffuse Axonal Injury* (DAI) or *Diffuse White Matter Shearing Injury* (DWSI) is a form of diffuse brain injury with prolonged loss of consciousness (more than 24 hours) and brainstem dysfunction. This type of brain injury involves considerable anatomical disruption (shearing) of white matter fibers and only 30% of the cases have good to complete recovery.

As a summary, table 4.3 indicates the relative importance of various types of head injury according to hospitalization, fatal outcome and disability after sustaining these injuries.

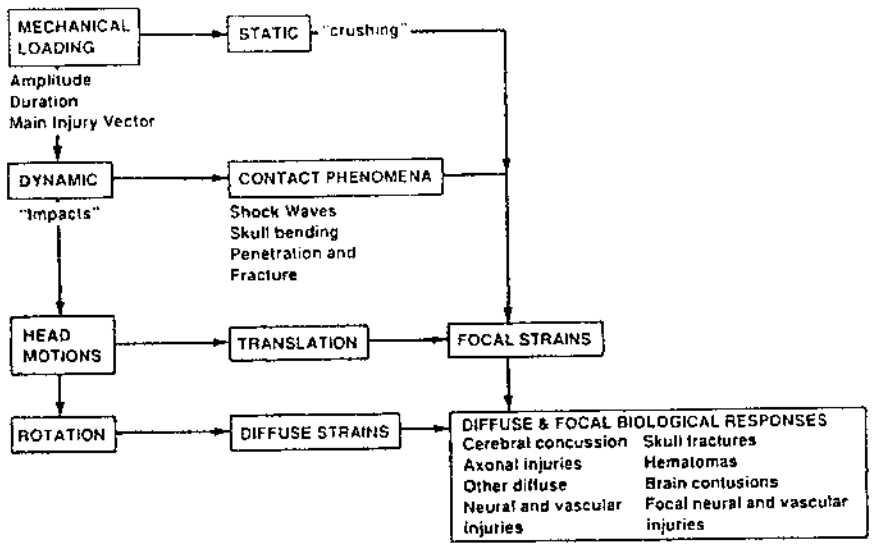

Figure 4.7: *Relation between external head load and local tissue response (adapted from [64]).*

4.4 External head loads and internal mechanical response

In this section, a rather qualitative description of external head load and internal mechanical response is given, which is summarized in figure 4.7. A more detailed discussion about assessment of local brain load is presented in sections 4.8 and 4.9.

4.4.1 Static and dynamic load

Dependent on the time duration of the load, *static* and *dynamic* load is distinguished. Generally a load is considered static if it lasts longer than 200 ms although this distinction is rather arbitrary. A (quasi-) static head load is also a focal load: it acts on a limited part of the head. Thus it induces focal strains in the skull and the brain. Dynamic load, the most frequently occurring type of mechanical load to the human body in accidents, usually lasts in the order of a few ms to 50 ms.

4.4.2 Contact and inertial load

The dynamic load may result from contact of the head with its environment (e.g. impact on the steering wheel), or from a force transmitted to the head through the neck (e.g. when the torso is restrained by a belt). These cases are referred to as *contact* and *inertial* load, respectively.

In the contact case, several *contact phenomena* occur:

- at the impact site, local strains are induced in skull and brain;
- dependent on the duration of the impact, (longitudinal, transverse, or surface) strain waves are induced in skull and brain; focusing of these waves may lead to strain concentrations at locations, distant from the impact site;

- inbending and subsequent snap-back of the skull at the impact site may serve as a source of pressure waves in the brain

In the inertial case, the head is loaded only because of its inertial properties. These *inertial phenomena* also occur in the contact case, if the total momentum provided by the contact is large enough. If the skull is accelerated, either by a contact with its environment or through the neck, the brain will lag behind because of its inertial properties.

4.4.3 Translational and rotational inertial load

In case of a *translational* (or linear) acceleration of the skull, the brain is compressed at one side of the skull. At this side, the brain experiences compressive strains, resulting in a positive pressure. At the opposite site, the brain will experience tensile strains, either through direct connections between brain and skull, or through a pressure decrease in the subdural space. These tensile strains are reflected in a negative pressure. This pressure distribution is known as the *coup contre-coup effect.*

In case of a *rotational* acceleration, there is a tendency of the skull to rotate around the brain. Let us think of the brain as a sphere, surrounded by a spherical shell, representing the skull. Then, in the case of a rotational acceleration around the center of the sphere, the connecting elements between brain and skull, i.e. the bridging veins and the brain stem, would be stretched, and transmit the rotational load from the skull to the brain. Next, the load would be transmitted from the superficial layers towards the deeper layers of the brain, as a shear load between successive layers.

In the real head, the absence of spherical symmetry, and the presence of falx and tentorium limit the rotational freedom of the brain within the skull. Thus these factors have a protective function for the bridging veins and the brainstem, since they take over part of the rotational load transmission from skull to brain.

Moreover, in the real head the center of rotation will be located in the neck, rather than in the center of gravity of the head. The resulting combination of rotational and translational acceleration is also called *angular* acceleration.

4.4.4 Classification of tissue strain

Tissue strains, induced by the external load, can be a normal strain, either *compressive* or *tensile*, or a *shear* strain.

Apart from the nature of the strain, strains are also classified by their spatial distribution. As will be apparent from the discussion above, static load, contact load, and translational load will induce *focal strains*, i.e. strains in a relatively small region. Rotational loading will lead to *diffuse strains*, i.e. strains that are distributed over a larger spatial region.

4.5 Injury mechanisms

In this chapter the term *injury mechanism* will be used for the cascade of events, by which an external head load leads to injury. This cascade comprises two steps: the first step through which an external load leads to an internal mechanical response, and the

second step through which this response, in combination with the spatial distribution of tissue components and their tolerance levels, leads to injury. The former step was discussed in the previous section, and is discussed in more detail in sections 4.8 and 4.9. The latter step is discussed in more detail in section 4.7. Often, a classification into *contact injury* and *inertial injury* is made [27].

4.5.1 Contact injury mechanisms

Contact injuries are defined as injuries that occur through contact impact without head motion. We distinguish between *local contact effects*, i.e. effects that occur at the site of impact, and *remote contact effects*.

Local contact

Injuries due to *local contact effects* comprise scalp injuries, (linear or depressed) skull fracture, epidural hematomas, and coup contusions. The occurrence of *skull fracture* depends on the magnitude of the contact force and the area over which it is distributed, and on the local skull material properties and thickness. Depressed skull fracture may cause macroscopic brain tearing (laceration).

Epidural hematoma, i.e. tearing of dural vessels, can occur if a skull fracture propagates across a vessel. But even in the absence of skull fracture, the inbending of the skull can load the vessel to above its failure limits.

Coup contusions, i.e. mixtures of vascular and brain damage, may occur beneath the site of impact. They are caused by compressive strains, due to skull inbending or depressed skull fracture, or by tensile strains, due to skull snap-back.

Remote contact

Injuries due to *remote contact effects* include remote vault and basilar fractures, and contracoup injuries. If the impact occurs on a thick portion of the skull, locally the load may remain below the failure level, and the load is transmitted to other portions of the neurocranium and the base. Remote *fractures* will occur if the load exceeds the failure load. Remote vault and basilar fractures can also be caused by the propagation of *waves* in the skull, emanating from the point of impact. Some basilar fractures (especially the transverse type) may also result from facial impact [39].

Contact loads may also induce *pressure (or longitudinal) waves* in the brain. Focusing of these waves may lead to sites of strain concentration and consequently brain damage in the form of *contrecoup contusion*. The occurrence of pressure waves depends on the frequency content of the load that is transmitted to the brain. Combining the speed at which pressure waves travel (1500 m/s), and the dimensions of the human head (15 cm), it is obvious that wave phenomena become important if the load contains enough energy in the frequency range above 10 kHz. In traffic accidents, the duration of the head load is typically in the order of ms, so the role pressure waves might be minor. In this case, the pressure distribution within the brain will display a monotonic decrease from a positive pressure at the site of impact, causing coup contusions, to a negative pressure opposite the side of impact, causing contre-coup contusions.

Table 4.4: *Prevalence, cause of death and disability of head injury for 434 hospitalizations [26].*

injury and mechanism	prevalence (% of all lesions)	cause of death (% of all death)	cause of poor survival (% of all survivals)
Focal contact	36	6	12
scalp laceration	13	0	0
vault fracture	15	0	0
epidural hematoma	2	2	8
cortical contusion	6	4	4
Remote contact	18	16	9
basal skull fracture	7	0	0
contusion - contre coup	8	7	4
intracerebral hematoma	3	9	5
Acceleration	33	64	62
concussion	18	4	4
diffuse injury	5	11	40
shearing injury	2	20	6
subdural hematoma	8	33	12
Secondary injury/other	13	13	17

4.5.2 Inertial injury mechanisms

Injuries may also be induced by *translational* or *rotational* accelerations of the head. As described before, translational inertial load will lead to a coup- contracoup effect, with positive pressures at the coup site and negative pressures at the contracoup site. This loading condition mainly will cause *contracoup contusions*, because of tensile loading at the contracoup site [27]. Translational loading can also produce other focal injuries, including intracerebral and subdural hematoma [27].

Already in the 1940's and 1950's [38, 31] it was indicated that rotational acceleration could develop tensile and shear stresses in the brain resulting in concussive brain injuries. Later studies have postulated that especially rotational acceleration is the most important cause for severe head injury: SDH and shearing injury [26, 63]. The injuries, induced by rotational acceleration, depend on the duration of the loading. Short duration loading is considered to cause *subdural hematoma* (SDH), i.e. disruption of the bridging veins between skull and brain. The explanation for this lies in the fact that the veins are particularly sensitive to high strain rate loading. If the rotational loading lasts longer, with lower magnitude, the bridging veins remain intact, and the loading is transferred to the brain. There it can cause *diffuse axonal injury*. At even lower loading, only *cerebral concussion*, i.e. a transient neurological dysfunction, may be induced.

Table 4.4 gives the relative importance of injuries to the head in terms of prevalence, cause of death and cause of poor survival of 434 hospitalized head injured patients [26]. The injuries are divided in three categories, depending on their (supposed) injury mechanism. From this table it can be seen that contact impact comprises more than

half of the patients (54%) but is responsible for only one-fifth (22%) of all deaths and similar number of poor outcome. Acceleration induced injury comprises only one-third of all hospitalizations but is responsible for two-thirds of all deaths and patient with poor outcome. Generally, acceleration is the most important injury mechanism in human head injury with regard to death and disability.

Finally, it must be noted that in real world accidents, head load is often a combination of contact load and (translational and rotational) inertial load. Consequently, the observed injuries may be the result of several injury mechanisms.

4.6 Head injury criteria and tolerances

For over 30 years, research has been undertaken to assess the mechanisms causing head injury in impact conditions and to establish associated tolerance levels of the human head. As discussed before, in principle tolerance levels should be formulated for each of the constituent tissues of the head, e.g. nerve, vascular and bone tissue, separately. These tolerance levels would be formulated in terms of stresses and strains. Unfortunately, in practical cases local tissue load is unknown. Consequently, the external load is often used as a measure of the local tissue load, and head injury criteria and tolerances are mostly formulated in terms of global kinematic data, e.g. head accelerations. Sometimes, the global kinematic data are used as input for simple lumped mass models, and some aspect of the behavior of the model is taken as a predictor for the occurrence of injury.

This section deals with the most commonly used tolerances and injury criteria. Today, these are the criteria that form the basis for both legislation and evaluation of injury prevention measures.

4.6.1 The Wayne State Tolerance Curve

The first extensive quantification of head tolerance to impact was the Wayne State Tolerance Curve (WSTC) [51, 32]. Still being basis for the most currently accepted injury criteria, the WSTC gives a relationship between a linear acceleration level and pulse duration that give similar head injury severity in head contact impact.

Figure 4.8 shows the now accepted form of the WSTC. The ordinate represents the 'effective' or average acceleration (measured at the rear of the head) and the abscissa represents the time duration of this acceleration. Combinations of acceleration and time which lie above the curve are likely to result in considerable brain damage (AIS 3 or higher) and combinations that lie below this curve stay below human tolerance. The experimental data used to develop this curve were [79]:

- for short pulse duration (1-6 ms): acceleration levels necessary to produce linear skull fracture (known to be highly associated with brain concussion) in embalmed cadaver heads;
- for intermediate pulse duration (6-10 ms): acceleration levels in experiments in which cadaver and animal brain pressure responses were compared;
- for long pulse duration: acceleration levels obtained in human volunteer tests, not producing brain injury and thus to be considered as asymptotic value of the curve.

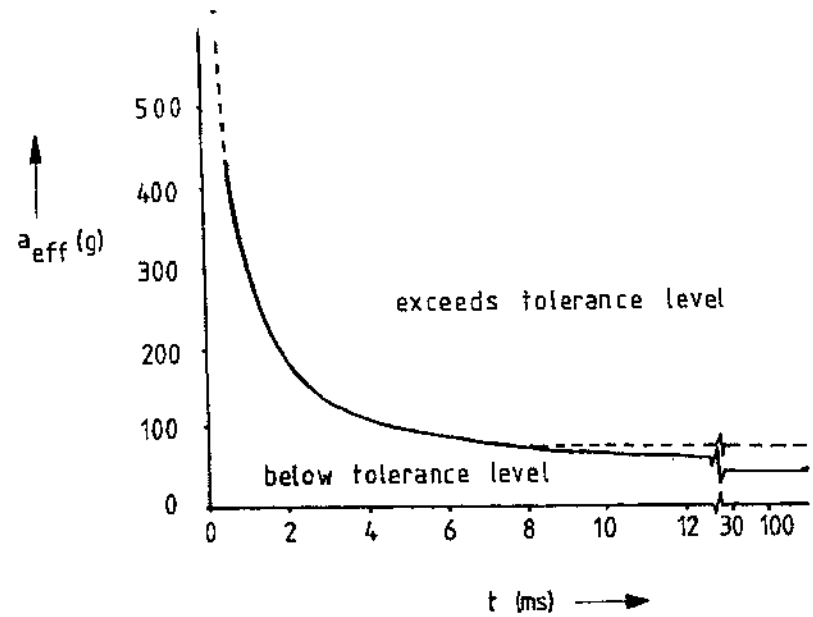

Figure 4.8: *The Wayne State Tolerance Curve.*

This asymptotic value was originally proposed to be 42 g but later proposed to be raised to 80 g.

When using the WSTC, one should bear in mind that the curve was established using embalmed cadavers (opposed to fresh cadavers), impacting a rigid or padded flat plate at their foreheads, instrumented with pressure transducers penetrating the skull and an accelerometer mounted on the rear center of the head. The WSTC is supported by experiments conducted in Japan [65] from which a Japan Head Tolerance Curve was developed (JHTC). The WSTC and JHTC are quite similar, especially for impulse durations between 1 and 10 ms [65, 5, 60].

4.6.2 Severity Index

For evaluating complex acceleration-time pulses to the WSTC, difficulties arise in the determining the effective acceleration. To overcome this problem Gadd developed a weighted impulse criterion for establishing a *Severity Index* SI, which for the head is:

$$SI = \int_T^0 a^{2.5}(t)dt \tag{4.1}$$

where $a(t)$ represents the acceleration in g's, T the pulse duration, and t the time in seconds.

The weighting factor 2.5 only applies to the head and is primarily based on a straight-line approximation of the WSTC plotted on log-log paper between 2.5 and 50 ms. The threshold - tolerance level - proposed by Gadd of concussion for frontal impact is 1000 (thus SI should not exceed 1000) [21, 22]. Gadd also used the uni-axial acceleration of the head, measured at the occiput in the direction of impact. For non-contact impact, Gadd proposed a tolerance of 1500 for concussion [79].

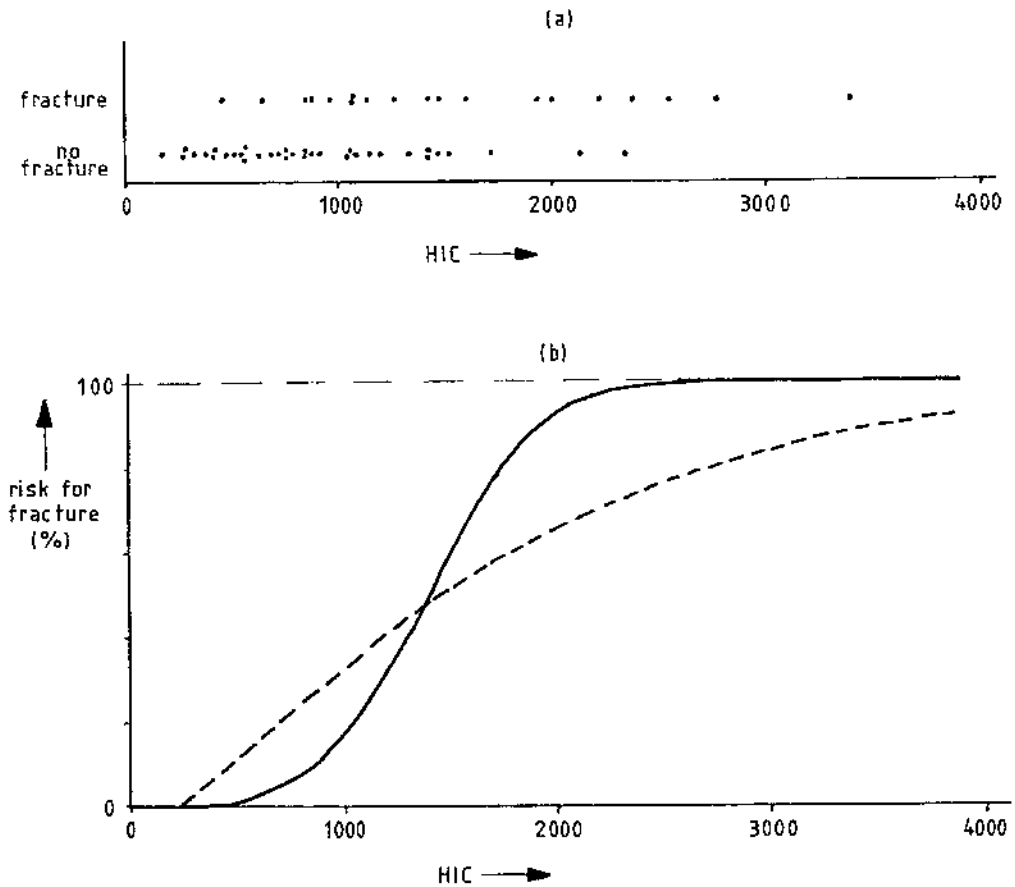

Figure 4.9: *Injury probability of the head: skull fracture vs. HIC [71].*

4.6.3 Head Injury Criterion

In response to a study by Versace on comparison of the WSTC and the SI [95], a new injury criterion for the head was defined by the U.S. government, the *Head Injury Criterion* (HIC):

$$HIC = \left\{ (t_2 - t_1) \left[\frac{1}{t_2 - t_1} \int_{t_1}^{t_2} a(t)dt \right]^{2.5} \right\}_{max} \tag{4.2}$$

where $a(t)$ is the resultant head acceleration in g's (measured at the head's centre of gravity), and t_1 and t_2 are the initial and final times (in seconds) of the interval during which the HIC attains a maximum value.

As for the SI, a value of 1000 is specified for the HIC as concussion tolerance level for concussion in frontal (contact) impact. For practical reasons, the maximum time interval $(t_2 - t_1)$ which is considered to give appropriate HIC values was set to 36 ms [79]. This time interval greatly affects HIC calculation and recently, this time interval has been proposed to be reduced to 15 ms [41] in order to restrict the use of the HIC to hard contact impacts [37].

Mainly because of human variability, no precise separation between a non-injurous and an injurous load condition can be defined. This raises the problem of *injury*

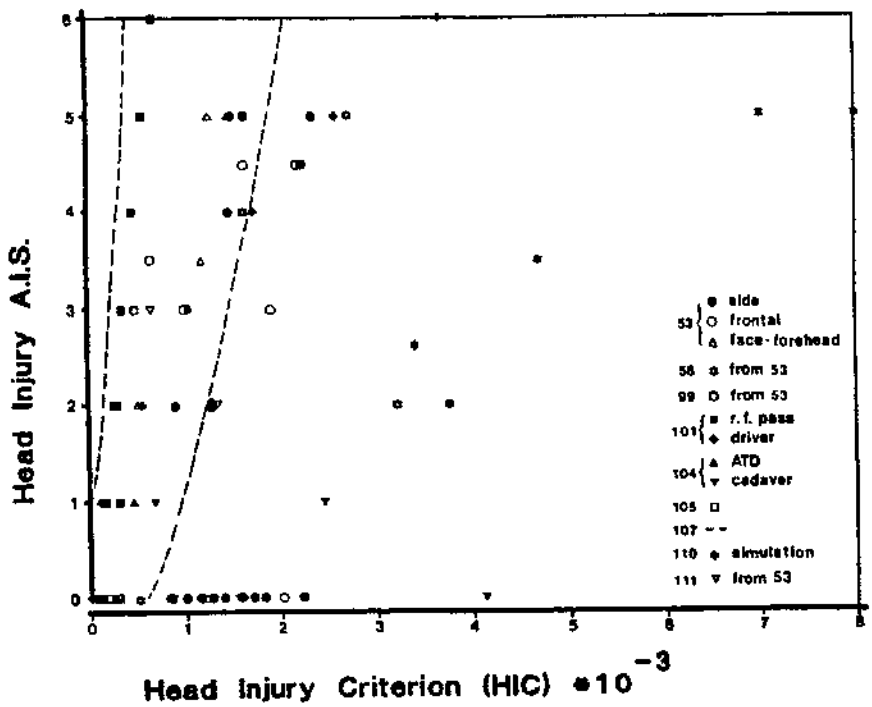

Figure 4.10: *Head Injury Severity (in AIS) as function of HIC [59].*

probability. In chapter 3 the general principle of injury probability is explained using statistical methods. Censored data, obtained by a discrete classification of injury severity, can be handled using the method of Maximum Likelihood [20]. Below an example is given for the head, regarding skull fracture and HIC [71].

The data used for this example concern HIC values obtained form 54 cadavers showing cranial fracture after impact [40]. These -censored- data are shown in figure 4.9-a. To the data in the overlap region (43 data points), a normal distribution was fitted, which results in the risk function shown in figure 4.9-b as a solid line [40]. Applying a Weibull distribution to all the data, according to the Maximum Likelihood Method, results in the function shown in figure 4.9-b as a dashed line [71]. The Maximum Likelihood Method fit shows a continuous increase in risk vs. HIC value, in contrast to the suggested Normal distribution, which has a more 'sudden' transition from 0 to 100% in the range from 1000 to 2000 HIC units.

Supposing the injury data, shown in figure 4.9, are representative of the population at risk and the HIC is suitable as an injury criterion for cranial fracture, a risk level of 50% corresponds to a tolerance level for HIC of 1400 and 1470 for the Normal and Weibull distribution respectively.

HIC values obtained in reconstructed accidents using dummies, cadavers and mathematical models, have been gathered by Newman [59] and are shown in figure 4.10. Newman concludes from these data that HIC and AIS do not correlate. Most important drawbacks of the HIC are that the WSTC lacks a functional relationship between human head injury and human surrogate head acceleration-time response and that HIC

Table 4.5: *Human brain tolerance to angular acceleration $\ddot{\alpha}$ and velocity $\dot{\alpha}$; all references from [69]; t denotes duration of impact.*

reference	injury	tolerance	
Ommaya et al. (1967)	cerebral concussion	50% probability:	
		for $t < 20$ ms: $\ddot{\alpha} = 1800$ rad/s^2	
		for $t \geq 20$ ms: $\dot{\alpha} = 30$ rad/s	
Löwenhielm (1975)	bridging vein rupture	$\ddot{\alpha} < 4500$ rad/s^2 and/or $\dot{\alpha} < 70$ rad/s	
Advani et al. (1982)	brain surface shearing	$2000 < \ddot{\alpha} < 3000$ rad/s^2	
Ommaya (1984)	brain (general)	$\dot{\alpha} < 30$ rad/s:	safe: $\ddot{\alpha} < 4500$ rad/s^2
			AIS 5: $\ddot{\alpha} > 4500$ rad/s^2
		$\dot{\alpha} > 30$ rad/s:	AIS 2: $\ddot{\alpha} = 1700$ rad/s^2
			AIS 3: $\ddot{\alpha} = 3000$ rad/s^2
			AIS 4: $\ddot{\alpha} = 3900$ rad/s^2
			AIS 5: $\ddot{\alpha} = 4500$ rad/s^2

only takes into account the linear aspects of head motion.

Despite its drawbacks, HIC is the most commonly used criterion for head injury in automotive research. It is believed to be an appropriate discriminator between contact and non-contact impact response and shows higher values in contact impact (as is consistent with basic laws of mechanics [5]). Furthermore, the data presented in figure 4.10 are not limited to impact condition and subject variability and thus implicitly show great variety in head impact response. If only cadaver data in frontal impact is selected HIC shows to be a reasonable discriminator between severe and less severe impact [89].

Important conclusions that can be drawn from HIC vs. injury severity analyses:

- HIC only considers linear acceleration, while biomechanical response of the head also includes angular motion which is believed to cause head injury;
- HIC is only valid if hard contact occurs thus the time duration of impact is limited;
- HIC is based on the WSTC, which is derived from subjects loaded in anterior-posterior (A-P) direction.
- More detailed injury severity classification is needed to fully investigate the relationship between head injury and head impact response.

4.6.4 Criteria and tolerances for angular acceleration

The WSTC, SI and HIC, concern linear head impact response. In the previous section, the importance of rotational acceleration of the head was noted, especially with respect to ASDH and diffuse brain injury. A summary of various tolerances of the human brain to angular acceleration (and angular velocity) is given in table 4.5. This table gives the reference, the injury considered and the proposed tolerance level, all concerning sagittal head motion.

An attempt to combine translational and rotational head acceleration response

was made by Newman [61]. Considering these accelerations as the cause for stresses generated in the brain and resulting in brain injury, a *Generalized Acceleration Model for Brain Injury Threshold* (*GAMBIT*) is proposed. The general GAMBIT equation is:

$$G(t) = \left(\left(\frac{a(t)}{a_c} \right)^n + \left(\frac{\ddot{\alpha}(t)}{\ddot{\alpha}_c} \right)^m \right)^{\frac{1}{s}} \tag{4.3}$$

where $a(t)$ and $\ddot{\alpha}(t)$ are the instantaneous values of translational and rotational acceleration respectively; n, m and s are empirical constants selected to fit available data; and a_c and $\ddot{\alpha}_c$ are the critical values of the accelerations (tolerances).

On the assumption that the tolerances derived from experiments with only translational or only rotational head motion are also valid for combined head response, and on the assumption that translational and rotational acceleration equally contribute to head injury, Newman simplified this equation to become:

$$G(t) = \frac{a_m}{a_c} + \frac{\ddot{\alpha}_m}{\ddot{\alpha}_c} \leq 1 \tag{4.4}$$

where a_m and $\ddot{\alpha}_m$ are the mean values of linear and angular acceleration; and $a_c = 250$ g and $\ddot{\alpha}_c = 10.000$ rad/s^2 are the maximum allowable values for linear and angular acceleration. However, thus far the GAMBIT lacks extensive validation.

4.6.5 Head injury criteria based on lumped mass models

The injury criteria discussed thus far (WSTC, SI and HIC) are set up empirically. They can be derived directly from measured accelerations of the head.

It has been discussed before, that the risk of injury is more directly related to the local mechanical load, imposed on the head tissues, than on the external head load, expressed in terms of head acceleration. A first attempt, to translate head acceleration to internal load has been made through the use of lumped mass models. In these models, the inertial, viscous and elastic behaviour of the head is lumped into one or more masses, dampers and springs, respectively. The response of the models upon an external load is formulated in terms of displacements of the masses, and their derivatives.

Still, discrete head injury models lack the quantitative relationship between head trauma and its actual cause. These models concern overall head response in stead of detailed modeling of the strains and stresses inside the structures of the head.

Using the WSTC as a basis, Slattenscheck [84] introduced a damped single mass-spring-system to model the head (figure 4.11, left). The compression of the spring x was interpreted as the relative displacement of the brain with respect to the skull. The maximum compression (x_{max}) was determined for different levels of impact. The model was validated to the WSTC. This validation resulted in a maximum tolerable relative displacement (x_{tolr}) of 2.35 mm. The injury criterion set up is called the *Vienna Institute Index* (J) and the tolerance for this index is 1:

$$J = \frac{x_{max}}{x_{tolr}} < 1 \tag{4.5}$$

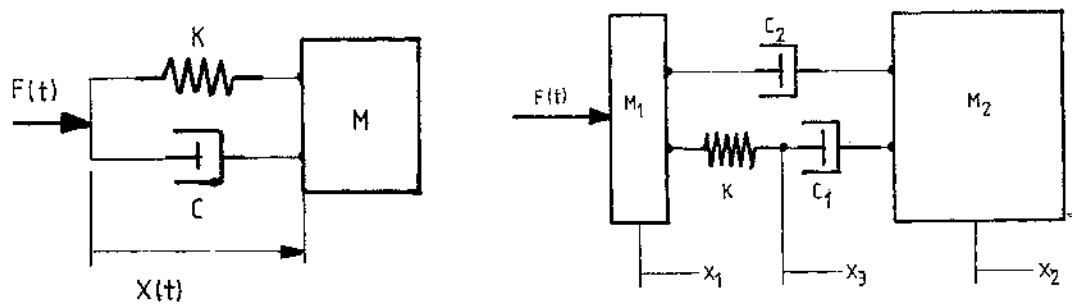

Figure 4.11: *Lumped mass models, used for defining head injury criteria; left: single mass spring-damper model; right: Translational Head Injury Model (THIM).*

Revision of the Vienna Institute Index by further validations to the WSTC (especially concerning short duration pulses: 3-5 ms), resulted in the *Effective Displacement Index* (EDI) [10]. A new maximum tolerable relative displacement was assessed: $x_{tol\tau} = 3.78$ mm. Also based on the single mass system of the Vienna Institute Index is the *Revised Brain Model* (RBM) [19]. With this model the injury criterion for short duration pulses (< 20 ms) was based on the velocity of compression of the spring, while for longer pulses, it was based on the maximum compression.

Using a 2 mass spring-damper system, Stalnaker et al. postulated a head injury criterion using mean strain, considered to be representative of brain deformation, as the parameter to predict head injury severity: *the Mean Strain Criterion MSC* [85, 86, 72]. The head model consisted of 2 masses, connected by one spring and one damper (parallel). Later studies indicated inconsistent behaviour of this model compared to cadaver responses and the model was changed by adding a second damper in series with the spring [87]. The new model is called the *Translational Head Injury Model* (THIM) and shown in figure 4.11.

The physical meaning of the model elements (derived from cadaver experiments) is considered to be:

- summation of masses M_1 and M_2 will always add up to the total head mass;
- M_1 is the mass of the skull moving directly under rigid impact;
- stiffness K and damper C_1 form the non-linear skull stiffness in a given direction;
- damper C_2 is believed to be primarily the damping of the brain and found to be constant for all directions;
- $F(t)$ is the impact force in rigid or padded head impacts.

The THIM concerns translational response to contact impact only. It is used to develop a new head injury criterion, based on energy dissipated or stored by elements of the model, rather than strain derived from relative motion between the masses of the model. This new criterion is called the *Translational Energy Criterion* (TEC) [88, 72].

Knowing head response usually includes both translation and rotation, an increasing interest can be noticed in modeling rotational head response. An example: similar to the THIM, Low and Stalnaker [52] developed a 2 dimensional lumped mass model to simulate the head response in terms of rotation: the *Rotational Head Injury Model*

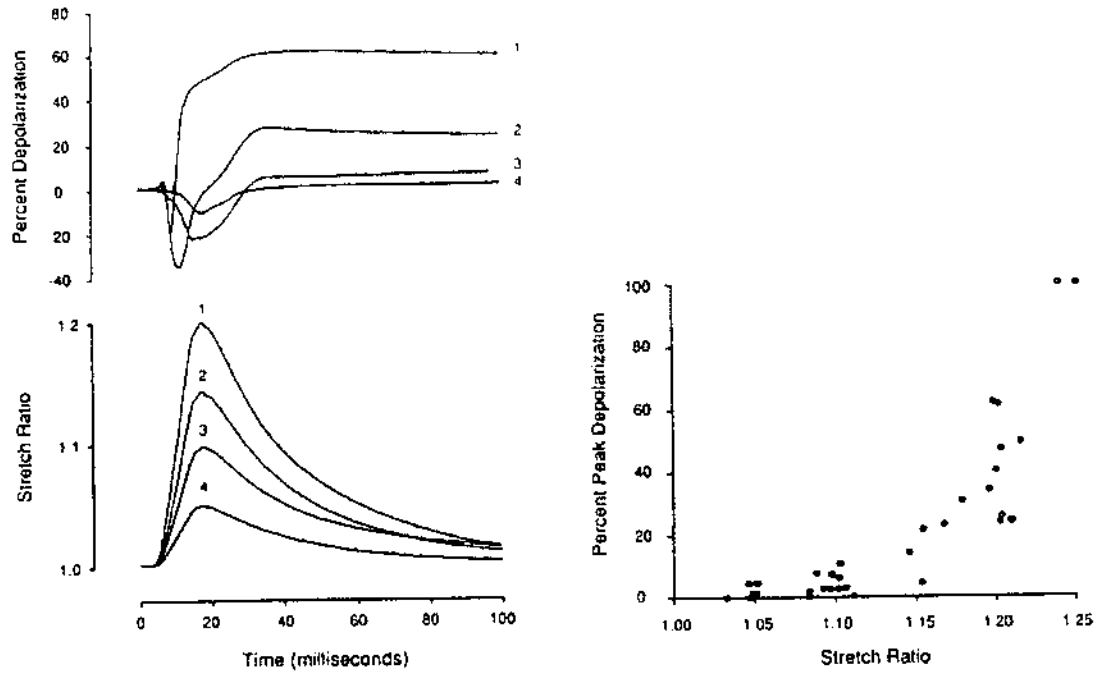

Figure 4.12: *The influence of dynamic stretching on the rest potential of the giant squid axon; left: time course of change in potential, normalized to the resting potential (top) and time course of applied stretch (bottom); right: relation between peak stretch ratio and peak depolarization; from [24].*

(RHIM). Currently attempts are being made to combine the THIM and RHIM into a Unified Head Injury Model (UHIT).

4.7 Failure behaviour of intracranial contents

Ultimately, head injury is related to functional or structural failure of the tissues, the head is composed of. The main tissues are bone, brain, and vascular tissue. As discussed before, during impact these tissues may be subjected to a combination of compressive, tensile and shear strain.

Bone is stronger in compression and tension, than in shear. Also, it is stronger than the vascular and nerve tissues. The strength of these soft tissues can be best understood if they are regarded as a mixture of solid components (fibers, membranes) and fluid. During compression, the load will be transmitted by the fluid component, and the risk of damage is low. However, during stretch and shear the load will be transmitted by the solid components, and the risk of damage is higher. Moreover, since the tissue behaves viscoelastically, tissue strength will be dependent on the strain rate.

In the following, we will concentrate on the failure behavior of brain and vascular tissue.

4.7.1 Failure of neural tissue

The failure behaviour of neural tissue has been studied in experiments on animals, on complete nerves containing thousands of neurons, and on isolated neurons. Animal experiments have the advantage that the neurons are loaded in their natural environment. On the other hand, exact loading of the individual neurons remains unknown: the applied load is distributed in a complex, inhomogeneous way over the tissue. Thus, unambiguous coupling of mechanical load to neuronal damage is impossible.

Complete nerves, such as the optic nerve, have also been used to study axonal injury. A single, rapid, controlled elongation (tensile strain) in the optic nerve of the albino guinea pig was found to induce axonal swelling, axolemmal blebs, and accumulation of organelles identical to those seen in human and experimental brain injury [28]. Still these results must be interpreted as the average response of a large population of neurons to external load.

To improve the understanding of how mechanical load affects neural function, experiments have been conducted on a single fiber, the giant squid axon [24]. The giant axon was subjected to controlled uniaxial loading and its mechanical and physiological responses were monitored. The physiological response of the axon to mechanical load was measured as the change in its resting potential (depolarization), which normally is in the order of 60 mV. Quasi-static loading was found to yield a small reversible hyperpolarization; however, as the rate of loading was increased, the axon depolarized and the magnitude and the time needed to recover to the original resting potential increased in a nonlinear fashion (see figure 4.12). At elongations greater than twenty percent an irreversible injury occurred and the membrane potential did not completely recover to baseline.

The temporary, reversible loss of neural function is also called *functional damage.* At higher load levels, a cascade of events is hypothized to lead to *structural damage.* Calcium is thought to play a crucial role in this process [64]. Under normal circumstances, cellular mechanisms maintain a low intracellular calcium concentration, despite a higher extracellular concentration. Dynamic elongation of the cell is hypothesized to create 'pores' in the membrane, thereby increasing membrane permeability to calcium, and allowing a large influx of calcium into the cell. Once intracellular calcium concentration reaches a critical threshold, cytoskeletal depolimerization occurs. The resulting proteins cause an increase of intracellular concentration, an increased intracellular osmotic pressure, attraction of extracellular water and subsequent cell swelling, eventually leading to disruption of the cell membrane. This sequence of events is shown in figure 4.13

Cellular damage, occurring according to this sequence of events, is also called *secondary cell disruption.* Of course, at higher loading levels, the cell can be disrupted directly without the swelling process being involved. This process is called *primary cell disruption.*

4.7.2 Failure of vascular tissue

The failure behaviour of vascular tissue seems less well documented than that of neural tissue. But, analogous to neural tissue, a distinction between functional, secondary and

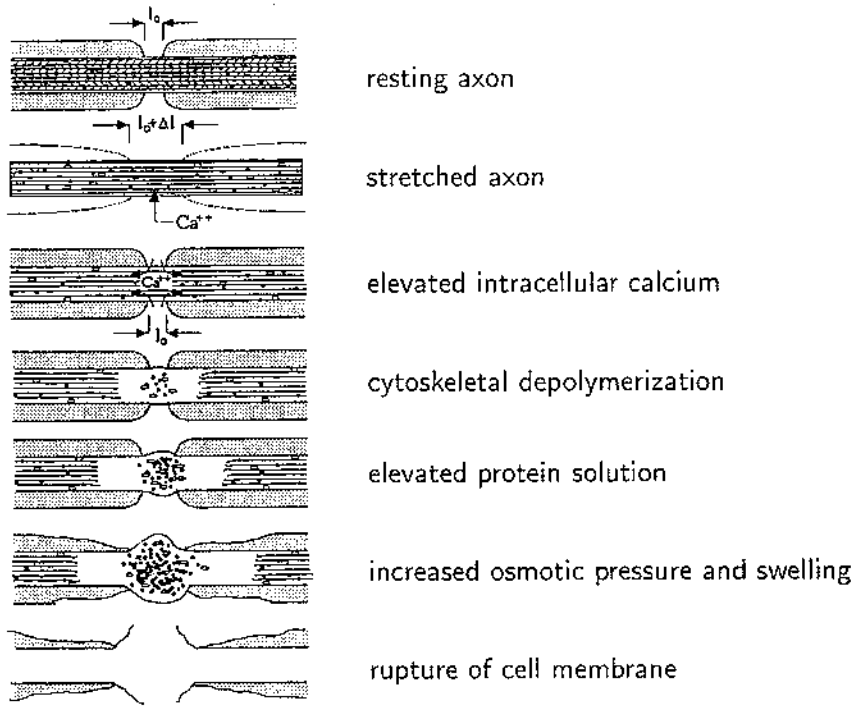

Figure 4.13: *Illustration of the cascade of events, hypothesized to lead to secondary cell rupture after mechanical loading; from [64].*

primary damage is appropriate.

Functional damage of a blood vessel must be interpreted as functional damage to the smooth muscle cell in the blood vessel wall. Like in the neural cell, also in the smooth muscle cell a dynamic stretch seems to lead to an increase in intracellular calcium concentration [91]. In the muscle cell, increased calcium levels lead to increased cross-bridge binding and thus increased contraction. On a more macroscopic level, vasospasm might occur, which might lead to reduced blood perfusion and ischemia. Finally, prolonged ischemia will lead to cell death.

Structural damage to the blood vessel might be secondary, caused by cell swelling, or primary, caused by direct disruption. Direct rupture of the bridging veins has been reported to occur at 50% tensile strain [48].

4.8 Experimental assessment of local mechanical brain response

An accurate quantitative picture of local mechanical brain response is crucial for full understanding of head injury mechanisms, since the local response forms the link between external load and tissue failure. In section 4.4, a qualitative description of the local mechanical brain response has been given. In this section, we will discuss experimental methods, through which insight into local mechanics can be increased.

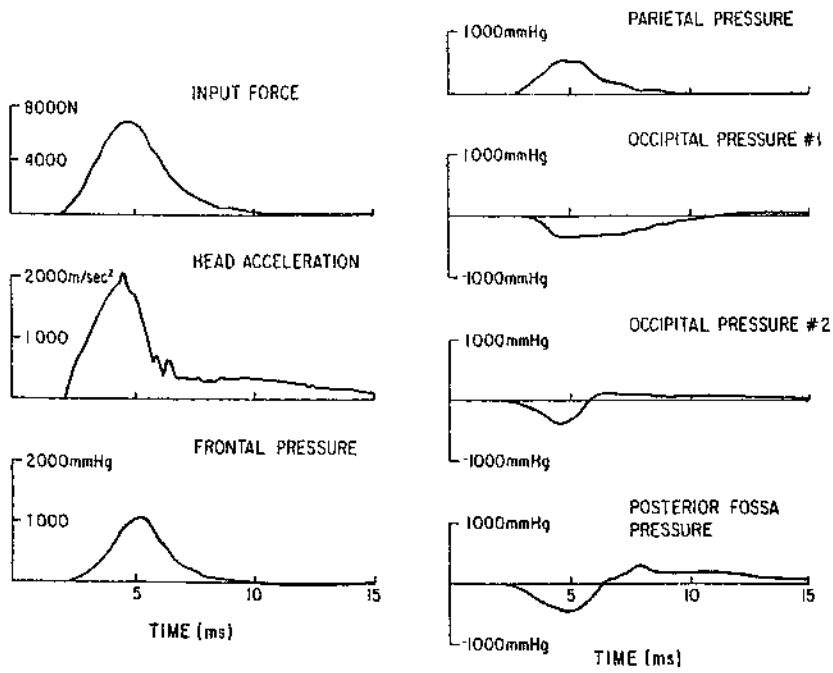

Figure 4.14: *Experimental results of frontal impact on a cadaver head, showing impact force, head acceleration, and intracranial pressures at several sites [58].*

4.8.1 Animal and cadaver tests

Experimental assessment of the brain response is hampered by the inaccessibility of the brain in the cranial cavity and the small time scale on the order of milliseconds, at which phenomena take place. Nevertheless, several experimental studies employing various techniques have given an indication of the local brain response.

Intracranial pressure measurements

In a study by Nahum *et al.* [58] cadaver heads were impacted with masses ranging from about 5 to 23 kg at speeds ranging from about 8 to 13 m/s. Resulting intracranial pressure response was measured at several sites. A typical result is shown in figure 4.14. The positive pressure at the impact ('frontal') site and the negative pressure at the opposite site ('posterior fossa') illustrate the coup contre-coup effect.

Radiographic techniques

Brain motion during impact has been studied using x-ray techniques [36, 33]. Here, lead markers were inserted into the brain, and the marker motion during impact was recorded on film. Brain movement was found to be in the order of 2 mm. In later studies, socalled neutral-density targets were used, i.e. markers having the same density as brain tissue [35]. Typically, displacements between closely-spaced targets (order 10 mm), corresponded to stretches in the order of 10% during a 100 G impact [35].

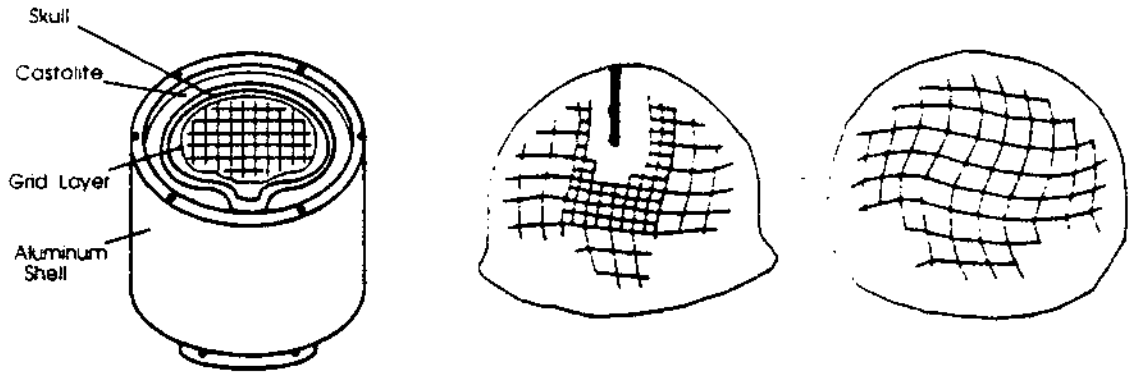

Figure 4.15: *A physical head model; left: model configuration; middle and right: response upon noncentroidal rotation for models with and without falx; note the increased deformation in the model without falx; from [53].*

Cranial windows

Several investigators used the technique of the translucent calvarium to directly observe brain motion during impact [81, 29, 30]. In this experiment, part of the skull is removed and replaced by a translucent implant. Through this window, direct observation of brain motion during impact is possible.

Intracranial accelerometry

Local brain kinematics has also been assessed through miniature accelerometers, implanted in the brain. Here, the problem has been to develop a method through which the complete vectorial translational and rotational motion can be deduced from the signal of multiple accelerometers. In the mid seventies, the socalled 3-2-2-2 arrangement of nine accelerometers was successfully applied [66, 13]. More recently, neutral-density accelerometers were used [35].

4.8.2 Physical models

To obtain more insight in local mechanical brain response, also physical models have been employed [2, 53, 96]. In some models the response in a coronal plane was studied. The outer (skull) boundary of the model was formed by the anterior half of a real skull (figure 4.15). In other models, the response in a saggital plane was studied. Here, the outer boundary was a cylinder, with a cross-sectional shape resembling the gross anatomy of the skull in a saggital cross-section [2, 96]. The dural folds, such as falx and tentorium, were represented by rigid or polyurethan plates. The brain material was represented by a silicon gel. The models were exposed to translational or rotational pulse. The strain response of the gel was derived from the motion of optical markers (dots or a grid).

Upon loading, representative for severe head impact, the models showed strains up to 25%. Experiments performed with and without falx and tentorium demonstrated that the presence of these structures reduced intracranial deformations (see figure 4.15).

Also, comparison of experiments with and without the possibility of slip between the skull and the gel, demonstrated that slip reduced the deformation of the outer layers of the gel. Thus, the combination of CSF and meninges may be expected to have a similar strain reducing effect in the real head. Moreover, regions with largest shear strains in the physical model seemed to correspond with those in the real brain most often associated with diffuse axonal injury [53].

Although the models provide insight into the local brain response, inevitable differences between the models and the real head prevent the derivation of quantitative critical strain levels from these experiments. On the other hand, because of the well defined model properties, the experimental results may be used for validation of numerical (FE) models.

4.9 Assessment of local mechanical brain response using finite element models

4.9.1 General methodology

From the previous section, it can be concluded that experimental assessment of the complete local mechanical brain response is practically infeasible. As an alternative, mathematical models are used, that are numerically solved using the finite element (FE) method.

From an engineering point of view, the local mechanical response of a continuum, such as the head, upon an external load is governed by the laws of conservation of mass and momentum, defined on a geometrical domain, supplemented by constitutive laws for the materials, and boundary conditions between internal subregions and with the environment. While the conservation laws are beyond any doubt, the descriptions of (or models for) the geometrical domain, the (distribution of the) material properties and the boundary conditions are approximations of reality.

Once models have been chosen for geometry, material properties and boundary conditions, the resultant mathematical model has to be solved. Since analytical solution for all but the simplest models is impossible, a numerical solution method, such as the finite element (FE) method, has to be used. Unfortunately, the FE method only yields an approximation of the solution of the mathematical model, while at the same time it may introduce numerical artefacts.

Finally, the quality of the head mechanics, as predicted by the model, has to be evaluated by comparison with experimental data. The limited availability of experimental data poses a major problem for the validation of FE models.

In the next paragraphs, we will discuss some of the above items in more detail.

4.9.2 Geometry

With the increasing power of imaging techniques (CT-scan, MRI) an increasing amount of geometrical information has become available. Whereas the distinction between hard and soft tissues can be made relatively easy, it is harder to distinguish between the various substructures in the brain. Moreover, it is not clear yet what level of geometric detail is necessary to provide a biofidelic prediction of local mechanical response. A

minimum demand seems to be incorporation of skull, right and left cerebrum, right and left cerebellum, brainstem, falx and tentorium.

4.9.3 Boundary conditions

Generally, the head model as a whole is subject to three boundaries with its surroundings: the head-neck junction, the foramen magnum, and, possibly, the contact with an external head load. The way in which the head-neck junction must be modeled, depends on not only on its anatomy, but also on the type of head loading and the type of fixation of the neck. Descriptions may vary from a free boundary condition, to a complete suppression of all degrees of freedom.

The foramen magnum is thought to act as a pressure-release mechanism, because cerebrospinal fluid can be pressed from the cranial cavity into the spinal canal. In principle, this fluid component should be modeled separately. In current models, this has not been realized yet, and the function of the foramen is at best approximated by a force-free opening, in combination with the possibility of the brain to slide along the skull.

More important boundary conditions are those between the various structures within the cranial cavity, especially the interface between brain and skull. As discussed before, the skull and brain are separated by the meninges, in between which cerebrospinal fluid is found. Until know, modeling each of these structures individually has been unfeasible, among others because of the problems associated with the combination of solid and fluid behaviour in one model. Instead, the interface is modeled with a description of the degree of suppression of the relative tangential and normal motion of skull and brain. For the tangential motion, descriptions range from no slip via different friction levels to frictionless motion. Normal motion is usually suppressed, although some models use a failure criterion, above which skull and brain can separate. Other models approximate the interface by a layer of soft, easily deformable elements.

4.9.4 Material properties

Like most soft biological tissues, brain tissue behaves nonlinearly viscoelastic, anisotropic, and almost incompressible.

As a very first approximation of this complex behaviour, an isotropic, linearly elastic law (Hooke's law) can be used, relating the Cauchy stress tensor σ to the linear strain tensor ε according to:

$$\sigma = \lambda \mathrm{tr}(\varepsilon) + 2\mu\varepsilon \tag{4.6}$$

where λ and μ are material parameters, the socalled Lamé parameters. In the case of brain tissue, linear material behaviour is more often described in terms of the *bulk modulus* B and the *shear modulus* G, which are related to λ and μ as:

$$B = \lambda + \frac{2}{3}\mu \quad ; \quad G = \mu \tag{4.7}$$

A first impression of the values of B and G can be obtained by looking at the speed, at which waves propagate through the brain tissue. Pressure (or longitudinal

or compressive or sound) waves travel through brain tissue at a speed c_p of about 1500 m/s, i.e. at a speed similar to that of sound in water. Shear (or transverse) waves, in which particle motion is perpendicular to the direction of wave propagation, travel at a speed c_s in the order of 10 m/s. In linear elastic theory, these speeds are related to the material properties as:

$$c_p = \sqrt{\frac{B + \frac{2}{3}G}{\rho}} \quad ; \quad c_s = \sqrt{\frac{G}{\rho}} \tag{4.8}$$

Inserting for the density ρ a value of 1000 kg/m^3, we arrive at the following, typical values for bulk and shear modulus:

$$B \approx 2 \text{ Gpa} \quad ; \quad G \approx 10 \text{ kPa} \tag{4.9}$$

It is important to note that brain tissue much stiffer in compression than in shear.

As a first extension of the linear elastic description, the behaviour in shear has been made viscoelastic by making the shear modulus G time-dependent. This linear viscoelastic behaviour has been characterized already in the early seventies [23, 82]. Since then, almost no further investigations have been conducted until the mid nineties. Recent studies concentrate on constitutive models for large deformations [56], differences between gray and white matter [4], regional differences [3], anisotropy [70], and high-frequency behaviour [67, 50].

4.9.5 Finite element approximation

The FE method can only yield an approximation of the solution of the original mathematical model since the mechanical response is computed for a limited number of point in space, at a limited number of time instants. Thus, a FE solution may be regarded as the real solution, filtered by a low-pass filter in space and time. The spatial points (or nodes) are grouped into volume elements. Most FE head models use linear 8-node bricks. Discretization should be such, that further refinement does not influence the relevant aspects of the solution anymore. In general, small dimensions of substructures, e.g. thickness of tentorium, lead to small elements. Sometimes, special purpose elements can be used, e.g. shell elements for tentorium. Also for the correct modeling of wave phenomena a fine mesh is required (typically 15 elements per wavelength) [7, 8, 9, 57].

Apart from yielding an approximation of the real solution, the FE method may also introduce numerical artefacts. A coarse spatial discretization may introduce numerical dispersion and artificial reflection of waves, while a coarse temporal discretization may introduce numerical instability [7, 8, 9, 57].

Finally, many commercially available FE codes, used to model the head, have difficulties with near-incompressibility and large rotations. To handle near-incompressibility, non-physical socalled 'hourglass' parameters are used, while large rotations may lead to severe errors in the predicted results [62].

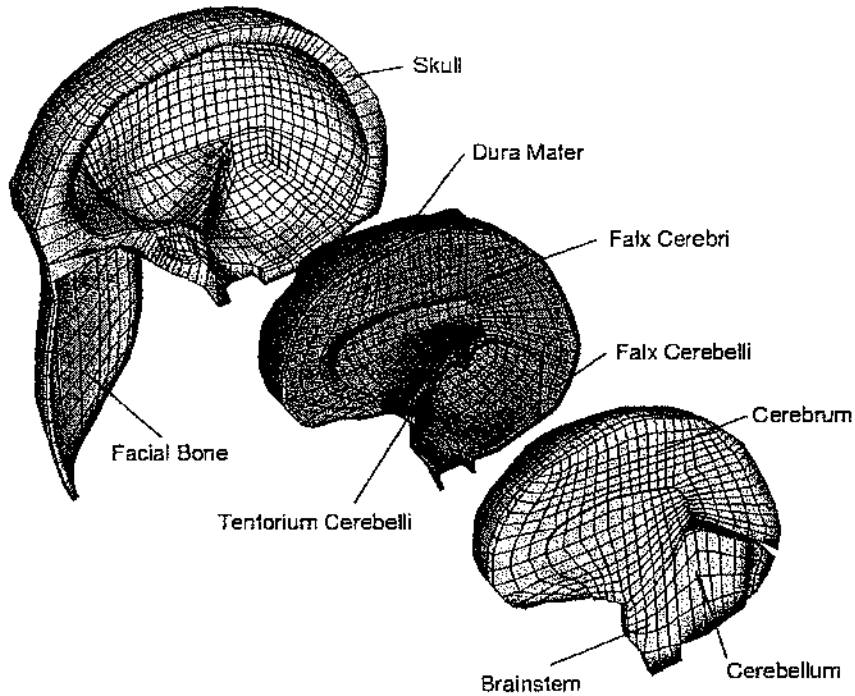

Figure 4.16: *The finite element head model, developed at the Eindhoven University of Technology.*

4.9.6 Early finite element head models

The development of finite element models of the head started in the early seventies. The early models [44, 83, 98], up to the beginning of the eighties, were reviewed by Khalil and Viano [45]. Essentially, the head was approximated as a two or three dimensional spherical or oval shell, representing the skull, filled by a linearly elastic or viscoelastic, homogeneous, isotropic material, representing the brain. Brain and skull were rigidly connected to eachother, or the interface between skull and brain was approximated by a thin layer of compliant elements. In the analysis, linear deformation theory was used. It was concluded that 'the models are a qualitative simulation of a simplified head surrogate, and as such, constitute merely the first approximation of one aspect of a highly complex biological problem' [45].

Models, published in the period 1982–1992, were reviewed by Sauren and Claessens [80]. They noted an increase in geometric complexity, leading to three-dimensional models [16, 17, 55, 73, 74, 75]. However, constitutive models still were predominantly linearly viscoelastic. More attention was paid to validation of the models, using experimental data obtained in physical models. Also, boundary conditions had been studied more extensively. Nevertheless, it was concluded that 'the existing finite element models are still far from explaining injury mechanisms and predicting type and severity of injuries in relation to loading conditions' [80].

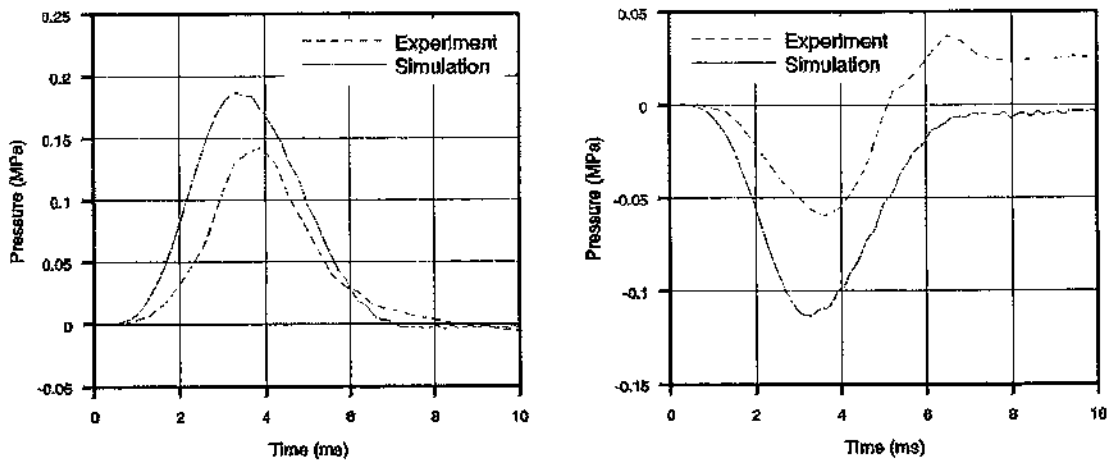

Figure 4.17: *Simulation of the Nahum-experiment with the EUT-model; frontal (left) and occipital (right) pressures as a function of time in model (solid line) and experiment (dashed line).*

4.9.7 Current finite element head models

A review of the most recent models was given by Verhoeve [94]. The basic properties, which these models have in common, are a linear elastic skull, a linear visco-elastic brain, and a linear elastic falx and tentorium.

At Wayne State University, Detroit, the original model by Ruan was further improved [73, 74, 75, 76, 77, 78]. Apart from the above mentioned basic properties, it includes a linear elastic scalp. The CSF layer is modeled as a soft solid. At the same university, a new model, the 'WSU brain injury model' was developed [102, 103]. In comparison with the original WSU model, a distinction was made between (both linear viscoelastic) grey and white matter. Moreover, the ventricles (linear visco-elastic) and the bridging veins (string elements) were included.

At the Université Louis Pasteur, Strassbourg, the socalled ULP model was developed [101, 93, 43]. Apart from the basic properties, this model includes a linear elastic scalp, a brittle skull, and a CSF layer, represented by soft solid elements. The model, developed by Dimasi, was also further improved [16, 17, 6, 18]. Its geometry is rather simple, lacking tentorium and cerebellum. But the skull-brain interface is modeled as a tie-break interface, and a socalled cumulative strain damage measure was introduced to predict brain damage. At the Eindhoven University of Technology, a brain model with the above mentioned standard configuration was developed [14, 15, 94].

In comparison to the older models, in the current models the amount of geometric detail is improved. However, brain material properties are still linearly visco-elastic, and values of material parameters differ a lot in between the models. The value of the bulk modulus differs orders of magnitude in between the models, leading to large differences with respect to propagation of pressure waves. The description of the CSF layer as a linear elastic compliant solid, is an attempt to describe fluid behaviour in a FE code, suitable only for solids. It may be doubted, whether the computed large deformations of the CSF layer, are reliable in view of the linear elastic theory used.

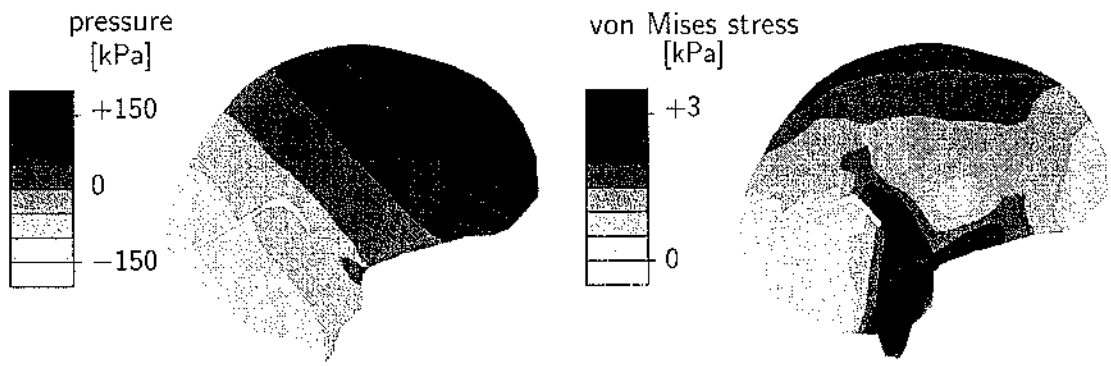

Figure 4.18: *Simulation of the Nahum-experiment with the EUT-model; distribution of pressure (left) and von Mises stress (right) distribution in a saggital plane, 10 mm outside the mid-saggital plane; pressure shown at $t = 4$ ms, von Mises stress at $t = 5$ ms.*

Modeling the CSF layer with a tie-break interface seems a more elegant option.

Systematic comparison between the models is difficult, because they differ in many respects. Possibilities for experimental validation are very limited, in view of the lack of experimental data. Nevertheless, the models provide an excellent tool for obtaining insight into the crucial determinants of brain response, by performing systematic parameter variation studies [47, 15].

As an example of the possibilities of current models, the EUT model, shown in figure 4.16, will be described in more detail. With this model, the Nahum-experiment was simulated [58]. Figure 4.17 shows a comparison between measured and predicted intracranial pressures. Figure 4.18 shows a the spatial distribution of pressures and von Mises stress. Note that the pressure distribution shows an almost linear gradient from coup site (upper right) to contre-coup site (lower right). However, the distribution of von Mises stress is more complicated.

In this simulation, the bulk modulus of the brain was 1.86 GPa. In a parameter variation study, it has been shown that lowering the bulk modulus will lead to oscillations in the predicted pressure response [15]. Also it was found that changing the skull-brain interface from no-slip to slip, influenced local brain response more than removing anatomical detail in the brain [15].

4.10 Discussion

It is obvious that an injury criterion and associated tolerance level, should relate to injury severity. The better this relationship, the better the injury criterion is a reflection of the injury mechanism and the better injury preventive measures can be evaluated. Several human surrogates are used to investigate this problem (animals, cadavers, etc.). Especially cadavers (Post Mortem Human Subjects) have been shown to be valuable models of the human being to determine tolerance levels. Practical problems that arise in setting up injury criteria are:

- the variability of cadaver data, primarily because of human variability (e.g. age, gender, etc.) but also caused by post-mortem changes, preservation of cadaver material, cause of death and by repeatability of the test methods;
- the 'translation' of a proposed injury mechanism into measurable physical parameters;
- the accuracy of clinical data and the extent to which injury severity can be scaled;
- the availability of cadavers;

Another way to assess injury mechanisms and set up injury criteria based on those mechanisms is to reconstruct real world accidents. This method involves three steps:

1. reconstruction of the external load, that acted on the head during the crash, based on estimated accident conditions (e.g. impact speed) and resultant car deformation; the victim may be modeled by a mathematical crash dummy model;
2. reconstruction of the internal mechanical head response, using a finite element head model;
3. comparison of predicted internal mechanical head response with head injury, observed using CT or MRI; identification of correlation between response and injury.

This approach was used in the European research project ADRIA (Advanced crash Dummy Research for Injury Assessment in frontal test conditions). Main advantage of this method is that it deals with the actual real-world situation. Main drawback is the summation of incertainties that occur during each step. In the ADRIA project it was found that, thanks to the current injury protection measures, in cases where relevant head injury occurred, car damage was that severe, that a reliable reconstruction of the external head load became problematic. Moreover, the lack of information about the victim seating position before the accident creates a fundamental uncertainty in the reconstructed head load.

At present, the HIC, despite its drawbacks, is the most commonly used head injury criterion. The HIC is based on the linear head response, expressed in terms of linear acceleration (as a function of time). More analytical approaches to head injury mechanics by means of simple mass-spring-damper systems have not (yet) reached the wide acceptance as the HIC, mainly because of lack of validation of these models. Anyhow, because of their discrete, simplified nature, these models will never be able to yield insight into the actual injury mechanisms.

In principle, such insight could be obtained with the use of finite element models. The main problem here lies in the lack of experimental data, needed for validation of the models. Nevertheless, the models provide an excellent tool for obtaining insight into the crucial determinants of brain response, by performing systematic parameter variation studies. Moreover, even if the current FE models still yield a simplified picture of the actual intracranial mechanics, they might already offer possibilities for defining head injury criteria that have more predictive capacity than HIC has.

4.11 References

[1] Association for the Advancement of Automotive Medicine: The Abbreviated Injury Scale - 1990 Revision. AAAM, Des Plaines (IL-USA); 1990

[2] Aldman, B., L. Thorngren, C. Ljung: Patterns of deformation in brain models under rotational motion. Head and Neck Injury Criteria - A Consensus Workshop, pp. 163-168. U.S. Dept. of Transport Publication DOT HS 806 434; 1983.

[3] Arbogast, K.B. and Margulies, S.S. Regional differences in mechanical properties of the porcine central nervous system. In *Proc. STAPP Car Crash Conf. SAE 973336*, pages 293–300, 1997.

[4] Arbogast, K.B., Prange, M.T., Meaney, D.F., and Margulies, S.S. Properties of cerebral gray and white matter undergoing large deformation. In *CDC-Proceedings*, pages 33–39, 1997.

[5] Backaitis, S.H.: The Head Injury Criterion. Head and Neck Injury Criteria - A Consensus Workshop, pp. 218-228, A.K. Ommaya ed., U.S. Dept. of Transport, NHTSA, Washington D.C., USA; 1981.

[6] Bandak, F.A. and Eppinger, R.H. A three-dimensional finite element analysis of the human brain under combined rotational and translational accelerations. In *Proc. 38th Stapp Car Crash Conf.*, 1994.

[7] Bazant, Z.P. Spurious reflections of elastic waves in nonuniform finite element grids. Comp. Meth. Appl. Mech. Eng. 16:91-100, 1978.

[8] Belytschko, T., R. Mullen. On dispersive properties of finite element solutions. In 'Modern problems in elastic wave propagation', ed. J. Miklowitz, J.D. Achenbach, Wiley Publ., New York, pp. 67–82, 1977.

[9] Brands, D.W.A. Wave propagation in head impact response: Assessment of physical possibility and numerical artefacts. (internal) WFW report 99.005, Eindhoven University of Technology, 1999.

[10] Brinn, J, S.E. Staffeld: Evaluation of Impact Test Accelerations: a Damage Index for Head and Torso. SAE Paper, Proc. 14th Stapp Car Crash Conf., pp. 188-202, Society of Automotive Engineering, New York (USA); 1970.

[11] Bull, J.P.: Injury Scoring Systems. Injury, 14, pp. 2-6; 1982.

[12] Chapon, A., J.P. Verriest, J. Dedoyan, R. Trauchessec, R. Artru: Research on Brain Vulnerability from Real Accidents. ISO/TC22/Sc12/WG6-Document N 139; 1983.

[13] Chou, C.C., S.C. Sinha. On the kinematics of the head using linear acceleration measurements. J. Biomech. 9:607-613, 1976.

[14] Claessens, M.H.A. *Finite element modeling of the human head under impact conditions.* PhD thesis, EUT, 1997.

[15] Claessens, M., Sauren, F., and Wismans, J. Modeling of the human head under impact conditions: a parametric study. In *Proc. STAPP Car Crash Conf. SAE973338*, pages 315–328, 1997.

[16] Dimasi, F., R.H. Eppinger, H.C. Gabbler III, J.H. Marcus. Simulated head impacts with upper interior structures using rigid and anatomic brain models. Auto & Safety. Summer 1991a, 20–31, 1991.

[17] Dimasi, F. Marcus, J. and Eppinger, R. 3-D Anatomic Brain Model for Relating Cortical Strains to Automobile Crash Loading. In Proc. 13th Int. Techn. Conf. on Experimental Safety Vehicles, Paris, France.

[18] DiMasi, F., R.H. Eppinger, F.A. Bandak. Computational analysis of head impact response under car crash loadings. In *Proc. 39th Stapp Car Crash Conf.*, 1995.

[19] Fan, W.R.S.: Internal Head Injury Assessment. SAE Paper No. 710870, Proc. 15th Stapp Car Crash Conf., pp. 645-665, Society of Automotive Engineering, New York (USA); 1971.

[20] Fisher, R.A.: Statistical Methods for Research Workers. First ed. Edinburgh, 1925, many later editions.

[21] Gadd, C.W.: Criteria for injury potential. Impact Acceleration Stress, Publication 977, NAS-NRC, pp 141-145; 1962

[22] Gadd, C.W.: Use of a weighted-impulse criterion for estimating injury hazard. SAE Paper No. 660793, Proc. 10th Stapp Car Crash Conference; 1966.

[23] Galford, J.E., J.H. McElhaney. A viscoelastic study of the scalp, brain and dura. J. Biomech. 3:211–221, 1970.

[24] Galbraith, J.A., L.E. Thibault, D.R. Matteson: Mechanical and electrical responses of the squid giant axon to simple elongation. J Biomech Eng, 115 pp. 13-22; 1993.

[25] Gennarelli, T.A.: Analysis of Head Injury Severity by AIS-80. Proc. 24th Annual Conf. of the American Association of Automotive Medicine, pp. 147-155, AAAM, Morton Grove (IL-USA); 1980.

[26] Gennarelli, T.A.: Mechanistic Approach to the Head Injuries: Clinical and Experimental Studies of the Important Types of Injury. Head Injury Criteria - A Consensus Workshop, pp. 20-25; U.S. Government Printing Office, Washington D.C. (USA); 1981.

[27] Genarelli, T.A. Head injury biomechanics: a review. In *???*, pages 9–20, 1987.

[28] Gennarelli T.A., L.E. Thibault, R. Tipperman, G. Tomei, R. Sergot, M. Brown, W.L. Maxwell, D.I. Graham, J.H. Adams, A. Irvine: Axonal injury in the optic nerve: a model simulating diffuse axonal injury in the brain. J Neurosurg, 71, pp. 244-253; 1989.

[29] Gosch, H.H., E. Gooding, R.C. Schneider: Distortion and displacement of the brain in experimental head injuries. Surgical Forum, 20-425-6, 1969.

[30] Gosch, H.H., E. Gooding, R.C. Schneider: The lexan calvarium for the study of cerebral responses to acute trauma. J. Trauma, 10, pp. 370– 376; 1970.

[31] Gurdjian, E.S., J.E. Webster, H.R. Lissner: Observations of the Mechanisms of Brain Concussion, Contusion and Laceration. Surgery, Gyneacology, and Obstetrics, 101, pp. 680-690; 1955.

[32] Gurdjian, E.S., H.R. Lissner, L.M. Patrick: Protection of the head and neck in sports. J. Amer. Med. Assoc., v. 182, pp 509-512; 1962.

[33] Gurdjian, E.S., V.R. Hodgson, L.M. Thomas, L.M. Patrick. The significance of relative movements of scalp, skull and intracranial contents during impact injury of the head. J. Neurosurg. 29:70–72, 1968.

[34] Hardy, W.N., Khalil, T.B., and King, A.I. Literature review of head injury biomechanics. *Int. J. Impact Engng.*, 15:561–586, 1994.

[35] Hardy, W.N., Foster, C.D., King, A.I., and Tashman, S. Update on the study of head-injury kinematics. In *CDC-Proceedings*, pages 177-184, 1998.

[36] Hodgson, V.R., E.S. Gurdjian, L.M. Thomas: Experimental skull deformation and brain displacement demonstrated by flash X-ray technique. J. Neurosurg. 25:49–52, 1966.

[37] Hodgson, V.R., L.M. Thomas: Effect of Long-duration Impact on Head. SAE Paper No. 720956, Proc. 16th Stapp Car Crash Conference, Detroit (MI), USA; 1972.

[38] Holbourn, A.H.S.: Mechanics of Head Injury. Lancet, 2: pp. 438-441; 1943.

[39] Huelke, D.F., W.S. Smock, P.M. Fuller, G.R. Nichols,II: Basilar Skull Fractures Produced by Facial Impacts - Case histories and a review of literature. SAE Paper No. 881711; 1988.

[40] International Organization for Standardization, Working Group 6, U.S. delegation: Position Paper on HIC Levels. ISO/TC22/SC12/WG6-Document N 146; 1983.

[41] Resolution of ISO/TC22/SC12/WG6 (Working Group on Biomechanics); 1991.

[42] Staggering cost of serious auto crashes continues. Journal of American Insurance 59:10–13, 1983.

[43] Kang, H., R. Willinger, B.M. Diaw, B. Chinn Validation of a 3d anatomic human head model and replicatio n of head impact in motorcycle accident by finite element modeling. In *Proc. 41th Stapp Car Crash Conf.*, pages 329–338, 1997. pages 329–338, 1997.

[44] Khalil, T.B. and Hubbard, R.P. Parametric study of head response by finite element modeling. *J. Biomech.*, 10:119–132, 1977.

[45] Khalil, T.B. and Viano, D.C. Critical issues in finite element modeling of head impact. In *Proc. 26th Stapp Car Crash Conf.*, pages 87–102, 1982.

[46] Krischer, J.P.: Indices of Severity: Underlying Concepts. Health Services Research, 11, pp. 143-157; 1976.

[47] Kuijpers, A.H.W.M., Claessens, M.H.A., and Sauren, A.A.H.J. The influence of different boundary conditions on the response of the head to impact: a two-dimensional finite element studyIn *Traumatic brain injury: Bioscience and mechanics.* , edited by Bandak, F.A., Eppinger, R.H., and Ommaya, A.K., chapter 22, pages 197–206. Mary Ann Liebert Inc., 1995.

[48] Lee, M.C., R.C. Haut. Insensitivity of tensile failure properties of human bridging veins to strain rate: implications in the biomechanics of subdural hematoma. J. Biomech. Eng. 22:537–542, 1989.

[49] LeFort, R.: Experimental Study of Fractures of the Upper Jaw, Part III. Plast. Reconstr. Surg. 50 (4), pp. 600-607; 1972.

[50] Lin, S.-C. and Grimm, M.J. Characterization of the mechanical properties of brain tissue using ultrasound. In *CDC-Proceedings*, pages 59–64, 1998.

[51] Lissner, H.R., M. Lebow, F.G. Evans: Experimental studies on the relation between acceleration and intracranial pressure changes in man. Surg. Gyn. Obst., v. 111, pp 320-338; 1960.

[52] Low, T.C., R.L. Stalnaker: A Lumped Parameter Approach to Simulate the Rotational Head Motion. Proc. of the 1987 Int. IRCOBI Conf., IRCOBI Secr., Bron (F); 1987.

[53] Margulies, S.S., Thibault, L.E., and Gennarelli, T.A. Physical simulations of brain injury in the primate. *J. Biomech.*, 8:823–836, 1990.

[54] McElhaney, J.H., R.L. Stalnaker, V.L. Roberts: Biomechanical Aspects of Head Injury. Human Impact Response - Measurement and Simulation, Proc. of the Symposium on Human Impact Response, W.F. King and H.J. Mertz eds., pp. 85-110, Plenum Press, New York (USA); 1973.

[55] Mendis, K.K. Finite element modeling of the brain to establish diffuse axonal injury criteria. PhD dissertation, Ohio State University, 1992.

[56] Mendis, K.K., Stalnaker, R.L., and Advani, S.H. A constitutive relationship for large deformation finite element modeling of brain tissue. *J. Biomech. Eng.*, 117:279–285, 1995.

[57] Mullen, R., T. Belytschko. Dispersion analysis of finite element semidiscretizations of the two- dimensional wave equation. Int. J. Num. meth. Eng. 18:11–29, 1982.

[58] Nahum, A.M., Smith, R., and Ward, C.C. Intracranial pressure dynamics during head impact. In *Proc. 21th STAPP Car Crash Conf.*, pages 339–366, 1977.

[59] Newman, J.A.: Head Injury Criteria in Automotive Crash Testing. SAE Paper No. 801317, Proc. 24th Stapp Car Crash Conf., pp. 701-747, Society of Automotive Engineering, New York (USA); 1980.

[60] Newman, J.A.: Temporal characteristics of translational acceleration in the prediction of helmeted head injury. Impact Injury Caused by Linear Acceleration: Mechanics, Prevention and Costs, AGARD Conf. Proc. No. CP-322, pp. 4.1-4.7, Advisory Group for Aerospace Research and Development, Neuilly Sur Seine, France; 1982.

[61] Newman, J.A.: A Generalized Acceleration Model for Brain Injury Threshold (GAMBIT). Proc. of the 1986 Int. IRCOBI Conf., IRCOBI Secr., Bron (F); 1986.

[62] Nusholtz, G.S. and Shi, Y. Physical reality in FE head models: rotation and strain. In *Proc. STAPP Car Crash Conf. SAE980355*, pages 37–54, 1998.

[63] Ommaya, A.K.: Mechanisms and Preventive Management of Head Injuries, a Paradigm for Injury Control. Proc. 32nd AAAM conference; 1988.

[64] Ommaya, A.K., Thibault, L.E., and Bandak, F.A. Mechanisms of head injury. *Int. J. Impact Engng.*, 5:5350–560, 1994.

[65] Ono, K., A. Kikuchi, M. Nakamura, H. Kobayashi, N. Nakamura: Human head tolerance to sagittal impact reliable estimation deduced from experimental head injury using subhuman primates and human cadaver skulls. SAE Paper 801303, Proc. 24th Stapp car Crash Conference, Northfield Hilton, Troy (MI), USA, October 15-17; 1980.

[66] Padgaontar, A.J., K.W. Krieger, A.I. King. Measurement of angular acceleration of a rigid body using linear accelerometers. J. Appl. Mech. 42:552–556, 1975.

[67] Peters, G.W.M., J.H. Meulman, A.A.H.J. Sauren. The applicability of the time/temperature superposition principle to brain tissue. *Biorheology*, 34:127–138, 1997.

[68] Pike J.A.: Automotive safety - Anatomy, Injury, Testing and Regulation. Society of Automotive Engineering, Inc., 400 Commonwealth Drive, Warrendale, PA 15069-0001, USA; 1990.

[69] Prasad, P., J.W. Melvin, D.F. Huelke, A.I. King, G.W. Nyquist: Chapter 1 - Head. from : Review of Biomechanical Impact response and Injury in the Automotive Environment., J.W. Melvin and K. Weber eds., report No. DOT HS 807 042, U.S. Dept. of Transport - NHTSA, Washington D.C., USA; 1985.

[70] Prange, M.T., Meaney, D.F., and Margulies, S.S. Directional properties of gray and white matter tissue. In *CDC-Proceedings*, pages 65–71, 1998.

[71] Ran, A., M. Koch, H. Mellander: Fitting Injury versus Exposure Data into a Risk Function. Proc. 1984 Int. IRCOBI Conf. on the Biomech. of Impact, held at Delft (NL); IRCOBI Secr., Bron (F); 1984.

[72] Rojanavanich, V., R.L. Stalnaker: Sensitivity Analysis for the Translational Energy Criteria: Overall Head Injuries. Proc. of the 1989 Int. IRCOBI Conf., held at Stockholm (S), IRCOBI Secr., Bron (F); 1989.

[73] Ruan, J.S., T. Khalil, A.I. King. Human head dynamic response to side impact by finite element modeling. J. Biomech. Eng. 113:276–283, 1991.

[74] Ruan, J.S., T. Khalil, A.I. King. Intracranial response of a three-dimensional human head finite element model. Proc. Injury Prevention through Biomechanics Symposium, Wayne State University, p 97-103, 1991.

[75] Ruan, J.S., T. Khalil, A.I. King. Finite element analysis of the human head to impact. Advances in Bioengineering, ASME-BED 22: 249–252, 1992.

[76] Ruan J.S., T. Khalil, A.I. King Dynamic response of the human head to impact by three-dimensional finite element analysis. J. Biomech. Eng. 116:44-50. 1994.

[77] Ruan J.S., P. Prasad Coupling of a finite element human head model with a lumped parameter Hybrid III dummy model: preliminary results. J. Neurotrauma 12:725-34, 1995.

[78] Ruan J.S., P. Prasad Study of the biodynamic characteristics of the human head. In *1996 Int. IRCOBI Conf. Biomech. Impacts*, pages 63–73, 1996.

[79] SAE J885 JUL86: Human Tolerance to Impact Conditions as related to Motor Vehicle Design. Society of Automotive Engineering, Inc. (USA); 1986.

[80] Sauren, A.A.H.J. and Claessens, M.H.A. Finite element modeling of head impact: the second decade. In *1993 Int. IRCOBI Conf. Biomech. Impacts*, pages 241–254, 1993.

[81] Sheldon, C.H., R. Pudenz, J.S. Restarski, W.M. Craig. The lucite calvarium – a method for direct observation of the brain. J. neurosurg. 1:67–75, 1944.

[82] Shuck, L.Z., S.H. Advani. Rheological response of brain tissue in shear. J. Basic Eng. 94:905–911, 1972.

[83] Shugar, T.A. A finite element head injury model. Report no. DOT HS 289-3-550-TA, vol. I, 1977.

[84] Slattenscheck, A., W. Tauffkirchen: Critical Evaluation of Assessment Methods for Head Impact Applied in Appraisal of Brain Injury Hazard in Particular Head Impacts on Windshields. Int. Automobile Safety Conf. Compendium, pp. 280-301, Society of Automotive Engineering, New York (USA); 1970.

[85] Stalnaker, R.L., J.H. McElhaney: Head Injury Tolerance for Linear Impacts by Mechanical Impedance Methods. ASME 70-WA/BHF-4, American Society of Mechanical Engineers, New York (USA); 1970.

[86] Stalnaker, R.L., J.H. McElhaney, V.L. Roberts: MSC Tolerance Curve for Human Head Impacts. ASME Winter Anual Conf. 71-WA/BHF-10, American Society of Mechanical Engineers, New York (USA); 1971.

[87] Stalnaker, R.L., A.C. Lin, D.A. Guenther: The Application of the New Mean Strain Criterion (NMSC). Proc. of the 1985 Int. IRCOBI/AAAM Conf., held at Goteborg (S), pp. 191-209, IRCOBI Secr., Bron (F); 1985.

[88] Stalnaker, R.L., T.C. Low, A.C. Lin: Translational Energy Criteria and its Correlation with Head Injury in the Sub-human Primate. Proc. of the 1987 Int. IRCOBI/AAAM Conf., held at Birmingham (UK), IRCOBI Secr., Bron (F); 1987.

[89] Tarriere, C.: Head Injury Criterion (HIC). Head and Neck Injury Criteria - A Consensus Workshop, pp. 218-228, A.K. Ommaya ed., U.S. Dept. of Transport, NHTSA, Washington D.C., USA; 1981.

[90] Tarriere, C.: Relationship between Experimental Measuring Techniques and Real World Accidents. Head Injury Mechanics, Symposium Report, New Orleans (LO-USA), Published by AAAM, Des Plaines (IL-USA); 1987.

[91] Thibault, L.E. Brain injury from the macro to the micro level and back again: What have we learned to date? In *1993 Int. IRCOBI Conf. Biomech. Impacts*, pages 3–25, 1993.

[92] Tortora, J.A.: Principles of Human Anatomy.

[93] Turquier, F., H. Kang, X. Trosseille, R. Willinger, F. Lavaste, C. Tarrierre, A. Domont. Validation study of a 3d finite element head model against experimental data. In *Proc. 40th Stapp Car Crash Conf.*, pages 283–293, 1996.

[94] Verhoeve, R. final report SAI, 1999.

[95] Versace, J.: A Review of the Severity Index. SAE Paper No. 710881, Proc. 15th Stapp Car Crash Conference, Coronado (CA), USA, November 17-19; 1971.

[96] Viano, D., Aldman, B., Pape, K., van Hoof, J., and von Holst, H. Brain kinematics in physical model tests with translational and rotational acceleration. *I.J. Crash*, 2:191–205, 1997.

[97] Viano, D., H. von Holst, E. Gordon. Serious brain injury from traffic-related causes: Priorities for primary prevention.

[98] Ward, C.C., R.B. Thompson. The develpment of a detailed finite element brain model. Proc. 19th Stapp Car Crash Conference, SAE, 641–674, 1975.

[99] Ward, C.C.: Finite Element Models of the Head and Their Use in Brain Injury Research. SAE paperno. 821154; 1982.

[100] Ward, C.: Finite Element Modeling of the Head and Neck. Impact Injury of the Head and Spine, Ewing C.L., D.J. Thomas, A. Sances Jr., S.J. Larson eds; ISBN 0-398-04702-2, Charles C. Thomas publisher, Springfield (IL-USA); 1983.

[101] Willinger, R., L. Taleb, C.M.J. Kopp. Modal and temporal analysis of head mathematical models. Neurotrauma 12:743-54, 1995.

[102] Zhou, C., T.B. Khalil, A.I. King. A new model comparing impact responses of the homogeneous and inhomogeneous human brain. Proc. 39th Stapp Car Crash Conference, SAE, 121–137, 1995.

[103] Zhou, C., T.B. Khalil, A.I. King. Viscoelastic response of the human brain to saggital and lateral rotational acceleration by finite element analysis. In *1996 Int. IRCOBI Conf. Biomech. Impacts*, pages 35–48, 1996.

CHAPTER 5

SPINE INJURY BIOMECHANICS

5.1 Introduction

The spine consists of three parts: the lumbar, the thoracic and the cervical spine. Since thoracic and lumbar spine injuries are less common in traffic accidents than cervical injuries, the emphasis in this Chapter will be on the cervical spine (or neck). The incidence of neck injuries in traffic accidents appears to be relatively low compared to for instance head injuries, except for specific accident configurations like a rear end collision where more than 50% of the injuries appear to be in the neck area (see Table 2.2). The longterm consequences of neck injuries however are often very serious, even in case of "minor" injuries (so-called whiplash injuries) which are rated as AIS=1 according to the AIS anatomical injury scale discussed in Chapter 3. It is estimated that 20% of all traffic fatalities in the United States are due to cervical injuries and about 500 cases of quadriplegia per year result from a traffic accident [1]. The IPR (Injury Priority Rating) which weighs motor vehicle injuries by body region in terms of total societal costs (see Table 3.5), rates neck injuries about 5% of the total IPR, which makes neck injuries the fifth most important injury category (after head, face, chest and abdomen).

One important mechanical function of the spinal column is to provide protection to the spinal cord. This protective role is comparable to the function of the skull in protecting the brains. Injuries of the spinal cord can result in severe disability (para- or quadriplegia) and death. Another important function of the the neck is to act as the principal load-bearing structure of the head and to provide mobility between head and torso. Due to this multitude of functions the cervical spine is a rather complex structure. Section 5.2 provides a brief description of the relevant anatomy.

Injuries of the neck are usually caused by indirect loading through the head, either by inertial loading or by an impact on the head. The incidence of injuries due to a direct loading on the neck itself is relatively small and will not be discussed here further. Section 5.3 introduces the most important injury mechanisms and injury types which can be observed in the cervical column.

The mechanical response of the cervical column under impact conditions can be studied by biomechanical models. Section 5.4 discusses several methods. Special attention is given to biofidelity performance requirements for crash dummies derived from an extensive series of human volunteer tests.

Various injury tolerance values for the cervical column and their limitations will be discussed in Section 5.5. Some directions for future research will be given in Section 5.6.

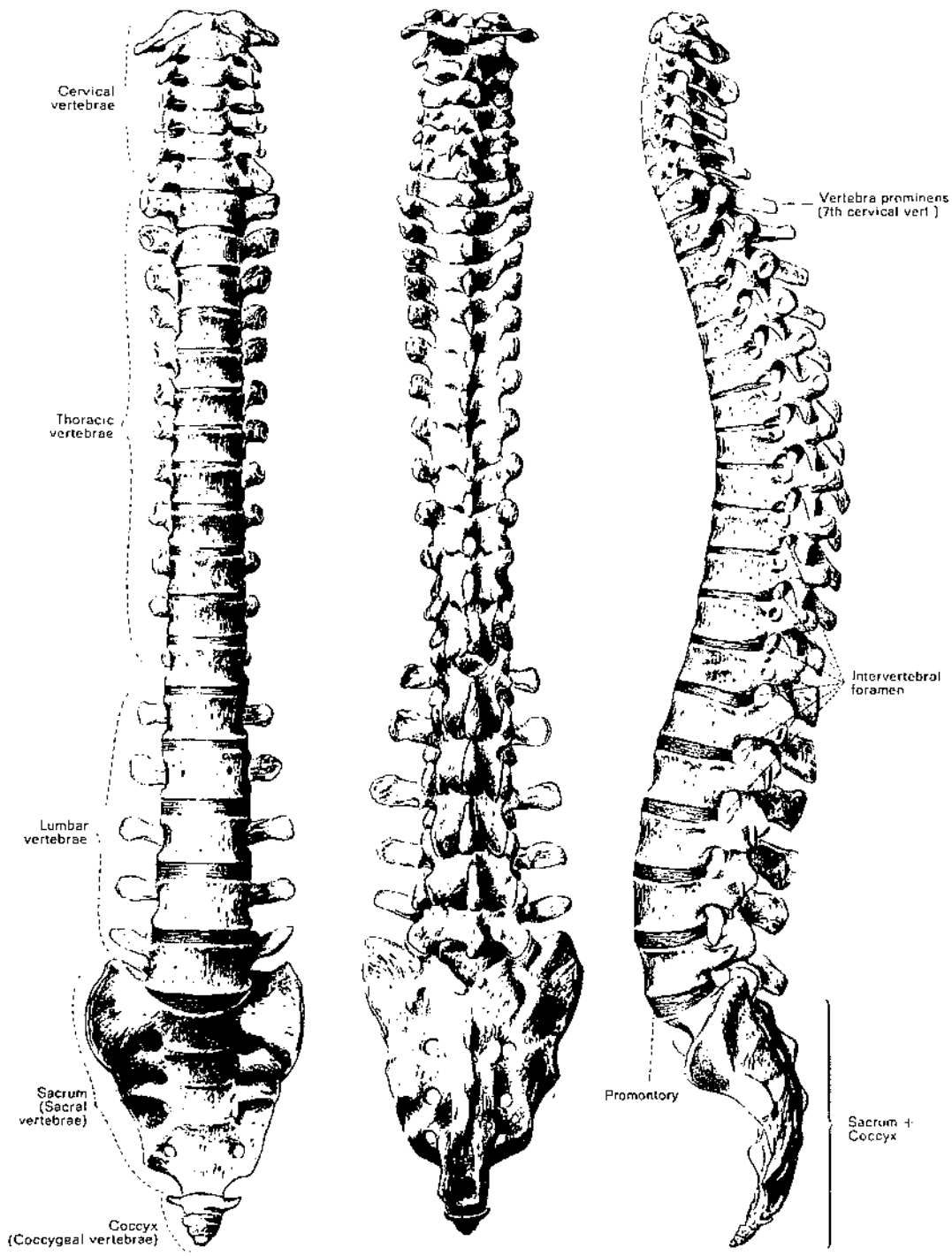

Fig. 5.1 *Anterior (left), posterior (middle) and lateral (right) view of the vertebral column [2].*

5.2 Anatomy

The cervical spine consists of seven bones, called vertebrae, which are connected by soft tissue like intervertebral disks, ligaments and muscles. These vertebrae usually are referred to as C1....C7 where C1 represents the upper vertebra (Fig. 5.1). In a similar way the thoracic spine is made up of 12 vertebrae (T1...T12) and the lumbar spine of 5 vertebra (L1....L5). The entire vertebral column is supported by the sacrum, which is connected to the pelvic girdle.

Except for C1 and C2, the vertebrae are quite identical in structure although the cervical vertebrae are smaller than the thoracic and lumbar vertebrae. A vertebra is made up of the "body" at the anterior side and the "neural arch" at the posterior side. The body consists of spongy bone surrounded by a layer of compact bone. The neural arch is a bony ring that ends posteriorly in the spinous process and lateral on each side in the transverse process. The processes are the attachment points for the ligaments and muscles. The neural arch surrounds an open area called vertebral foramen which forms together with the other vertebral foramina the vertebral canal through which the spinal cord passes. Fig. 5.2 shows a vertebra schematically.

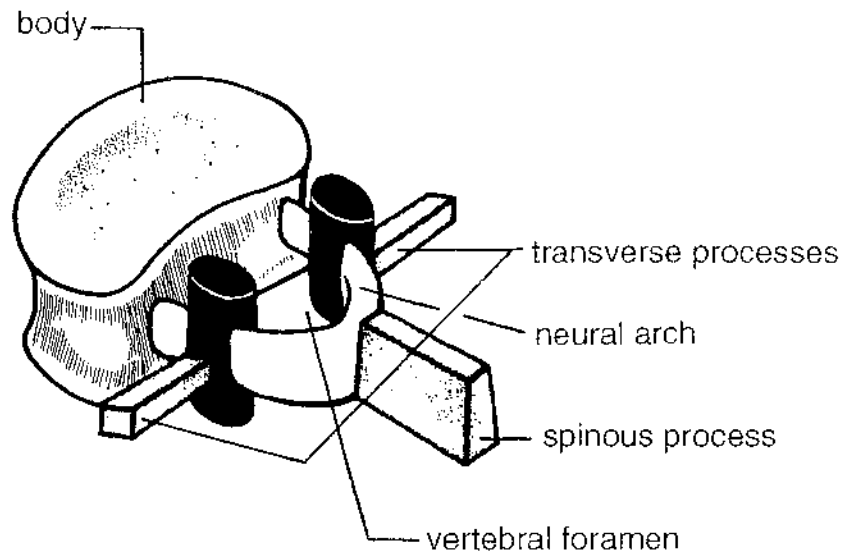

Fig. 5.2 A schematic representation of a vertebra [3].

The load-bearing function of the vertebral column is realized by two load paths: one at the posterior side and one at the anterior side. The first load path is through the bodies of the vertebrae which are connected by intervertebral disks. A disk is a fibro-cartilaginous structure which allows a certain amount of movement between the connected bodies and which can act as a shock absorber. The second load path is through the neural arch of a vertebra which is provided for this purpose by four articulation surfaces, called facets: two at the superior side and two at the inferior side. These surfaces articulate with the facets of the vertebrae above and below, the so-called facet joints.

The two upper cervical vertebra (C1 and C2) differ considerably in structure from the other. The first cervical vertebra (C1) is called atlas and can be considered as a ring of bone (Fig. 5.3). The atlas is provided at the superior side with a pair of facets, each covered with cartilage, which articulate with the base of the skull, the atlanto-occipital joint. The skull part of this articulation is formed by the condyles of the occipital bone referred to as occipital condyles. This articulation allows a nodding motion of the head. The second cervical vertebra (C2) is called axis. It has at the superior side of the body a small process of bone, the dens. This dens fits in the anterior side of the vertebral foramen of the atlas. The atlanto-axial joint allows rotational movement of the head.

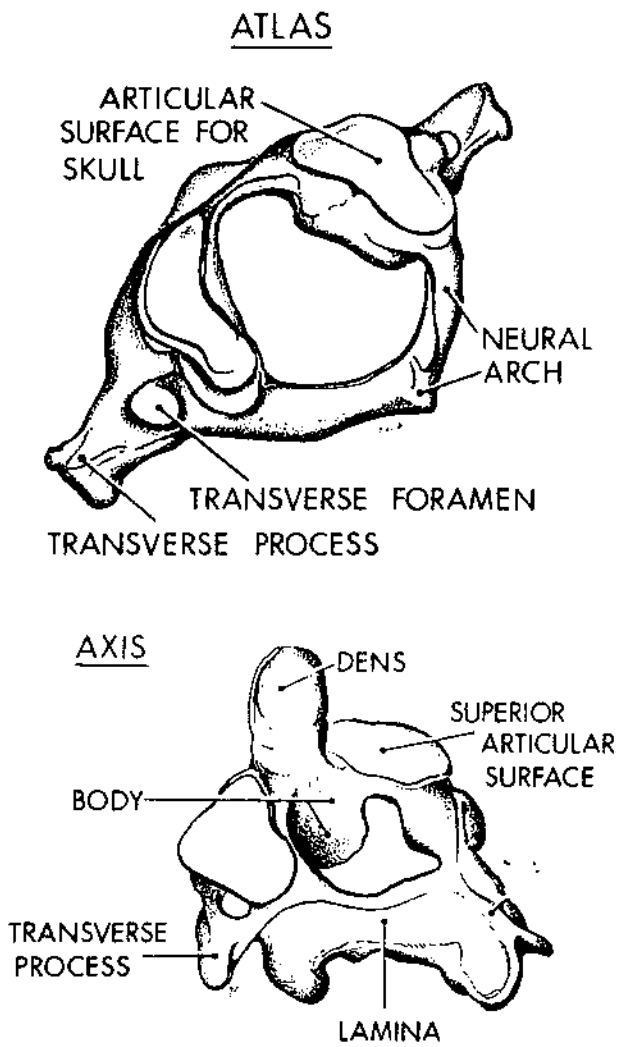

Fig. 5.3 *The atlas and axis [8]*

Finally the most important ligament structures will be mentioned here. At the anterior side the bodies of the vertebra are connected by the anterior longitudinal ligament which runs over the entire length of the spine, i.e. from the skull to the tailbone. It limits the range of extension motion. A similar ligament is located at the posterior side of the bodies: the

posterior longitudinal ligament. Also this ligament is a continuous ligament connecting all vertebrae. Inside the vertebral canal is a series of ligaments called ligamentum flavum connecting adjacent vertebrae but not continuous like the anterior and posterior longitudinal ligaments. The facet joints mentioned before are completely surrounded by ligamentous tissue: the capsular ligaments. Important ligaments at the posterior side of a vertebra are the interspinous ligaments and superspinous ligament. This last ligament also connects the entire spine. It is called ligamentum nuchae in the cervical area. Flexion motion of the head is partly controlled by this ligament.

5.3 Injuries and injury mechanisms

The cervical spine offers a relatively large mobility in a multitude of directions. This mobility in relation to the various loading conditions which may arise in case of an accident can cause a large number of different injury mechanisms. This Section shall be limited to loading in the mid-sagital plane. The following four important categories of injury mechanisms will be discussed here [4]: "tension-flexion", "tension-extension", "compression-flexion" and "compression-extension".

In case of the "tension" mechanisms inertial loading of the head plays an essential role. The "tension-flexion" mechanism is typical for a frontal vehicle collision in which the torso is restrained by a restraint system and where the head is pulled forward by inertial forces resulting in (hyper)-flexion of the neck. Laboratory experiments by Schmidt [5] with 100 unembalmed human cadavers restrained by a 3-point belt system showed damage in the C7-T1 area in 46 out of the 100 tests. The deceleration levels were relatively small (16.9-25.6 g). In cadaver tests by Cheng [6] at higher load levels (34-38 g) separation injuries in the upper neck area (atlanto-occipital and atlanto-axial joint) were reported. Field accident studies, however, show that the risk of serious injuries in this loading condition is small. An exception might be small children under extreme loading conditions due to their relatively large head mass compared to the strenght of the neck [7].

The "tension-extension" mechanism is typical for a rear-end collision. Inertial loading pulls the head backwards due to which the neck comes into (hyper)-extension. This mechanism is considered to be the most important cause of so-called "whiplash" injuries, an AIS=1 injury with often long-lasting effects. The injury causing mechanism for this injury is not well understood yet. Soft tissue "damage" is involved but can not be determined clinically with current available techniques. In severe loading conditions the "tension-extension" mechanism can cause fracture of the vertebral body (i.e. chip of bone pulled off at the anterior side) due to extreme stretching of the anterior longitudinal ligament (Fig. 5.4). More severe fractures, like a "Hangman's fracture" (i.e. a fracture-dislocation of C2), can occur if a frontal head impact, for instance due to the chin impacting the instrument panel or the forehead impacting the windshield, causes the "tension-extension" mechanism.

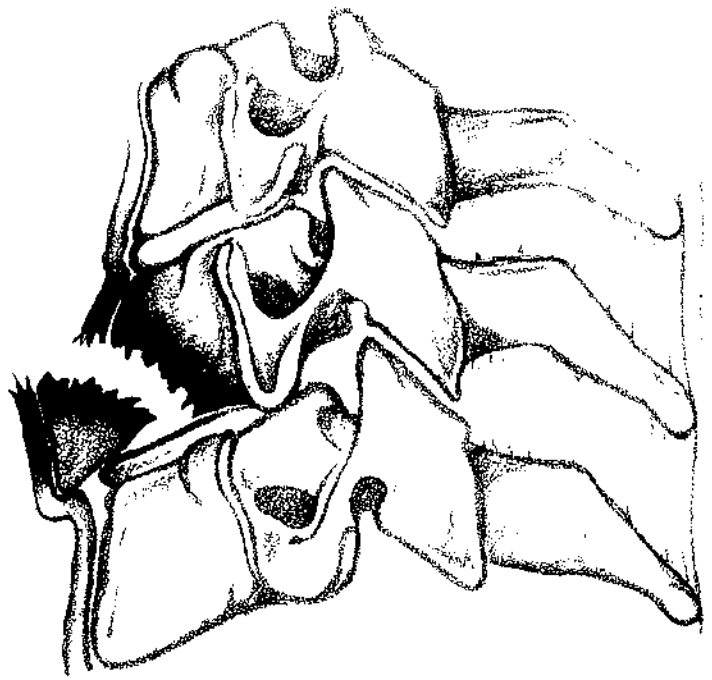

Fig. 5.4 *Fracture of the vertebral body due to the "tension-extension" mechanism [8]*

In case of a "compression" mechanism a contact force is acting on the head, directed in such a way that compression of the cervical column occurs. Depending on the location of the contact point and the initial position of the head either a "compression-flexion" or a "compression-extension" mechanism will take place.

The "compression-flexion" mechanism can result in several types of fracture of the vertebral body (wedging and bursting fractures). Also dislocations, locked facets and torn posterior ligaments may be the result of this injury mechanism (Fig. 5.5). Damage of the cord is likely in this latter case as well.

Fig. 5.5 *Ligament rupture and facet dislocation due to the "compression-flexion" mechanism [8]*

The "compression-extension" mechanism finally can cause fracture of the neural arch components (including spinous process) of one or more vertebrae. In case of severe impacts also inferior facets may fracture and dislocation might occur.

It should be noted here that above descriptions represent idealized loading conditions and that not all mechanisms are completely understood yet. In laboratory experiments with human cadavers it appeared to be often difficult to reproduce above mechanisms due to absence of muscle tone. In real accidents loading conditions will be often much more complicated and as a consequence also the resulting injuries, particularly if lateral bending and twist of the neck is involved.

5.4 Biomechanical response

5.4.1 Introduction

Several reasons can be identified why biomechanical reponse data for the human neck are needed. First of all they are needed to identify neck injury mechanisms and associated injury criteria and tolerance data. Furthermore they represent the basis for definition of biofidelity performance requirements for mechanical neck simulators. Realistic simulation of the neck response in a dummy is of particular importance to get a humanlike dynamical behaviour of the dummy head. Trajectories of the head and the nature of the head contact with vehicle interior or exterior are critically dependent on the dummy's neck design. Finally also the thoracic response of a dummy to impact will be dependent on the response of the mechanical neck.

Biomechanical response data for the cervical spine have primarily been studied in the past on the basis of tests with human volunteers and cadavers. Such tests can be subdivided into static tests, dynamic tests without head impact and dynamic tests with head impact. Human cadaver tests can be subdivided into tests on isolated neck structures, tests on head-neck assemblies and tests involving a complete cadaver. An example of a static volunteer test is given in Fig. 5.6. The purpose of this test conducted by Mertz and Patrick [9] was to determine the neck loads a volunteer is willing to tolerate. Results of such tests are presented in Section 5.5. Fig. 5.7 shows various test methods using complete cadavers for the study of neck response in case of head impact, including drop and impacter tests.

This Section further will deal specifically with tests conducted to determine biofidelic neck performance requirements in case of no head impact. First a brief review will be given of work conducted in the seventies dealing with neck response in the mid-sagittal plane which still is the basis of the biofidelity performance requirements of current frontal impact dummies (Section 5.4.2). In subsequent Sections 5.4.3-5.4.8 an extensive review will be given of human neck response in several impact directions based on voluminous data

acquired at the Naval Biodynamics Laboratory in New Orleans which were analyzed by TNO. First a description of the human volunteer test methodology is given (Section 5.4.3), followed by an analysis of the motion of T1 in these tests (Section 5.4.4) and the motion of the head (Section 5.4.5). Resulting performance requirements are presented in Section 5.4.6 followed by a comparison with frontal cadaver tests which were conducted in similar test conditions (Section 5.4.7). A general discussion concludes this biomechanical response Section (Section 5.4.8).

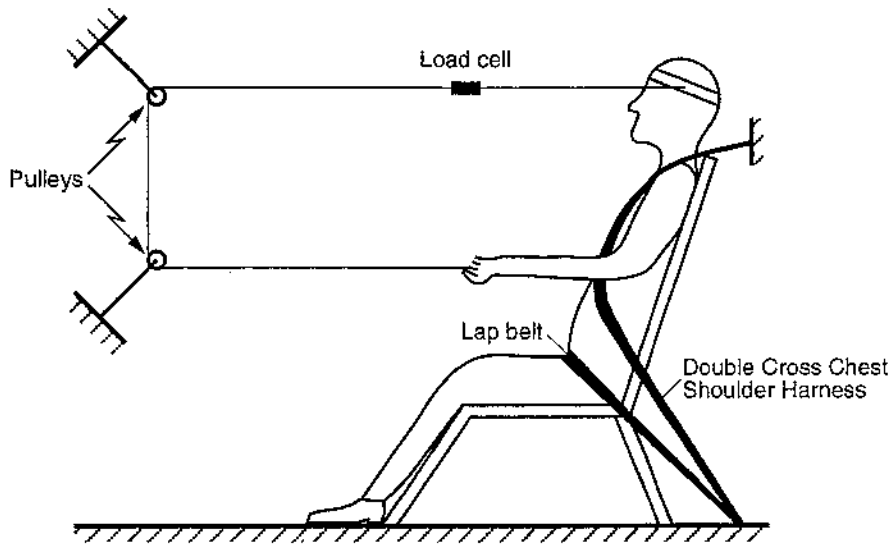

Fig. 5.6 *Static human volunteer test [9]*

5.4.2 Earlier neck performance requirements in frontal direction

In the early seventies performance requirements for dynamical head-neck behaviour in frontal impacts were proposed by Mertz and Patrick [9] based on tests with volunteers and human cadavers. Neck response was defined by the relation between the torque about the occipital condyles and the angular position of the head. Resulting performance corridors specifically for the loading phase are shown in Fig. 5.8.

For unloading motion a ratio was defined for the area under the unloading curve with respect to the area under the loading curve. Separate corridors for flexion and extension motions were developed. Human volunteer dynamical tests in this study were limited to one subject, partly tested with an additional weight attached to the head.

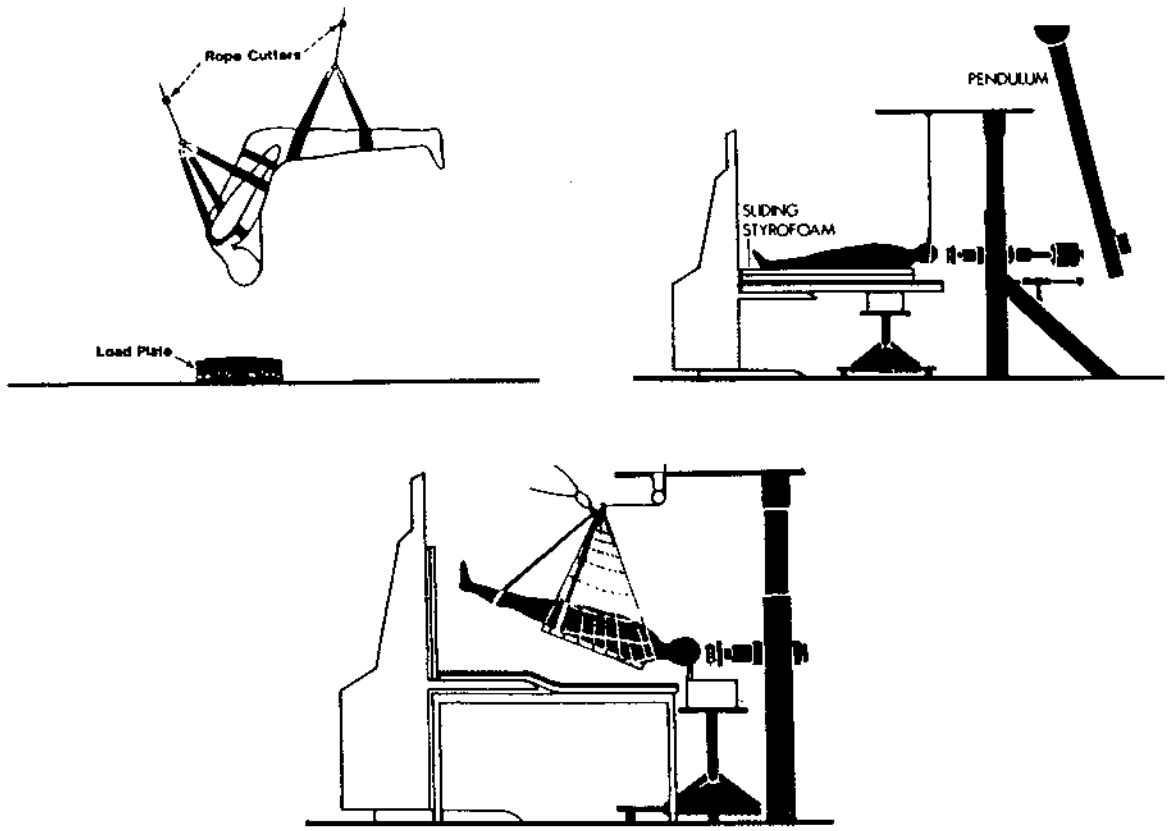

Fig. 5.7 *Different test methods to study neck response using a complete cadaver [10]*

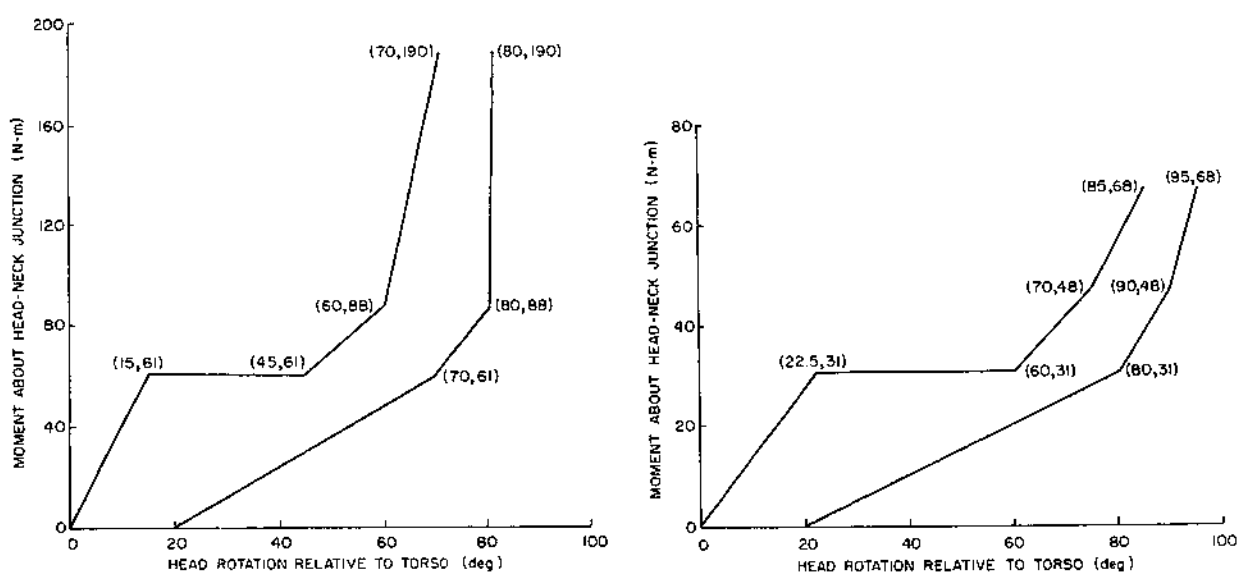

Fig. 5.8 *Head-neck response envelops in flexion and extension for the loading phase according to Mertz and Patrick [9]. (Left: flexion; Right: extension)*

Such requirements, however, are not sufficient conditions to ensure humanlike response, since they are limited to the head rotation. Additional requirements are needed such as the head center of gravity trajectory. A study by Muzzy and Lustick [11] illustrates the need for these type of requirements. In their study displacements of the Hybrid II head-neck system (i.e. a crash dummy specified in regulations in the USA; see also Chapter 7) were compared with human volunteers in 10 g frontal impacts. The complete dummy was tested in a restraint system similar to that of the human volunteers. Significant differences in the head center of gravity and the head angle relative to the torso were observed: the Hybrid II neck was found to be stiffer than the volunteer.

5.4.3 Test methodology human volunteer tests

The Naval Biodynamics Laboratory (NBDL) in New Orleans has conducted an extensive research program over the past years to determine the head-neck response of volunteer subjects to impact acceleration. In the tests the subjects are seated in an upright position on a HYGE Accelerator and exposed to short duration accelerations simulating frontal, oblique or lateral impacts. The resulting three-dimensional motions of the head and first thoracic vertebral body (T1) are monitored by anatomically mounted clusters of accelerometers and photographic targets (Fig. 5.9). A detailed description of the instrumentation and test methods is provided in [12,13].

In the frontal impact tests, the subjects are restrained by shoulder straps, a lap belt and an inverted V-pelvic strap tied to the lap belt. Upper arm and wrist restraints were used to prevent flailing [13]. In addition a loose safety belt around the chest is employed. The same restraint system is used in lateral and oblique tests along with a 25 cm wide chest strap to minimize the load on the right shoulder. In addition a lightly padded wooden board is placed against the right shoulder of the subject to limit the upper torso motion. Fig. 3.1 shows the initial position of an instrumented volunteer.

TNO has analyzed a large number of tests involving 15 different subjects [15]. Mean values of the sled acceleration-time histories for the most severe frontal, lateral and oblique tests are shown in Fig. 5.10. The volunteers were willing to accept higher impact severities in frontal than in lateral impacts as can be seen in this Figure. The impact severity for oblique impacts is in between.

Fig. 5.11 illustrates the location of the head and T1 anatomical coordinate systems as defined by NBDL. Both coordinate systems are orthogonal and right-handed. Three dimensional X-ray techniques were used to specify in each test these coordinate systems relative to head and T1 anatomical landmarks. The initial nominal orientation (i.e. before moving of the sled) of these systems relative to the laboratory and the sled coordinate systems for the 3 impact directions, is illustrated in Fig. 5.12. More details on the definition of the NBDL coordinate systems are provided in [5,15].

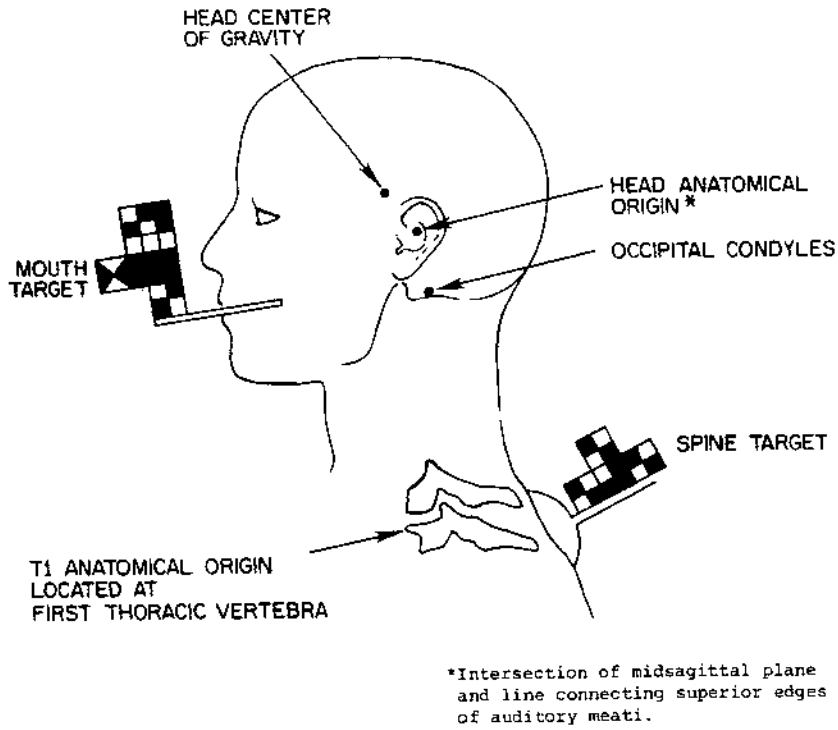

Fig. 5.9 *NBDL human volunteer test.*

The distance between T1 and head anatomical origin just before impact (time = 0) is called initial neck length. For different tests with the same subject considerable variations in this initial neck length, and also in the initial orientation of the T1 coordinate system, were observed [14]. These differences were attributed in part to errors in the specification of the T1-instrumtation. Therefore a new corrected T1 coordinate system has been introduced which was obtained in the following way:

- For each subject an average initial neck length is determined on the basis of calculated initial neck length values for each test.
- The origin of the T1 coordinate system is shifted vertically with respect to the laboratory in such a way that the initial neck length becomes identical to the subject's average initial neck length.
- Finally the T1 coordinate system is rotated so that it becomes aligned with the sled (laboratory) coordinate system. As a consequence the orientation of the corrected T1 coordinate system relative to the T1 vertebral body will be dependent on the impact direction. In lateral (oblique) direction it is rotated nominally 90 degrees (45 degrees) with respect to its orientation in frontal direction. Fig. 5.12 includes the orientation of the corrected T1 coordinate system.

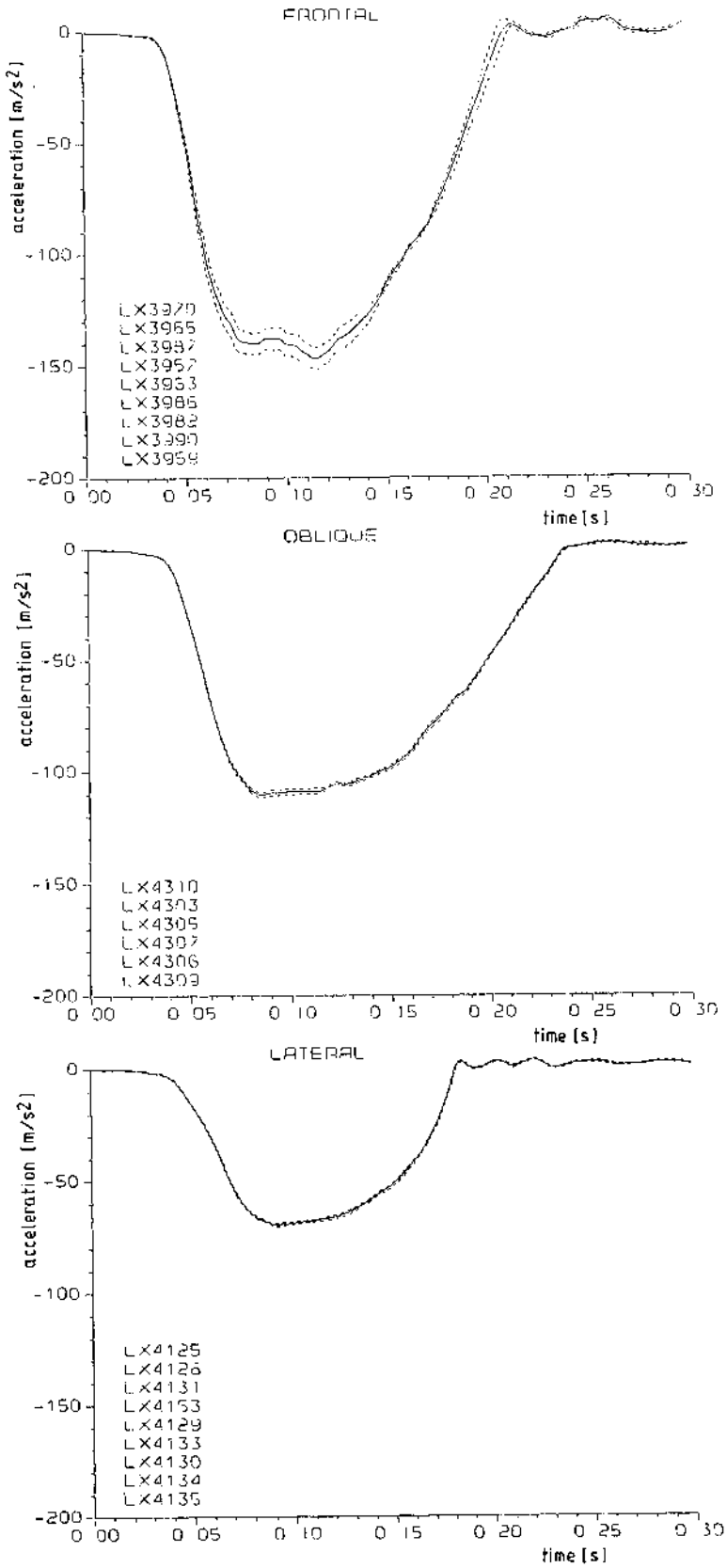

Fig. 5.10 *Mean sled acceleration-time histories for most severe frontal, oblique and lateral impacts. (———— mean value, ------ corresponding standard deviation, LX .....: test number)*

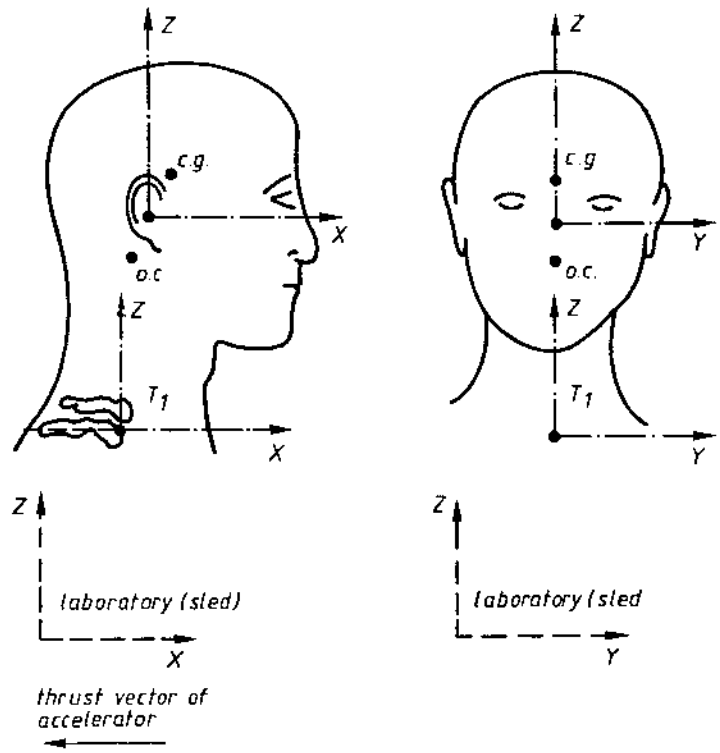

Fig. 5.11 *Location of anatomical coordinate systems according to NBDL (o.c. = occipital condyles, c.g. = center of gravity).*

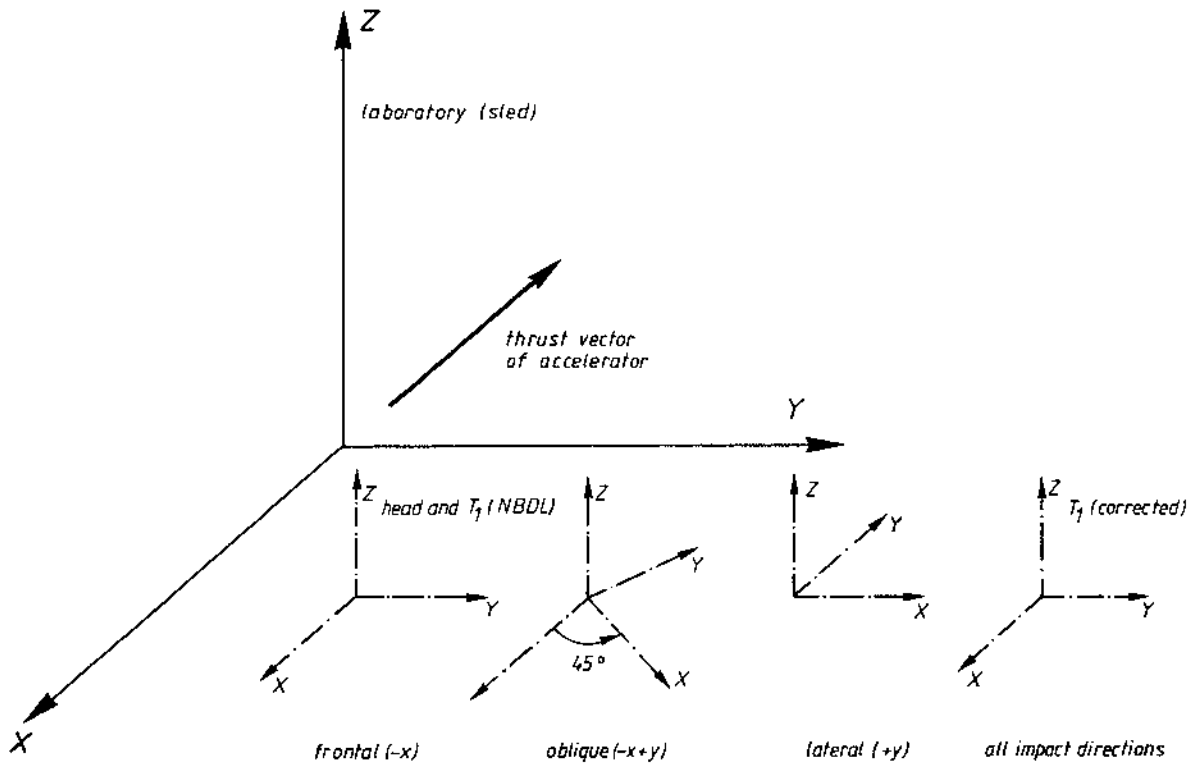

Fig. 5.12 *Nominal initial orientation of head and T1 (NBDL) anatomical coordinate systems relative to laboratory and sled coordinate system in case of frontal, oblique and lateral impacts. Also the orientation of the corrected T1 coordinate systems is included.*

At NBDL detailed anthropometric measurements are conducted for each subject as part of the test protocol. In order to calculate neck load, estimates had to be made for the head mass distribution. The subjects head mass and the principal moments of inertia have been based on regression equations proposed by McConville et al. [17] using measured head anthropometry data. For details on the selected regression equations see [18].

The orientation of the principal inertia axes, location of center of gravity and location of occipital condyles are assumed to be subject independent. Assumptions for these parameters are based on data in literature [15]. Table 5.1 summarizes these data.

Table 5.1 *Subject independent anthropometric data estimated on the basis of data in the literature (relative to head anatomical coordinate system).*

	x (cm)	y (cm)	z (cm)
center of gravity*)	1.2	0	2.9
occipital condylar point	-1.1	0	-2.6
principal axis system	rotated -36° about anatomical y-axis (backwards)		

* including correction for instrumentation

5.4.4 T1 motions

A detailed analysis has been performed of the displacements and accelerations of T1. It was shown that the only significant displacement of T1 exists in the direction of impact (i.e. along the sled thrust vector) [14]. Therefore vertical and lateral T1 displacements have been neglected further. In addition also rotation of T1 was observed (see Section 5.4.7). For the analysis of the head motion, to be presented in the next Section, this T1 rotation has been neglected.

Fig. 5.13 shows for each impact direction separately mean values resulting from the most severe tests for the T1 horizontal acceleration as a function of time. The corresponding standard deviation is incorporated in this Fig.. It can be seen that the T1 accelerations deviate considerably from the sled accelerations presented in Fig. 5.10. For all impact directions initially a large spike can be observed due to the interaction between the thorax and the restraint system. As a consequence the peak input acceleration experienced by the head neck system is about twice the peak sled acceleration.

Further it follows that the 15 g frontal tests clearly are the most severe tests in terms of input to the head-neck system.

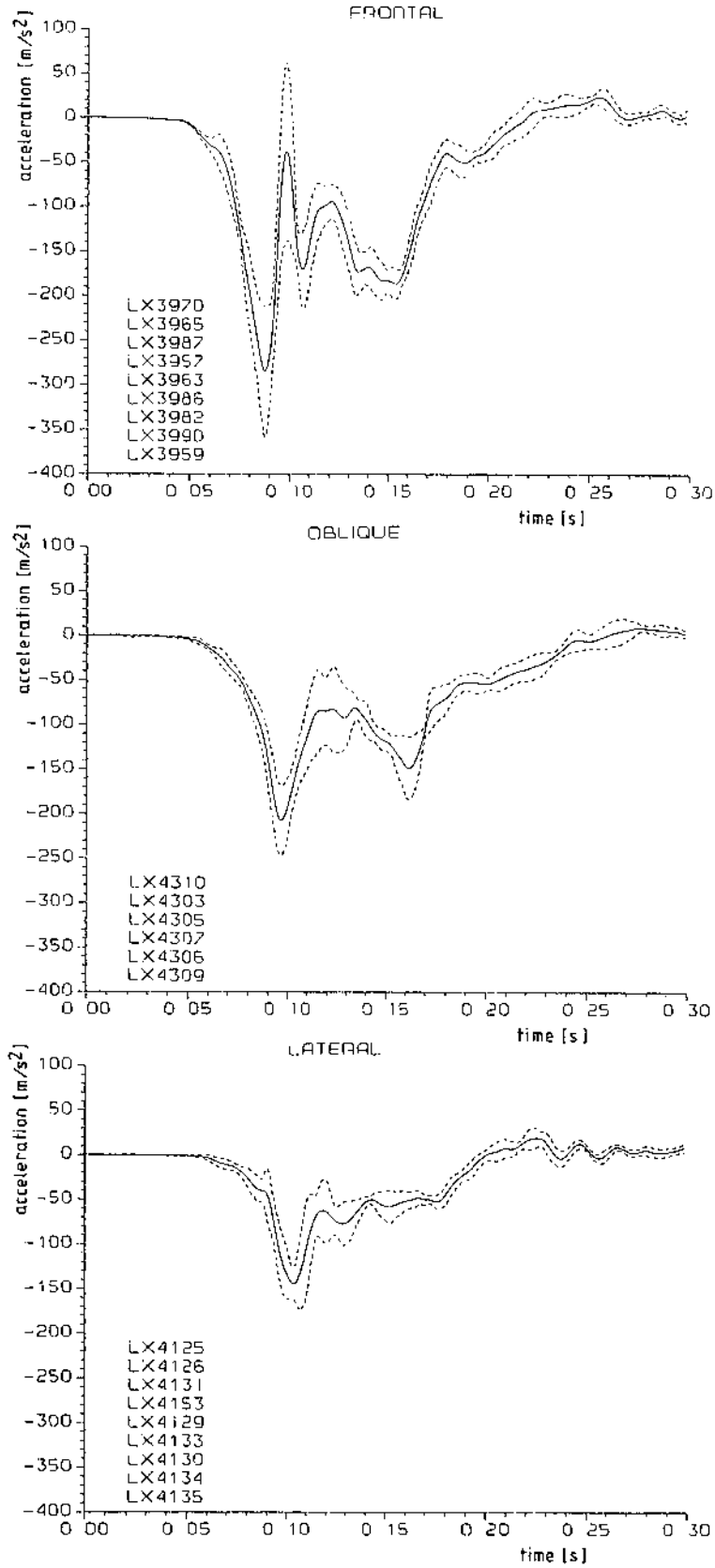

Fig. 5.13 *Mean T1 horizontal acceleration-time histories for the most severe tests in three impact directions*
(——— mean value, ----- corresponding standard deviation; LX .....: test number)

5.4.5 Head motions

This Section deals with the motions of the head during the loading phase i.e. up to maximum head excursion. Head motions will be expressed relative to a corrected T1 coordinated system as defined in the preceding Section. Since T1 rotations will be neglected here, head motions will be presented with respect to a coordinate system which stays aligned with the laboratory coordinate system.

First an analysis has been made of the occipital condyle trajectories. Fig 5.14 illustrates trajectories of several tests with different impact severity with the same subject in frontal, lateral and oblique impact direction. It follows that [14]:

- trajectories for different tests with the same subject are quite close to each other;
- maximum head excursions in frontal impacts are slightly larger than in oblique impacts and much larger than in the lateral ones;
- all trajectories quite well can be approximated by a circular arc segment.

This last finding is the most interesting one. Because displacements of the occipital condyles in a direction perpendicular to the plane of impact are small, a 2-pivot linkage mechanism can be used to characterize the observed motions. Fig. 5.15 illustrates this linkage mechanism. The upper link represents the head, the middle link the neck and the lower link the torso. The upper pivot is located in the occipital condyles and the lower pivot in the center of the circular arc approximating the occipital condyle trajectories. This lower pivot is a pin joint i.e. a joint with one degree of freedom with the rotation axis perpendicular to the plane of impact. The rotation in this joint is denoted by θ and is defined as the angle between neck link and z-axis of the corrected T1 coordinate system.

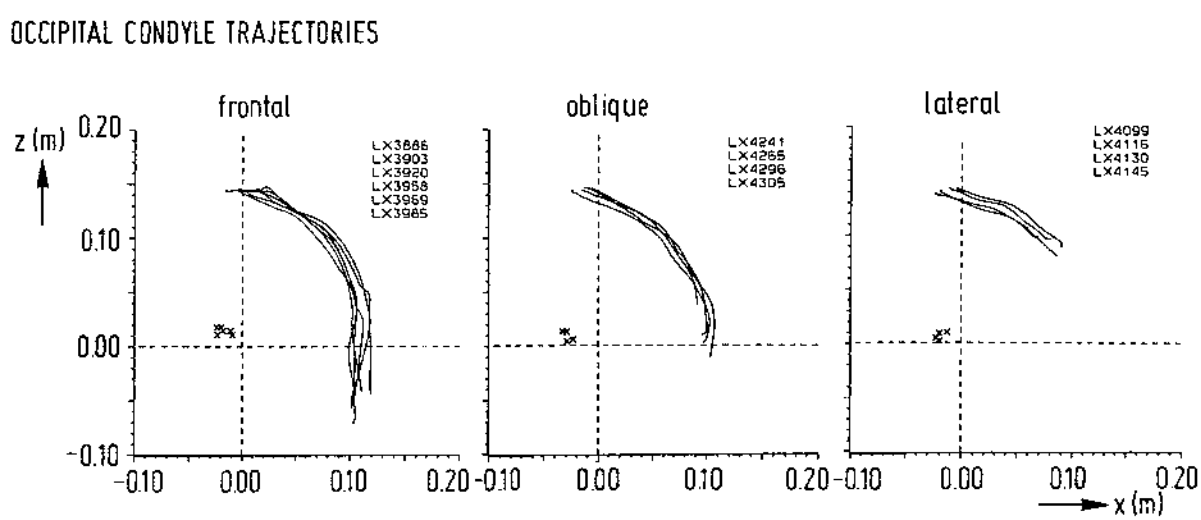

Fig. 5.14 Occipital condyle trajectories for tests with the same subject in different impact directions.

The upper pivot is a joint with two degrees of freedom (universal joint). The first degree of freedom of this joint allows the head link to rotate relative to the neck link in the plane of impact. This rotation angle will be denoted by ϕ and is defined here as the angle in the plane of impact between the z-axis of the head anatomical coordinate system and the corrected T1 coordinate system. The second degree of freedom of this upper joint is the rotation ψ of the head about the head anatomical z-axis indicating the head torsion or twist. In frontal impacts this twist motion can be neglected. The rotations of the head link (i.e. head anatomical z-axis) out of the plane of impact will be neglected here because such rotations were found to be very small.

On the basis of the occipital condyle trajectories the neck link length of the analog system and the lower pivot location relative to the torso have been determined for all of the tests [14]. The average radius was found to be 129 mm with a standard deviation of about 2 mm. The optimal location of the lower pivot of the linkage mechanism has been calculated for this average link length. Fig. 5.14 includes this location for the presented trajectories. It was found that for most of the tests the x-coordinate of this pivot has a negative value, i.e. opposite to the direction of the motion of the head if viewed from the corrected T1 coordinate system.

The head motions will be presented now using the linkage rotations presented in Fig. 5.15. The head flexion ϕ and head twist ψ can be calculated directly from the NBDL test results (i.e. the head rotation matrix) and are independent of the selected geometrical linkage parameters. The neck link rotation θ is calculated from the occipital condyle trajectories and the lower pivot location.

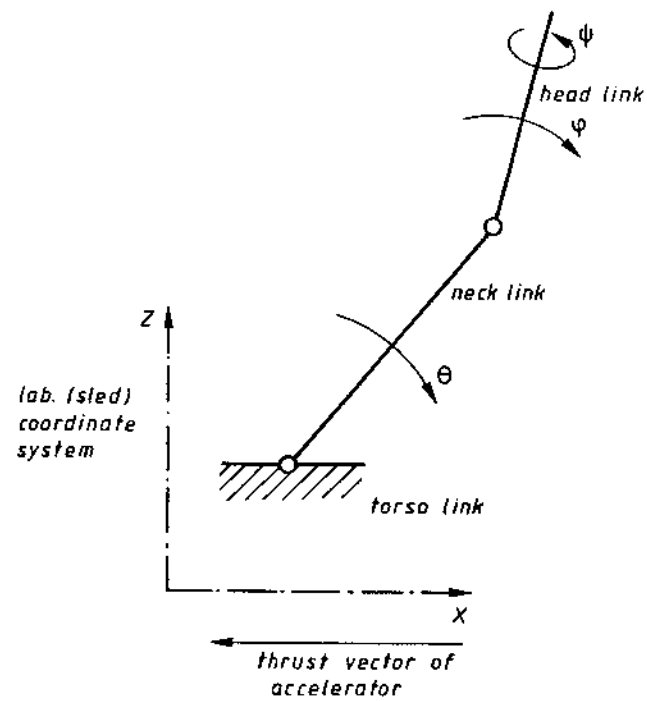

Fig. 5.15 Analog system for the description of the relative head motions.

The magnitude of the angles ϕ, ψ and θ in the initial position (time = 0) will be denoted by ϕ_0, ψ_0 and θ_0, respectively. Maximum values for these rotations are denoted by ϕ_{max}, ψ_{max} and θ_{max}. Mean values for $(\phi_{max} - \phi_0)$, $(\theta_{max} - \theta_0)$ and $(\psi_{max} - \psi_0)$ as function of impact direction and impact severity are presented in Fig. 5.16. Both the head flexion and the neck link rotation appear to be strongly dependent on the peak sled acceleration. The influence of the impact direction is most clearly present in the neck link rotation: frontal impacts show larger neck link rotations (for the same impact severity) than oblique ones and oblique impacts show larger neck link rotations than the lateral ones. Finally it can be seen that lateral impacts show a much larger twist than oblique ones.

Fig. 5.17 presents for the three impact directions the neck link rotation $(\theta - \theta_0)$ as function of head flexion $(\phi - \phi_0)$. Results for the most severe tests are given. In the initial phase of the motion for all impact directions the head flexion is smaller than the neck link rotation illustrating the translational nature of the initial head motion. As soon as the relative angle $(\theta - \theta_0) - (\phi - \phi_0)$ reaches a certain level the head and neck link become more or less locked. For most of the tests this relative angle appears to decrease slightly in the final part of the loading phase.

The maximum relative angle i.e. $((\theta - \theta_0) - (\phi - \phi_0))_{max}$ between head and neck link has been calculated for all tests. The influence of impact direction and impact severity on this angle is presented in Fig. 5.18. The impact direction appears to have a significant influence while the effect of impact severity is small. Average values for the upper pivot maximum rotation are 30 degrees in frontal, 20 degrees in oblique and 10 degrees in lateral impacts. In addition to above relations between linkage angles also information on the head twist as function of head flexion is available [14]. The value of the head torsion angle appears to be, in general, smaller than the head flexion angle.

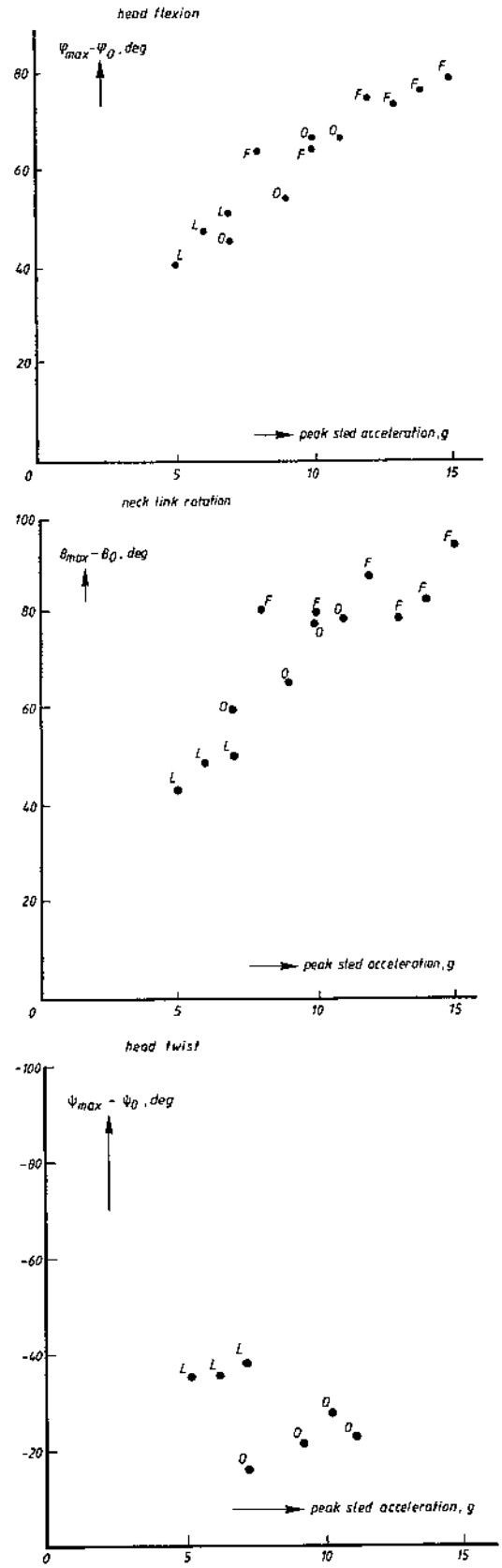

Fig. 5.16 *Mean values for peak rotations as function of impact direction and impact severity. (F = Frontal, O =Oblique, L = Lateral).*

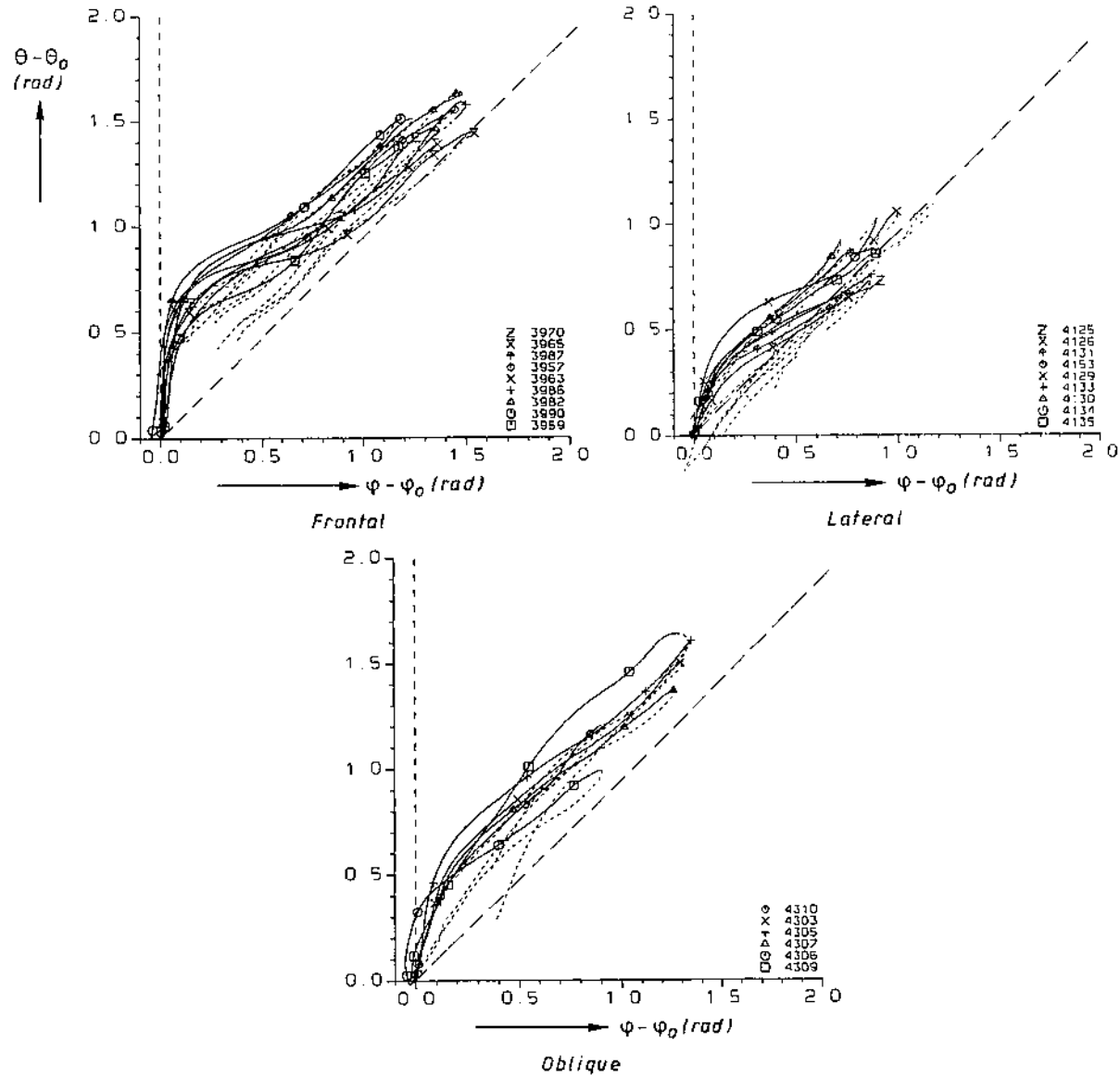

Fig. 5.17 *Neck link rotation (θ - θ_0) as function of head flexion (ϕ - ϕ_0) for the most severe tests as function of impact direction. (——— loading ——— unloading)*

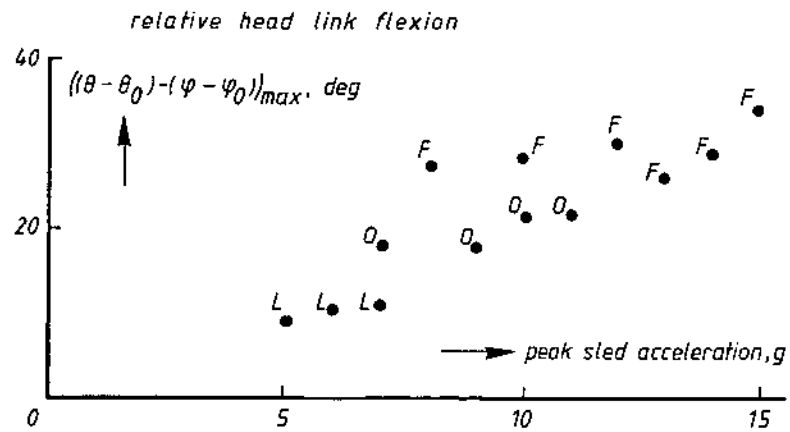

Fig. 5.18 *Influence of impact severity on maximum upper pivot angle (relative head link flexion). (F = Frontal, O = Oblique, L = Lateral)*

5.4.6 Performance requirements

The analog system proposed in the preceding Section specifies as such completely the dynamical response of the head-neck system for the NBDL test conditions, provided that also dynamical properties of the linkage joints are available. In other words the analog system with dynamic joint elements constitutes a necessary and sufficient set of performance requirements.

The loads applied by the neck to the head can be calculated using measurements of head acceleration and angular velocity provided that the head can be regarded as a rigid body and does not come into contact with any other object or body part. For all tests incorporated in this study neck loads have been calculated under the assumption that neck inertia effects can be neglected. Detailed results are presented in [14]. The following is a summary of the findings:

As discussed before, for the upper pivot a free range of motion can be observed initially, which varies per impact direction: about 30 degrees in the frontal, 20 degrees in the oblique and 10 degrees in the lateral direction. The joint stiffness after locking of this joint shows no significant differences per impact direction: this joint behaviour can be quite well approximated by a linear function with a slope (i.e. joint stiffness) of 3 Nm/degree. The largest occipital joint torques are found in the frontal tests and vary between 60-90 Nm.

For the head twist a linear function is proposed to characterize the stiffness against torsion motion. The stiffness appears to be relatively small and varies per impact direction: about 0.4 Nm/degree in the lateral direction and 0.75 Nm/degree in the oblique direction (note: no torsion motion is present in frontal impacts).

For the lower pivot also linear functions were selected resulting in the following stiffness values:

Frontal : 1.2 Nm/degree
Oblique : 1.5 Nm/degree
Lateral : 2.2 Nm/degree

5.4.7 Comparison with cadaver tests in frontal flexion

The human volunteer tests discussed in above Sections were extended with a small set of human cadaver tests in order to study the effect of muscle tone and to study the head-neck response, including possible injuries, under more severe impact conditions [19]. Tests were carried out by the University of Heidelberg. Only tests in frontal impact direction have been conducted. NBDL test conditions were reproduced as far as possible. Head and T1 accelerations and displacements were monitored by accelerometers and phototargets

directly screwed to the head and T1, rather than using the NBDL instrumentation. Fig. 5.19 illustrates the head instrumentation.

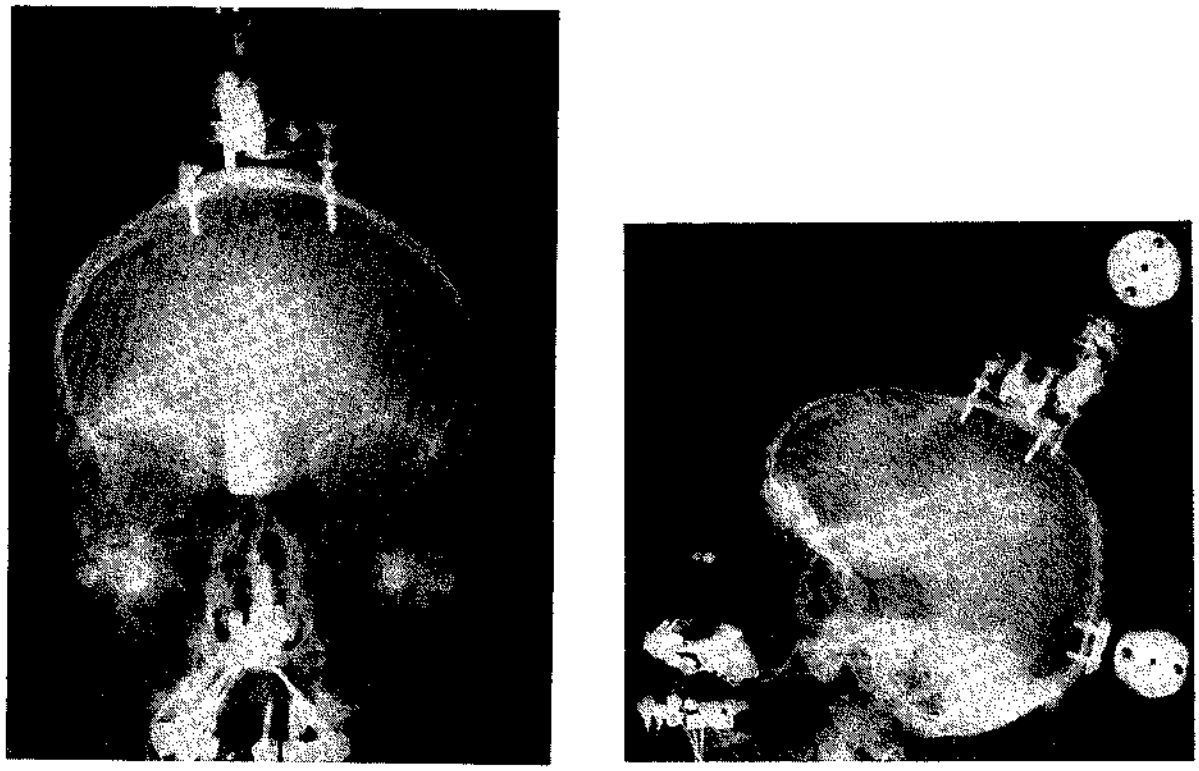

Fig. 5.19 *Anterior-posterior and lateral x-rays with head instrumentation.*

In total 12 tests have been conducted, 5 tests of which were fully analyzed, as far as the kinematics are concerned, and compared with volunteer response. Three of these tests had a similar severity as the most severe volunteer tests (15 g) and 2 tests were conducted at a higher severity level (23 g). The age of the cadavers varied from 24 to 61 years.

No injuries occured in 3 out of the 12 tests. In seven cases strains in the vertebral discs and small lacerations of the ligaments flava and within the joint were observed (AIS 1). In 2 tests a severity of AIS 2 was determined, one being a moderate test (T2 fracture) and one being a severe one (laceration of T2/T3 ligamentum flavum) [19].

T1 accelerations in the moderate cadaver tests were found to be within the envelope of the volunteer tests, indicating that the input to the head-neck system in the cadaver tests was close to the volunteer tests. Differences were found in vertical T1 displacements, which in the cadaver tests showed up to 9 cm downward displacement while this displacement was almost absent in the volunteer tests, and in the T1 rotations which was larger in the cadaver tests as is illustrated in Fig 5.20. Note in this Fig. the backward rotation in the volunteer tests which is not present in the cadaver tests.

The same linkage mechanism as used for the human volunteer tests was applied to characterize the cadaver motions. Fig. 5.21 shows a comparison of the neck link versus head rotations in case of the moderate impacts. Also in the cadaver the initial translational motion of the head can be observed but it is less evident than in the volunteer tests. Head rotations are found to be larger in the cadaver tests most likely due to absence of muscle tone.

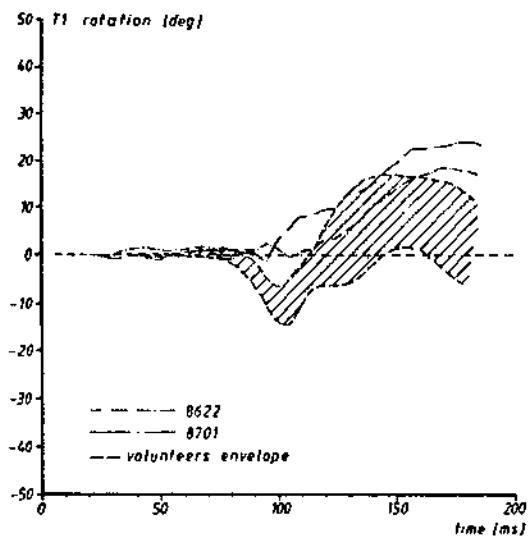

Fig. 5.20 *Comparison of T1 rotation-time history.*

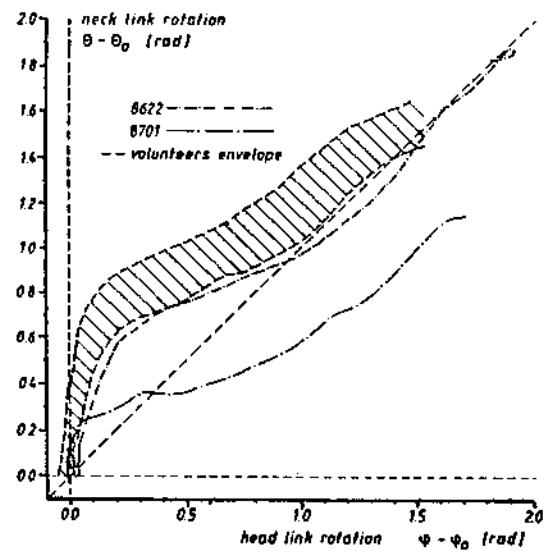

Fig. 5.21 *Comparison of neck link rotation as function of head rotation.*

Further it was observed that centre of gravity excursions do not differ significantly in the severe tests from the moderate tests while head rotations are slightly larger in the more severe tests.

5.4.8 Discussion

The most important finding of the analysis of the human volunteer and cadaver tests is that the observed human head-neck response can be represented adequately by a linkage system with 2 pivots. One link represents the head, one link the neck and one link the torso. This analog system should not be considered as a representation of the very complex anatomical structure of the cervical articulations and the associated structures, however; it is rather a model which describes the head motions realistically in case of non head impact conditions, assuming that T1 rotations can be neglected. It is expected that similar mechanisms can be developed if T1 rotations are not neglected.

Torques calculated in this study near the occipital condyles and near T1 represent the resultant torque in the head-neck and neck-torso interface, respectively. These torques are developed by tension forces in the musculature, internal neck compression forces, etc. More detailed neck models are needed to study the load contribution of the various neck structures (see Section 5.6).

The proposed analog system implicitly constitutes a performance requirement. As an alternative, performance requirements could have been formulated explicitly by means of kinematic requirements like displacements and accelerations for several impact levels. Such a formulation is desirable for instance when establishing a standard to be used in the laboratory for verifying the dummy response. Such criteria can be derived directly from the NBDL (and cadaver) test data or indirectly from the analog system.

The cadaver tests conducted learn that muscle tone has an effect on the head-neck response: head rotations appear to be larger in the cadaver than in the volunteer tests. Furthermore significant differences in T1 rotations can be observed which are not completely understood yet. The observed injuries in the cadaver tests (including two AIS 2 injuries) indicate that the impact severity levels in the volunteer tests are quite high.

Although the developed analog system is not intended as a design principle for a future omni-directional mechanical neck it illustrates some important design principles:

- The basic geometrical set-up of the neck design can be identical for the various impact modes. In other words it is expected that one neck design can be used for all impact directions.
- The stiffness of a dummy neck is dependent on the impact direction. In lateral direction for instance the neck should be stiffer (almost twice as stiff) than in forward direction.
- A feature should be incorporated in the design which surpresses large head flexions but allows relatively large neck link rotations. In order to realize this the effect of the locking mechanism which was identified for the upper pivot, should be approximated in a future dummy neck design.

5.5 Injury criteria and tolerances

The various kinds of biomechanical response tests indicated in Section 5.4.1 can give us some information on the tolerance of the cervical spine and its components. First some tensile, compressive and torsional strength data of vertebrae and intervertebral discs will be summarized here (Table 5.2), based on tests on isolated neck structures conducted by Sonoda and presented by Yamada [20].

Mertz and Patrick [9] and Patrick and Chou [21] conducted static tests on human volunteers to determine the maximum loads they can resist near the occipital condyles. The test set-up was presented in Fig. 5.6. Loads were applied in several directions. Results for axial loads, shear forces and bending torques are summarized in Table 5.3. The neck was in a normal position (i.e. no flexion of the head) for the presented test results. In addition to the results shown in Table 5.4 also data are available for the neck in a flexed and extended position and for loads applied in an oblique direction [22]

Table 5.2 *Breaking strength of cervical neck elements in tension, compression and torsion by age group [20]*

	Age group (years)		
	20-39	40-59	60-79
Cervical vertebrae			
Tension (KN)	1.12	0.89*	
Compression (KN)	4.09	3.30	1.86
Cervical disc			
Tension (KN)	1.03	0.78*	
Compression (KN)		3.13	
Torsion (NM)	5.5	4.7**	

* 40-79 years
** 40-69 years

Mertz [23] has used data from several sources including dynamic cadaver tests and accident reconstructions using a Hybrid III dummy to develop protection criteria (i.e. injury assessment guidelines) to be measured at the Hybrid III dummy neck. The tolerance level proposed for the occipital condyle torque in frontal flexion is 190 Nm and in extension 57 Nm. For axial compression, tension and shear the proposed protection criteria are illustrated in Fig. 5.22. The proposed criteria are a function of the duration of the loading.

Table 5.3 *Maximum static forces and bending torques developed at the occipital condyles by human volunteers [22].*

	Bending Torque [Nm]
Forward flexion	50.2
Extension	20.3
Lateral flexion	47.5
	Force [N]
Anterior-posterior (shear)	845
Posterior-anterior (shear)	845
Lateral shear	400
Axial tension	1134
Axial compression	1112

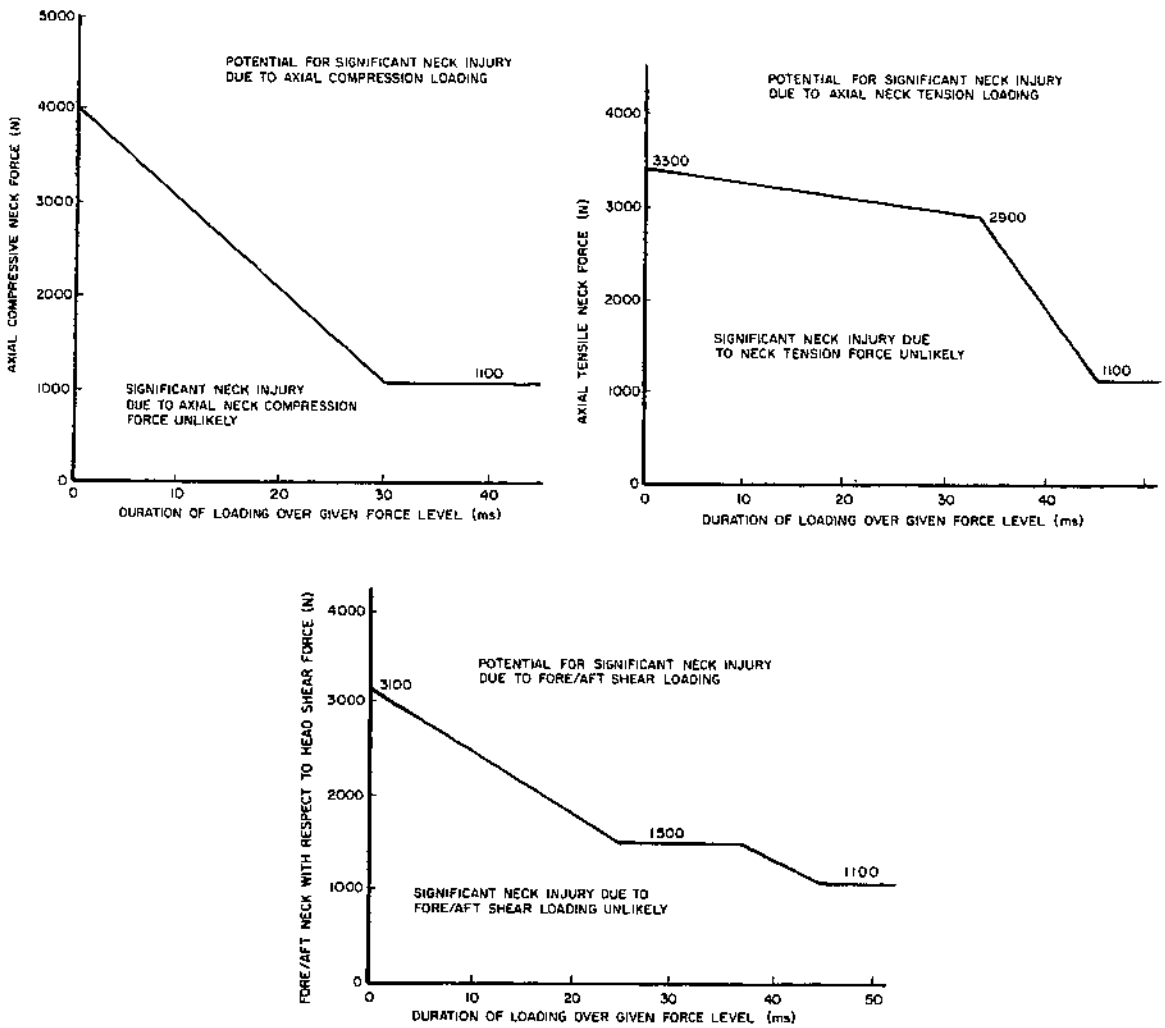

Fig. 5.22 *Injury assessment criteria for neck axial compression, tension and shear [4]*

In addition to above type of data also results are available from cadaver tests in which an impact load has been applied to the head. In this way information is obtained for the effect of combined loading on the neck structure. A review of some of this work is given in Ref. [4]. The initial position of the head was found to be important for the injuries produced in the neck. In general it is concluded that the status of the knowledge on the tolerance of the neck is still rather limited [4].

5.6 Discussion

The human cervical column is a rather complex structure that provides support to the head and allows movement of the head relative to the torso. Due to the large number of loading conditions that can exist and variations in initial conditions a number of different injury mechanisms can take place. The knowledge on the various mechanisms and corresponding injury tolerance levels is still rather limited. In this respect it should be emphasized here that tolerance criteria discussed above partly are based on accident reconstructions and as such they are only valid if the dummy neck used in the reconstructions responses in a humanlike manner. The proposed bending torque level for frontal flexion of 190 Nm seems to be rather high when compared to the occipital condyle torques determined for the NBDL tests (below 60 Nm). The finding of AIS 1 and 2 injuries in the Heidelberg cadaver tests indicates that the 190 Nm tolerance value should be applied with much care.

Additional research certainly is needed in this field, not only for severe neck injuries but also for minor (whiplash type of) injuries due to their high frequency and long-term effects. In addition to well-defined biomechanical experiments, detailed mathematical models of the human neck are required, which take the actual neck anatomy into account, to study and understand the various injury mechanisms and to analyze the effect of different loading conditions. Furthermore such models can be very usefull for the analyses and reconstruction of real accidents. An example of such a model is shown in Fig. 5.23 [24]. This model is a lumped-parameter model. Rigid bodies are used to represent the vertebra fom T1 to C1. Also the head is represented by a rigid body. Muscles are represented by non-linear spring elements. The model has been compared with NBDL human volunteer response with good correlation according to the authors. Current research at the Eindhoven University of Technology seeks to improve and extend this type of models for future injury analysis.

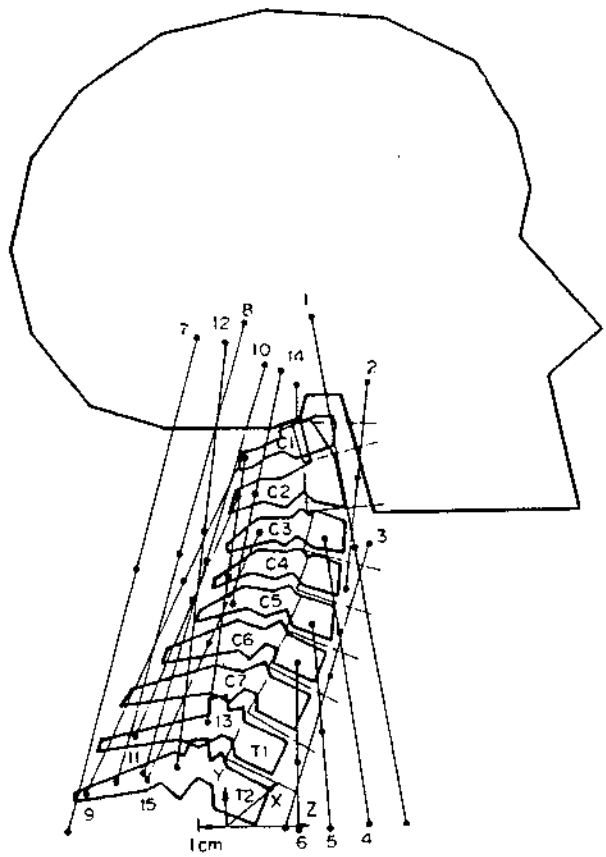

Fig. 5.23 3D Mathematical model of the neck by Deng and Goldschmidt [24]

REFERENCES

1. King, A.I.: "The vertebral column: experimental aspects". In: The Biomechanics of Trauma. Eds. Nahum and Melvin. Appleton, Century-Crafts, Norwalk, Connecticut, 1985.

2. Sobotta/Figge: "Atlas of the human anatomy", Urban & Schwarzenberg, Baltiomore-Munich, 1977.

3. Kapandji, I.A.: 'The physiology of the joints', Vol. III The trunk and the vertebral column. Churchill Livingstone Edinburgh London and New York, 1974.

4. Nyquist, G.W. and A.I. King: Chapter 2 (Spine) In: "Review of Biomechanical Impact Response and Injury in the Automotive environment", Technical report DOT HS 807 042, U.S. Department of Transportation National Highway Traffic Safety Administration, 1986.

5. Schmidt, G., Kallieris, D., Barz, J., Mattern, R. and F. Schulz: "Belastbarkeitsgrenze und Verletzungsmechanik des Angegurteten Fahrzeuginsassen, "FAT, Schriften Reihe, frankfurt, 1978.

6. Cheng, R., Yang, K.H., Levine, R.S., King, A.I. and Morgan, R.: "Injuries to the cervical spine caused by a distributed frontal load to the chest", Proceedings of the 26th Stapp Car Crash Conference, 1983.

7. Langwieder, K. and Hummel, Th.: "Children in cars -their injury risks and the influence of child protection systems", ESV Conference, Gothenburg, 1989.

8. Huelke, D.F., Moffatt, E.A., Mendelsohn, R.A. and J.W. Melvin: "Cervical fractures and fracture dislocations - an overview", In: 'The human neck -Anatomy, Injury Mechanisms and Biomechanisms'. SAE Warrendale SP-438. Paper 790130, 1979.

9. Mertz, J.H. and Patrick, L.M.: "Strength and response of the human neck", Proceedings of the 15th Stapp Car Crash Conference, 1971.

10. Huelke, D.F., Husholtz, G.S.: "Cervical spine biomechanics: A review of the literature", J. Orthop. Res. 4:232 1986.

11. Muzzy III, W.H. and Lustick, L.:"Comparison of kinematic parameters between Hybrid II head and neck system with human volunteers for -Gx acceleration profiles", Proceedings of the 20th Stapp Car Crash Conference, SAE-paper 760801, 1976.

12. Ewing, C.L., Thomas, D.J., Lustick, L., Williams, G.G., Muzzy III, W.H., Becker, E.B. and Jessop, M.E.: 'Dynamic response of human and primate head and neck to + Gy impact acceleration'. Report DOT HS-803 058, 1978.

13. Ewing, C.L., Thomas, D.J. and Lustick, L.: 'Multiaxis dynamic response of the human head and neck to impact acceleration'. Aerospace Medical Panel's Specialist's meeting. Paris, AGARD Conference Proceedings no. 153. North Atlantic Treaty Organisation. Advisory Group for Aerospace Research and Development, 1978.

14. J. Wismans, H. van Oorschot and H.J. Woltring: "Omni-Directional Human Head-Neck response". 30th Stapp Car Crash Conference, Proceedings P-189, p. 313-332, San Diego, Society of Automotive Engineers Inc., 1986.

15. Wismans, J. and Spenny, C.H.: 'Performance requirements for mechanical necks in lateral flexion'. In: Proceedings of the 27th Stapp Car Crash Conference. SAE Paper No. 831613, 1983.

16. Ewing, C.L. and Thomas, D.J.: 'Human head and neck response to impact acceleration'. NAMRL Monograph 21. Naval Aerospace Medical Research Laboratory, Pensacola, Florida, 32512, 1973.

17. McConville, J.T., Churchill, T.D., Kaleps, I., Clauser, C.E. and Cuzzi, J.: 'Antropometric relationships of body and body segment moments of inertia'. Report AFAMRL-TR-80-119. Air Force Aerospace Medical Research Lab. Wright Patterson Airforce Base, Ohio 45433, 1980.

18. Wismans, J.: 'Preliminary development head-neck simulator'. Vol. 1: Analysis of human volunteer tests. Final report Phase I Project SRL-59. Vehicle Research and Test Center, East-Liberty, Ohio, 1985.

19. J. Wismans, M. Philippens, E. van Oorschot, D. Kallieris and R. Mattern: "Comparison of Human Volunteer and Cadaver Head/Neck Response in Frontal Flexion". 31st Stapp Car Crash Conference, Proceedings P. 202, Society of Automotive Engineers, Inc. 1987.

20. Yamada, H.: "Strength of biological materials", pp 75-80, Eds. F.G. Evans, Williams and wilkins, Baltimore, 1970.

21. Patrick, L.M. and chou, C.: "Response of the human neck in flexion, extension and lateral flexion", Vehicle Research Institute Report No VRI-7-3. Society of Automotive engineers, Warrendale, Pa, 1976.

22. "Human tolerance to impact conditions as related to motor vehicle design", SAE information report SAE J885 JUL86, Society of Automotive Engineers, Inc. 1986.

23. Mertz, H.J.: "injury assessment values used to evaluate Hybrid III response meausurements", General Motors Corp. NHTSA Docket Submission VSG 2284 Part III, Attachment I, Enclosure 2.

24. Deng, Y.C. and W. Goldsmith: "response of a human head/neck/upper-torso replica to dynamic loading - II analytical-numerical model", Journal of Biomechanics, 20:471-486, 1988.

CHAPTER 6

THORAX INJURY BIOMECHANICS

6.1 Introduction

The thorax is after the head the next most critical region to protect from injuries. The IPR (Injury Priority Rating) which weighs motor vehicle injuries by body region in terms of total societal costs (see Table 3.5), rates thoracic injuries about 19% of the total IPR. The thorax consists of the ribcage and the vital organs for blood circulation and respiration. Section 6.2 provides a brief description of the relevant thorax anatomy.

The nature of thoracic injuries is basically different from e.g. head injuries. There are few long-term disabilities and a victim either dies soon after the accident or recovers completely [1]. Therefore accurate diagnoses of thoracic injuries and quick surgical repair is essential for recovery of the victim. Chest injuries can occur in two basic forms: blunt trauma and penetrating injuries. Blunt trauma is caused by a relatively flat or blunt object striking the chest without penetration, which can result in for instance rib fractures, lung contusion or disruption of vessels. Penetrating injury may result often in damage of the different pleura, injury to the internal organs of the chest with possible bleeding from the heart and great vessels or disruption of the lung. Penetrating injuries are relatively uncommon in traffic accidents and therefore will not be considered here further. Section 6.3 introduces the most important thoracic injury mechanisms and injury types due to a blunt impact.

The mechanical response of the thorax under impact conditions can be studied by biomechanical models. Section 6.4 discusses several methods and findings from research conducted in the past. Injury criteria and injury tolerances for the thorax and their limitations will be presented in Section 6.5. In particular attention is given to the Thoracic Trauma Index (TTI) and the Viscous Criterion (VC). Directions for future research will be discussed in Section 6.6.

6.2 Anatomy

The thorax is the upper part of the torso, extending from the base of the neck to the lower ribs. It contains the following important organs: the heart, the lungs, the bronchi, the trachea, the great vessels, the nerves and the oesophagus, which are surrounded and protected by the bony ribcage. The outside of the thorax consists of the skin, a variety of muscles, fat and other soft tissue. The ribcage structure consists of twelve thoracic vertebrae (the thoracic spine), the sternum and twelve pairs of ribs, which form a relatively

rigid though movable shell around the organs (Fig. 6.1). All ribs are connected in a flexible way to the thoracic vertebrae. The sternum is a flat elongated bone at the anterior side of the thorax, directly beneath the skin, which extends from the first upper rib to the soft abdominal wall structure. The upper seven pairs of ribs have a direct flexible connection to the sternum while the next five pairs articulate indirectly with the sternum. The lower three pairs, referred as floating ribs, are not connected to the sternum at all, but to the muscles of the abdominal wall. The ribs are interconnected with each other by the internal and external intercostal muscles, forming a flexible muscle barrier between the ribs.

The size, shape and strength of the ribcage depends on the age and sex. Its general shape is a truncated ovoid with its depth less than its breadth. The function of the ribcage is to protect the internal organs and to facilitate respiration. The chest cage of children is very flexible and is therefore not able to protect the chest contents very well. During growth the chest stiffness increases but the rib cage still remains flexible so that an optimal protection is created. In the elderly the movable joints between the ribs and the sternum and the vertebrae become stiffer and also the ribs become more brittle because of calcium loss, so injuries are more likely to occur.

The diaphragm, a dome-shaped thin muscle, is the lower thoracic boundary which separates the thoracic and abdominal cavity. Portions of the lower ribs are below the diaphragm and partially protect the organs in the abdominal cavity (liver, stomach, spleen, pancreas and the kidneys).

At the superior side of the ribcage the shoulder structures are located (clavicle, scapula) which extend the protective function of the ribcage with respect to the internal structures.

The interior of the ribcage is divided into three regions, two regions at the left and right side which contain the lungs and in the centre the mediastinum which contains a group of structures including the heart, the trachea and the large vessels (Fig 6.2). The lungs are connected with the left and the right bronchi which join together in the trachea. They are surrounded by two layers of membranes, the visceral pleura which enclose the outside of the lungs like a sac and the parietal pleura which cover the entire inside of the ribcage, including the top of the diaphragm and the bodies of the thoracic vertebra. The small space between visceral and parietal pleura is called pleural cavity and is an enclosed space with no access to the outside air. Due to elasticity of the lungs a continuous underpressure is maintained in the pleural cavity in order to keep the lungs in their normal (i.e. inflated) shape. If this underpressure cannot be maintained due to for instance a perforation in the chest wall or the lungs, the lungs will deflate (move inwards) due to their elasticity and the pleural cavity will be filled with air (pneumothorax).

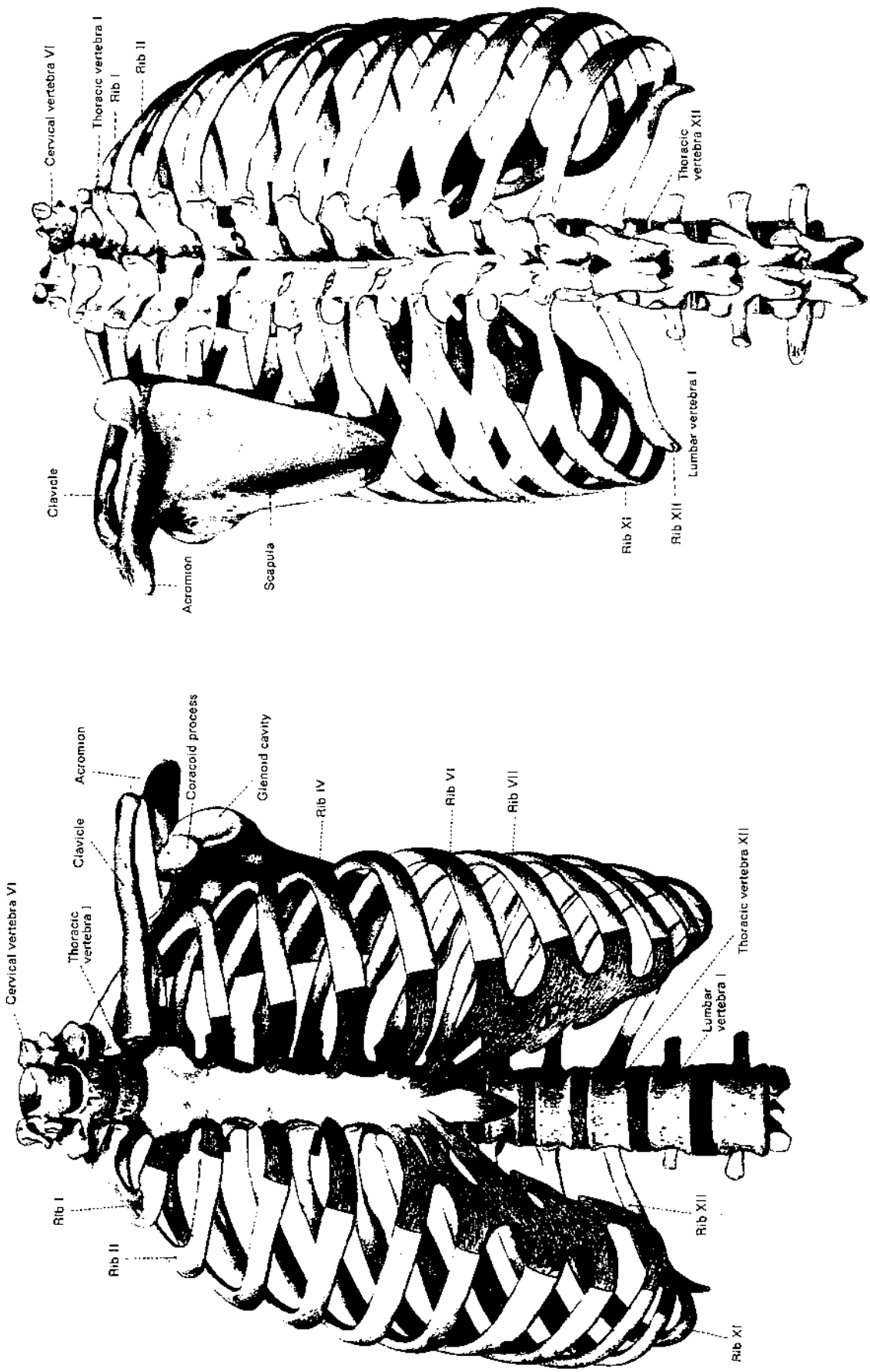

Fig. 6.1 *The ribcage: anterior view (left) and posterior view (right) [2]*

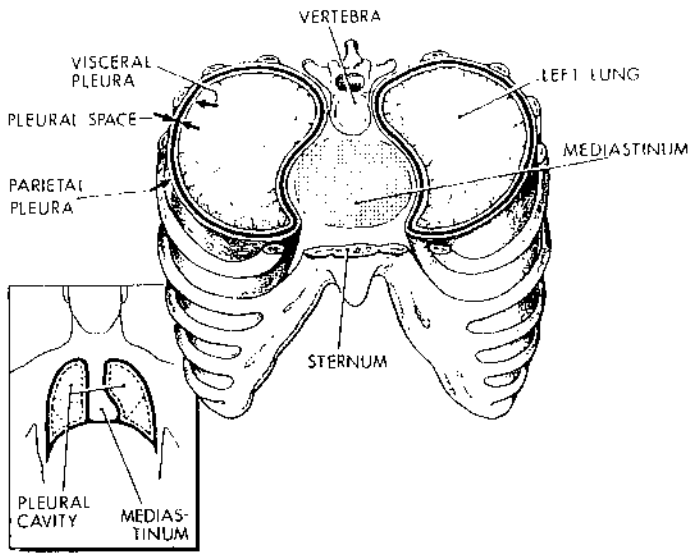

Fig. 6.2 *Subdivision of regions in the thoracic cavity [3]*

The diaphragm and the rib cage and its muscles function as a pump, drawing air into the lungs (inspiration) and expelling air from the lungs (expiration) as shown in Fig. 6.3. Inspiration takes place if the thoracic volume is enlarged by lifting the rib cage and by lowering the diaphragm. The sub-atmospheric pressure in the pleural cavity drops from 2-3 N/m^2 during expiration to 8-10 N/m^2 [4]. Due to this the lungs will stretch and air is sucked through the trachea and the bronchi to ventilate the lungs. Expiration takes place by relaxing the muscles, due to which the elastic energy stored in the lungs, diaphragm and the rib cage during inspiration, will cause the air to expel from the lungs.

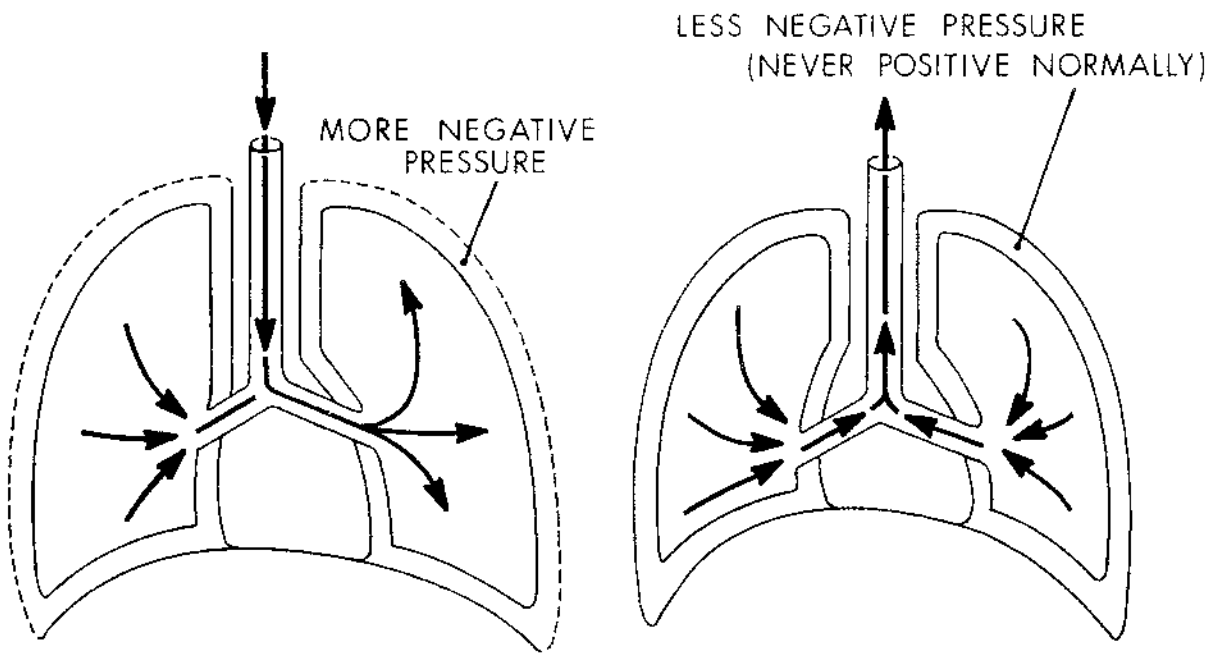

Fig. 6.3 *Inspiration (left) and expiration (right) in the lungs [3]*

The mediastinum, containing the heart and the great vessels, is located between the sternum and the thoracic vertebrae. It should be noted here that the available space between sternum and thoracic vertebrae is rather small (less than 15 cm). As a consequence compression of the anterior ribcage may easily cause injuries to the structures in the mediastinum. The great vessels are the pulmonary arteries (left and right), the pulmonary veins (left and right), the thoracic aorta and the vena cava. The thoracic aorta is the largest vessel, with the highest internal pressure peaks, which supplies the head and the body with blood containing a high oxygen level. The heart which is a bundle of muscular fibres acts as a double pump with two chambers on each side. Each chamber has an atrium and a ventricle, referred as the left and right atria and ventricles. The heart is surrounded by a two-layered membrane, the pericardium. Between the two separate layers there is a space called the pericardial space.

6.3 Injuries and injury mechanisms

6.3.1 Introduction

The description of thoracic injuries and injury mechanisms to be presented here will be limited to injuries due to blunt impacts, i.e. a relatively flat or blunt object (e.g. a steering wheel or a dash board) striking the chest, without penetrating the surface. When the thorax is suddenly decelerated due to a blunt impact basically three different injury causing mechanisms can take place, as was discussed already in Section 3.3.3: compression of the thorax, viscous loading within the thorax cavity and inertia loading of the internal organs (see Fig. 3.3). Often these mechanisms will take place in combination with each other, depending on the loading situation.

Chest compression may injure ribs or the lungs, heart or great vessels directly by causing a contusion, a bruising or even more severe a rupture. Shock waves also can cause contusion and rupture but, also for instance, ventricular fibrillation. Due to inertia the interior structures will continue to move after the chest cage itself is arrested in case of an impact. This can cause for instance disruption of the great blood vessels in the chest.

Thoracic injuries may be subdivided into three categories: ribcage fractures, lung injuries like a pneumo- or hemothorax and injuries of the other thoracic organs like rupture of the thoracic aorta, which is a frequent and mostly fatal injury. The mechanisms of ribcage fractures and some of the lung injuries are reasonably well understood in contrast to injury mechanisms in the other thoracic organs. Knowledge on injuries in the thoracic organs appears to be mainly based on clinical experience up to know, rather than biomechanical testing. In the next Sections briefly rib cage fractures and some important lung injuries will be discussed. For a detailed review of thoracic injuries see Ref. [5].

6.3.2 Rib fractures

Most single rib fractures are self healing and not too serious on its own. In Table 3.2 it was shown that one single rib fracture is an AIS 1 injury according to Abbreviated Injury Scale while 2-3 rib fractures are scaled as AIS 2. Multiple fractures however, can have life threatening complications. They decrease the strength of the ribcage, and therefore decrease the ability to inhale air in the lungs. Ribs can have fractures at any point but usually they break at the site where the force is applied and at the place where the greatest curvature is located. Sharp edges of broken ribs can perforate the muscular chest wall and the skin, which is called an open fracture. These open fractures are of particular concern because this situation can lead to a pneumothorax, lung collapse or an infection. The sharp edges of a broken rib can also perforate the visceral or parietal pleura, which can lead to various respiratory problems. They can injure the lung, the heart, the great blood vessels, the intercostal nerves, arteries and veins between the ribs and cause abdominal haemorrhage. The occurrence of rib fractures is therefore an important diagnostic indication for treatment of the victim. If the skin and the soft tissue overlaying the fracture remains intact the fracture is called a closed or simple fracture. If a rib fractures in more than one fragments it is referred as a comminuted fracture.

If an injury of the chest results in multiple rib fractures the chest wall may lose its overall strength and become instable. This can result in a chest motion that is opposite to normal. During inspiration the disrupted chest wall is sucked in and thus reducing the expansion volume of the chest. On expiration the chest wall moves outwards, which decreases the ability of the chest to push all the air out of the lungs. There are three factors which influence the development of this process: the extent of the injury, the control of the pain involved and the mechanical properties of the lung. The greater the area of the chest which is moving in and out during breathing, the lesser the amount of air which can be refreshed in the lungs. This condition of the thorax is called a *flail chest.* As a result a life threatening situation can occur due to low oxygen levels in the blood (hypoxemia), high carbon dioxide levels or radical pH changes [5].

6.3.3 Lung injuries

The pleural cavity, the space between the parietal pleura and the visceral pleura, can be filled with air or blood, in case of a thoracic injury. The first case (air) is called a *pneumothorax* and the latter (blood) a *haemothorax.* A combined situation, a haemo-pneumothorax can also occur. A pneumothorax is most likely the result of a fractured rib, perforating the pleura and the lung. On inspiration the drop in the intrapleural pressure causes air to suck into the pleural cavity through the leak in the lung. During expiration the laceration (a wound made by cutting or tearing) of the lung falls together, blocking the escape of the air from the pleural cavity. During each breath a certain amount of air is accumulated in the

pleural space, which can lead to a collapse of the lung. A haemothorax is usually the result of a laceration of the lung or a blood vessel. The blood can accumulate in the chest which results in a further loss of available lung volume.

Lung contusion (or bruising) can occur due to chest compression both with or without rib fractures involved and often in combination with a flail chest. Lung contusion increases the risk of pneumonia, which is one of the most serious complications. In combination with a severe thoracic trauma, pneumonia often causes the death of the victim. Lung contusion can also lead to airless areas in the lung yealding in artery-to-vein shunting which causes local pneumonitis. This shunting leads to increased strain on the heart because of shortness of oxygen in the blood flowing in the coronary arteries.

6.4 Biomechanical response

6.4.1 Introduction

The purpose of this Section on biomechanical response is to review some of the experimental thoracic impact work conducted in the past with the emphasis on mechanical response data, as opposed to injury response which will be discussed in Section 6.5. Mechanical response data are used in particular to develop biofidelity performance requirements for crash dummies or mathematical analogs of the human thorax.

Thoracic biomechanical response studies have been conducted by many researchers in the past using volunteers, embalmed and unembalmed cadavers and various types of animals (rabbits, dogs, monkeys and pigs). For biofidelity performance requirements in particular human cadaver tests are of importance. Cadaver thorax tests can be subdivided into impactor tests, drop tests, sled tests and full scale crash tests [6]. In an impactor test the thorax is loaded by a rigid or padded surface connected to a moving mass. The main advantage of this type of tests is that the load is applied in a very controlled way and that the interaction with the adjacent body parts is minimized. Most of the current thoracic biofidelity requirements are based on this type of tests. Also injury response data in human cadavers or animals usually have been obtained through impactor tests. A possible concern of this type of tests is the representativety of the impact conditions (i.e. the impactor mass, impactor velocity, impact surface characteristics and impact locations) for the real world accident situation.

In a drop (i.e free fall) test the cadaver is dropped from a certain height, for instance 1 or 2 meters, on a rigid or padded surface. It is a relatively simple test which sometimes has been used for side impact response studies [7,8]. A special concern of a drop test is the limited control of the impact conditions. Particularly the problem of unique horizontal initial positioning of the cadaver, which is done by suspending the cadaver by means of a number of

ropes, and the lack of control of the motion during the fall, causes this type of test to be rather inaccurate. We shall not consider these tests here further.

A sled test in which the test subject is not restrained is, in principle, rather similar to a drop test. The initial position and kinematics of the subject however are much better controlled in this test. The subject is seated on the sled seat well supported in the back. The sled is decelerated (or accelerated in case of an acceleration sled) and the subject impacts with one or more contact surfaces. The biomechanical response of several body parts can be studied by using different impact surfaces for each body region of interest. An impact surface can be rigid or padded and is instrumented by a load cell. A limiting factor, however, to use such test data for biofidelity requirements in case of a specific body region, is the large interaction between the various body parts. Only for global (whole-body) biofidelity evaluation these tests are suitable.

The same disadvantages of drop and sled tests, as far as the suitability for biofidelity requirements is concerned, also apply to real world crash tests (e.g. vehicle accident reconstructions): the variability of the test conditions of the cadaver before impacting any structure is large, because of the complex nature of the test environment and different collapse modes possible in the vehicle [6]. Moreover such tests are rather expensive, partly due to the extensive preparations needed and the required instrumentation. The main advantage of this type of tests is that the cadaver is loaded in a more realistic way.

In this Section we shall mainly concentrate on impactor and, to a lesser extent, on sled tests. Moreover some quasi-static tests with human volunteers will be discussed. This Section is organised in 2 subSections: Section 6.4.2 dealing with frontal loading and Section 6.4.3 with lateral loading.

6.4.2 Frontal loading

The earliest work dealing with thoracic loading was part of the whole-body response research programs with human volunteers, which was briefly discussed in Section 3.6. In these tests the subjects were seated on a sled, usually restrained by a harness type of seat belt system. The thorax is not actually impacted by a surface but loaded inertially due to the sled deceleration. Information on biomechanical response data in terms of changes in the body position and shape as function of time is not available from these tests due to absence of adequate instrumentation. The quality of available high speed films and the visibility of landmarks is too poor to generate additional information afterwards.

Most thoracic impact research described in literature has been conducted with human cadavers. One concern is the absence of muscle tension in a cadaver. To investigate this effect, Lobdell [9] studied the thorax frontal stiffness at seven male human volunteers

under quasi-static loading conditions. The volunteers were sitting in an upright position with the back supported by a rigid structure. The load was applied manually through a lever arm using a sudden pre-selected displacement input. The peak loading was reached after about 0.1 sec. The volunteers were loaded mid-sternally with a circular flat rigid "impactor" (diameter 0.152 m). The applied load was recorded with a load-cell and the displacement of the "impactor" with a string potentiometer. This displacement was taken as the anterior-posterior (A-P) thorax deflection.

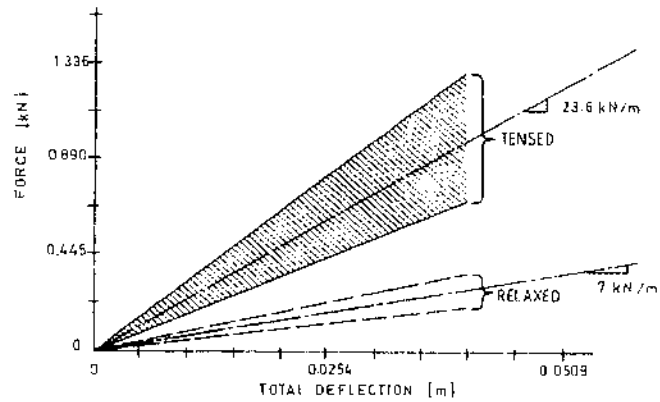

Fig. 6.4 *Comparison of volunteer quasi-static frontal thorax stiffness in tensed and relaxed state [9]*

Tests were conducted with the volunteers in a tensed and a relaxed state. Fig 6.4 shows corridors of the force-deflection characteristics derived from these tests. Zero deflection was defined at 22.2 N pre-load. A large difference between the tensed and the relaxed condition can be observed. The tensed condition appears to result in a 3-4 times larger thorax stiffness which is clearly a benefit from the standpoint of injury tolerance. An additional benefit of being tensed is that the thorax size increases [10].

An extensive review of human cadaver tests conducted in the sixties and early seventies was conducted by Kroell [10]. These tests still represent the basis of current biofidelity performance requirements for frontal impact dummies. Initially sled tests and impactor tests with embalmed cadavers were conducted followed in a later stage by unembalmed cadaver impactor tests. Embalmed responses in general showed somewhat higher forces than unembalmed ones. In the impactor tests an identical impactor face was used as for the volunteer tests discussed earlier. The subjects were seated upright and in most of the tests the back of the cadavers was not restrained. Tests were conducted with different impactor masses and impact velocities. The impact load was determined by a load cell located in the impactor.

Different techniques for determining the thoracic (i.e. sternum) deflection were employed in the tests. Initially use was made of a deflectometer rod attached anteriorly to the sternum

and passing through the thoracic cavity to one side of the thoracic spine and protruding through a bushing in the back tissue. At the free end of the rod a target was mounted of which the position was measured photographically relative to the bushing in the back. A disadvantage of this technique is a possible contribution to the injury mechanisms in the thorax and the fact that it prevents pressurisation of the arterial system. Another technique involved the use of an induction coil deflection gage, however this device did not record the initial deflection correctly. So both techniques were not employed in later tests. Instead thoracic deflection was determined directly from highspeed films as the differential motion between impactor and back of the spine. Corrections have to be introduced for the interface (tissue) deflections in order to obtain sternum deflections.

Typical force-deflection curves obtained from unembalmed cadaver tests in which the same impactor mass (about 23 kg) and the same impactor velocity (about 7 m/s) was used are summarized in Fig. 6.5. The deflections presented here are not corrected for the interface deflections. A couple of observations can be made:

- The general shape of the curves is that of a sharply rising force during the initial deflection followed by a plateau region up to maximum deflection.
- This plateau is followed by a large drop in force level indicating a high hysteresis in the thorax system.
- Comparison with Fig. 6.4 in which human volunteer static response is displayed, shows a large difference between static and dynamic thoracic response. The dynamic stiffness appears to be much larger than the static one. (This is not due to possible differences between static cadaver and human volunteer thoracic stiffness since they are from the same order of magnitude).

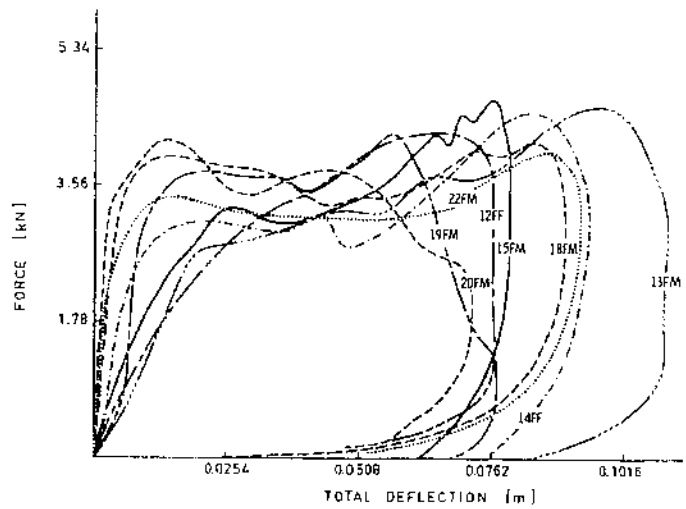

Fig. 6.5 *Dynamic force-deflection characteristics in frontal impacts [10]*

Similar shaped curves are reported for other combinations of impactor masses and impactor velocities. It was found that the plateau force increases with the impactor velocity. An exception was the condition of low mass, high velocity, impacts where the force rises sharp early in the loading event, but than shows a sharp decline without a constant force level (plateau).

Fig. 6.6 shows the relationship between impactor velocity and plateau force [1]. In addition to data from Kroell in this Fig. also impactor tests with one volunteer [11] in similar test conditions are included. Data of Kroell are presented in original form and corrected for absence of muscle tension. This correction was estimated from the differences in tensed and relaxed human volunteer tests presented in Fig. 6.4. Fig. 6.6 suggests a linear relationship between plateau force and impact velocity above impact speeds of 4 m/s.

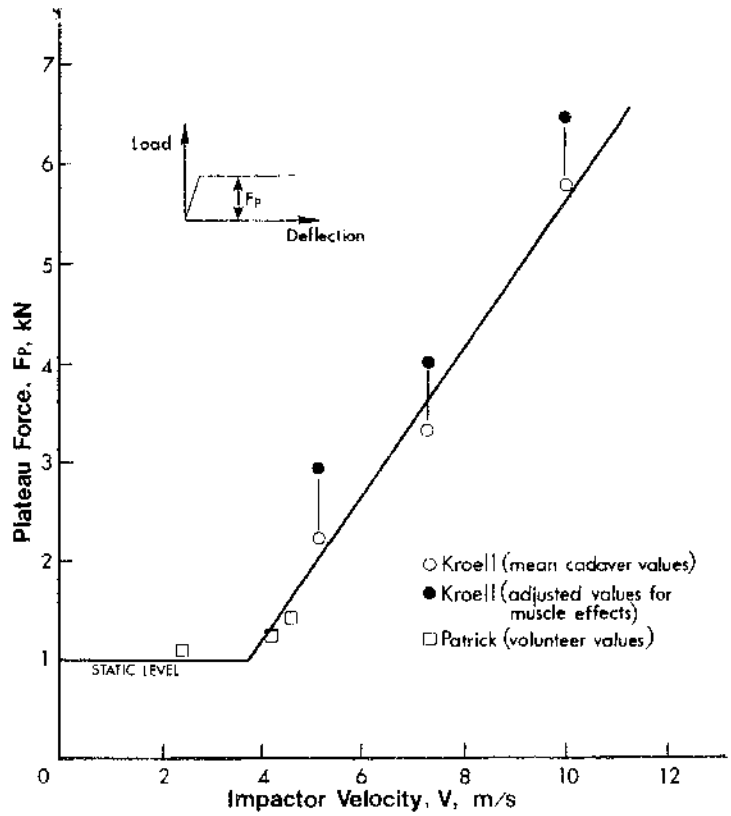

Fig. 6.6 Plateau force versus impactor velocity for frontal chest impacts [1]

On the basis of the cadaver tests, force-deflection corridors for 2 combinations of impactor mass and velocity were developed to be used as performance requirements for crash dummies [10]. The corridors are often referred to as the Kroell corridors.

In 1973 Lobdell [9] developed a mathematical thoracic analog which consists of 3 masses m1, m2 and m3 connected by springs and dampers (Fig. 6.7). Mass m1 represents the impactor and masses m2 and m3 the sternal and vertebral effective mass. Spring k_{12}

represents the skin and flesh between impactor and sternum. The internal spring and dampers represent the connection between sternum and thoracic spine. The model response correlated well with the Kroell cadaver corridors even if the spring-damper in series was removed [12]. The Lobdell thorax model has been frequently applied, for instance in dummy thorax design studies.

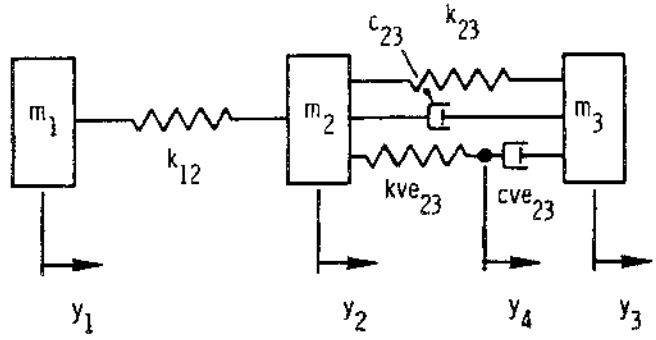

Fig. 6.7 The Lobdell thorax model [9]

In addition to above tests with circular flat impactors also a number of sled tests have been conducted in which the biomechanical response due to belt loading was investigated. A review of a number of studies is given in Ref. [1]. It was shown that belt loading produces a significantly different load distribution than a flat circular impactor. The constant level of the "plateau force" was not found for belt loading; in fact the force-deflection responses under dynamic conditions were reported to be close to linear. Average dynamic stiffnesses at the sternum level were reported in the range of 120-140 kN/m. Dynamic thoracic stiffness were found to be much larger than static values like in the circular flat impactor tests. Furthermore it was found that the static thorax stiffness under belt loading is about twice as high as due to static circular plate loading [1].

The studies described above all relate to cadaver or human volunteer tests. Experiments with animals have shown a number of similarities with the cadaver tests. For instance the plateau force was also observed in many animal tests as is illustrated in Fig. 6.8, while moreover a very strong sensitivity of the plateau force level to impact velocity could be demonstrated [10]. Fig 6.8 shows the force as function of normalized deflection (i.e. deflection expressed as a percentage of the anterior-posterior chest diameter). The level of the plateau force appears to correlate well with the weight of the animal. Further it can be observed in this Fig. that the difference between embalmed versus in vivo animal tests is less than 20%.

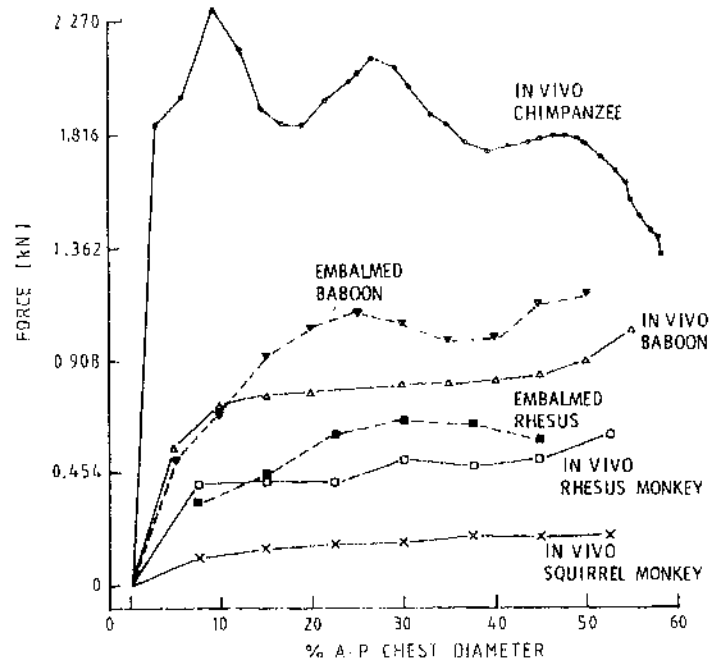

Fig. 6.8 Force-deflection response in several animal tests [10]

6.4.3 Lateral loading

The earliest lateral thorax impacts with unembalmed human cadavers were conducted by Stalnaker in the seventies [13]. Tests with a flat rigid circular impactor (diameter 0.152m and mass 10 kg) and with a padded armrest simulating impactor were carried out. Thoracic deflections were obtained from high speed films. Results of these tests are summarized in Fig. 6.9 and 6.10. It follows that the padded impact tests do not exhibit a sharp initial rise in impact load like in the rigid impact tests. Fig. 6.9 also includes a corridor of frontal thorax impactor tests using the same test procedure. It can be seen that the lateral thorax "stiffness" is less than the frontal one. Comparing the corridor of frontal impact response in Fig. 6.9 with the test results presented by Kroell (see Fig. 6.5) shows that a plateau force as observed by Kroell is less apparent in the Stalnaker tests. A good explanation of this difference has not been given in literature but most likely the relative inaccuracy of a single defection measurements as such, is an important contributing factor.

To overcome the problems related to a single deflection measurement, Robbins [14] developed a new method using 12 accelerometers which were fixed to different well-defined locations at the ribcage (see Table 6.1). This array of sensors allows the measurement of the kinematic response of the flexible ribcage in a more accurate way and is moreover suited for different impact directions. It was intended to be used for cadavers as well as dummies.

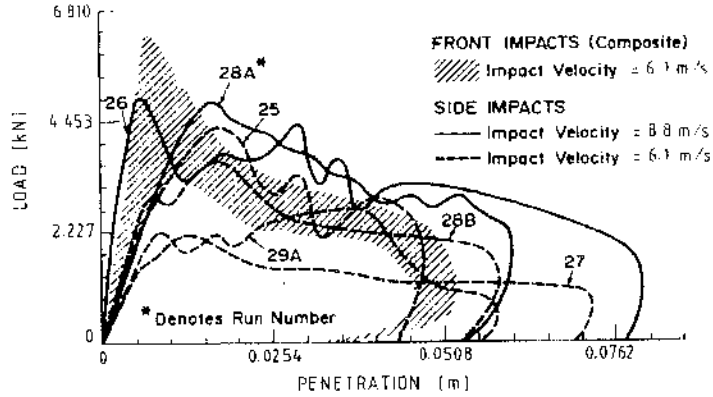

Fig. 6.9 *Dynamic force-deflection characteristics in lateral impacts with a flat circular impactor [13]. A corridor of frontal response is included as well.*

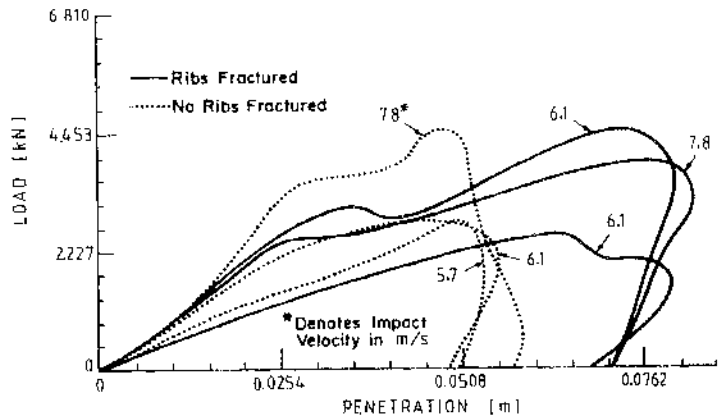

Fig. 6.10 *Dynamic force-deflection characteristics in lateral impacts with a padded armrest simulated impactor [13].*

Table 6.1 *Accelerometer locations in thoracic impact tests [14]*

Location	Active Axis Direction
Most lateral point on fourth left and right rib	Left to right, normal to body
Most lateral point on eight left and right rib	Parallel to body pointing to front
Top of sternum	Pointing to front of body
Bottom of sternum	Pointing to front of body
Spinous process of first thoracic vertebra	Triaxial mount with head to foot, left to right, and front to back axes
Spinous process of twelfth thoracic vertebra	Triaxial mount with head to foot, left to right, and front to back axes

Using this instrumentation a large number of tests have been conducted, particularly in lateral direction. Both impactor and sled tests were carried out. After the tests detailed autopsies were performed and resulting injuries were correlated with the accelerometer measurements. This resulted in the so-called Thoracic Trauma Index (TTI) which will be briefly discussed in Section 6.5. Biofidelity performance requirements available from these tests are force-time and acceleration-time histories rather than force-deflection data since deflections could not be determined accurately from the accelerometer measurements. Fig. 6.11 illustrates typical results for the rib acceleration at the fourth rib at the struck side (referred to as left upper rib (LUR)) obtained from 4 lateral rigid impactor tests. A summary of the available data base (status 1985) of cadaver tests using the 12 accelerometer array and resulting response corridors is provided in Ref. [15]. Currently the data base of lateral impacts consists of 84 cadaver tests [16]

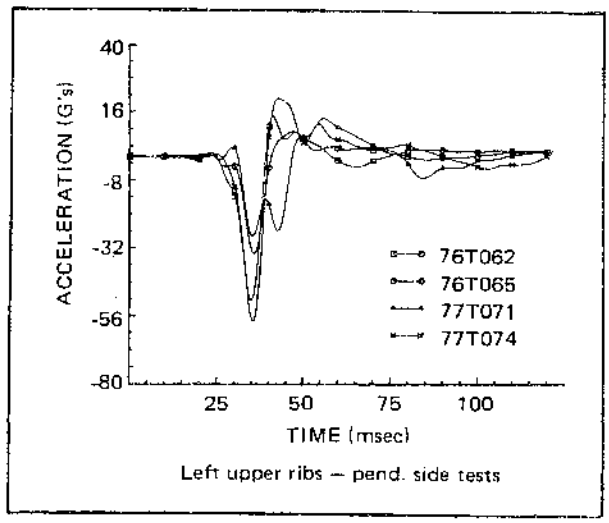

Fig. 6.11 Left upper rib accelerations (i.e. struck side rib) in lateral impactor tests [14]

One important factor in lateral thorax impacts is the placement of the arm of the subject. The arm can be placed partly or completely between the striking object and the thorax or the arm can be raised. In a study by Cesari [17] the effect of arm placement was studied by means of cadaver tests. It was concluded that the arm has some protective effect, comparable with a reduction in impactor velocity of about 10%.

6.5 Injury criteria and tolerances

6.5.1 Introduction

In Section 6.3 three principal injury mechanisms for the thorax were identified: compression, viscous response and inertial loading. It was noted that often these mechanisms will occur in combination with each other. Proposed thoracic injury criteria in literature relate to

one or more of these mechanisms. The most important criteria are chest deflection in relation to the compression mechanism, acceleration and force based criteria related to compression and inertial loading and the viscous criterion related to both compression and viscous response. In the next Section first a description of simple acceleration or force based criteria will be given followed, in Section 6.5.3, by a discussion on a more complex acceleration based criterion: the Thoracic Trauma Index (TTI). Thorax compression criteria will be described in Section 6.5.4 and finally in Section 6.5.5 the so-called viscous tolerance criterion will be discussed.

6.5.2 Single acceleration and force based injury criteria

The first thoracic injury criteria were acceleration or force based. In Section 3.6 some of the earliest whole-body tolerance tests with human volunteers were reviewed. In these tests the subjects were not instrumented yet. Most data obtained were limited to acceleration levels measured at an impact sled on which the subject was seated, restrained by a harness system. Based on these tests and additional sources it was shown that the whole-body deceleration tolerance decreases if the duration of the exposure increases. The use of a single acceleration criterion for the prediction of chest injuries is rather attractive for measurements in crash dummies since such measurements relatively easy can be performed. United States regulations (i.e. MVSS 208) specify a resultant chest acceleration at the dummies centre of gravity as being acceptable if it does not exceed 60 g, except for intervals whose cumulative duration is not more than 3 ms.

As an alternative chest criterion in an earlier stage the chest severity index (SI) has been used which is identical to the head SI discussed in Chapter 4. This criterion is calculated from the chest resultant acceleration in the centre of gravity and like for the head a tolerance level of 1000 was proposed. The value of the chest SI is meaningless however according to Nahum [18] who observed that sternum SI exceeded sometimes 20.000 in cadaver tests, while in similar experiments spinal SI usually was found to be below 50!

The reliability of a single acceleration criterion as a general injury parameter for description of the different thoracic injury mechanisms is rather limited. A single acceleration criterion namely is based on Newton's second law, which states that the force on a rigid mass is proportional to its acceleration. The real situation is that the human chest is not a single mass, but should be represented as a more complex system built of masses, springs and dampers like illustrated by the Lobdell thorax model shown in Fig. 6.7. The response of this complex system cannot be simply accounted for by a single mass, as is done in a single acceleration criterion. For this reason Robbins [14] started the research program discussed in Section 6.4.3 in which accelerations were measured at more locations in the ribcage. In Section 6.5.3 some of the findings in terms of injury prediction functions will

be discussed with special emphasis on the Thoracic Trauma Index (TTI), which uses the accelerations at the struck side ribs and at T12.

Closely related to acceleration based tolerance requirements (through Newton's second law) are force based requirements. The first tests reviewed by Kroell (see 6.4) were tests with human cadavers seated unrestrained on a deceleration sled. These cadavers were arrested by energy absorbing structures instrumented with load cells. The purpose of these tests was to establish force based tolerance levels for the development of energy absorbing steering columns. From these test a 3.29 kN maximum force on the sternum and a 8.00 kN maximum distributed load on the shoulder and chest were proposed with only minor risk of injury in case of a well-centred impact [19]. These values are much lower than a tolerance of 17.6 kN which can be calculated from the 60 g deceleration tolerance value, assuming an effective thorax mass of 30 kg. In addition to tolerable "steering column" loads also tolerance levels for shoulderbelt loads have been defined from cadaver tests [20]. These values were slightly below the 8.00 kN level. A disadvantage of using such force levels as an injury criterion is that they are very sensitive to the parameters of the steering column or the seat belt system. Moreover like a single acceleration requirement a force applied to the thorax can not account for the complex response in the thorax itself. Kroell [10] concluded that for the spectrum of loading conditions used in his study, peak thoracic force did not correlate well with injury produced in the cadaver.

6.5.3 The Thoracic Trauma Index (TTI)

The TTI is an acceleration criterion for lateral thoracic injuries derived from a large bio-mechanical data base in which the 12 accelerometer array was used for determination of the ribcage kinematics (see Section 6.4 for details). The TTI formulation was developed using regression analysis techniques. It followed that the occurrence of injuries is strongly related to the average of the peak lateral acceleration, experienced by the struck side rib cage and the lower thoracic spine. The specific benefit of the TTI is that it allows, in principle, to assess the injury risk for a certain population at risk since the weight and age are included in the formulation.

The TTI is defined by the following equation [21]:

$$TTI = 1.4 * AGE + 0.5 * (RIBY + T12Y) * MASS / M_{std} \qquad (6.1)$$

where:

TTI = Thoracic Trauma Index (dimension: g)
AGE = age of the test subject in years

RIBY = maximum absolute value of lateral acceleration in g's of the 4th and 8th rib on struck side after filtering of the acceleration signal

T12Y = maximum absolute value of lateral acceleration in g's of the 12th thoracic vertebra after filtering of the acceleration signal

MASS = test subject mass in kg

M_{std} = standard reference mass of 75 kg

There is also a definition for the TTI which could be used for 50th percentile dummies [16]

$$TTI(d) = 0.5 * (RIBY + T12Y) \tag{6.2}$$

It is important to emphasize here that in order to compute a meaningful TTI or TTI(d), the acceleration signals have to be processed according to a prescribed filtering procedure.

The predicting capability of the TTI is demonstrated in Fig. 6.12, which shows the AIS as function of TTI for a large number of cadaver tests, including an initial series of tests mainly conducted in the USA (indicated by O) and more recent tests conducted by the University of Heidelberg. These last tests were conducted on a sled with an Opel Kadett car body as side structure. L indicates impacts at the left side thorax and R at the right side.

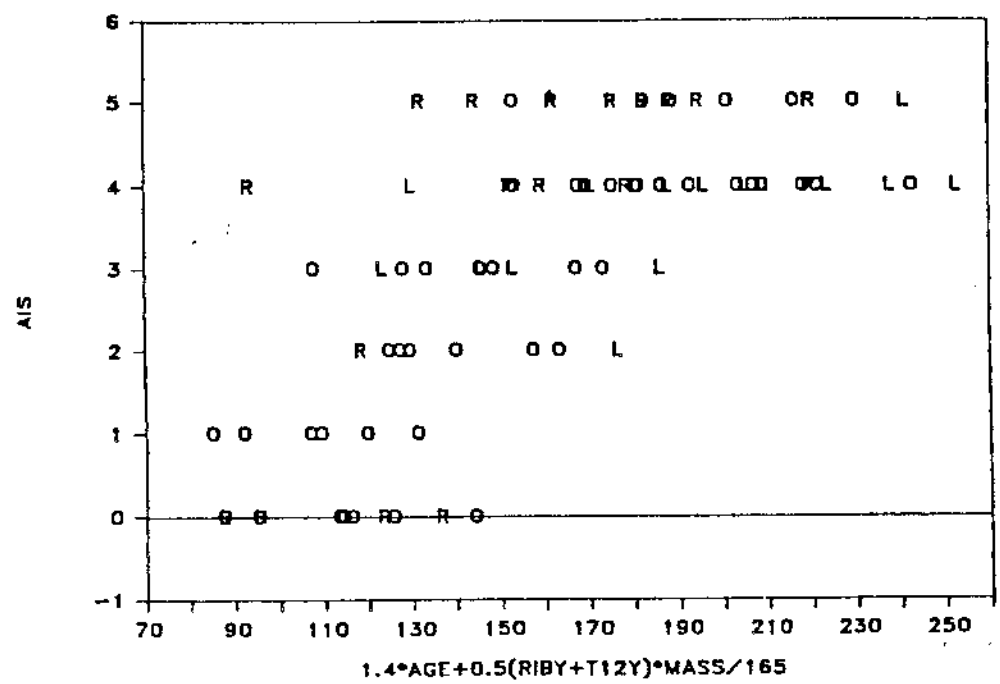

Fig. 6.12 AIS as function of TTI [21]

The "Maximum Likely Hood" method using a Weibull distribution (see Section 3.6) was applied on these data to determine the probability of injury for several AIS levels. Also the difference between the probability of injury in the left and right thorax side was investi-

gated. Fig. 6.13 shows the probability of risk at the right and left side as function of TTI, for severe injuries (AIS = 4 or greater). It follows that the body has a lower thoracic impact injury tolerance on the right side than on the left side, which was explained by the contribution of liver injuries.

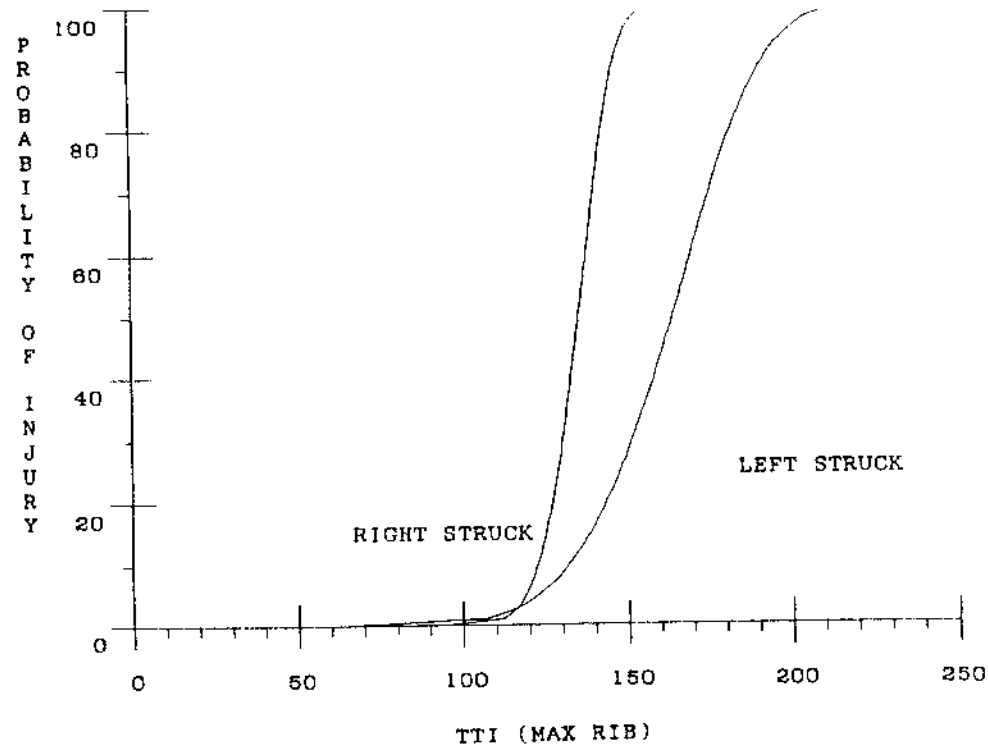

Fig. 6.13 *Comparison of probability of severe injuries (AIS = 4 or greater) for left side and right side impacts [21].*

An important criticism on the TTI is that it reflects a pure statistical function rather than a physical one. In other words there is not a physical basis which explains the relation between TTI and the injury mechanisms involved. Such a physical relation clearly is present for the compression as injury criterion, as will be shown in the next Section. In the TTI formulation simply 2 peak accelerations, which moreover occur at different times, are added. Attempts have been made to calculate the deformation of the ribcage by double integration of the spine and rib acceleration and by subtracting these values subsequently. But the results were rather disappointing since the accuracy of the accelerometer values appeared to be too limited for this calculation.

6.5.4 The Compression Criterion (C)

Because of the insufficient prediction of the risk of internal injuries by thorax accelerations and the impact force, several attempts have been made to find better indicators for chest injuries. From the cadaver and animal tests analyzed by Kroell [10] which were discussed

in Section 6.4.2, it was concluded that maximum chest compression is a much better indicator of chest injury severity than acceleration or force. Fig. 6.14 according to Kroell [10] presents for frontal impacts the AIS as function of chest compression resulting from cadaver and animal tests. Compression is defined here as the amount of deformation divided by the thickness of the thorax. A linear regression line based on the cadaver tests is included. It follows that human volunteers can sustain about 20% of chest compression under quasi-static frontal loading conditions without injuries. The regression line indicates 35% compression for an AIS 3 injury.

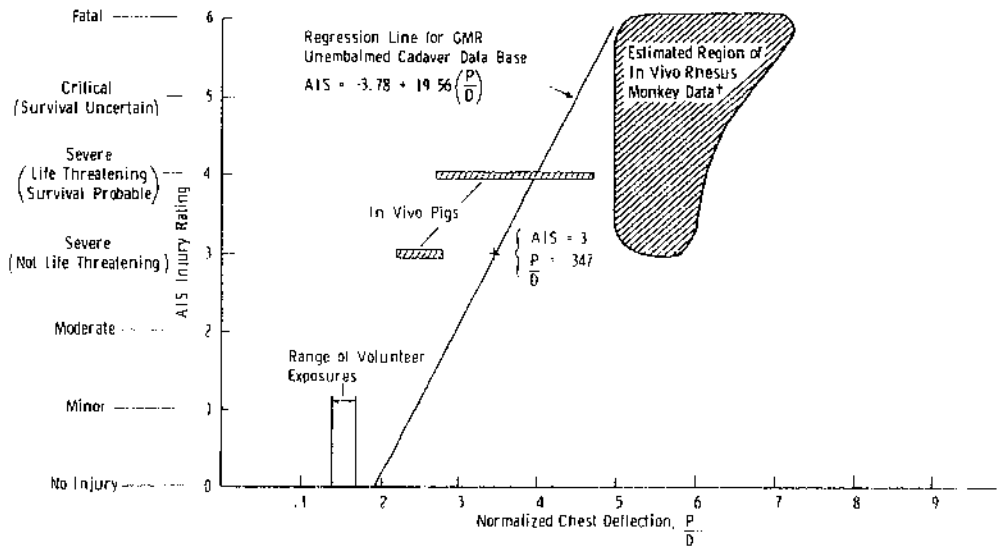

Fig. 6.14 Summary of injury tolerance vs. thorax deflection in frontal blunt thoracic impact [10]

Viano [19] suggests to make a distinction between skeletal damage and internal organ injuries. After reviewing the cadaver data of Kroell he concluded that the linear relationship between injury and compression only holds to a certain point. Beyond this point the thorax collapses (flail chest) and the likelihood of "life-threatening" heart, lung and vessel injuries increases dramatically. Statistical analysis resulted in a 25% probability of severe injury (i.e. AIS 4 and higher) at a compression of 35% in frontal blunt impacts [19].

6.5.5 The Viscous Criterion (VC)

A large series of animal tests has shown that a compression criterion does not properly reflect the probability of injury for higher impact velocities. See Viano [19] for a review of these tests. In situations with constant maximum compression and different impact velocities, injuries are more severe (on the AIS scale) for the higher velocities. Less compression is required to produce similar injury levels when the impact velocity is increased. This relationship was found both for frontal and lateral thoracic impacts but also for abdominal

impacts. For impact velocities below 3 m/s a compression criterion appears to be adequate (Fig. 6.15), but for impact velocities up to 30 m/s both compression and the velocity of compression have to be taken into account. For higher velocities only the velocity of compression is important (blast injuries).

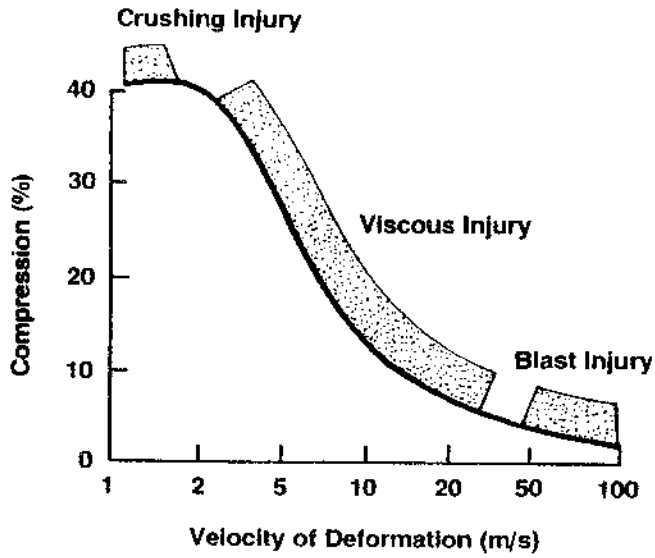

Fig. 6.15 *Ranges of validity for the viscous criterion [22]*

The Viscous Criterion, denoted as VC, is a time function formed by the product of the velocity of deformation, V(t) and the instantaneous compression function C(t). The velocity of the deformation V(t) is calculated by differentiation of the deformation, D(t): V(t) = d[D(t)]/dt and C(t) is defined as D(t)/D, where D is the initial torso thickness. So :

$$VC = \frac{d[D(t)]}{dt} \times \frac{D(t)}{D} \tag{6.3}$$

VC has the same dimension as V(t): [m/s]. Like for the TTI the method of filtering of the signals is very important. Analysis of several series of animal as well as cadaver tests has shown that the maximum Viscous response, defined as VC_{max} is highly correlated to the risk of injuries. For example in case of the Kroell cadaver data the Viscous response was found to correlate better with injury risk than maximum compression [19]. The tolerance level for a 25% probability of severe injuries (i.e. AIS 4 and greater) in the Kroell cadaver data base was VC_{max} = 1 m/s.

The physical interpretation of VC can be explained by means of the Lobdell model presented in Fig. 6.7. Let y(t) = y1(t)-y3(t) represent the chest deflection. The velocity of deformation V(t) is given then by $v(t) = \dot{y}(t)$

The viscous response VC can be written as:

$$V(t)\,C(t) = y(t)\,\dot{y}(t)/D \tag{6.4}$$

The Lobdell model will be reduced now to a more simple system without spring K_{12}, spring KVE_{23} and damper CVE_{23}. Further the damper C_{23} is a linear damper with the damping force F_c given by $F_c(t) = \dot{y}(t)$. The adsorbed energy in the damper takes the form:

$$E_v(t) = \int_0^t F_c(t)\,dy = \int_0^t (\dot{y}(t))^2\,dt \tag{6.5}$$

Since the differential of $y\dot{y}$ is:

$$\frac{d(y\dot{y})}{dt} = (\dot{y})^2 + y\ddot{y} \tag{6.6}$$

eq. (6.5) can be written as:

$$E_v(t) = \int_0^t \frac{d(y\dot{y})}{dt}\,dt - \int_0^t y\ddot{y}\,dt \tag{6.7}$$

or:

$$E_v(t) = y(t)\,\dot{y}(t) - \int_0^t y\ddot{y}\,dt \tag{6.8}$$

By using eq. (6.4) for the first term in (6.8) and assuming a thickness D of unity it follows:

$$E_v(t) = v(t)\,c(t) - \int_0^t y\ddot{y}\,dt \tag{6.9}$$

Thus VC is related to the absorbed energy in the thorax.

To illustrate this relationship we shall consider an example in which the velocity of deformation is a sinusodial function: $\dot{y}(t) = \sin t\ (0 \le t < \pi)$. Fig. 6.16 shows the velocity of deformation, the chest deflection, the absorbed energy and the viscous response for this situation. Also the risedual integral in eq. 6.9 is included. It follows that the viscous

response reaches a maximum before the absorbed energy approaches its maximum. The residual integral in this example is small and negative until VC reaches its maximum.

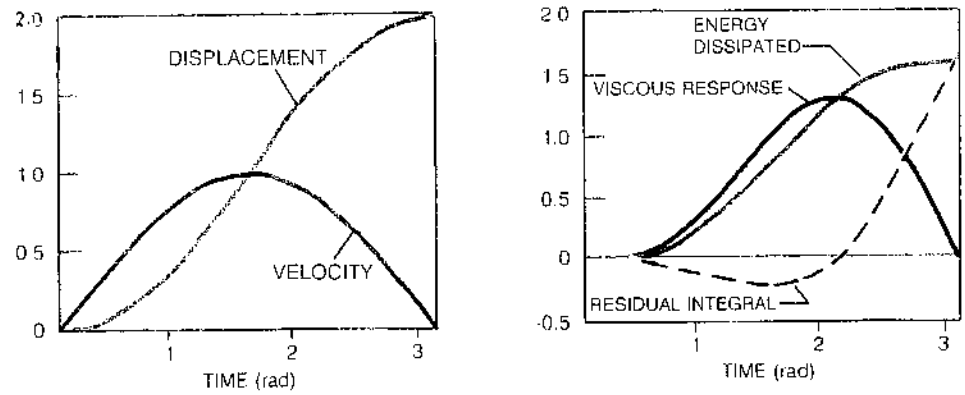

Fig. 6.16 *Example of viscous response and absorbed energy for a velocity of deformation* $\dot{y} = \sin t$ *[19].*

6.6 Discussion and conclusions

Injuries to the human thorax can be subdivided into skeletal and soft tissue injuries of the internal organs. The latter injuries are the most critical ones and the knowledge on the injury mechanisms involved in case of blunt impacts are not well understood yet. Various injury criteria have been proposed including accelerations, forces, deflections and a combination of deflection and velocity of deflection called viscous response VC, to predict thoracic injuries. This last criterion seems to be the most promising one, since it appears to be closely related to the physical mechanisms taking place during impact loading. In order to calculate this criterion accurately, information on the thoracic deflection is required, but research conducted in the past has shown that the accuracy of current deflection measurements is still questionable.

Several attempts have been made in the past to obtain more detailed information on the thoracic deformation during an impact, instead of using a single deflection measurement. An example of this approach is the 12 accelerometer array discussed in Section 6.4.3. The statistical analysis which was conducted on these data resulted in an injury criterion called Thoracic Trauma Index (TTI) which however lacks a clear physical relationship with the injury mechanism. One explanation for this might be the limited reliability of integrated accelerometer data which are needed to obtain relative velocities and deformations in the thorax, i.e. parameters which have been shown to correlate well with thoracic injuries. Alternative measurement techniques which currently are under development and which are intended to assess the spatial deformations of the thorax more accurately, certainly are of interest in this respect. An example is the chest band, a thin metal band equipped with straingages which surrounds the thorax [23].

Like for the other body area's discussed in this course, i.e. the head and the cervical spine, relatively simple mathematical models of the anatomical structure have been developed which can be of help to explain some of the mechanical phenomena involved. The Lobdell model discussed here, has obtained much attention from researchers and has been applied successfully to support dummy design studies and to study the effect of injury reduction strategies like the effective use of padding materials. More detailed models which take the actual thoracic anatomy into account are needed, in close conjunction with well-defined biomechanical tests, in order to study and understand the various injury mechanisms and to analyze the effect of different loading conditions in detail.

REFERENCES

1. Melvin J.W., R.L. Hess and K. Weber: "Thorax", In: "Review of Biomechanical Impact Response and Injury in the Automotive environment", Chapter 3, Technical report DOT HS 807 042, U.S. Department of Transportation National Highway Traffic Safety Administration, 1986.

2. Sobotta/Figge: "Atlas of the human anatomy", Urban & Schwarzenberg, Baltiomore-Munich, 1977.

3. Huelke D.F.: "The anatomy of the human chest", In: The human Thorax, anatomy, injury and biomechanics, P-67, Society of automotive engineers inc., Warrendale, 1976.

4. Peters, M: "Biomechanics of chest injuries", In: The Biomechanics of Trauma. Eds. Nahum and Melvin. Appleton, Century-Crafts, Norwalk, Connecticut, 1985.

5. G. William et. al.: "An introduction to the understanding of blunt trauma", In: The human thorax, anatomy, injury and biomechanics, P-67, Society of automotive engineers inc., Warrendale, 1976.

6. A.K. Roberts, E.G. Janssen and D. Cesari: "Review of cadaver responses to lateral impact and derived biofidelity targets for dummies". IRCOBI Conference, Bron, September 1990.

7. Stalnaker, R.L., Tarriére, C., Fayon, A., Walfisch, G., Baltlazard, M., Masset, J., Got, C. and Patel, A.: "Modification of Part 572 dummy for lateral impact according to biomechanical data", Proc. 23rd Stapp Car Crash Conference, pp. 843-872. Society of Automotive Engineers, Warrendale, Pa, 1979.

8. Fayon, A., et al: Contribution to Defining the Human Tolerance to Perpendicular Side Impact, Proceedings of the 3rd IRCOBI Conference. Berlin FR Germany. Spetember 1977.

9. Lobdell T.E.: "Impact response of the human thorax", In: Human impact response: Measurement and simulation, pp 201-245, Plenum Press, New York, 1973.

10. Kroell, C.K.: "Thoracic response to blunt frontal loading", In: The human thorax, anatomy, injury and biomechanics, P-67, Society of automotive engineers inc., Warrendale, 1976.

11. Patrick, L.M.: Impact force-deflection of the human thorax. Proc. 25th Stapp Car Crash Conference, pp. 471-496. Society of Automotive Engineers, Warrendale, Pa.

12. Neathery, R.F. and Lobdell, T.E.: "Mechanical simulation of human thorax under impact", Proc. 17th Stapp Car Conference, pp. 451-466, Society of Automotive Engineers, New York, 1973.

13. Stalnaker, R.L., Roberts, V.L. and McElhaney, J.H.: "Side impact tolerance to blunt trauma, Proc. 17th Stapp Car Conference, pp. 377-408, Society of Automotive Engineers, New York, 1973.

14. Robbins, D.H., Lehman, R.J. and Augustyn, K.: "Prediction of thoracic injuries as a function of occupant kinematics", 7th International Technical Conference on Experimental Safety Vehicles, pp. 374-383. U.S. Government Printing Office, Washington, D.C. 1979.

15. Melvin, J.W., King, A.I. and Alem, N.M.: "AATD System Technical characteristics, design concepts, and trauma assessment criteria", Task E-F, Final Report, Contract, DTNH22-83-C-07005. USDOT NHTSA, Washington, 1985.

16. Federal Register, Part II, VS-DOT, MHTSA, 49 CFR Part 571, et al. Federal Motor Vehicle Safety Standards, Side impace protection, Rules, Vol. 55, No 210, Oct 30 1990.

17. Cesari, D., Ramet, M. and Bloch, J.: "Influence of arm position on thoracic injuries in side impact", Proc. 25th Stapp Car Conference, pp. 271-297, Society of Automotive Engineers, Warrendale, Pa., 1981.

18. Nahum, A.M., Schneider, D.C. and Kroell, C.K.: "Cadaver skeleton response to blunt thoracic impact", Proc. 19th Stapp Car Conference, pp. 259-293, Society of Automotive Engineers, Warrendale, Pa., 1973.

19. Viano, D.C. and Lau, I.V.: "A viscous tolerance criterion for soft tissue injury assessment", J. Biomechanics 21 (5): 387-399, 1988.

20. "Human tolerance to impact conditions as related to motor vehicle design", SAE information report SAE J885 JUL86, Society of Automotive Engineers, Inc. 1986.

21. Morgan, R.M., Marcus, J.H. and Eppinger, R.H.: "The biofidility of NHTSA's proposed ATD and Efficacy of TTI", SAE 861877, Proc. 30th Stapp Car Crash Conf, 1986.

22. Lau I.V., Viano, D.C.,: "The Viscous Criterion: Bases and Applications of an Injury severity Index for Soft Tissues", SAE 861877, Proc 30th Stapp Car Crash Conf, 1986.

23) Hagedorn, A.V., Eppinger, R.H., Morgan, R.M., Pritz, H.B. and Khaewpong, N.: "Application of a deformation measurement system to biomechanical systems", Ircobi Conference, Berlin, 1991.

CHAPTER 7

MECHANICAL HUMAN BODY MODELS

7.1 Introduction

Every year thousands of people die in road accidents and many more are injured seriously. Scientific research can assist in preventing part of the fatalities and injuries. The risks involved in road use can be effectively reduced by translating research results into legal measures or by implementing them in the automobile industry. European accident statistics over the last decade show impressive results. The compulsory use of seat belts and crash helmets, for instance, has reduced the number of fatalities significantly.

Thorough knowledge of the characteristics of the human body and its behaviour under heavy mechanical loads is essential in research with the aim to prevent serious consequences of accidents. Injury mechanisms and human tolerance levels should be known in order to improve, for instance, the safety of passenger cars. International automotive standards have been developed to evaluate the crash performance of motor vehicles. In these standards road accidents are simulated by well-defined laboratory experiments. For obvious reasons it is impossible to perform such experiments with human beings. Therefore approval tests in accordance with these standards are carried out with 'mechanical models' or 'crash dummies'. These substitutes have similar characteristics as human beings and, being fitted with special instrumentation, they enable injuries to be assessed.

This Chapter gives a summary of design requirements and specifications for crash dummies (Section 7.2). Section 7.3 describes the physical parameters measured by the dummies to assess injury risk. In Section 7.4 some examples are presented of dummies used in approval testing, while trends in future dummy design are summarized in Section 7.5.

7.2 Dummy design requirements and specifications

7.2.1 Introduction

Mechanical models or *crash dummies* normally consist of a metal or plastic skeleton, including joints, covered by a flesh-simulating plastic or foam. They are constructed such that dimensions, masses and mass-distributions, and therefore the kinematics in a crash, are humanlike. The dummy is fitted with instrumentation to measure accelerations, forces and deflections during the test, that correlate with injury criteria for human beings. Dummies are often used in approval tests on vehicles or safety devices, in which the measured values

should remain below certain (human tolerance) levels. Very important in this respect is a repeatable response of the dummy in identical tests.
Most dummies used to evaluate vehicles or safety devices are used in one specific impact mode; frontal or lateral. Dummies with a vertical performance capability are mainly used in aircraft research concerned with ejection seat testing. This 'impact direction' is the most important design requirement. Attempts have been made to design 'omni-directional' dummies, however without much succes. The following sections will show that it is already difficult to design a dummy suitable to be used in one impact direction. Of course, not all requirements should necessarily be fulfilled, this depends strongly on the dummy application.

7.2.2 Simplicity

Mechanical human models are not necessarily complex pieces of equipment. Depending on the application, (quasi) two-dimensional models rather than three-dimensional models can be used. Sometimes it takes only half a dummy to evaluate a product. The 'body-block impactor', for instance, consists of only the front of the dummy (see Fig. 7.1). This 'device' is used to evaluate the flexibility of the steering systems in accordance with ECE-Regulation 12 (see also 7.4.2). The torso-stiffness and the mass (35 kg) are prescribed. When the dummy impacts a steering system with 24 km/h, the force on the dummy should remain below 11110 N to pass this Regulation.

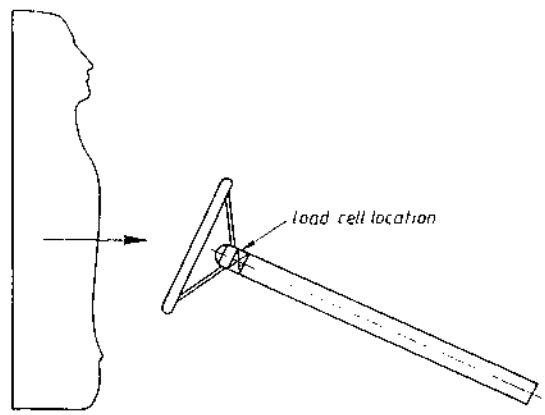

Fig. 7.1 Body-block dummy for the evaluation of the flexibility of steering systems.

In general three levels of complexity can be distinguished:
- complete (crash) *dummies* for the evaluation of vehicles and/or safety systems in full-scale tests;
- *body segment* impactors for the evaluation of vehicle sub-systems;
- *impactors* for the evaluation of vehicle components.

In sub-system tests a part of the vehicle is tested by a part of the dummy. The surrounding vehicle structure should be included to avoid 'edge-effects' and to obtain realistic boundary conditions. The body segment impactor should have an effective mass (see 7.2.4), impact velocity and -angle corresponding with the kinematics of a complete dummy (see Fig. 7.2). Dummy tests and mathematical model simulations are performed to obtain these test values. Vehicle components (e.g. dashboard) are normally tested by rigid impactors having a standard mass and a standard impact velocity.

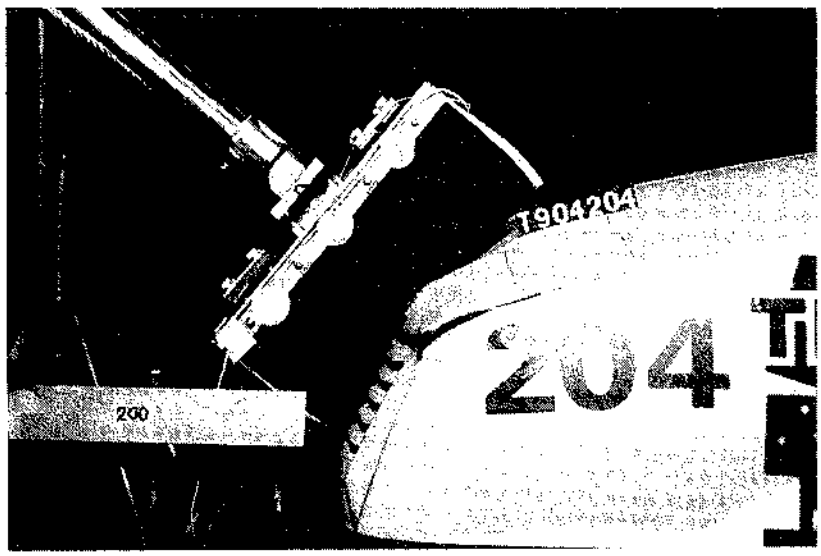

Fig. 7.2 *Subsystem test representing an impact of a pedestrian's upper leg against the bonnet leading edge of a passenger car.*

Complex pieces of equipment with extended instrumentation are more likely to fail. Servicing and certification (see also 7.2.6) is frequently expensive and sometimes difficult, therefore ease of maintenance and serviceability must also be considered during the design phase.

The following requirements and specifications mainly relate to 'complete dummies'.

7.2.3 Anthropometry

Crash dummies should represent the human being in terms of selected size and corresponding mass and mass-distribution. The dummy should interact correctly with the vehicle seat and the safety belt system. Moreover, the dummy should sit in the seat in a lifelike manner.

In automotive tests a 50th *percentile* adult male dummy is most frequently used. In a frequency-distribution of a certain anthropometric measurement, 'one percentile' is a column with an area of 1% under the frequency-curve. So the 50th percentile value indicates the measurement value for which 50% of the population shows a lower value (and therefore

also 50% a higher value). Therefore a 50th percentile measurement represents an 'average'. All these 50th percentile values are combined in one 'mid-sized' dummy, which then represents a 'defined average' adult male dummy. Occasionally two other sizes are used in vehicle crash tests, a 95th percentile (large) male and a 5th percentile (small) female. Many anthropomorphic studies have been published, whereas the study of Schneider and Robbins [1] is mostly referred to nowadays. An extensive measurement program has been carried out to define the external dimensions, coordinate system definitions, location of body segment centers of gravity and joint center locations of a small female, a mid-sized male and a large male in a 'driving position'. Fig. 7.3 illustrates the general configuration of these dimensions. The specific gravity (i.e. density) of body segments measured on cadavers is used together with the volume of the body segment measured on the volunteers to calculate the mass for the body segments. Segment inertial properties are based on these calculated masses. A total body mass of 77.5 kg and a standing height of 175 cm were defined for a 50th percentile adult male.

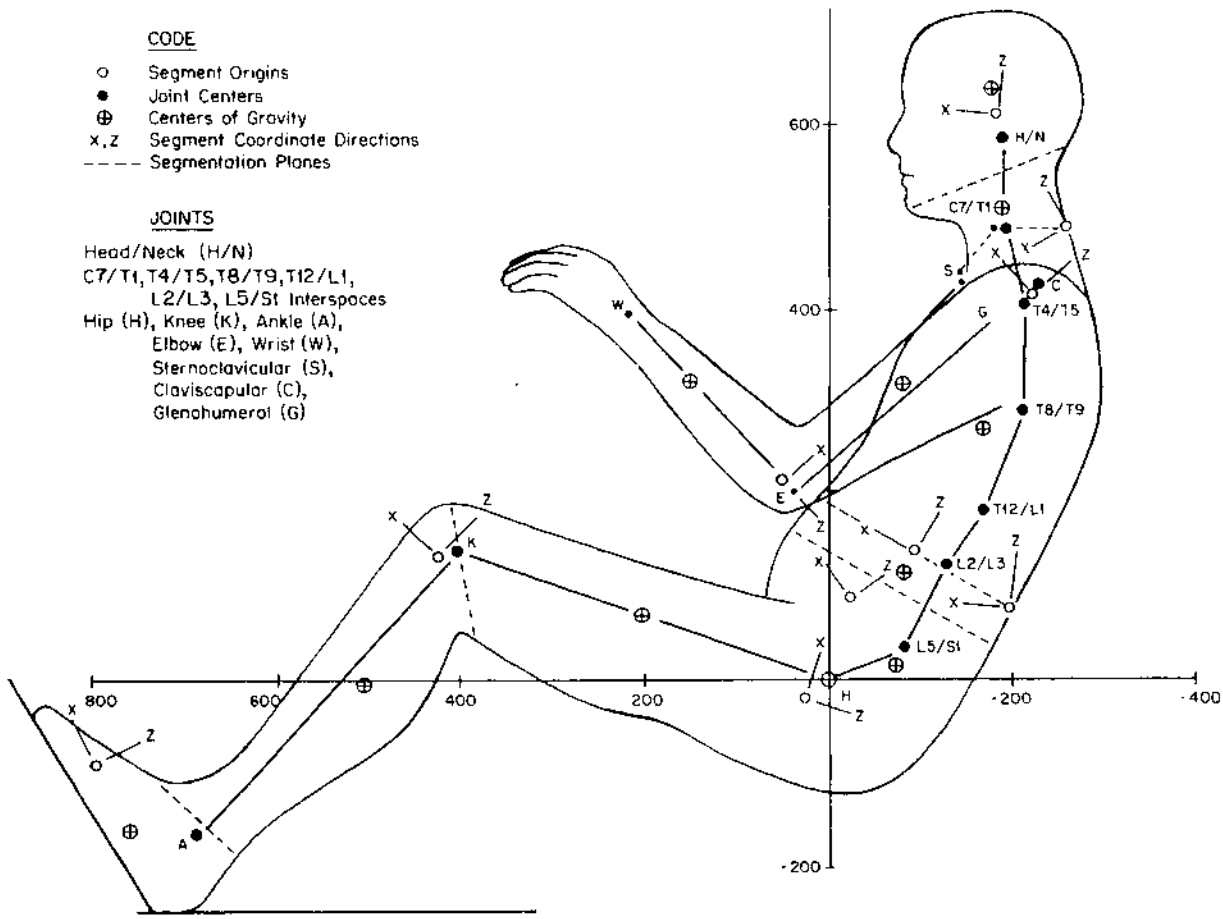

Fig. 7.3 *Anthropometric specifications for a mid-sized male dummy.*

These anthropometric data are not commonly used yet, very often a dummy design is based on the anthropometry of a predecessor. Currently *scaling methods* have been developed to specify the geometric, inertial and impact response requirements for a specially-sized dummy, based on an existing dummy. Mertz [2] applied this method on an advanced midsize adult male dummy, called the Hybrid III, to obtain the design requirements for a 5th percentile female dummy and a 95th percentile male dummy. The purpose of this study was to define specifications for these two dummies having at least the same level of 'biofidelity' (see 7.2.4) and measurement capacity as the Hybrid III dummy. Furthermore, development time and cost can be reduced by using an existing dummy rather than starting with the original anthropometric data for the small female and the large male. The key body dimensions and segment weights of the Hybrid III were taken from the design specifications and drawings. The key body segment dimensions and the overall body weights for a small female and a large male were taken from the anthropometric data [ref. 1]. The body segment weights for these two sizes of people had to be calculated since the body sectioning scheme used in the anthropometric study is not the same as that used for the Hybrid III dummy. Therefore geometric and inertial scale factors were determined. As an example the head scaling factors are presented here.

The head masses for the small female and large male were calculated by assuming that their heads are geometrically similar to the Hybrid III head and have equal density. The characteristic length chosen for the geometric similitude was the sum of the head circumference (C), width (W) and length (L). For geometrically similar objects, the length scale factors (λ_x, λ_y, λ_z) are equal and are calculated by dividing the subject (s) characteristic length by the Hybrid III (H) characteristic lenght, or,

$$\lambda_x = \lambda_y = \lambda_z = (C+W+L)_s / (C+W+L)_H \qquad (7.1)$$

Using these scaling factors, for instance the distance of the vertex and the center of gravity to the occipital condyles can be calculated for the two new dummies.
For geometrically similar objects with equal density, the ratio of their masses is defined as the mass ratio, R_m, and is equal to the cube of their characteristic length ratio, or,

$$(\text{Head Mass})_S/(\text{Head Mass})_H = R_m = \lambda_x^3 \qquad (7.2)$$

Using this equation the head masses for the small female and large male can be calculated.

The biomechanical head impact response requirements (or 'certification'; see 7.2.6) for the Hybrid III dummy are limits placed on the peak resultant head center of gravity acceleration for a 14.8 inch drop of the head onto a flat rigid surface. For such a forehead impact, the peak resultant head acceleration has to lie between 225 g and 275 g (1 g is the gravitational acceleration). The response of the two new heads had to be scaled from this Hybrid III response requirement.

Assume that the head impact test condition can be represented as a single spring-mass system of mass m and stiffness K, which is allowed to impact a rigid surface with a velocity V_0. For such an impact, the peak displacement D, acceleration a and force F are given by,

$$\frac{1}{2} mV_0^2 = \frac{1}{2} KD^2 \quad > D = V_0 m^{1/2}/K^{1/2} \tag{7.3}$$

$$F = KD = ma \quad > a = V_0 K^{1/2}/m^{1/2} \tag{7.4}$$

The ratios of peak responses of two different spring-mass systems (system s and system H) which impact the same rigid surface at the same impact velocity can be expressed as,

$$R_D = R_s/R_H = R_m^{1/2}/R_k^{1/2} \tag{7.5}$$

$$R_a = R_k^{1/2}/R_m^{1/2} \tag{7.6}$$

$$R_F = R_k^{1/2} R_m^{1/2} \tag{7.7}$$

where

$$R_k = K_s/K_H \tag{7.8}$$

$$R_m = m_s/m_H \tag{7.9}$$

The forehead stiffness can be expressed as,

$$K = F/D \tag{7.10}$$

where F is the impact force and D is the deflection that occurs. The impact force can be expressed as the stress, σ, times the impact area A, or,

$$F = \sigma A \tag{7.11}$$

The stress can be expressed as the modulus of elasticity E, times the strain which is the deflection D, divided by the material thickness T, or,

$$\sigma = ED/T \tag{7.12}$$

Noting that E will be the same for all heads, combination of the equations 7.8, 7.10, 7.11 and 7.12 gives,

$$R_k = (A_S/A_H)/(T_S/T_H) \tag{7.13}$$

Since the heads were assumed to be of equal density and geometrically similar, all lenght ratios will scale as λ_x, area ratios as λ_x^2 and mass ratios as λ_x^3. Combining these relationships with those given by equations 7.6, 7.8, 7.9 and 7.13 gives,

$$R_a = a_S/a_H = 1/\lambda_x \tag{7.14}$$

Using this scale factor the biomechanical response ranges for the small female and the large male dummy head can be calculated.

This procedure described by Mertz [2] can be presented in a more general way as follows [3]:

For dimensional analysis or -scaling it is sufficient to scale the basic parameters length (L), mass (M), temperature (T) and time (t). Geometrical scaling implies that the scaling factor for geometry is linear:

$$L(m) :: \alpha \tag{7.15}$$

Using the same material means that the specific gravity (φ), elasticity and stiffness (E,G,K) and heat transfer (λ) are not changing due to scaling:

$$\rho \quad (kg/m^3) :: 1 \rightarrow M\,(kg) :: \alpha^3 \tag{7.16}$$

$$E,G,K \quad (N/m^2) :: 1 \rightarrow t\,(sec) :: \alpha \tag{7.17}$$

$$\lambda \quad (W/m/K) :: 1 \rightarrow T\,(K) :: \alpha \tag{7.18}$$

The effects of these equations yields the following relationships between all other physical parameters:

$$V\,(m/s) :: 1 \tag{7.19}$$

$$a\,(m/s^2) :: \alpha^{-1} \tag{7.20}$$

$$F\,(kg\ m/s^2) :: \alpha^2 \tag{7.21}$$

$$K\,(N/m) :: \alpha \tag{7.22}$$

From equation 7.20 it follows that acceleration scales as α^{-1}, however the acceleration of gravity can not be scaled. So this scaling technique should be used only when the influence of the earth's gravity can be neglected.

7.2.4 Biofidelity

Achieving desirable human like reponses is probably the most difficult part of the design. Mechanical characteristics, such as the stiffness of the dummy at the points at which it is struck, and where it is likely to strike the vehicle, should be similar to those of similar parts of the human body. This means that the dummy should inflict damage on the vehicle similar to that found from human impacts in accidents or cadavers in tests. Similarly the dummy should deform where struck in a representative manner as particularly specified for each body component. If the detailed dummy response is wrong the impact measurements at those points on the dummy will be wrong. Then the dummy could guide the vehicle design in a wrong direction.

The articulation of joints and the flexibility of parts of the dummy should be sufficient so as not to distort the reponse of the dummy for the intended impact conditions of those parts of the dummy whose reponses are to be measured.

The dummy is used in an environment in which a human may well be injured. In addition, in a situation were a human would have incurred injury and would have been 'broken', the dummy must not fail but be able to carry on recording the impact so that the degree of overload can be assessed.

The International Organization for Standardization (ISO) has defined a series of biofidelity requirements for side-impact dummies [4]. ISO describes a series of impact tests, including impactor tests, drop tests and sled tests using the head, neck, shoulder, thorax, abdomen and/or pelvis of the dummy. The proposed dummy responses are based on identical cadaver and human volunteer impact tests. These test subjects have large variations in their physical characteristics such as size, shape, and inertial properties. Since a subject's impact response is dependent on its physical characteristics, testing of such a sample of subjects will produce widely varying response data. Mertz [ref. 5] developed a procedure for normalizing impact response data. One example will be presented here.

Fig. 7.4 shows the impact force versus time response obtained from a series of cadaver drop tests. The cadavers were subjected to 1 meter free fall drops onto a rigid surface. The Fig. shows the load on the thorax due to its interaction with the impact surface. For normalizing purposes, Mertz defined an equivalent simple-mass system shown in Fig. 7.5. The task is to calculate the same interaction impulse and velocity change as that experienced by the free-body mass of the cadaver. Such a mass is called the *'effective mass'* M_e.

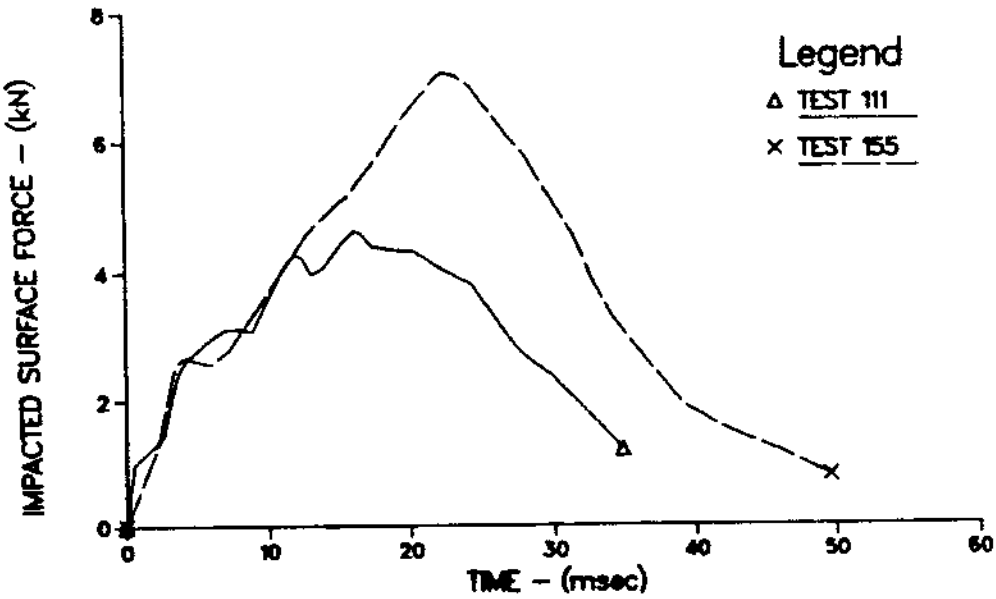

Fig. 7.4 *Lateral thoracic impact surface force for cadavers subjected to 1 meter drops onto a rigid surface.*

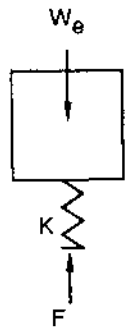

Fig. 7.5 *Spring-mass model of cadaver drop test.*

Impulse-momentum consideration of the simple spring-mass system of Fig. 7.5 gives,

$$\int_0^T F\,dt = W_e V_o/g + W_e T \quad \rightarrow \quad W_e/g = \left[\int_0^T F\,dt\right] / (V_o + Tg) = M_e \qquad (7.23)$$

Where
- F = load on subject due to interaction with impact surface
- T = impact duration
- g = acceleration of gravity
- V_o = initial velocity
- K = stiffness of subject
- W_e = effective weight of subject
- M_e = effective mass

The effective mass for all cadaver tests can be calculated now. Then an effective mass for a standard subject M_S must be selected. Mertz calculated the percentage body mass (i.e. M_e divided by the total body mass) involved in the cadaver tests. The average of these percentages (41.2%) was applied to the 50th percentile adult male's body mass (76 kg according to Mertz) to obtain the standard effective mass M_S (31.3kg). The mass ratio used to normalize the cadaver data is,

$$R_m = M_S/M_e \tag{7.24}$$

The stiffness ratio is defined as:

$$R_k = K_S/K_i \tag{7.25}$$

where K_S is the stiffness of a standard subject and K_i of the i-th cadaver. Cadaver stiffness data were not available, so it was assumed that the thoracic stiffness is proportional to a characteristic lenght,

$$K_i = C\, L_i \tag{7.26}$$

where L_i = a characteristic thoracic dimension of the i-th cadaver (chosen is the thoracic depth)
C = proportionality constant which is the same for all cadavers

Since the thoracic depth of the 50th percentile male and of all cadavers is known, the stiffness ratio R_k can be calculated.

Using the same simple spring-mass system, Mertz [ref. 5] calculated the normalizing factors for force, acceleration, displacement and time using these mass and stiffness ratios (see also 7.2.3):

$$R_f = (R_m)^{1/2}\,(R_k)^{1/2} \tag{7.27}$$

$$R_a = (R_k)^{1/2}\,(R_m)^{-1/2} \tag{7.28}$$

$$R_x = (R_m)^{1/2}\,(R_k)^{-1/2} \tag{7.29}$$

$$R_t = (R_m)^{1/2}\,(R_k)^{-1/2} \tag{7.30}$$

All cadaver responses are now normalized using these normalizing factors. Fig. 7.6 shows the normalized force versus time curves. Based on these normalized cadaver responses ISO defined a corridor for a dummy response in the same test condition. The dummy response should be normalized also to adjust for changes in effective mass due to slight differences in the position of the dummy on impact. The effective mass should be calculated, while the stiffness ratio for a 50th percentile adult male dummy is defined to be equal to 1. Fig. 7.7

shows the ISO biofidelity requirement corridor and the response of the European Side Impact Dummy (see 7.4.6) in a 1m thoracic drop test.

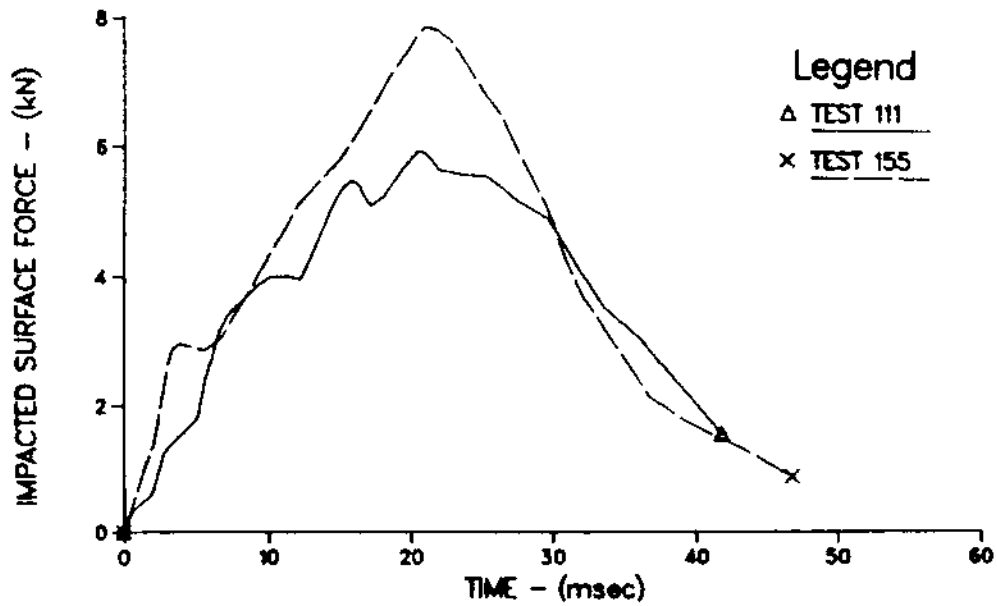

Fig. 7.6 *Normalized thoracic impact surface force for cadavers subjected to 1 meter drops onto a rigid surface.*

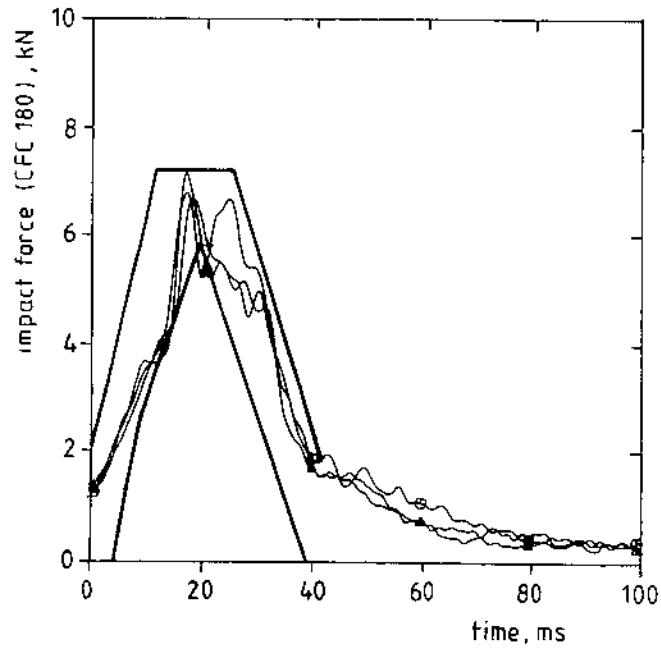

Fig. 7.7 *ISO response requirement corridor and EUROSID responses in 1 meter thoracic drop test.*

In order to reduce the variability of cadaver-based impact response data, the techniques of *dimensional analysis* as presented in Section 7.2.3 can also be applied to normalize the data to that of the mid-sized (cadaver) male.

7.2.5 Repeatability

In order for a dummy or subcomponent test device to function as an effective industry and government standard, or even as a useful research tool, it must not only provide reponse biofidelity, but it must also demonstrate that it can give the same results in repeated tests. Each dummy should be repeatable in use; whichever size and design is chosen, it is essential that a dummy always reacts to a given impact in the same way so that the same measurements can be recorded. A coefficient of variation, i.e. the standard deviation of the peak values divided by the mean peak value, of 5% or less is considered to be good; a CV of 10% or less is considered acceptable.

In an attempt to define a root-mean squared (RMS) based measure of dummy performance, a *cumulative variance* technique has been created by Morgan et al. [6, 7]. The cumulative variance is defined by:

$$CV = \sum_{t=1}^{T} [a_1(t) - a_2(t)]^2 \tag{7.31}$$

where: CV = cumulative variance
t = time data point
T = maximum number of data points
$a_1(t)$ = acceleration response of first signal at time t
$a_2(t)$ = acceleration response of second signal at time t

Two dummy tests or a cadaver and a dummy test can be compared. If the dummy exactly follows the cadaver the CV equals 0. Generally, more than one cadaver test is available, therefore a Mean Cadaver Response (MCR) is computed by the following:

$$MCR(t) = \frac{1}{n} \sum_{i=1}^{n} a_i(t) \tag{7.32}$$

where: MCR(t) = Mean Cadaver Response at time t
n = number of cadaver tests
$a_i(t)$ = response at time t of the i^{th} cadaver

In order to properly compute the MCR, the signals must be aligned in time. The alignment is selected to minimize cumulative variance between the curve to be aligned, and a particular curve arbitrarily selected as the 'alignment standard'. Assuming that the signals are correctly aligned, and while the MCR is computed, the variability in the cadavers is measured. At each point in time of the signal, the variance of each cadaver signal with the MCR is calculated and summed over each point in time. This sum is called the Cadaver Cumulative Variance (CCV):

$$CCV = \frac{1}{n-1} \sum_{t=1}^{T} \sum_{i=1}^{n} [a_i(t) - MCR(t)]^2 \qquad (7.33)$$

where: CCV = cadaver cumulative variance
T = number of time data points
n = number of cadaver tests
$a_i(t)$ = response of cadaver i at time t
MCR(t) = mean cadaver response at time t

The CCV is a measure of the variability of cadavers among themselves for a given test condition. This equation can also be used to measure the repeatability of a dummy design. The various dummy responses would be entered into the above presented MCR and CCV equations. The lower the resulting value of CCV the more repeatable a dummy is. The biofidelity of a dummy can be partially evaluated and graded by using CV, CCV and MCR. After calculating the MCR and CCV, the cumulative variance between the MCR and the dummy response is computed. This is called the DCV (Dummy Cumulative Variance). Then the ratio DCV/CCV is computed and interpreted in the following manner:

DCV / CCV = 0.0 (dummy response exactly matches the MCR)

0.0 < DCV / CCV < 1.0 (dummy response is no more variable from MCR than cadaver data is)

DCV / CCV > 1.0 (dummy is more variable than cadaver data by the amount of the ratio)

Other methods have been developed as well to evaluate the repeatability of test results. The NISE (Normalized Integral Square Error) estimates the influence of phase, amplitude and shape of curves on their similarity [8].

Among the sources of inter-test variability, both the level of expertise of technicians and problems in repeating dummy initial position are important. Environmental aspects, such as ambient temperature, also influence the repeatability. Finally, it should be noted that the

goal of designing for humanlike response characteristics (i.e. biofidelity) and the goal for designing for repeatability may not be completely compatible. That is, a design that accurately represents the human in response characteristics may be so sensitive to small changes in test conditions or vehicle manufacturing variations that it has inherent repeatability problems. For the industry user and for the government standard, the features of repeatability and reproducibility (see 7.2.6) should not be sacrificed in the effort to achieve improved biofidelity and injury assessment capability.

7.2.6 Reproducibility

Reproducibility is repeatability between one dummy and another of the same type. Any dummy built to a particular design must respond in a manner similar to any other. A repeatable and reproducible response to known impact stimuli is very important for all dummies, in particular in approval testing. Of course, input conditions such as vehicle impact speed and the initial position of the dummy should be well defined. A special 'H-point manikin' (see Fig. 7.8) is often prescribed to set the seat into the defined positions. Certain procedures should be followed to position the dummy onto the seat. An important aspect in this connection is that the dummy sinks slowly into the seat due to the visco-elastic properties of the flesh-simulating material. The position of the dummy's H-point (= Hip rotation point), as well as the position of the arms/hands and the legs/feet are often prescribed. However, this is all senseless if the dummy responds differently to similar impacts.

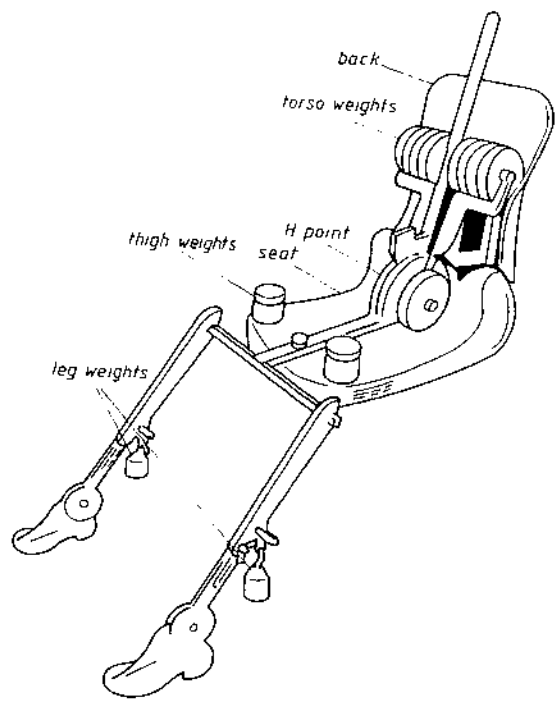

Fig. 7.8 H-point manikin used to define the position of the vehicle seat.

In order to maintain reproducibility, dummies have to be certified in the body areas that will be used to predict injury. *Certification* is the tuning or checking of dummy components that they are within a predefined corridor or set of limits. These limits are not only dimensional or static, but are also dynamic. A visual check of the dummy is always necessary before a test. Dummy parts should be undamaged and mechanisms should function well. Furthermore, adjustable joints should be set to their correct torque resistance. A well-known procedure in this respect is the so-called 'one-g' position of the joints; the joints are tensioned such that they can just bare the weight of the limb. The dummy is fitted with the necessary instrumentation and subsequently subjected to a standard stimulus in a certification test. Certification of the complete dummy should be performed at least after every ten tests. Before every important test (e.g. the testing of a prototype vehicle) the dummy should be certified as well. Also, if extreme values were recorded in a specific test, the dummy should be certified again. *Calibration* of the instrumentation is often described by its manufacturer.

Certification tests range from simple drop testing of the head onto a rigid surface, to rigid impactor testing on, for instance, the knees and chest. The tests are performed under standard humidity and temperature conditions. A complete certification program for the European Side Impact Dummy has been developed by TNO (see Fig. 7.9). The most advanced procedure was developed for the thorax; if a rib module does no longer comply with the specification, it can be tuned by replacing a spring.

7.2.7 Sensitivity

A design requirement not mentioned so far concerns 'sensitivity'. A dummy should be highly sensitive to parameters that relate directly to injury mechanisms (e.g. impact speed). On the other hand, it should not be sensitive to external parameters such as ambient temperature. Measurements should clearly distinguish between loadings which are just above critical from those just below critical for human beings. In other words the *performance criterion* measured (e.g. rib deflection) should be such that the rate of change of the measured quantity on the dummy should not be close to zero at the loading corresponding to the maximum tolerable human loading. Fig. 7.10 shows, as an example, the sensitivity of a EUROSID performance criterion (i.e. pelvis pubic symphysis force) to the impact velocity in rigid side impact tests. The *tolerance level* for pelvic (i.e. pubic ramii) fracture is 10000 N. The influence of a protective padding fixed to the rigid impact surface is also shown in Fig. 7.10.

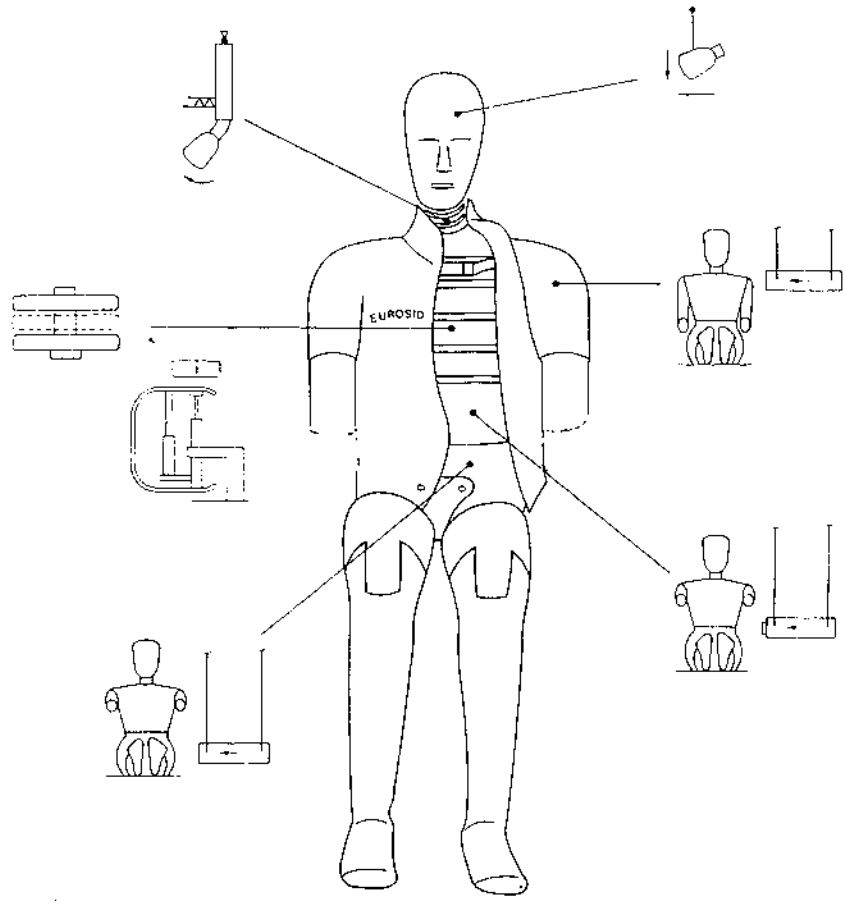

Fig. 7.9 *Overview of dynamical certification tests performed on the European Side Impact Dummy.*

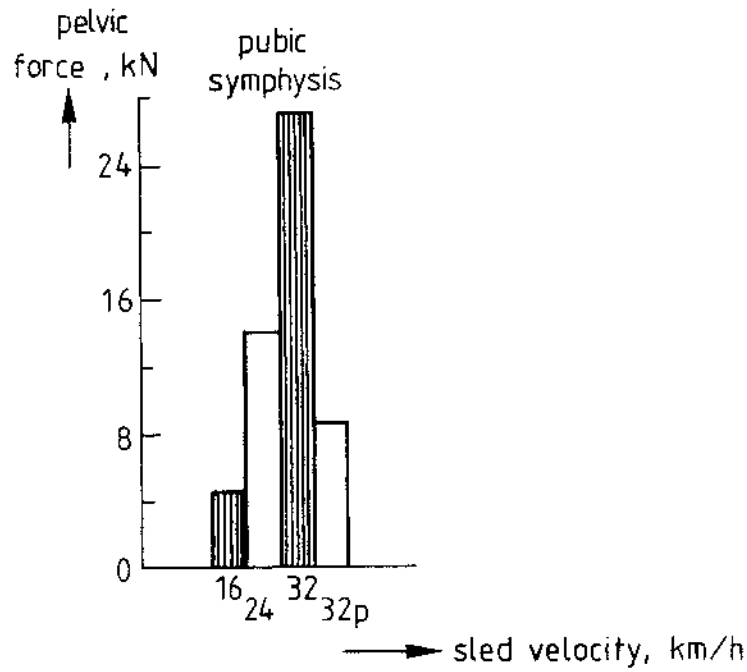

Fig. 7.10 *Relation between EUROSID pelvic forces measured at the pubic symphysis and the impact velocity in rigid and padded ('p') sled tests.*

Measuring devices should be fitted which are appropriate to each injury situation. For example an impact force may be critical only if spread over a small area of contact, whereas it might be acceptable if distributed over a larger area. So not only the dummy design should 'feel' this difference, it should also be recorded by the instrumentation. Measurements should not prevent the dummy response to each local impact being similar to a human response. The design of the dummy may slightly differ in detailed design features from the human being represented and so the human tolerance loads may have to be replaced by slightly different loads on the dummy. Biomechanical response testing should show this difference and a transfer function can be computed. Frangible components which break at the critical loadings may be acceptable or even necessary (e.g. from tests with (motor-)cycle and with pedestrian dummies it is known that a non-breakable dummy-leg will influence the kinematics of the dummy considerably), but it is likely that stronger components are preferable which represent stronger and heavier human beings. These then indicate the degree of overload imposed by the impact on a standard sized person. Possibly 50% overload without failure is desirable but may not be attainable.

7.2.8 Durability

Crash dummies must be robust. Each crash test dummy should 'survive' a number of tests without failure and should remain within the specified certification limits. Values of 20 to 100 tests with a 50% overload compared with the human tolerance are mentioned as durability requirement [9]. The dummy should withstand without damage for instance 20 unrestrained (i.e. no seat belts or airbag used) 30-40 mph frontal vehicle impact tests. This requirement can be contradictory to, for instance, requirements regarding 'biofidelity' and 'sensitivity' (see also 7.2.7). The materials used to simulate the human soft tissue should be strong (i.e. high tearing resistance) but light (weight and biofidelity requirements), and have the correct stiffness characteristics, which should not be influenced by temperature and humidity. Special foams and rubbers are used for this purpose.

7.2.9 Cost

Crash dummies are (mostly) complex tools. The more is demanded of a dummy (e.g. biofidelity) the more it is likely to cost. In addition spare parts are likely to be more expensive. Since the cost of impact testing is already high, high servicing costs should be avoided. As an example, the price of the most used frontal crash dummy, the Hybrid III, is approximately 35000 US$ without instrumentation. Including full instrumentation this price is more than tripled.

7.3 Performance criteria and instrumentation

7.3.1 Introduction

Injury criteria for human beings are transferred into *performance criteria* for dummies; the physical parameter that should be measured by the dummy. The injury tolerance limits for human beings are transferred by the legislation authorities into performance criteria limits; exceeding these values will lead to disapproval of the vehicle or safety device. These limits plus 50% overload (see 7.2.8) indicate the performance criteria range to be measured by the dummy.

Instrumentation should be available to measure the physical parameter. The transducer should be small (enough) and should withstand high-g loadings. Transducers with a possibility for 'shunt' calibration just prior to testing are preferable, because of improvement of the reliability of the test data obtained. This calibration is accomplished by sending a known signal in and comparing it to the output signal. The instrumentation and data acquisition system should be developed to meet the requirements as outlined in ISO 6487 (Road Vehicles - Techniques of Measurement in Impact Test - Instrumentation) or the Society of Automotive Engineers Recommended Practice SAE J211. These standards describe data amplitude and time accuracy, frequency response, sampling rate, etc. All dummy response signals are filtered through filters having prescribed characteristics. For instance, a cut-off frequency of 1650 Hz is normally used for the head acceleration signals.

The following Sections briefly describe the currently measured performance criteria and associated instrumentation.

7.3.2 Head

The current method of injury assessment in the head involves the measurement of resultant triaxial translational acceleration at the center of gravity of the dummy's head and subsequent analysis to produce a *Head Injury Criterion* (HIC) value. Linear *accelerations* in current dummies are routinely measured using piezoresistive (PR) accelerometers (see Fig. 7.11). The measurement capacity of these transducers varies from 200 to 2000 G. The biomechanical basis for the HIC method, is related only to direct impacts to the head. The difficulty in determining when head contact is taking place in some crash tests has led to the concept of limiting the HIC computation to a maximum interval time of 36 ms in any test. A HIC value of 1000 (seconds) is currently used in several regulations. Peak accelerations measured with current dummies go up to 200 g.

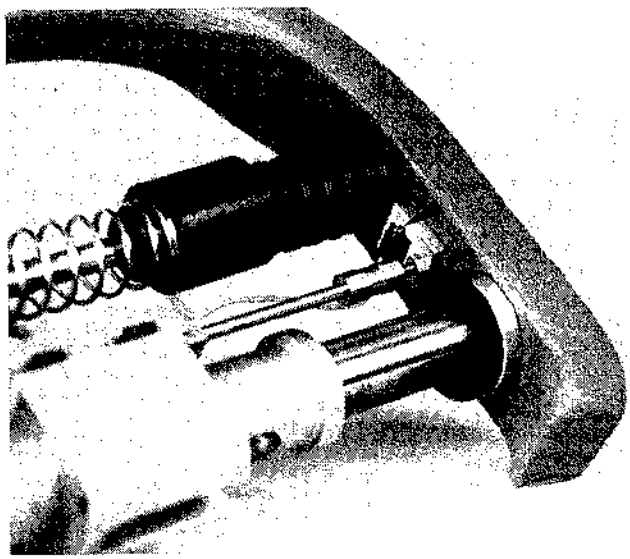

Fig. 7.11 *Miniature high-g accelerometer mounted on the rib of a EUROSID (see arrow).*

7.3.3 Spine

Currently maximum *bending moments* and maximum tension, compression and shear *forces* are proposed as injury criteria for the cervical and lumbar spine. The allowable forces depend on the time duration of a given force level. The technology to measure force and moment is well established. The most commonly used transducers are the piezoresistive (PR) types. The transducers are either uniaxial or multicomponent. All transducers follow the basic principle of utilizing strain gauge signals to measure the changes in deformable beams due to applied loads. Performance criteria limits up to 1235 Nm for flexion of the lumbar spine and up to 12700 N for the tension force on the lumbar spine are proposed.

7.3.4 Thorax

Thoracic injury mechanisms include rib-cage skeletal fractures, contusions of the heart and lungs, tearing and rupture of the vascular and pulmonary systems, and disruption of the heart-muscle conducting system. Many of the above injuries are thought to occur due to excessive deformations of the thorax when directly loaded. On the other hand, inertial reactions of the organs are thought to produce stresses and deformations in the tissues of the organs, resulting in injury. At high velocities, such injuries may occur with very little rib cage deflection. Current dummy performance criteria for judging injury potential to the thorax involve *deflections* of the rib cage at a specific location and/or *acceleration* of the spine or chest wall (i.e. ribs or sternum). The use of potentiometers and capacitive, induc-

tive or reluctive displacement transducers for measuring deformation is a well-established technology.

A 60 G spine acceleration during 3 ms in time and a sternum deflection of 75 mm are currently used as injury criteria in frontal vehicle impact tests. An acceleration-based injury criterion for lateral loading to the thorax is included in the US side impact regulation [10]. The *Thoracic Trauma Index* (TTI) combines the peak lateral lower thoracic spine (i.e. T12 vertebra) acceleration and the peak lateral rib acceleration. The mean value of these two accelerations (=TTI) should not exceed 90 g.

A General Motors research programme [11] showed a strong relation between thorax injuries and a *viscous tolerance criterion* using the combination of deformation velocity, V, and relative thoracic compression, C, in the form $VC_{max}=[V(t)*C(t)]_{max}$. The velocity is obtained by differential calculation of the displacement signal. Dividing the displacement by the thoracic depth gives the relative compression. A $VC_{max}=1.3$ m/s would correspond to a 50% probability of AIS≥3 in frontal impacts.

The proposed European side impact regulations [12, 13] combine the lateral VC_{max} (= 1.0 m/s) and the maximum lateral rib deflection (= 42 mm).

7.3.5 Abdomen

Injury mechanisms in the abdomen are primarily the result of deformation or *penetration* of the abdominal contents with associated generation of significant forces or pressures in the deformed organs. In addition, at high impact velocities, solid organs such as the liver may undergo severe damage due to *pressure* generation alone, with little deformation. Pressure transducers of various types are available and have been used in dummy and cadaver testing. Normally they are used to measure pressure in fluid- or gas-filled compartments.
In frontal impact tests abdominal penetration by the lap belt is measured by strain gaged force transducers mounted on the iliac crest. In lateral impacts the deflection and/or *force* are measured. The viscous criterion VC is also proposed for lateral abdominal impacts.

The proposed European side impact regulations [12, 13] describe an abdominal injury criterion limit of 2500 N measured at 40 mm from the outside dummy contour.

7.3.6 Pelvis

Lateral loading to the pelvis and associated hip-joint structures can result in fractures of the bony structure, including iliac wings, sacrum and pubic ramii. Frontal loading through the knees and upper legs may result in fracture of the acetabulum.

Normally the triaxial sacrum *acceleration* is measured in frontal impacts, however no tolerance value is prescribed. The US side impact regulation [10] allows a peak lateral sacrum acceleration of 130 g. The proposed European side impact regulations [12, 13] prescribe a *force* measurement at the pubic symphysis with a tolerance limit of 10000 N.

7.3.7 Lower extremities

The mechanisms of injury to the lower extremities due to blunt loading involve either fracture of bony structures or disruption and dislocation of joints by damage to ligamentous structures. For the knee/femur/pelvis complex, tolerance data consist primarily of axial loads along the femur. The axial loading tolerance of the femur has traditionally been characterized by a *compressive load* limit, measured by a force transducer mounted into the dummy femurs. The allowable force limit (in frontal impacts) is 10000 N. More recently the measurement of *bending moments* is proposed as well, since failure of the long bones is (partly) due to bending. Tolerance limits of 366 Nm for the femur and 244 Nm for the tibia are proposed [9]. *Shear load* through the knee joint due to proximal tibia impacts are also monitored by the Hybrid III dummy. Tolerance limits of 5000 N force and 15 mm displacement are proposed.

No measurements are performed in the lower extremities of side impact dummies.

7.4 Current dummies and their application

7.4.1 Introduction

Various types of crash tests are used to assess vehicle impact behaviour, both for legislative and research purposes. For both purposes it is necessary to analyse the performance of the vehicle and to evaluate the possible injuries sustained by the occupants. Anthropomorphic test devices -i.e. dummies-are used for crash safety research as well as for the approval testing of vehicles, components and products for impact safety. These dummies are often designed for one special purpose: a frontal impact, a side impact, for the evaluation of seat belts or child restraint devices and so on. The type of dummy prescribed in a regulation is a function of the requirements of the test, the cost of the test and the potential savings to be gained from the test. Each application requires a dummy of a different degree of sophistication. Sometimes the dummy has to act merely as a loading device; more often a human-like response to that loading is also required. For approval testing a dummy should give repeatable results. Moreover, it should be durable in order to reduce the cost of testing. Some examples of approval testing and the dummies used are presented in this Chapter.

7.4.2 Legislation

In the past motor vehicles intended for the conveyance of goods and passengers had to comply with certain technical requirements. These requirements differed from one country to another and consequently formed an impedement to international trade. So, there was obviously a need for harmonization of vehicle regulations to facilitate trade and improve safety. Therefore, the EEC laid down a Council Directive on Motor Vehicle Type Approval in 1970. According to this Directive, Member States of the Economic Community may not refuse to register or prohibit the sale, entry into service or use of any new vehicle that complies with the technical requirements of '*EEC Directives*'. These directives are to a substantial extent duplications of '*ECE Regulations*'.

In 1958 the United Nations Economic Commission for Europe (ECE) already finalized an Agreement in this respect. Under this Agreement, vehicle components that complied with the prescribed requirements and that had been approved by the government in one country would automatically be accepted by other governments that have ratified the Regulation in question.

In the 1970s the ECE adopted many standards from the USA. These *Federal Motor Vehicle Safety Standards* are 'self-certifying', i.e. vehicle conformity is ensured by spotchecks by the government. To satisfy an inquiry by the government into a vehicle meeting a certain standard, manufacturers should show 'good faith attemps to meet the standard'. Furthermore, vehicle conformity will be ensured by the knowledge that individuals in the USA can take legal action and claim compassionate allowance, if they can prove that injuries have resulted from a vehicle not complying with the safety standards.

7.4.3 Seat belt tests

The TNO Road-Vehicles Research Institute has been involved in the development of dummies since the early 1960s. The first relatively simple dummies were made of wood, leather, rubber and steel, to evaluate the performance of seat belts. They were used mainly as loading device to test the strenght of the belt system.

On the basis of these studies a new, simplified dummy, the so-called '*TNO-10*', was developed and introduced about 1970. The dummy is prescribed in ECE-Regulation 16 and EEC Directive 82/319/EEC for the approval testing of seat belts. The pertinent test procedure includes a dynamical sled test in which a relatively severe vehicle crash is simulated (see Fig. 7.12). The impact speed is 50 km/h and the deceleration of the sled with the dummy seated on a simulated car seat is approximately 28 g. In this test the displacement of the dummy should remain within certain limits, while no components of the belt system should break or come loose. So, in this test the dummy is used primarily as a dynamic loading device.

The TNO-10 dummy consists of a head, a neck, a torso, two upper legs and one lower leg (see Fig. 7.13). As the required motion of the dummy is two-dimensional, hinge joints have been used to connect head and neck, torso and upper legs, and the upper legs with the lower leg. The friction of these joints can be adjusted. The greater part of the TNO-10 dummy is made of polyurethane rubber, reinforced with steel plates and tubes. The standing height of the dummy is 174 cm and the weight can be varied by means of correction weights from 70 kg up to 82 kg.

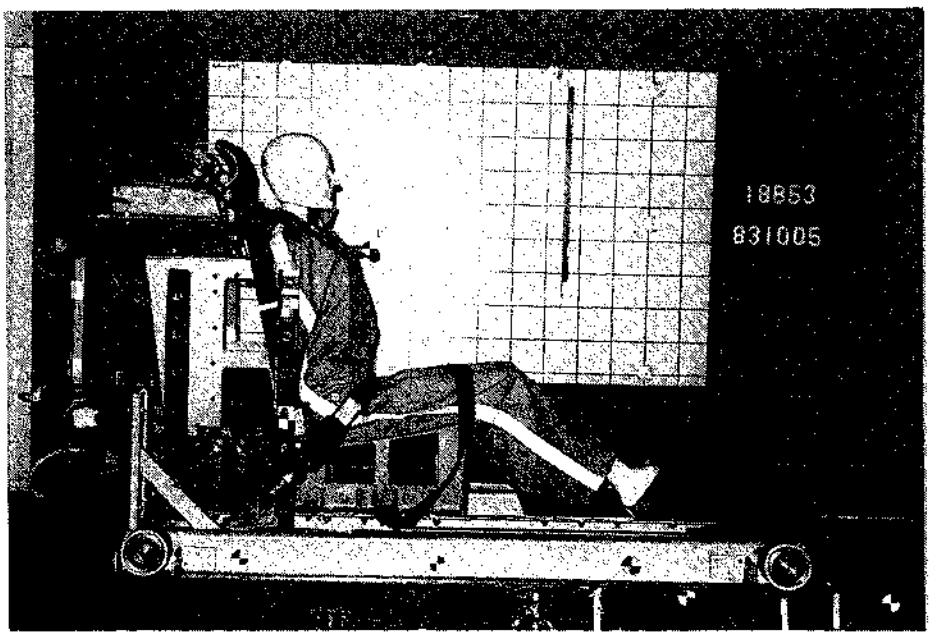

Fig. 7.12 *TNO-10 dummy on a dynamical sled for a seat belt approval test.*

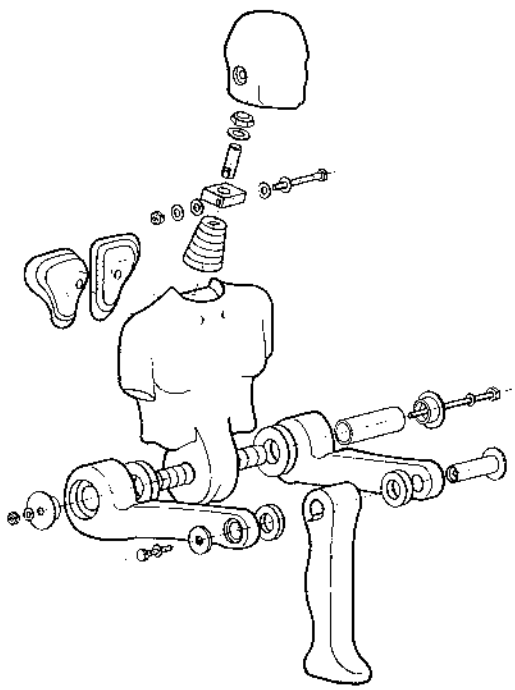

Fig. 7.13 *Exploded view of a TNO-10 dummy*

7.4.4 Child safety devices

Over the years, TNO has gained considerable experience in the field of safety devices for children. The institute was involved in the drafting of ECE-Regulation 44: "Uniform provisions concerning the approval of restraining devices for child occupants of power-driven vehicles (1980)". Along with the development of testing methods a series of child dummies was designed. The procedure for evaluating a child safety device in accordance with ECE-R44 includes the performance of a dynamical sled test (see Fig. 7.14). A maximum head excursion (550 mm horizontal) and maximum chest acceleration (55 g resultant acceleration during 3 ms and 30 g vertical acceleration during 3 ms) of the child dummy is prescribed, while no abdominal penetration should occur. So, in this test the dummy is not only used as a loading device, but is also supposed to show a humanlike response to the load applied. As to the latter requirement, the specific anatomical characteristics of children, resulting in a relatively high frequency of abdominal and neck injuries, was taken into account.

Fig. 7.14 TNO child dummy on a dynamical sled for the evaluation of a child restraint system.

In view of these specific characteristics, TNO has developed the *P3/4*, *P3*, *P6* and *P10* child dummies. The 'P' stands for 'Pinocchio' (the first child dummy developed by TNO in the early 1960s), while the number indicates the age (expressed in years). The weight of the dummies (9, 15, 22 and 32 kg respectively) and the standing height (71, 98, 117 and 138 cm respectively), as well as other anthropometric characteristics are based on data of West-European and Nord-American children. Fig. 7.15 shows an exploded view of a child

dummy. To allow for realistic motions of the dummies, ball-and-socket joints have been used for the hip and shoulder, and hinge joints for the elbows and knees. The head can rotate around a vertical axis as well as around a horizontal lateral axis (atlas-axis vertebra). The TNO child dummies have for the larger part been made of polyurethane rubber, reinforced with steel and aluminium strips and tubing. The neck and lumbar vertebrae have been made of polyamide and the abdominal insert has been made of a soft, open cell foam. Provisions have been made for mounting accelerometers in the head and chest of the dummies. As it was required to obtain an indication of abdominal penetration, a realistic pelvis shape was necessary together with a soft abdominal region and a flexible lumbar area. Abdominal penetration is indicated by impressions on a piece of plasticine located between the soft abdominal insert and the lumbar vertebrae. Recently a new technique, based on pressure measurement in an oil-filled flexible tube, has been developed. A prototype neck force and moment transducer for the P3/4 dummy has been developed and tested in 1990/91. Both new measurement methods are not (yet) included in the regulation.

In 1984 a fifth child dummy has been included in ECE-R44. This *P0*, or 'newborn infant dummy', consists of a head, torso, arms and legs as one single unit. This 3.4 kg dummy is used to test baby carrycots.

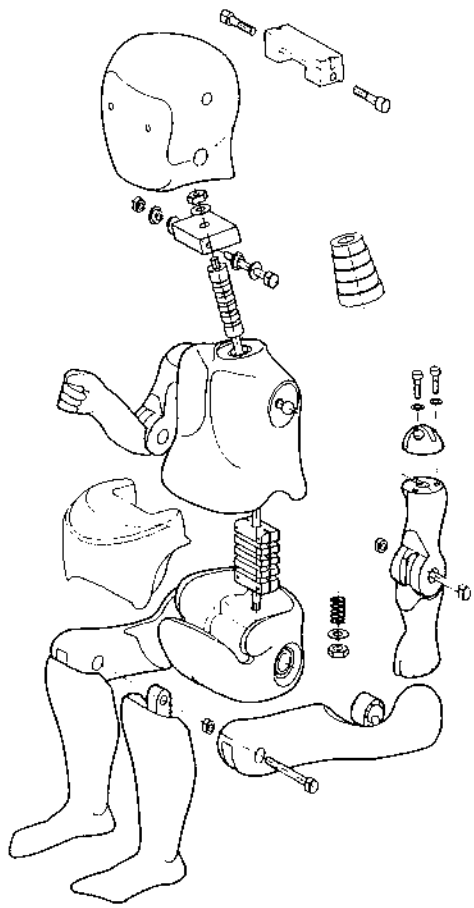

Fig. 7.15 *Exploded view of a TNO child dummy.*

7.4.5 Frontal vehicle tests

For many years automotive research and regulations have focussed primarily on the protection of car occupants involved in a frontal crash. Reinforced occupant-compartments, crush zones, collapsible steering columns and seat belts have been introduced.

Sophisticated dummies are required to evaluate a complete vehicle. In the USA several generations of frontal crash dummies have been developed. Well-known examples are the '*Hybrid II*' and its successor the '*Hybrid III*' dummy, developed by General Motors in the early and late 1970's, respectively. Dummies representing children of three and six years old have also been developed in the USA (see Fig. 7.16). The Hybrid II and III are used all over the world in 30 mph standard vehicle crash tests in accordance with FMVSS 208 (see Fig. 7.17), and for all kind of research in this field. They have also been used as pedestrian and (motor-)cyclist dummy. In a 208 test all portions of the dummy should be contained within the passenger compartment. Furthermore, the dummy responses should not exceed certain levels (HIC $\leq$ 1000, chest acceleration $\leq$ 60 G over 3 ms, femur forces $\leq$ 10000 N).

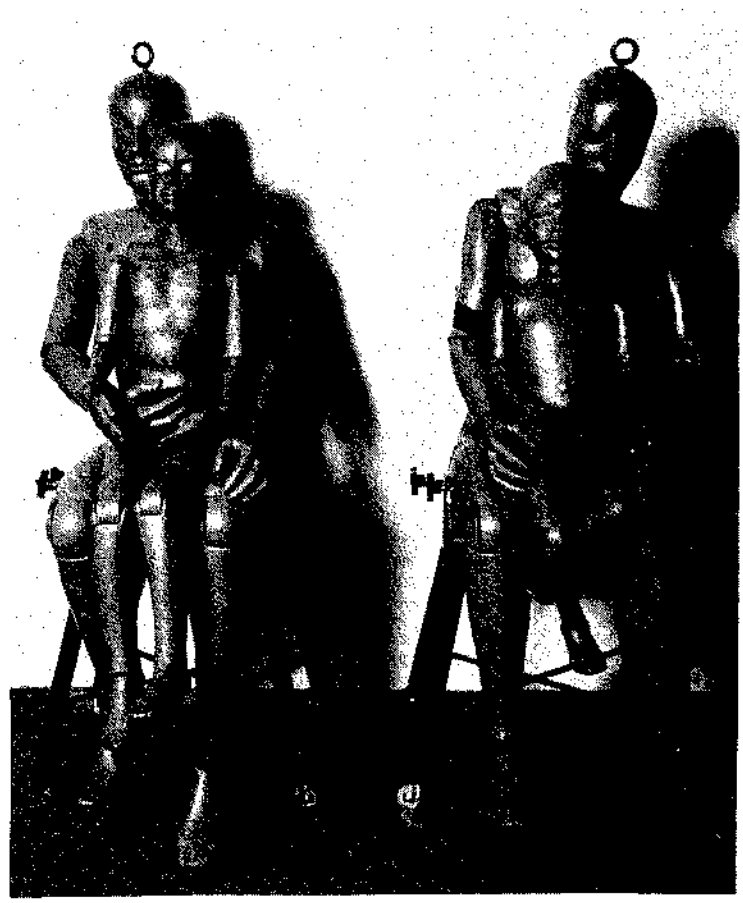

Fig. 7.16 *A family of US crash dummies.*

The Hybrid II represents a 50th percentile adult male (a 5th percentile female and a 95th percentile male also exist). The dummy is made of a metal skeleton including joints, covered by flesh-simulating plastic. The neck and lumbar spine are represented by rubber cylinders. A complete and well-specified set of certification requirements has been developed together with the dummy. In the Hybrid III design special attention has been given to repeatability and reproducibility, as well as to humanlike response and seating position. Provisions have been made for more than 60 data channels, distributed over the dummy from the ankles up to and including the head. The 50th percentile adult male version of the Hybrid III has been used as standard dummy for development of larger and smaller versions (see also 7.2.3).

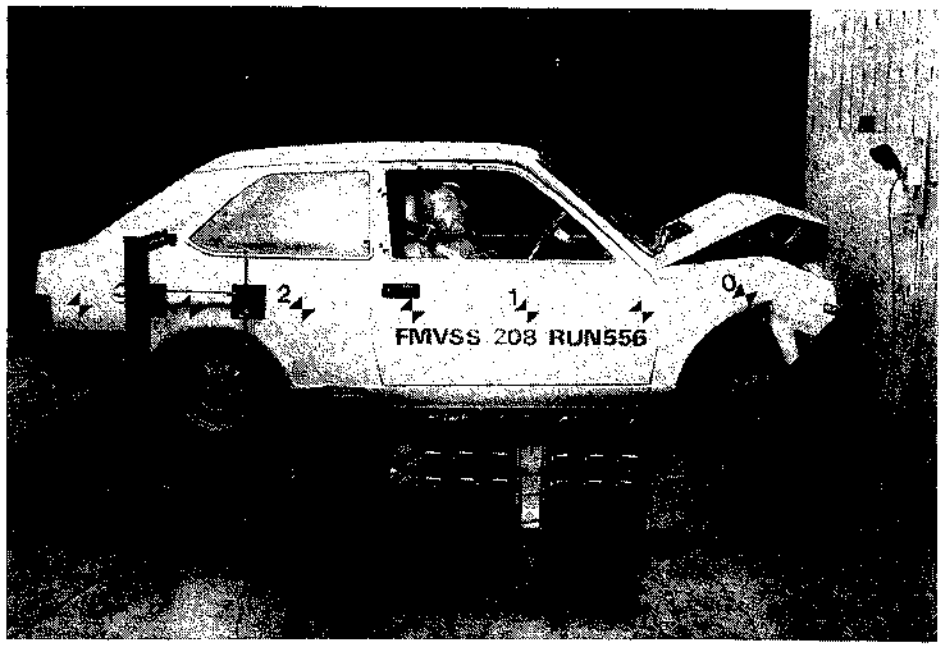

Fig. 7.17 *A head-on collision of a passenger car against a fixed barrier (concrete block) in accordance with a US standard.*

7.4.6 Lateral impact tests

In the 1980's research has been concentrating especially on protection against side impact injuries. Special dummies are required for side impact tests: kinematics, response and injury assessment capabilities should be suitable for this purpose. TNO has been involved in the development of the so-called '*EURO*pean *S*ide *I*mpact *D*ummy' (see Fig. 7.18). EUROSID has been designed and constructed by a group of European research laboratories which worked together under the auspices of the European Experimental Vehicle Committee. Design and performance criteria are based on human cadaver tests. The EUROSID represents a 50th percentile adult male, however without lower arms (all three

existing side impact dummies do not have lower arms, since they disturb the repeatability too much). The instrumentation of the head, chest, abdomen and pelvis allows for the assessment of injuries sustained under lateral impact conditions. EUROSID can be converted from a left-hand impact dummy to a right-hand impact dummy.

Fig. 7.18 The European Side Impact Dummy EUROSID-1.

As an example of an integrated design method the thorax and abdomen of EUROSID will be presented in more detail. In side impact accidents the thorax is injured by direct impact on most occasions. The actual blow is usually from the distorted door. If the blow is from a flat panel, severe injury usually only occurs when several ribs fracture. If the door is more distorted the blow is more localized and penetration of the thorax may occur with one or a few ribs being fractured and displaced into the thorax. To be able to distinguish between distributed and localized loads on the thorax, it was decided to split the thorax into three similar horizontal rib sections covering the region of the upper rib cage ('hard thorax'). The thorax section of dummies usually includes only those ribs which protect the lungs and heart (i.e. head of 11th rib to costal end of 6th rib). Besides, the ribs of a dummy are positioned perpendicularly to the thoracic spine instead of downwards. The region of the lower ribs is included in the abdomen of EUROSID and this includes the region of the liver.

Fig. 7.19 shows a side-view of a 50th percentile adult male and a part of the EUROSID dummy. The EUROSID thorax consists of a rigid thoracic spine and three identical rib modules. The ribs are attached to the spine by a system of piston/cylinder, springs and a damper (see Fig. 7.20). Deflection of the ribs is recorded by a linear potentiometer (not shown in Fig. 7.20). To obtain the required parameters of this design a simple mathematical model has been used (see Fig. 7.21). To study the influence of for instance the rib mass and the skin characteristics a large number of parameters variations have been conducted using this model [14]. It was shown that the skin plays a very important role in the response of the thorax, especially if it is required to match the acceleration response of various parts of the thorax with the response recorded in cadaver experiments. For the 'flesh' on the EUROSID ribs 'Confor-foam' is used, a light material with a very high energy-absorption capacity. These simulations and impactor tests on the prototype dummy showed that the 'moving' rib mass should be very low to obtain a humanlike response.

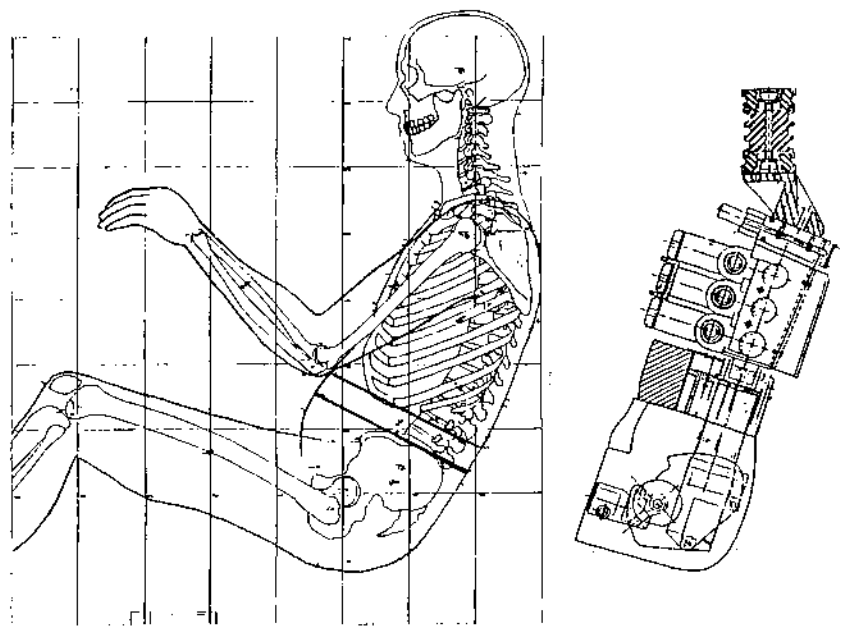

Fig. 7.19 *Side view of a 50th percentile adult male and a (part of a) 50th percentile dummy (EUROSID).*

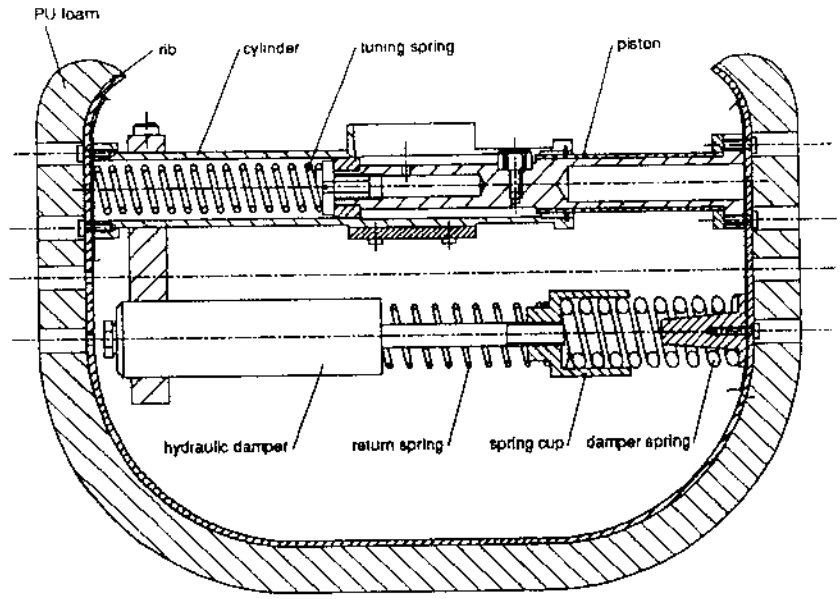

Fig. 7.20 *Cross-section of EUROSID rib module.*

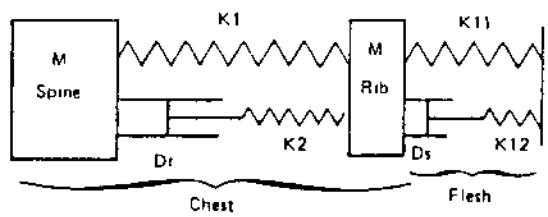

Fig. 7.21 *Mathematical model of the EUROSID rib module.*

The base for the (TNO) design of the EUROSID abdomen was a force-deflection corridor and tolerance values established from cadaver drop tests [15]. Cadavers were dropped laterally on a rigid hardwood simulated armrest (see Fig. 7.22). The principle was to choose a flexible material for the abdomen that would give a dynamical force-deflection response from the armrest impact which could be inside the cadaver corridor up to the critical force and penetration (see Fig. 7.23).

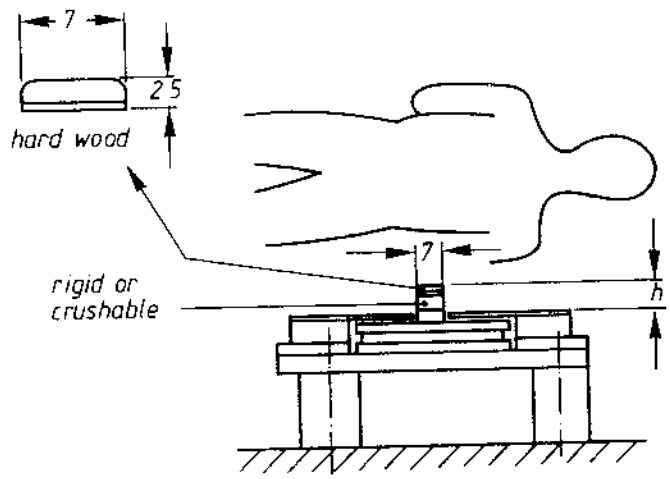

Fig. 7.22 *Test set-up for cadaver abdominal drop tests.*

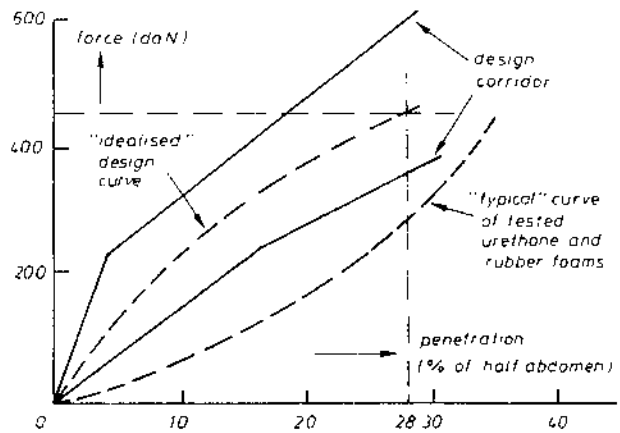

Fig. 7.23 *Design requirements for EUROSID abdomen.*

Impact tests on specimens of urethane and rubber foams showed that these materials were unable to produce responses in agreement with the cadaver design corridor (see Fig. 7.23). The construction does not provide any inertia, this in contradiction to the human abdomen. The desired dynamical characteristics (see Fig. 7.23) could be achieved by making the outside of the dummy of a relatively heavy but flexible material, such as solid rubber filled with lead pellets, which is supported by a soft foam underlayer to allow the necessary penetration. A problem then was to find the combination of mass carrying rubber and foam, which together would give the desired dynamical response. To avoid the making and testing of a large number of material compositions it was decided to use Computer Aided Design to find the design parameters. The MADYMO program, developed by TNO [16],

was used to formulate a dynamical non-linear finite segment model for a 2-dimensional simulation of a cross section through a half abdomen (see Fig. 7.24). Fig. 7.25 shows the comparisons of model simulations and experimental tests for:

a. no mass in outside layer,
b. 1 kg mass in outside layer,
c. 2 kg mass in outside layer.

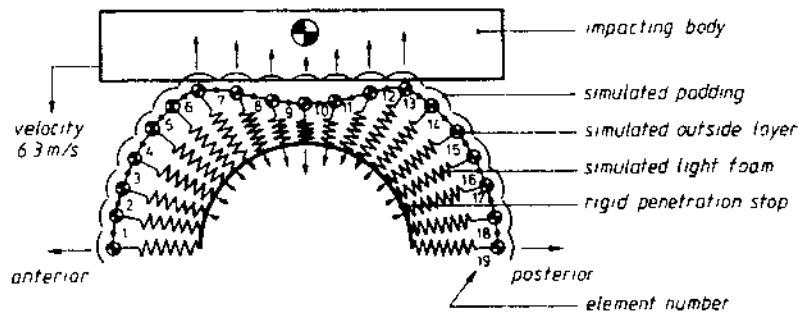

Fig. 7.24 Concept of MADYMO model of EUROSID abdomen.

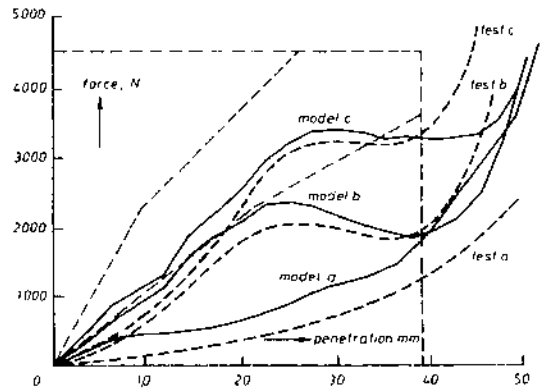

Fig. 7.25 Model predictions compared with experimental results.

This clearly shows that the added masses in the outside layer of the abdomen resulted in a force-deflection response which was more in conformity with those of cadavers. From an extensive number of computer tests it was concluded that for a prototype abdomen a mass of 1.5 kg in a section of the outside layer of about 200 mm of length would be the best choice (see Fig. 7.26).

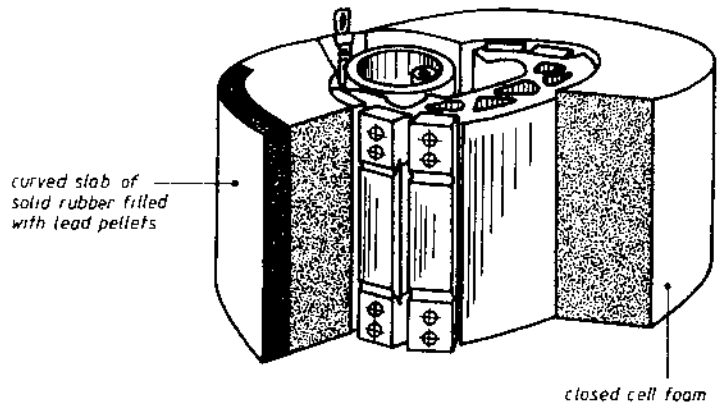

Fig. 7.26 *Prototype of EUROSID abdomen section.*

The latest version of the European Side Impact Dummy, EUROSID-1, is included in two proposed European Side Impact Regulations, one for EEC [12] and one for ECE [13]. In these regulations a moving barrier with a deformable front based on stiffness data of passenger cars is prescribed as an impacting vehicle (see Fig. 7.27).

Fig. 7.27 *Side impact of a moving deformable barrier against a passenger car.*

In the US Side Impact Regulation (1990) another Side Impact Dummy (*SID*) is prescribed [10]. Besides the dummy and performance criteria, also the test method, including moving barrier and impact direction, differs from the European proposal. For the American (and

other) car industry this Side Impact Dummy is not acceptable and they designed the Biofidelic Side Impact Dummy (*BIOSID*). This dummy is now considered, together with EUROSID-1, by the US administration as an alternative dummy. The European car industry proposes a combination of quasi-static tests on the vehicle and mathematical model simulations as worldwide side impact regulation.

7.5 Future dummy designs

There are several types of dummies used in automotive research or prescribed in regulations; they vary from simple loading devices to highly sophisticated devices for the evaluation of complete vehicles in a frontal or lateral impact.

Nowadays the design and development of dummies is more complex and costly than 30 years ago. Crash dummies have to comply with more and more stringent requirements, especially with respect to biofidelity. More and more international co-operation will be necessary to cover the cost of dummy research and development. Knowledge on accident statistics, impact biomechanics, injury mechanisms, materials and instrumentation is necessary to design and develop crash dummies. Design requirements for dummies and dummy parts are partly based on biomechanical analysis of volunteer and cadaver test responses. Mathematical model simulations are used for analysis purposes, but also to simulate prototype dummy parts and evaluate the influence of certain design parameters.

Recently TNO started a research program aimed to develop a new generation of child dummies, based on new anthropometric data and cadaver responses. It should be noted that very little test data on child cadaver performance is available. Accident statistics will indicate the need for the measurement of certain 'injury criteria'.

In the US research programs have been set up to develop a new advanced anthropometric test device (*AATD*) with humanlike response in frontal to lateral as well as roll over impact directions [9]. This dummy will interact realistically with restraint systems and the interior of the vehicle. The dummy will be durable and it will be easy to maintain and certify. The design will be based on recent biomechanical data and will have biofidelity in all directions. Furthermore, the seated configuration will be compared with recent dummies. New measuring techniques will be applied in the chest and abdomen. For instance, the dummy will be fitted with fluid-filled bag compartments (e.g. to simulate the heart, the lungs, etc.) connected to pressure transducers in order to indicate loading. Fig. 7.28 and Table 7.1 summarize the concept design of this AATD. A total of 72 to 100 data channels on the dummy will be required. An on-dummy instrumentation system with integral memory is recommended. A microprocessor-based system should allow for on-dummy analysis, self tests of individual data channels as well as the transfer of data to an external computer.

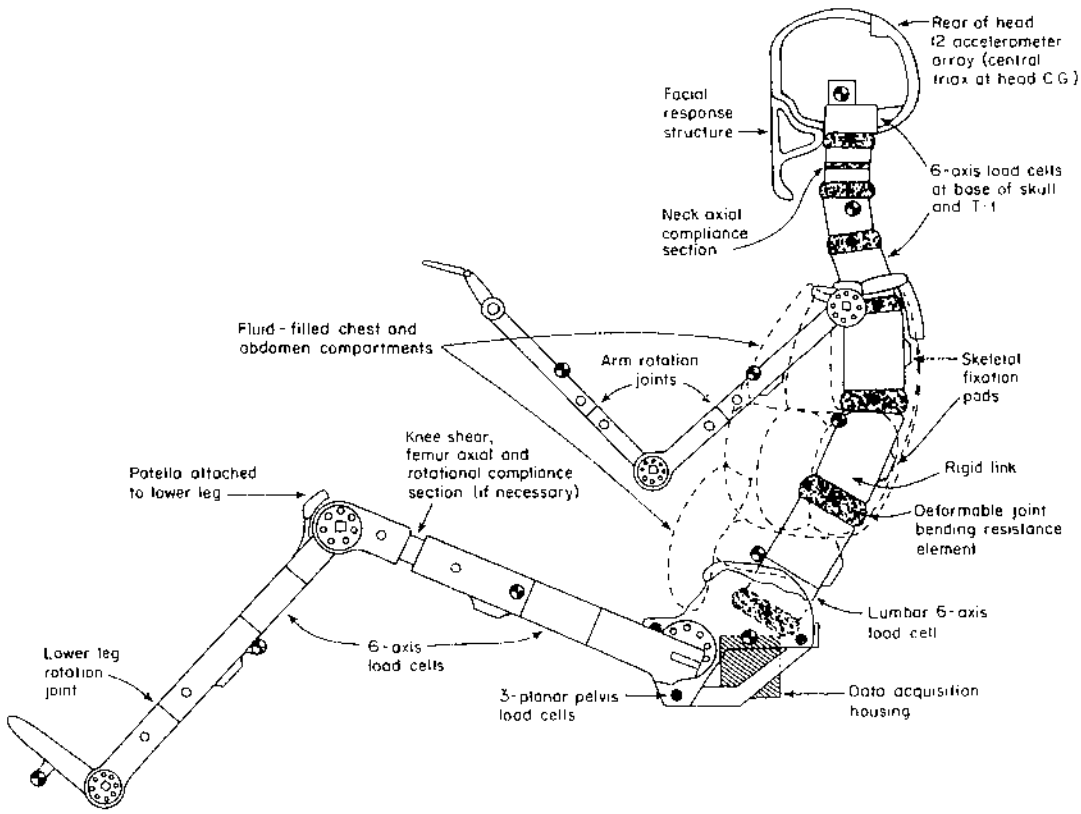

Fig. 7.28 AATD design concepts.

Biomechanical research indicates that rotational accelerations of the head may contribute to brain injuries. Prototype dummy heads have been developed, able to measure 9 linear accelerations in a special configuration. After the test a computer program calculates the translational and rotational accelerations. Computer programs using Finite Elements Methods are also proposed to assess brain injuries. The input for the model will be obtained from the dummy kinematics.

The range of research and development activities in which TNO is involved has grown wider in recent years. Besides in research programs to develop, evaluate and improve crash dummies, TNO is also involved in activities concerned with non-automotive test dummies. In the field of home and sport accidents, biomechanical studies are performed to design dummies or parts with special features, such as assessment of skin injuries. In this field 'minor' injuries are important, where automotive safety research has focussed mainly on live-threatening injuries in the past. For the development of a sport shin guard test method, cadaver tests are performed to set up requirements for breakable dummy legs. Other areas of interest are dummies for medical applications and dummies for aerospace and railroad safety.

Table 7.1 Ideal and feasible AATD measures.

Ideal Measures	Feasible Measures
HEAD	
Skull • Global structural deformations. • Local contact forces. • Rigid body motion. Brain • Global pressure distributions. • Global tissue deformations and motions. Face • Bone structural loading • Soft tissue and nerve laceration	Skull • Continuous monitoring of skull deformation at selected sites. • Local contact force at selected sites, but not for the general case of any impact site. • Rigid body three-dimensional motion. Brain: • Continuous monitoring of pressure distributions or of tissue motions and deformations at selected sites. Face: • Facial bone load • Soft tissue lacerations and facial bone fractures, simulated with lacerable and frangible materials
SPINE	
• Motion and/or dislocation of vertebral elements • Local loads between vertebral elements • Input loads to spinal segments • Local deformations of the spinal cord • Muscle, blood vessel, and nerve deformations and lacerations	• Three-dimensional motions of vertebral elements • Local load measurement between vertebral elements at selected sites • Input loads to spinal segments from surrounding body • Continuous measurements of spinal cord, blood vessel, muscle, and nerve deformations at selected sites • Soft tissue, blood vessel, and nerve lacerations, simulated with lacerable materials
THORAX	
• Pressures in the heart, aorta, and lungs • Motions and deformations of the heart, aorta, and lungs • Rib cage motions, deformations, and loads	• Continuous monitoring of the pressure distributions in the heart, aorta, and lungs at selected sites • Continuous monitoring of motions, and deformations of the heart, aorta, lungs, and rib cage at selected sites
ABDOMEN	
• Pressures in the internal abdominal organs • Motions and deformations of the internal abdominal organs	• Continuous monitoring of the pressure distributions in the internal abdominal organs at selected sites • Continuous monitoring of the motions and deformations of the internal abdominal organs at selected sites
LOWER EXTREMITIES	
• Loads in the pelvis, upper leg, knee, and lower leg • Motions and dislocations of joints • Soft tissue and nerve lacerations	• Load measurements in the pelvis, femur, knee, and tibia • Measurement of motions and dislocations of joints • Soft tissue and nerve lacerations, simulated with lacerable materials

REFERENCES

1a. Schneider, L.W. et al., Development of anthropometrically based design specifications for an advanced adult anthropomorphic dummy family. 3v. UMTRI-83-53. The University of Michigan Transportation Research Institute, Ann Arbor, 1983.

1b. Robbins, D.H., Development of anthropometrically based design specifications for an advanced adult anthropomorphic dummy family. Volume 2: Anthropometric specifications for mid-sized male dummy. UMTRI-83-53-2. The University of Michigan Transportation Research Institute, Ann Arbor, 1983.

2. Mertz, H.J. et al., Size, weight and biomechanical impact response requirements for adult size small female and large male dummies. SAE 890756. Automotive frontal impacts SAE/SP-89/782, International Congres and Exposition, Detroit, 1989.

3. Jones, N., Scaling of inelastic structures loaded dynamically, In: Structural impact and crashworthiness Vol. 1, Keynote Lectures, ed. G.A.O. Davis, Elsevier Applied Science Publishers, London/New York, 1984.

4. ISO/DP 9790-1 to 9790-6, Road vehicles - anthropomorphic side impact dummy - impact response requirements to assess the biofidelity of the dummy. Technical Committee 22, Subcommitte 12, Geneva, November 1987 to August 1988.

5. Mertz, H.J., A procedure for normalizing impact response data. SAE 840884. Society of Automotive Engineers, Warrendale, 1984.

6. Morgan, R.M., Marcus, J.H. and Eppinger, R.H., Correlation of side impact dummy/cadaver tests. SAE 811008. Proceedings 25th Stapp Car Crash Conference, San Francisco, 1981.

7. Morgan, R.M., Marcus, J.H. and Eppinger, R.H., Side impact - The biofidelity of NHTSA's proposed ATD and efficacy of TTI. SAE 861877. Proceedings 30th Stapp Car Crash Conference, San Diego, 1986.

8. Donnelly, B.R., Morgan, R.M. and Eppinger, R.H., Durability, repeatability and reproducibility of the NHTSA side impact dummy. SAE 831624. Proceedings of 27th Stapp Car Crash Conference, San Diego, 1983.

9. U.S. Department of Transportation, National Highway Traffic Safety Administration, Advanced anthropomorphic test device (AATD) development program, phase 1 reports: concept definition. Washington, 1985.

10. National Highway Traffic Safety Administration, Federal Motor Vehicle Safety Standard No. 214, Side impact protection. Federal Register, Vol. 55, No. 210, October 30, 1990.

11. Viano, D.C. and Lau, I.V., Thoracic impact: A viscous tolerance criterion. Proceedings 10th International Technical Conference on Experimental Safety Vehicles, Oxford, 1985.

12. Ad hoc group ERGA Passive Safety, Proposal for a directive on the protection of car occupants during side impact collision. Document Erga S/65, Annex 10 of Final report, Brussels, September 1989.

13. Economic Commission for Europe, Experts on Passive Safety (GRSP), Proposal for draft Regulation: uniform provisions concerning the approval of vehicles with regard to the protection of the occupants in the event of a lateral collision. Document TRANS/SC1/WP29/GRSP/R.48/Rev.1, Geneva, January 1991.

14. Langdon, M.G., Modelling the lateral impact of the thorax in car side impact accidents. Proceedings 10th International Technical Conference on Experimental Safety Vehicles, Oxford, 1985.

15. Maltha, J. and Janssen, E.G., Design of injury detecting abdomen section for side impact dummies. EUR 8938. Proceedings of seminar Biomechanics of impacts in road accidents, Brussels, 1983.

16. Lupker, H.A. et al., Advances in the MADYMO crash simulation program. SAE 910879. SAE International Congres and Exposition, Detroit, 1991.

CHAPTER 8

DESIGN TOOLS: HUMAN BODY MODELLING

8.1 Introduction

In crash safety research and development, like in many other engineering disciplines, a strong increase could be observed during the last thirty years in the use of computer simulations. This is due in part to the fast developments in computer hardware and software, but in case of automotive safety, probably even more due to emphasis which has been placed on the development of reliable models describing the human body in an impact situation, as well as numerous validation studies which have been conducted using these models. Mathematical models of the human body in conjunction with a mathematical description of the vehicle structure and the various safety provisions and restraint systems, appear to offer a very economical and versatile method for the analyses of the crash response of complex dynamical systems.

In the crash safety field mathematical models can be applied in practically all area's of research and development including:

- reconstruction of actual accidents
- design (CAD) of the crash response of vehicles, safety devices and roadside facilities
- human impact biomechanics studies

Furthermore computer simulations may be part of safety regulations, much like standard crash tests.

Dependent on the nature of the problem, several types of crash analyses programs have been developed, each with their own, but often overlapping, area of applicability. Most of the models are of the deterministic type, that is, based upon measured or estimated parameter values, representing characteristics of the human body, safety devices, the vehicle and its surroundings and using well established physical laws, the outcome of the crash event is predicted. Another category of models used in the crash safety field is of a statistical nature. They are used for instance in injury biomechanics research to assess the correct relationship between loading conditions and resulting injuries by means of regression type of equations (the so-called injury risk function). This Chapter will concentrate on deterministic models for the human body.

Although the various deterministic models may differ in many aspects, they are all dynamic models. They account for inertial effects by somehow deriving equations of motions for all movable parts and solve these equations by an iterative method. The mathematical

formulations used for these models can be subdivided into lumped mass models, multi-body models and finite element models. Lumped mass models are usually one- or two-dimensional, multi-body models two- or three-dimensional and finite element models usually three-dimensional.

Lumped mass models

In a lumped mass model a system is represented by one or more rigid elements often connected by mass-less elements like springs and dampers. An example of a lumped-mass model is shown in Fig. 8.1. It is a one-dimensional model of the human thorax developed by Lobdell in 1973 [1]. This model simulates the thorax response in case of a loading by an impactor. The model consist of 3 rigid bodies with masses m1, m2 and m3 connected by springs and dampers. Mass m1 represents the impactor mass and masses m2 and m3 the sternal and vertebral effective mass. Spring k_{12} represents the skin and flesh between impactor and sternum. The internal spring and dampers represent the connection between sternum and thoracic spine. The response of this model was shown to correlate well with human cadaver tests.

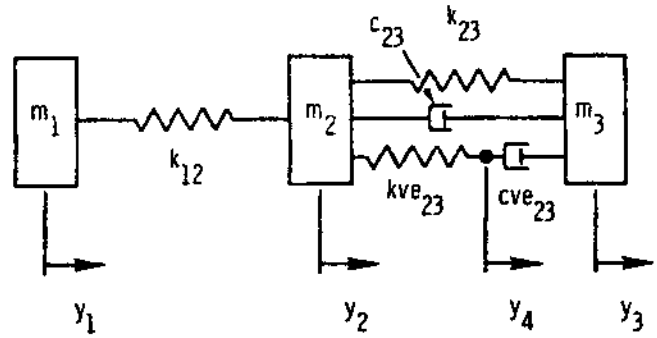

Fig. 8.1 Example of lumped mass model: the Lobdell thorax model [1]

Multi-body models

The most important difference between a lumped mass model and a multi-body model is that elements in a multi-body formulation can be connected by various joint types due which the number of degrees of freedom between the elements can be constrained. A lumped mass model in fact can be considered as a special case of the more general multi-body model formulation. The motion of the joint-connected elements in a multi-body model is caused by external forces generated by so-called force-interaction models.

Examples of force-interaction models in a multi-body model for crash analyses are the model to account for an acceleration field, spring-damper elements, restraint system models and contact models. Another difference with lumped mass models is that in a multi-body formulation instead of rigid bodies also flexible bodies can be specified.

A first historical example of a multi-body model is presented in Fig. 8.2. The model was developed in 1963 by Mc Henry [2]. The model which represents the human body together with restraint system and vehicle is 2-dimensional and has 7 degrees of freedom. The human body part of the model is represented by 4 rigid bodies representing thorax/head, upper arms, upper legs and lower legs. The rigid elements were connected by simple pin joints. The values for the parameters in the model were estimated. Mc. Henry compared his model calculations with experimental data to demonstrate the potential of this type of calculations. He was able to show quite good agreement for quantities like hip displacements, chest acceleration and belt loads.

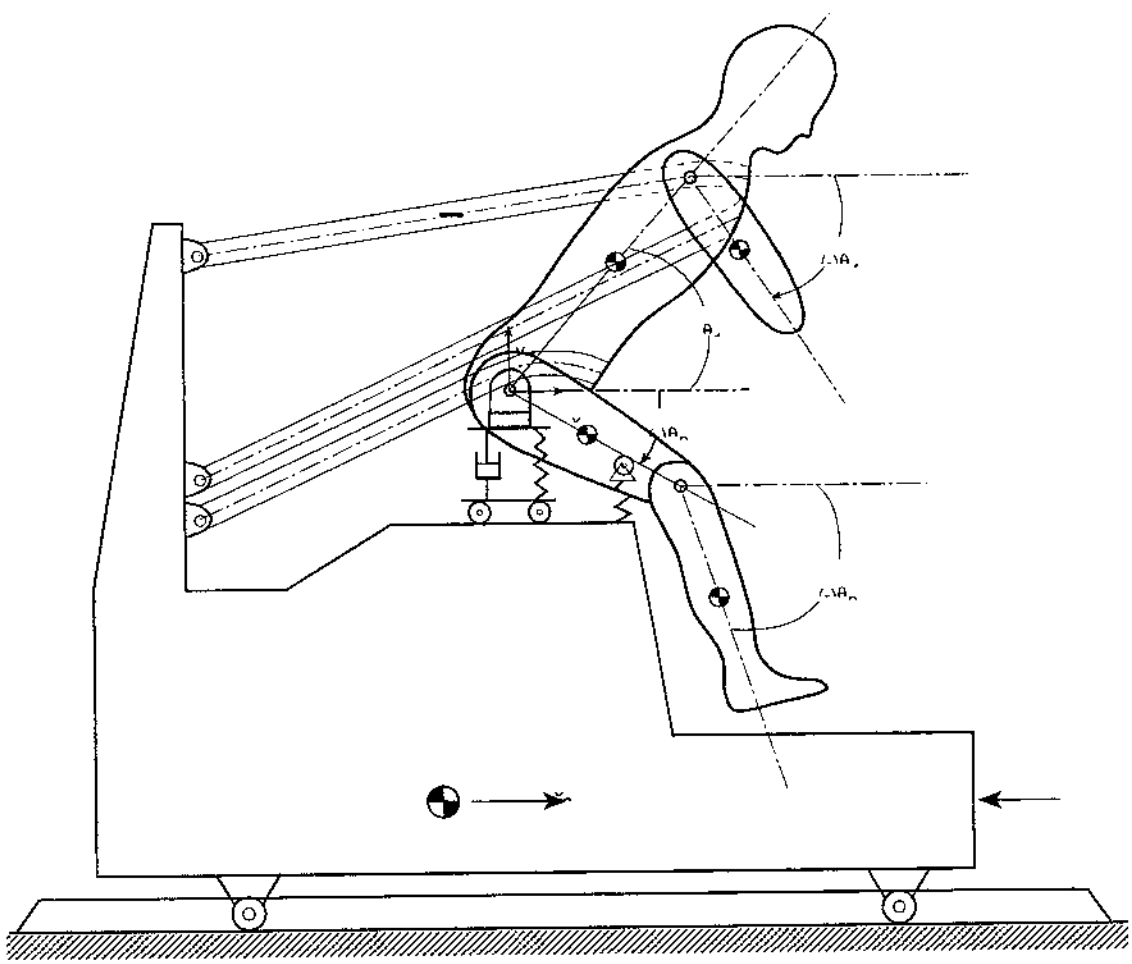

Fig. 8.2 Example of multi-body model: 7 degrees of freedom model for frontal collisions by Mc. Henry [2]

A second more recent example of a multi-body model is presented in Fig. 8.3. It is 3-dimensional MADYMO model of a Chrysler Neon vehicle suitable for frontal collisions.

The model was developed as part of a co-operative effort between the European Community and the NHTSA (DOT-USA) to study vehicle compatibility issues [3]. The vehicle part of the model has more than 200 elements and includes a description of interior, restraint system, suspension, steering wheel, bumper, engine, hood etc. The human body part of the model is a 32-segment model of the Hybrid III dummy. Model results were compared with rigid wall test and offset deformable barrier tests and quite realistic results were obtained.

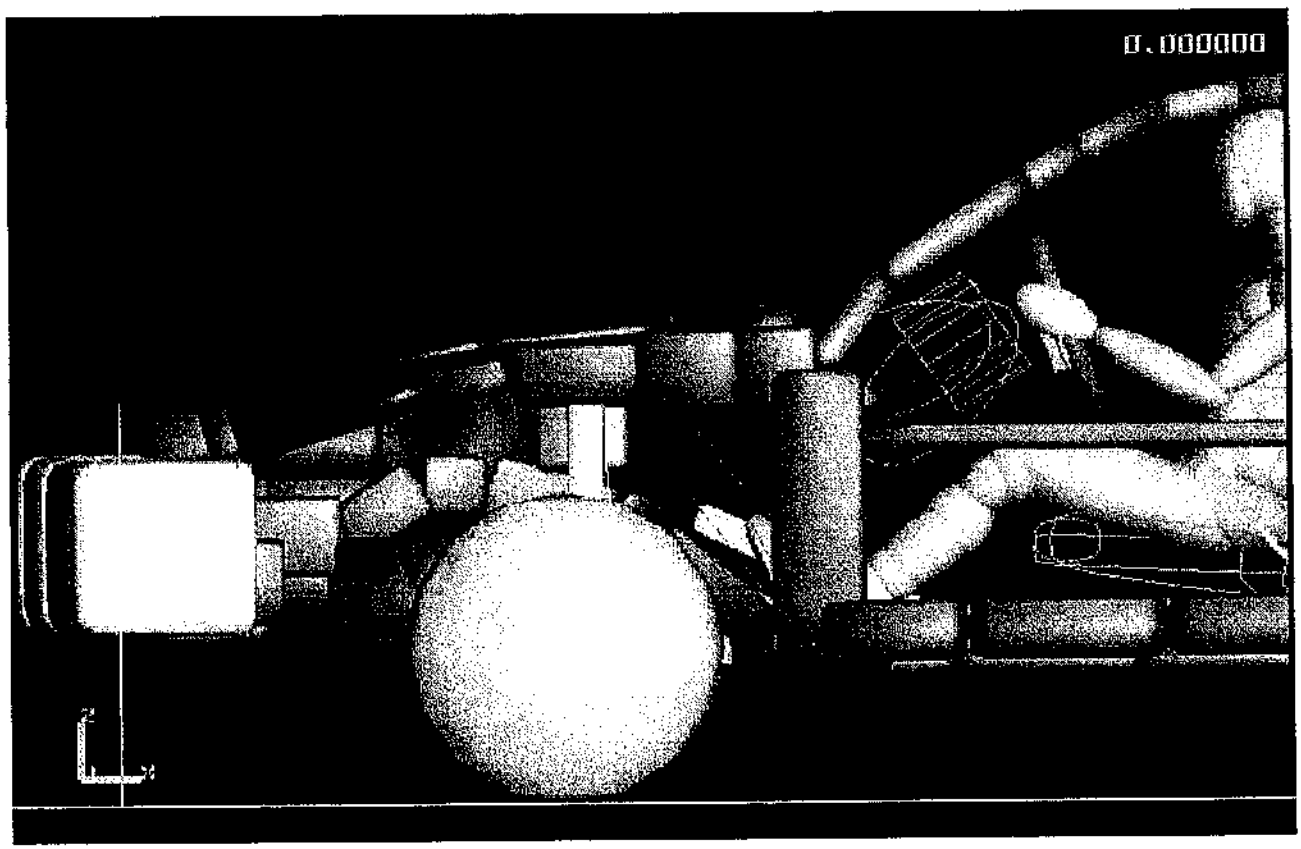

***Fig. 8.3** Example of multi-body model: 3-dimensional model for frontal collisions of Chrysler-Neon with Hybrid III dummy [3]*

Finite element models

In a finite element model the system to be modelled is divided in a number of finite volumes, surfaces or lines representing an assembly of finite elements. These elements are assumed to be interconnected at a discrete number of points: the nodes. In the displacement-based finite element formulation, which is applied in practically all major finite element software packages, the motion of the points within each finite element is defined as a function of the motion of the nodes. The state of stress follows from the deformations and the constitutive properties of the material modelled. Fig. 8.4 shows one of the earlier examples of using the finite element method for human body impact modelling: a model of the human head. The model was developed in the seventies by Shugar [4]. The model was 3-dimensional and included a representation of the skull and brain. Linear elastic and linear visco-elastic material behaviour was assumed. Skull bone response and brain response from the model was compared with experimental results of head impact tests with primates.

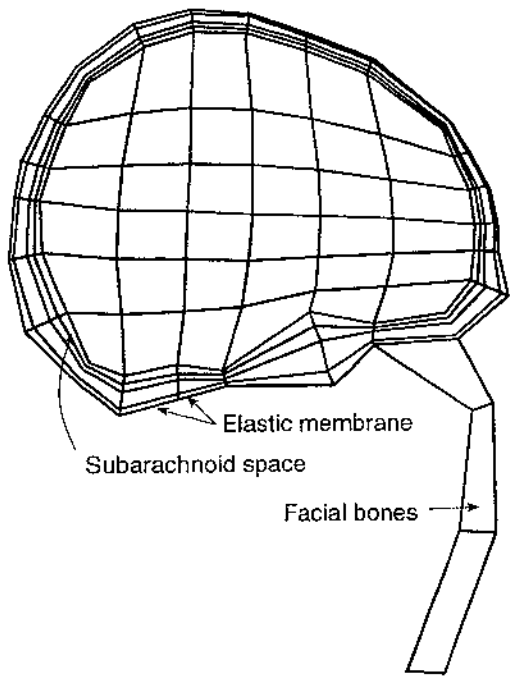

***Fig. 8.4** Example of a finite element model simulating the human body: a head model by Shugar [4]*

Multi-body models versus finite element models

Both the multi-body method and the finite element method offer their specific advantages and disadvantages in case of crash analyses. The multi-body approach is particularly attractive due to its capability of simulating in a very efficient way complex kinematical connections like they are present in the human body and in parts of the vehicle structure like the steering assembly and the vehicle suspension system. The finite element method offers the capability of describing (local) structural deformations and stress distribution, due to which it becomes possible to study for instance injury mechanism in the human body parts. Usually much larger computer times are required to perform a finite element crash simulation than a multi-body crash simulation, making the finite element method less attractive for optimisation studies involving many design parameters.

Fig. 8.5 shows an example in which both the multi-body approach and the finite element approach are used. This integrated approach is sometimes referred to as "hybrid" approach. It is model of a car occupant interacting with a passenger airbag developed in the eighties by Bruijs [5]. The airbag (and airbag straps) was modelled in the PISCES 3D-ELK program (now MSC-DYTRAN) using almost 2000 triangular membrane elements. For the gas inside the airbag was described using the perfect gas law. The model takes into account leakage through airbag material and exhaust orifices. The most important assumption in the airbag model is that the pressure and temperature in the airbag are constant and that inertia effects of the gas are neglected. The finite element airbag model interacts with a multi-body model of the Hybrid III crash dummy modelled in MADYMO 3D.

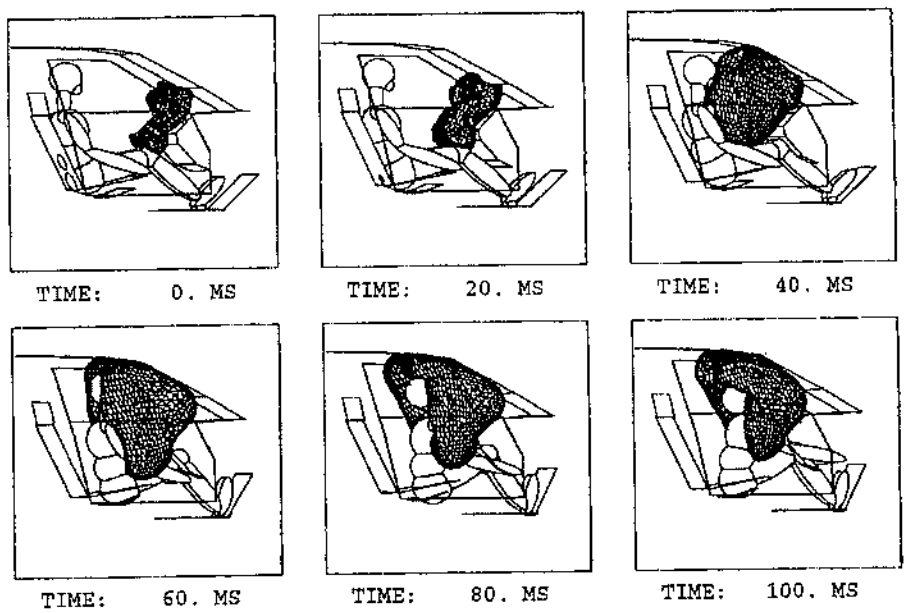

Fig. 8.5 Example of integrated multi-body finite element model: occupant-airbag interaction by Bruys [5]

Set-up of this Chapter

Multi-body models in which the complete human body is simulated for the purpose of crash analyses are often referred to as Crash Victim Simulation models (CVS), human body gross-motion simulators or whole body response models. The theoretical basis for this type of models will be presented in section 8.2. The finite element method as such is assumed to be known here, so this method will not be treated here further except for the aspect of integrated multibody-finite element simulations (section 8.2.5).

Human body models for crash analyses can be subdivided into models of crash dummies and models of the real human body. Section 8.3. discusses some aspects of crash dummy models. Real human body models will be presented in section 8.4. In the final section 8.5 some concluding remarks will be made and future trends will be discussed. Among others attention shall be given to the aspect of model validation in view of the increasing importance of virtual testing.

8.2 The multi-body method for crash analyses

8.2.1 Introduction

One of the first human body gross-motion simulation models was developed already almost 40 years ago by McHenry [2], see Fig. 8.1. The results of this model were so encouraging that since then many, more sophisticated, models have been developed. The most well known are the two-dimensional 8-segment MVMA-2D model and the three-dimensional 6-segment HSRI occupant model both developed by Robbins et. al. [6,7], the three-dimensional 12-segment UCIN model [8] and the three-dimensional Calspan 3D CVS (CAL3D) which allowed up to 20 elements [9]. For a review of the status of human body gross-motion simulators up to 1975 see King and Chou [10].

Two of the reviewed models, i.e. MVMA 2D and the CAL3D, have gone through an extensive further validation and development effort since then and are still frequently used at present. An example of these developments is the ATB (Articulated Total Body) program, which is a special version of CAL3D for aircraft safety studies, developed by the Air Force Aerospace Medical Research Laboratory in Dayton [11].

This section will be mainly related to a more recent program, i.e. MADYMO [12], which is a general multibody/finite element program with a number of special features for crash analyses. The program was developed in Europe by TNO Automotive in Delft, The Netherlands. For a comparison of the basic features between MADYMO, MVMA2D and

CAL3D the reader is referred to reviews of gross-motion simulation programs by Prasad [13,14] and Prasad and Chou [15]. MADYMO has a two- and a three-dimensional version referred to as MADYMO 2D and MADYMO 3D, respectively. This section will concentrate on the multibody part and the force interactions in MADYMO 3D.

8.2.2 MADYMO set-up

MADYMO consists of a number of modules (Fig. 8.6). The multi-body module of the program calculates the contribution of the inertia of bodies to the equations of motion; the other modules calculate the contribution of specific force elements such as springs, dampers, muscles, interior contacts and restraint systems or the effect of systems which are represented as a finite element model. Special models are available for vehicle dynamic applications including tyre models. A control module is available which offers the possibility to apply loads to bodies dependent on the body's motions. For this purpose motion quantities can be extracted from the bodies by sensors. The sensor signals can be manipulated with summers, transformers and controllers and used as input for actuators which apply forces and torques to the bodies. In the next section 8.2.3 the multi-body algorithm will be presented and in section 8.2.4 the most important force elements as used for crash analyses. The aspect of integrated multi-body/finite element analyses will be introduced in section 8.2.5.

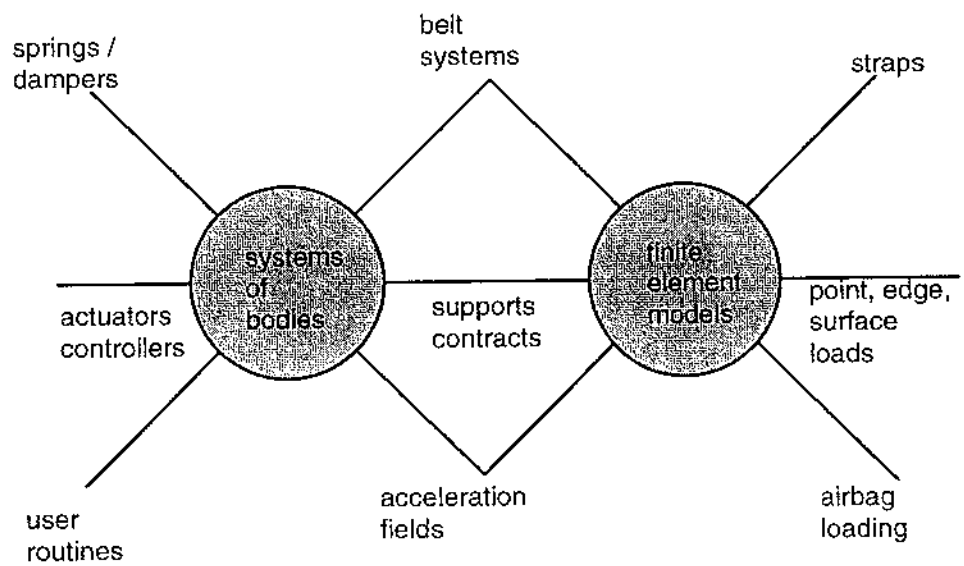

Fig. 8.6 MADYMO modules

8.2.3 MADYMO multi-body algorithm

The multi-body module analyses the motion of systems of bodies. Bodies can be interconnected by kinematic joints such as spherical joints, revolute joints, universal joints, and translational joints. More over, new kinematic joints can be added by user subroutines.

Topology of a system of bodies

Consider a system of N bodies with a tree structure (Fig. 8.7). A system of bodies has a tree structure if one can proceed from one arbitrary body to another arbitrary body along a unique sequence of bodies and joints. Systems with closed chains of bodies in it (like for instance a four bar linkage system) are permitted in the later MADYMO versions. For topology specification they have to be reduced to a tree structure however. The bodies are numbered in order to be able to specify which bodies are interconnected. One of the bodies is chosen as reference body and is given number 1. The other bodies are numbered from 2 till N in such a way that the numbers of the bodies on the path from the reference body to any other body are lower than the number of that specific body. The configuration of a system is completely defined by specifying for all bodies at the end of the tree (the peripheral bodies), the numbers of the bodies on the path to the reference body. The bodies on such a path form a branch. In the MADYMO input file the configuration of a system is defined by entering for each branch the numbers of the bodies in decreasing order. This table with branchnumbers is called configuration table. For the example in Fig. 8.7 the configuration specification is:

Branch 1: 3 2 1
Branch 2: 7 2 1
Branch 3: 6 5 1
Branch 4: 8 4 1

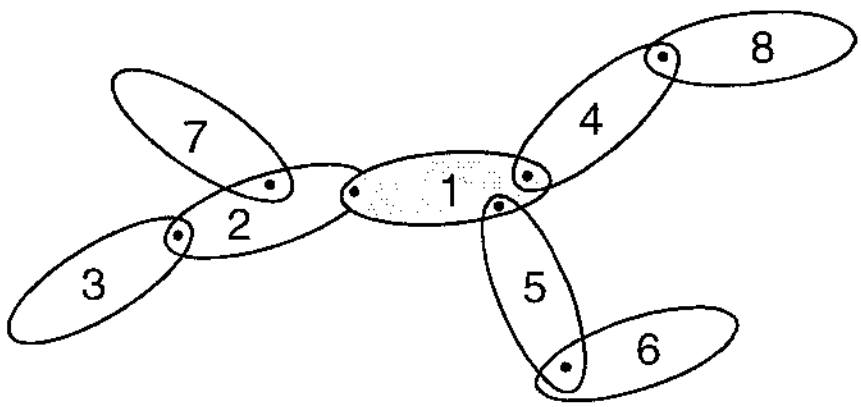

***Fig. 8.7** Example of body numbering*

Kinematics of a rigid body

Consider the rigid body i shown in Fig. 8.8. In order to describe its motion relative to an inertial space, a right-handed body-fixed base $\{\mathbf{e}\}_i$ is introduced. Its origin is chosen coincident with the centre of mass since then the equations of motion of a single body have their simplest form: the Newton-Euler equations. The motion of the body is defined by the position of the origin and the orientation of the body-fixed base relative to an inertial base $\{\mathbf{E}\}$.

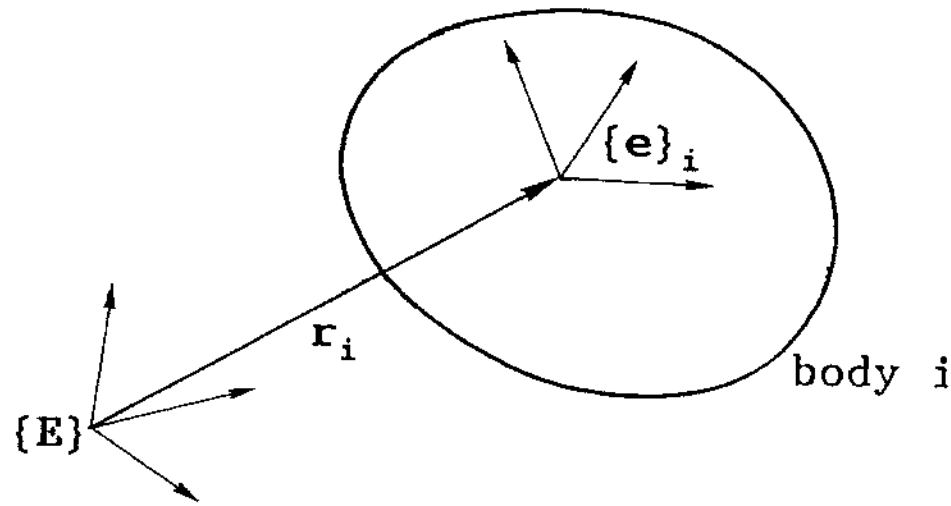

Fig. 8.8 Specification of the motion of a rigid body

The position of the origin of the body-fixed base relative to the origin of the inertial base is given by the vector $\mathbf{r}_i$; the orientation of the body-fixed base relative to the inertial base is defined by the rotation matrix $\underline{A}_i$. The elements of this matrix consist of scalar products of the inertial base vectors and the body-fixed base vectors.

Kinematics of a flexible body

In later versions of MADYMO 3D, bodies which experience small deformations can be modelled as flexible bodies. For a flexible body the motion of a point on a body is considered to be composed of a rigid body motion and a superimposed motion due to the deformation. The motions of the body due to the deformations are approximated by a linear combination of predefined displacement and rotation fields (deformation modes). Only at certain pre-defined points in the body (the so-called nodes) the deformation nodes are defined.

Kinematics of pair of bodies interconnected by a joint

Consider the pair of bodies interconnected by an arbitrary kinematic joint shown in Fig. 8.9. (A kinematic joint as defined here can connect only two bodies.) The bodies are numbered i and j. The number of the lower numbered body i can be obtained from the configuration table. In MADYMO the motion of a body j is described relative to the

corresponding lower numbered body i. This is done in terms of quantities that define the motion within the joint, the so called joint co-ordinates. Their number, n_{ij} equals the number of degrees of freedom of the joint. They will be put in the column matrix $\underline{q}_{ij}$.

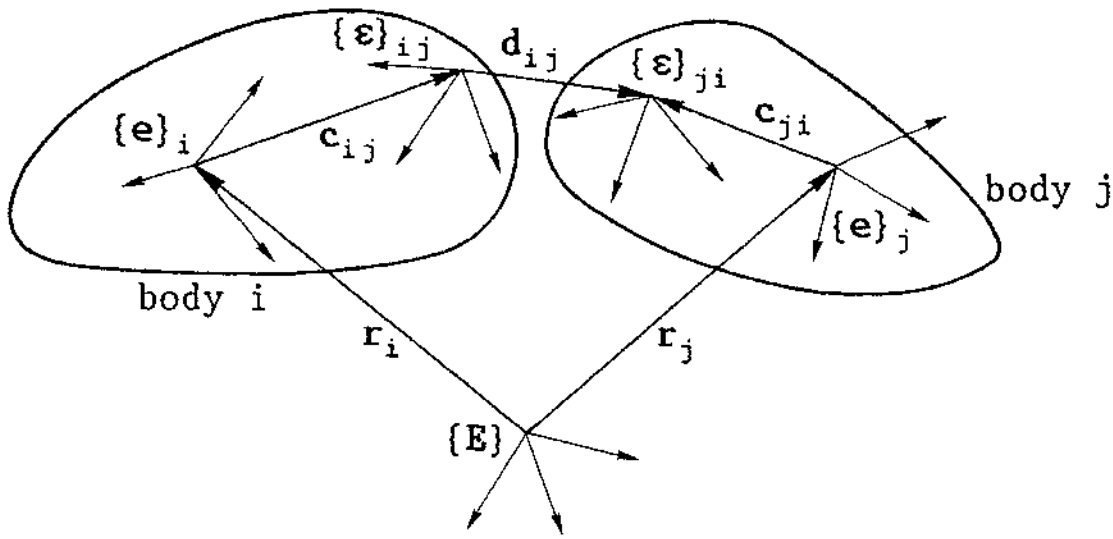

Fig. 8.9 Pair of interconnected bodies

On each body a body-fixed joint base $\{\varepsilon\}$ is introduced in order to describe the relative motion of body j relative to body i. The origins of these joint bases are chosen such that the mathematical expression for the relative translation of the joint base origins is as simple as possible. As an example, for a spherical joint the origins will be chosen coincident with the articulation points on the bodies. Then, the relative translation vector is identically **0**.

The selection of the orientations of the joint bases is made on the same ground. As an example, for a revolute joint one of the base vectors of each joint base will be chosen parallel to the rotation axis. The best choice for the origin and the orientation of joint bases depends on the specific joint which is considered.

Let the orientation of the joint base on body i (j) relative to the body base on body i (j) be specified by the time-independent rotation matrix $\underline{C}_{ij}$ ($\underline{C}_{ji}$). Let the orientation of the joint base on body j relative to the joint base on body i be specified by the rotation matrix $\underline{D}_{ij}$. This matrix is a function of the joint co-ordinates. Using these rotation matrices, the rotation matrix of the base of body j can be written as:

$$\underline{A}_j = \underline{A}_j \underline{C}_{ij} \underline{D}_{ij} \underline{C}_{ji}^{\ T} \tag{1}$$

Let $\mathbf{c}_{ij}$ and $\mathbf{c}_{ji}$ be the position vectors of the origins of the joint bases on body i and j, respectively, relative to the origin of the base of the corresponding body. For a rigid body, the components of these vectors relative to the corresponding body base are constant. The vector from the origin of the joint base on body i to the joint base on body j is given by the vector $\mathbf{d}_{ij}$. The components of this vector relative to the joint base on body i, $\underline{d}_{ij}$, is a function of the joint co-ordinates. The position vector of the origin of the body base of body j can be written as:

$$\mathbf{r}_j = \mathbf{r}_i + \mathbf{c}_{ij} + \mathbf{d}_{ij} - \mathbf{c}_{ji} \tag{2}$$

Applying equation (1) and (2) successively for body 1 till body N yields the positions and orientations of all body bases relative to the inertial base.
Taking the first time derivative of (1) and (2) yields the following expressions for the angular and linear velocity [16]:

$$\omega_j = \omega_i + \omega_{ij} \tag{3}$$

$$\dot{\mathbf{r}}_j = \dot{\mathbf{r}}_i + \omega_i \times \mathbf{c}_{ij} + \dot{\mathbf{d}}_{ij} - \omega_j \times \mathbf{c}_{ji} \tag{4}$$

where ω_i and ω_j are the angular velocity of body i and j, respectively and ω_{ij} the angular velocity of the joint.

Taking the second time derivative of (1) and (2) yields similar expressions for the angular and linear acceleration [16].

Example of a kinematic joint
Consider the joint shown in Fig. 8.10. This joint allows a relative translation s and a relative rotation φ. These joint co-ordinates are assembled in the column matrix $\underline{q}_{ij} = [s\ \varphi]^T$. The first base vectors of both joint bases are chosen parallel to the rotation/translation axis. The origin of the joint bases are chosen on the rotation/translation axis and are initially coincident. Then the components of the relative translation vector with respect to the joint base $\{\varepsilon\}_{i\,j}$ and the rotation matrix are given by:

$$\underline{d}_{ij} = \begin{pmatrix} s \\ 0 \\ 0 \end{pmatrix} \tag{5}$$

$$D_{ij} = \begin{pmatrix} 1 & 0 & 0 \\ 0 & \cos\varphi & -\sin\varphi \\ 0 & \sin\varphi & \cos\varphi \end{pmatrix} \tag{6}$$

The relative velocity of the origins of the joint bases is obtained by taking the first time derivative of (5). This yields:

$$\underline{\dot{d}}_{ij} = \begin{pmatrix} \dot{s} \\ 0 \\ 0 \end{pmatrix} \tag{7}$$

The relative angular velocity of the joint bases is the axial vector of the skew-symmetric matrix $\dot{D}_{ij} D_{ij}^{T}$. This yields:

$$\underline{\omega}_{ij} = \begin{pmatrix} \dot{\varphi} \\ 0 \\ 0 \end{pmatrix} \tag{8}$$

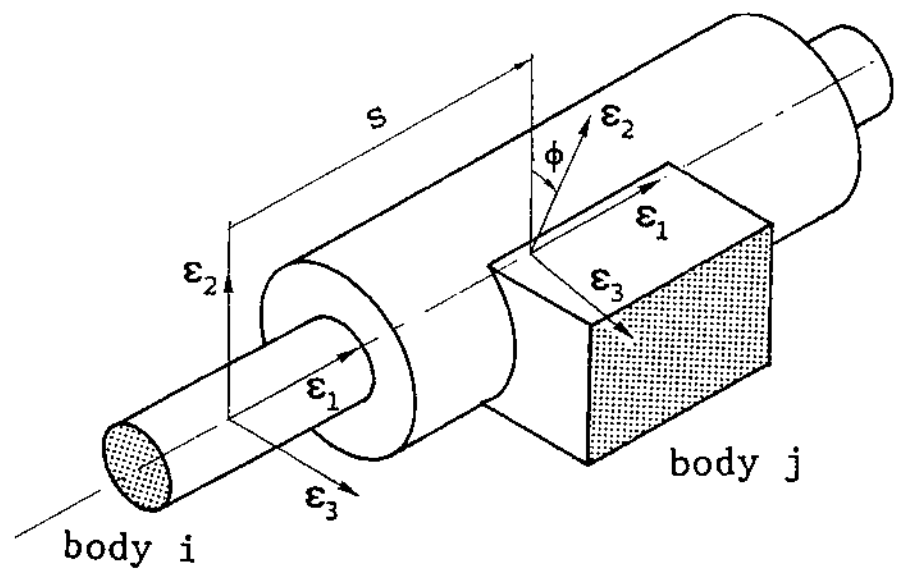

Fig. 8.10 Translational-rotational joint

In MADYMO 3D a library of kinematic joints is available. Fig. 8.11 summarises a number of the most frequently used joint types within MADYMO.

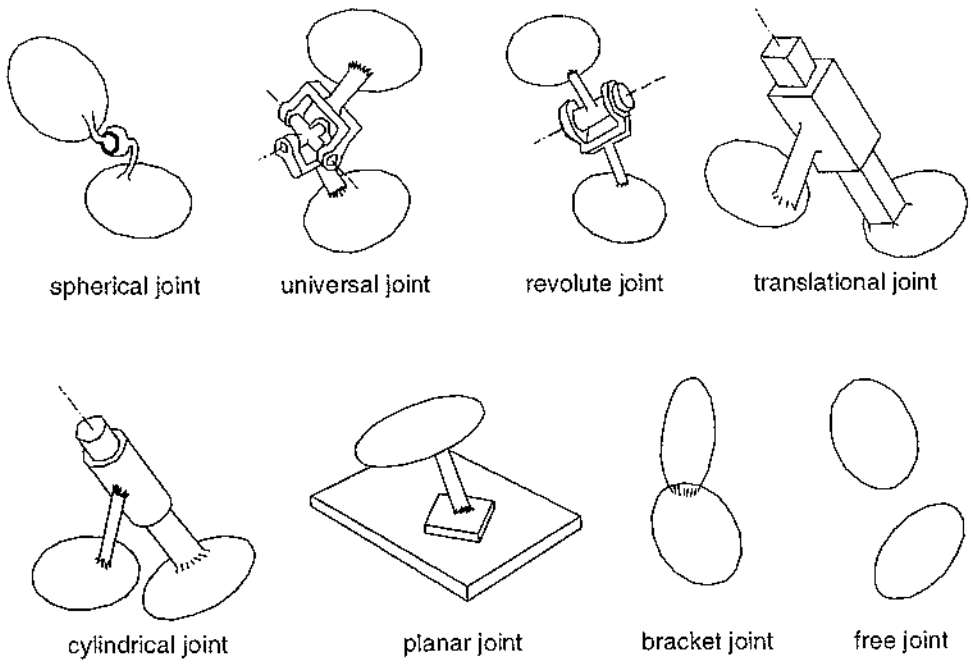

Fig. 8.11 Examples of kinematic joints

Equations of motion

The equations of motion (Newton-Euler) of a rigid body i referred to its centre of mass are [16]:

$$m_i \ddot{\mathbf{r}}_i = \mathbf{F}_i \tag{9}$$

$$\mathbf{J}_i \circ \dot{\omega}_i + \omega_i \times \mathbf{J}_i \circ \omega_i = \mathbf{T}_i \tag{10}$$

where m_i is the mass, $\mathbf{J}_i$ is the inertia tensor with respect to the centre of mass, $\mathbf{F}_i$ is the resultant force vector, and $\mathbf{T}_i$ is the resultant torque vector relative to the centre of mass. For a body in a system of bodies, $\mathbf{F}_i$ and $\mathbf{T}_i$ include the effect of the applied forces and torques acting on the rigid bodies as caused by the force-interaction models as well as the constraint forces and torques due to kinematic constraints in the joints. These constraint forces and torques cannot be determined until the motion of the system is known. This in contrast with the applied forces and torques which depend only on position and velocity quantities.

The constraint forces and torques can be eliminated using the principle of virtual work. First equations (9) and (10) are multiplied by a variation of the position vector, $\delta\mathbf{r}_i$, and a variation of the orientation, $\delta\pi_i$, and the resulting equations are summed for all bodies of the system:

$$\sum \left[\delta\mathbf{r}_i \circ \{ m_i \ddot{\mathbf{r}}_i - \mathbf{F}_i \} + \delta\pi_i \circ \{ \mathbf{J}_i \circ \dot{\omega}_i + \omega_i \times \mathbf{J}_i \circ \omega_i - \mathbf{T}_i \} \right] = 0 \tag{11}$$

In case the variations δr_i and $\delta \pi_i$ of connected bodies are such that the constraints caused by the joint are not violated, the unknown joint forces and torques will cancel (principle of virtual work). Such variations can be obtained from equations (1) and (2) by varying the joint co-ordinates. These expressions can be substituted in (8.11). Starting with bodies at the end of the tree, expressions for the second time derivative of the joint co-ordinates are obtained:

$$\underline{\ddot{q}}_{ij} = \underline{M}_{ij}\,\underline{\dot{Y}}_i + \underline{Q}_{ij} \tag{12}$$

$\dot{Y}_i$ is a 6×1 column matrix which contains the components of the linear and angular acceleration of the base of the lower numbered body i. The $n_{ij} \times 6$ matrix $\underline{M}_{ij}$ and the $n_{ij} \times 1$ column matrix $\underline{Q}_{ij}$ depend on the inertia of the bodies and the instantaneous geometry of the system. $\underline{Q}_{ij}$ depends additionally on the instantaneous velocity of the system and the applied loads. The matrices $\underline{M}_{ij}$ and $\underline{Q}_{ij}$ are calculated successively starting with body N to body 1. Then starting with the joint between the inertial space and body 1 the second time derivatives of the joint co-ordinates can be calculated from (12). Note that for this joint, i equals 0 and j equals 1 and the acceleration of the inertial space, $\dot{Y}_0 = \underline{0}$.

This algorithm yields the second time derivatives of the joint co-ordinates in explicit form. The number of computer operations is linear in the number of bodies in case all joints have the same number of degrees of freedom. This leads to an efficient algorithm for large systems of bodies.

Time integration of the second time derivatives of the joint co-ordinates gives the joint co-ordinates and there first time derivatives at a new point in time. These are used to calculate the motion and velocity of the body bases relative to the inertial base using equations (1) and (2) and their first time derivatives (3) and (4). At the start of the integration the joint co-ordinates and their first time derivatives have to be specified (initial conditions). For the time integration two explicit numerical integration methods are available, namely a fourth order Runge-Kutta method which uses a constant time step, and a fifth order Runge-Kutta-Merson method which uses a variable time step that is controlled by the local truncation error.

8.2.4 Force interaction models

The motion of a system of joint-connected bodies is caused by applied forces. MADYMO offers a set of standard force-interaction models. The various categories of force-interaction models are summarised below (see also Fig. 8.6):

- Acceleration field model
- Spring-damper elements
- Muscle models

- Contact models
- Belt model
- Dynamic joint models

In addition the user can make and link his own routines to the MADYMO multibody module.

Forces (and torques) are specified as a (non-linear) function of parameters like deflections, elongations, penetrations, joint rotations etc. Such functions are defined by means of a set of function pairs, which internally in the program are approximated either by a spline function or by a piece-wise linear interpolation. Generally, quasi-static tests have to be carried out to obtain these characteristics. Differences between loading and unloading responses can be approximated by various hysteresis models.

Often function characteristics will be rate dependent in a highly dynamical environment like a crash. For this purpose in a number of the force-interaction models, velocity dependent damping can be introduced. Moreover there is a possibility to prescribe a so-called dynamic amplification factor which multiplies a statically determined force with a rate dependent factor in order to approximate the dynamic response. For details on the physical background of dynamic amplification in a crash environment see Prasad and Padgaonkar [17]. In MADYMO several dynamic amplification factors have been implemented including polynomial and logarithmic function of the rate of deformation (or penetration, elongation etc..).

Acceleration field model

The acceleration field model calculates the forces at the centres of gravity of bodies in a homogeneous time-dependent acceleration field **a** (Fig. 8.12). This model can be applied for the simulation of the acceleration forces on a vehicle occupant during an impact. Consider as an example the impact of a vehicle against a rigid barrier. If the vehicle does not rotate during the crash, the actual recorded accelerations at the vehicle can be prescribed as an acceleration field acting on the occupant, while the vehicle is connected to the inertial space. The motion of the occupant relative to the vehicle is the same as when the actual recorded motion of the vehicle is prescribed. The components of the vector **a** are defined as a function of time relative to the inertial co-ordinate system.

Spring-damper elements

Three different types of massless "spring-damper" models can be specified: a Kelvin-, a Maxwell- and a Point-restraint element (Fig. 8.13). The Kelvin element is a uniaxial element which simulates a spring parallel with a damper. The Maxwell element is an uniaxial element which simulates a spring and damper in series. The point-restraint model can be considered as a combination of three Kelvin elements with infinite spring length, each parallel to one of the axes of an orthogonal co-ordinate system. All spring-damper

models can be attached to arbitrary points of any two bodies or between a body and the inertial space.

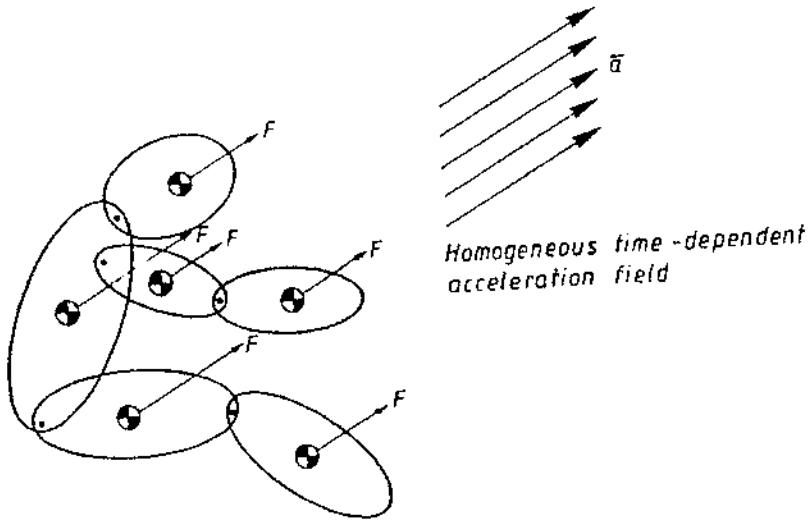

Fig. 8.12 *A homogeneous acceleration field*

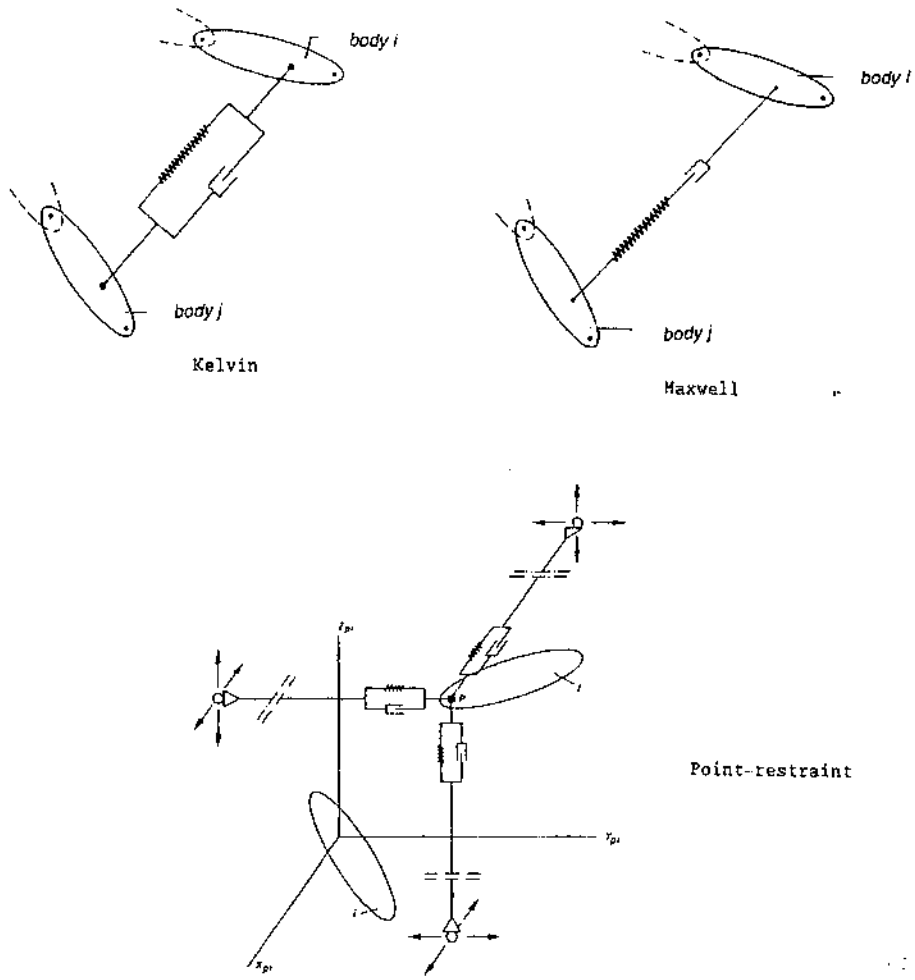

Fig. 8.13 *A Kelvin-, Maxwell- and Point-restraint element*

Muscle models

The most common muscle model in biomechanical research is the Hill model (Fig. 8.14). The model consists of a contractile element (CE) which describes the active force generated by the muscle, a parallel elastic element (PE) which describes the elastic properties of muscle fibers and surrounding tissue, 2 elastic elements (SE1 and SE2) which describe the elastic properties of tendons and aponeurosis and 2 masses (M1 and M2) to account for the muscle mass. The basic muscle model implemented in MADYMO consists of the combined contractile element CE and parallel elastic element PE. Muscles with varying complexity can be formulated using this basic model in combination with the standard MADYMO elements.

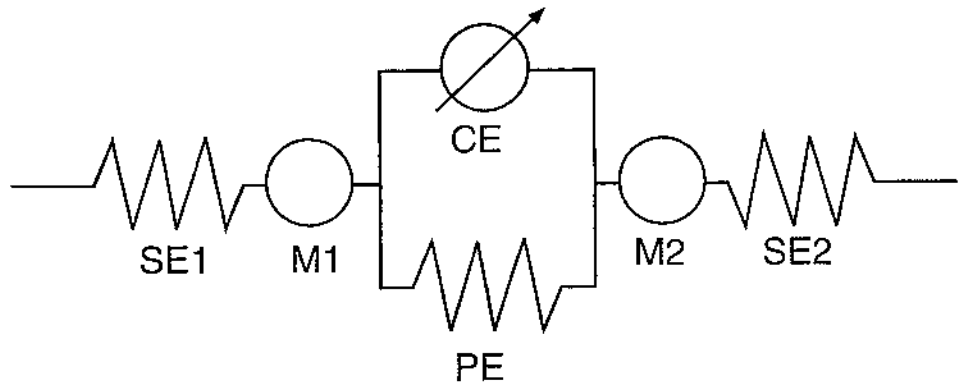

Fig. 8.14 *The Hill type muscle model*

Contact models

Planes, cylinders, ellipsoids and in later versions of MADYMO also arbitrary shaped surfaces (called facet surfaces) are used to model contact with other bodies or the surroundings. The contact surfaces are of major importance in the description of the interaction of the human body and an impacting surface like the vehicle interior. Apart from standard ellipsoids which are of the degree 2, also higher order ellipsoids can be specified:

$$\left(\frac{|x|}{a}\right)^n + \left(\frac{|y|}{b}\right)^n + \left(\frac{|z|}{c}\right)^n = 1 \qquad (13)$$

where a, b and c are the semi-axes of the (hyper)ellipsoid and n is the degree. If the degree n increases the (hyper)ellipsoid will approximate more and more a rectangular shape (Fig. 8.15).

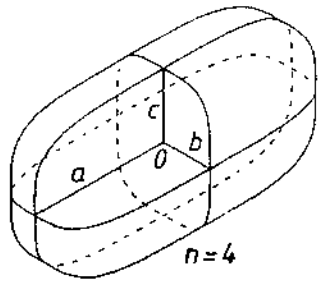

Fig. 8.15 *A hyper-ellipsoid of degree 4*

The surfaces cannot deform themselves; instead they are allowed to penetrate into each other. The basic principle of the contact models in MADYMO (and other human body gross-motion simulators) is that a contact force is generated between two colliding surfaces which is a function of the penetration of the two surfaces as well as of the relative velocity in the contact area (Fig. 8.16). In this way elastic (including hysteresis and dynamic amplification), damping and friction forces can be specified in the contact. If a facet surface is involved the contact force instead of "force-penetration" based also can be based on a "stress-penetration" function.

The belt model

The belt model consists of a chain of connected, massless, spring type of segments (Fig. 8.17). The end points of these segments are connected to rigid bodies or the inertial space at so-called attachment points. These attachment points cannot change during a simulation. An important feature is that belt material can slip through an attachment point from one segment to another. The belt model accounts for initial belt slack or pre-tension and rupture of belt segments. Elastic characteristics can be specified separately for each belt segment. Furthermore a retractor can be specified which is either of the vehicle sensitive type or of the webbing sensitive type. A vehicle sensitive reel can lock at a specified time or if a specific component of the calculated linear acceleration at the retractor location exceeds a prescribed level during a certain time interval. A webbing sensitive reel locks if the belt feed rate exceeds a specified limit. Finally also a pretensioner model is available.

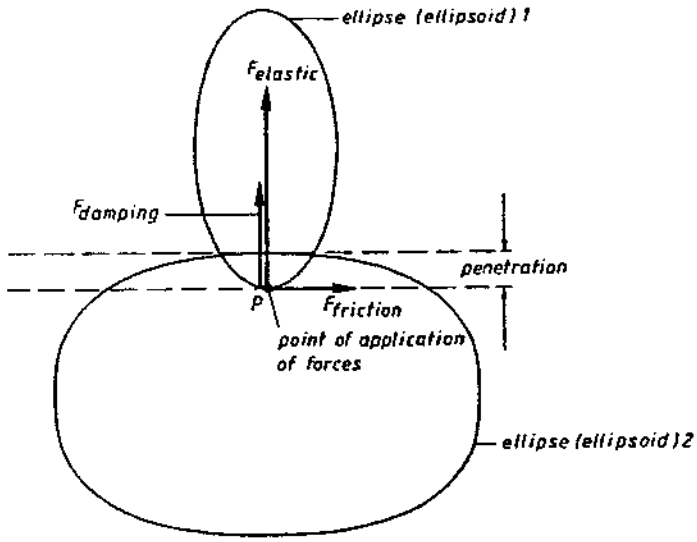

Fig. 8.16 *Contact loads in an ellipsoid-ellipsoid contact (only forces acting on the upper ellipsoid are shown).*

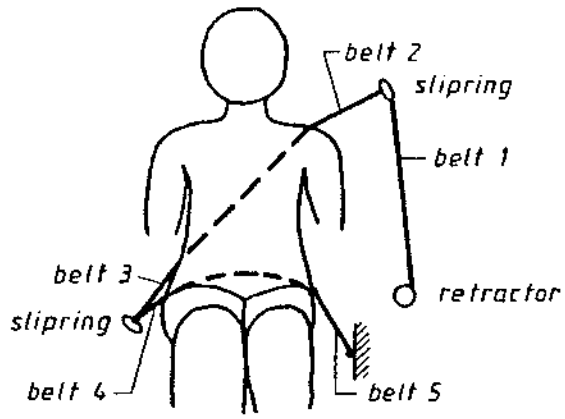

Fig. 8.17 *A 3-point belt with retractor.*

Dynamic joint models

The last type of force-interaction models to be discussed here is the category of dynamic joint models. As described earlier, in a joint two types of loads are acting, the internal forces and torques caused by the kinematic joint constraints, and the applied loads representing for instance passive type of loads due to friction or elastic resistance or active loads caused for instance by muscle activity. The applied joint loads are taken into account by the dynamic joint force models. The most simple type generates a force (or torque) as function of a single joint co-ordinate. An example is the torque as function of the rotation in a revolute joint (Fig. 8.18). In this model, elastic (including hysteresis and dynamic amplification), as well as damping forces (torques) can be prescribed, much like e.g. in a spring-damper model. Moreover in this model a friction torque can be introduced.

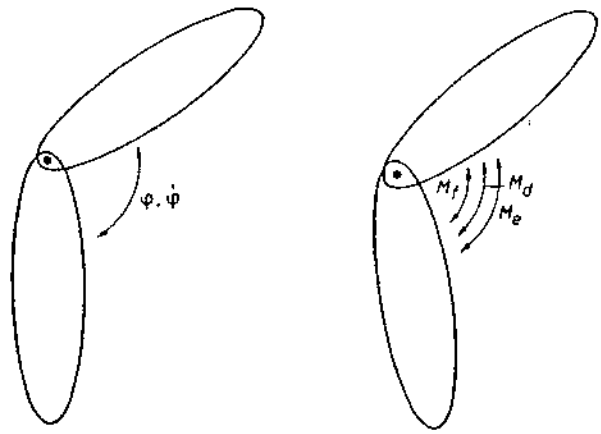

Fig. 8.18 *A revolute joint with joint torques*

A more complicated dynamic joint is the so-called "flexion-torsion restraint" model which can be applied for instance in case spherical joints are used to represent flexible rubber type structures like the neck and spine in crash dummies. In this model the relative joint position of the joint is considered to be the result of two successive rotations, i.e. a "bending" and a "torsion" motion of segment j relative to segment i. Both for the "bending" and "torsion" motion an elastic torque has to be defined where the bending torque can be defined directional dependent, this means that for instance the "bending" stiffness in forward direction can differ from the stiffness in backward or lateral "bending".

8.2.5 Integrated multi-body finite element simulations

In the MADYMO finite element module, truss, beam, shell, brick and membrane elements are implemented and material models like elastic, visco-elastic, elasto-plastic, hysteresis and Moonley-Rivlin can be applied. Also models are available for sandwich material, solid foam and for honeycomb material. A MADYMO model can be made of only multi-body systems, only finite element structures or combinations.

Fig. 8.19 illustrates the interaction between the multi-body and the finite element module. Two kind of interactions generate forces between the multi-body and the finite element model: support and contacts. A support is a finite element node rigidly connected to a body of a multi-body system (or to a belt segment of the belt model in order to model belt parts by membrane or truss elements). The necessity of these two types of interactions can be illustrated using the example of a finite element driver airbag simulation. The airbag unit is connected to the steering column which often is modelled as a multibody system. The airbag model can be attached to the multi-body steering column using supports while the interaction of the airbag with a multi-body occupant can be handled through contacts.

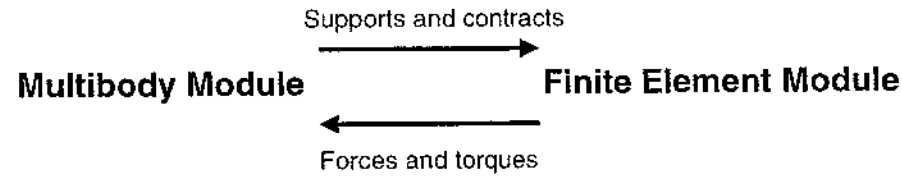

Fig. 8.19 Interaction between multi-body and finite element module

This approach allows the use of different integration methods for the equations of motion of the finite element module and the multi-body module. For an integrated MADYMO analyses the 4th order Runge-Kutta or Euler method is used for the time integration of the equations of motion of the multi-body system. The central difference method is used for the equations of motion of the finite element model. Actual body positions and velocities at each time step of the central difference method determine the support and contact forces. The forces acting on the multi-body system are accounted for in each mean time point of the 4t^{h} order Runge-Kutta and each time step of the Euler method. Due to the fine spatial discritization often required in a finite element model a much smaller time step is required in finite element model compared to a multi-body model. To improve the efficiency of the integrated analyses the finite element analysis is subcycled with respect to the multi-body analyses.

Apart from the finite element module within MADYMO using above principles also external interfaces between MADYMO and finite element programs like PAMCRASH, LSDYNA, RADIOSS and MSC DYTRAN have been developed.

8.3 Crash Dummy modelling

8.3.1 Introduction

Well-validated human body crash models presented in literature so far mainly have been developed for mechanical models of the human body, i.e. crash dummies, rather than for real human beings themselves. The rationale for this is that most model input data in case of crash dummy models can be measured relatively easy. Moreover, results of experiments with crash dummies often are available for model validation and if not, such experiments, unlike tests with biological models, readily can be carried out in many well-equipped crash laboratories. Another reason for the emphasis on modelling crash dummies so far is the need, particular from the design departments in the automotive industry, for well-validated design tools which can reduce the number of regulatory tests with crash dummies in order to shorten and optimise the development process of a new car model. In the next section (section 8.3.2) the modelling process of a (multi-body) crash dummy model will be described. In section 8.3.3 typical examples of crash dummy models will be presented.

8.3.2 Modelling methodology

The first step in the modelling process of a crash dummy is the division of the dummy in segments and the specification of the parts that belong to each segment. The segments are selected by dividing the dummy into functional components. Each part of the dummy having significant mass and a flexible connection with other parts is considered as a segment. Dummy parts which do not show any relative motion are usually considered to be part of another segment except if load information is required at the interface between the two segments. In present dummy designs usually four types of kinematic connections between segments can be distinguished: revolute (or pin joints), translational joints, universal joints and universal joints.

Furthermore often flexible structures are present in a dummy. Some are partly or completely made of rubber like the lumbar spine and neck. They are usually modelled by two universal joints located in the centres of the end planes of these structures or by a 6-degree of freedom joint. Flexible parts like the ribs in the dummies are usually represented by a number of rigid bodies, flexible bodies or by finite elements.

If the general model set-up has been specified the geometrical parameters have to be determined from technical drawings, CAD files and/or they have to be measured directly at the dummy. Information needed includes the joint locations within the individual segments, the joint axes orientations and the outside surface geometry. Three-dimensional measurements are conducted usually at a disassembled dummy. Some of the geometrical joint data have to be determined in an indirect way since the requested joint data may not be directly accessible a measuring device. Additional measurements of landmarks specifying segment local co-ordinate systems have to be conducted in order to express the data in a common body-fixed base.

The outside surfaces of the dummy segments are usually represented by means of ellipsoids or arbitrary shaped surfaces. The ellipsoids or arbitrary surfaces are used for visual presentation of the occupant kinematics as well as for the contact interactions between dummy segments and environment (e.g. the vehicle interior).

The next step is the determination of the inertial properties. The mass, location of the centre of gravity, the principal moments of inertia and the orientation of the principal axes must be determined for each dummy segment. In addition the position of segment landmarks have to be determined in order to express the inertia data in a body-fixed co-ordinate system. Experimentally the moments of inertia can be determined with a torsional vibration table [18]. The object which is fixed in a box is measured in several positions in order to get the complete inertia tensor.

The stiffness of the connections (joints) between the different segments is one of the

parameters having a major effect on the motions of the dummy segments in a crash environment. These joint resistive properties are determined using various static and dynamic test methods. In these tests the range of motion corresponding to a joint co-ordinate is determined as function of the externally applied load. If a joint has more than one degree of freedom, like in a universal joint, for each degree of freedom separate measurements are conducted, keeping the others fixed. Since the actual joint resistance often will depend on the value of multiple joint co-ordinates, large test series may be required. In practice up to now this dependency on more than one degree of freedom is neglected and joints are tested with the other degrees of freedom fixed.

The last step is the specification of the surface compliance properties. Static as well as dynamic measurements with several penetrating surfaces must be performed at different locations on the dummy segments. The surface compliance is dependent on the skin covering thickness and density as well as the compliance of the underlying structure. If the dummy part to be modelled will be represented by a finite element model, material parameters describing the involved dummy materials have to be determined. The surface compliance tests can be used for model validation purposes in this case.

On the basis of these measurements a model of the dummy can be compiled now. After formulating a model, verification simulations are carried out to insure that the model adequately represents the complete dummy. For this purpose well controlled impactor tests and sled tests with the assembled dummy at different acceleration levels are used. If results are not completely satisfying further model refinements with corresponding input measurements may be required. A well validated computer model allows the user to apply the model for predictive simulations of events outside the range of validated simulations.

8.3.3 Examples of crash dummy models

The need for well-validated databases of crash dummies has been recognised by many organisations in the past and has resulted in a number of (co-operative) research efforts to develop such databases. A detailed presentation of these efforts would be out of the scope of this Chapter. However worthwhile to mention here are the activities in the mid-eighties concerning the Hybrid III crash dummy. A series of frontal sled tests using a Hybrid III dummy at a rigid seat at 3 different severity levels was conducted in 1985 by Prasad [19]. The results were available for a SAE (Society of Automotive Engineers) subcommittee for the purpose of validation of dummy databases of the ATB and MADYMO programs. These validation efforts were presented at the 1998 SAE congress by several authors [20,21,22] which resulted in a number of recommendations for further improvement of the quality of the Hybrid III dummy database.

Figs. 8.20 illustrates some of the validated "standard" multi-body dummy databases currently available with the MADYMO program. In addition to the dummy models shown in Fig. 8.20 also models for the Hybrid II dummy, the various side impact dummies (EUROSID, BIOSID and DOT-SID) and various headforms and other impactors are available. Fig. 8.21 shows 2 different MADYMO models for the EUROSID dummy: a model with arbitrary (facet) surfaces (left) and a finite element model.

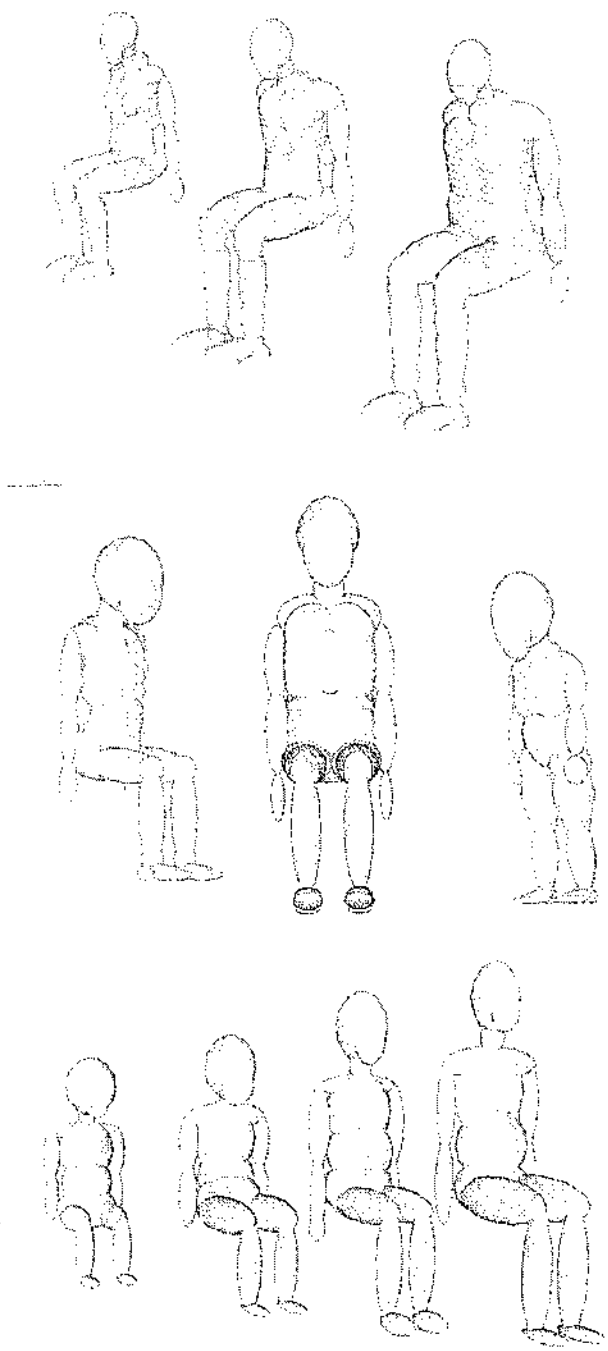

Fig. 8.20 *Examples of multi-body crash dummy models (Hybrid III dummy family(top): 5th, 50th and 95th%, USA child dummies(middle): Hybrid III 3yr, Hybrid III 6yr and Crabi 12 month and TNO child dummies(bottom): P3/4, P3, P6 and P10)*

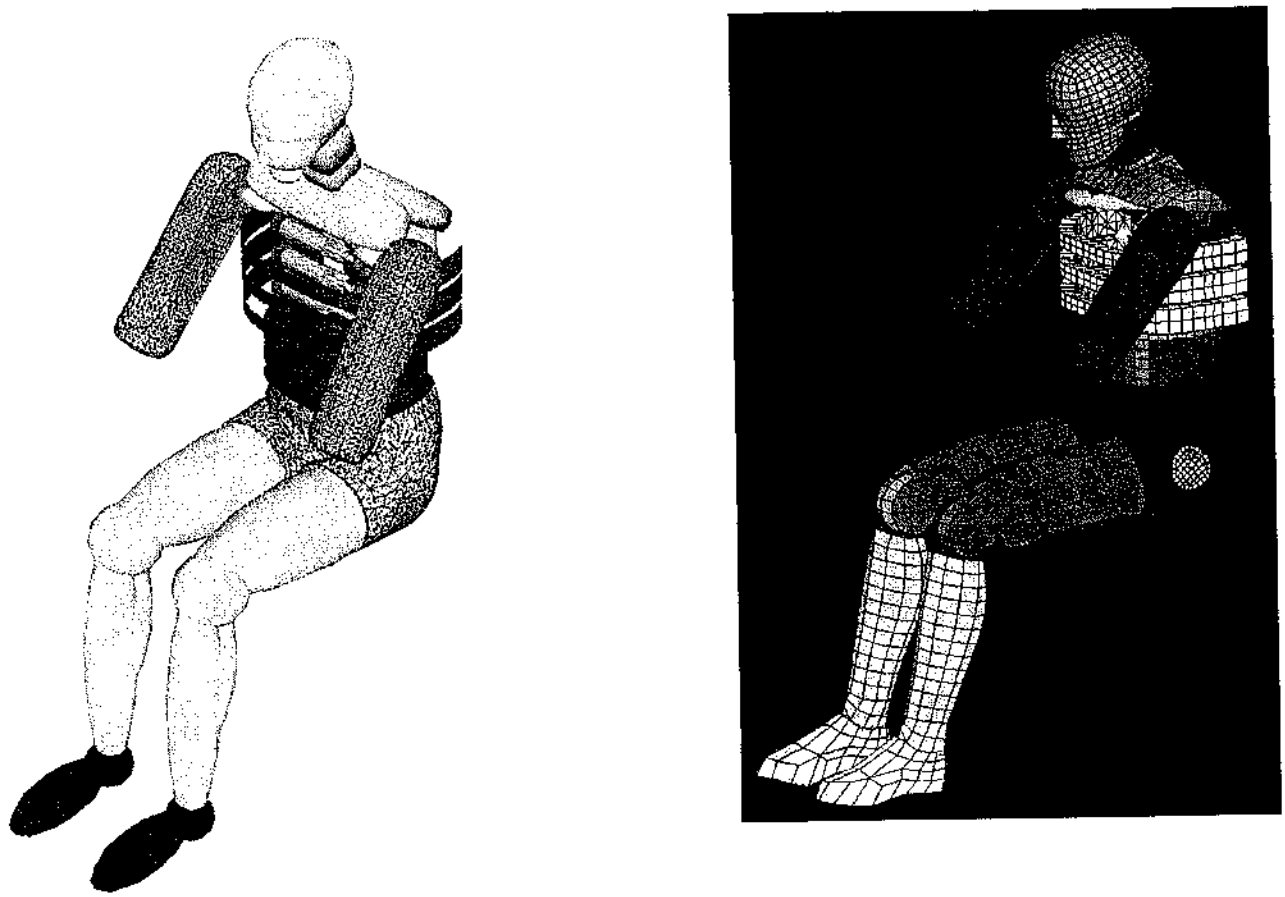

Fig. 8.21 MADYMO multi-body facet model (left) and finite element model (right) of the EUROSID dummy

8.4 Modelling the real human body

8.4.1 Introduction

A model of the real human body is much more difficult to develop than a model of a physical crash dummy. Mathematical modelling of the real human body potentially offers improved biofidelity compared to crash dummy models and allows the study of aspects like body size, body posture, muscular activity and post fracture response. Detailed human body models potentially allow analysis of injury mechanisms on a material level.

A large number of models describing specific parts of the human body have been published but only a few of these models describe the response of the entire human body in impact conditions. Models simulating the response of car occupants have been published for lateral loading by Huang [23,24] and Irwin [25], frontal loading by Ma et. al. [26] and rearward loading by Jakobsson et. al. [27] and van den Kroonenberg et. al. [28]. A model for vertical loading has been published by Prasad and King [29], pedestrian models have been published by Ishikawa et al. [30] and Yang et al. [31] and a child model in a child restraint system by Wismans et. al. [32].

In the next section 8.4.2 the aspect of anthropometry of human body models will be presented. In section 8.4.3. some examples will be shown.

8.4.2. Anthropometry

In occupant crash simulations the program GEBOD is often used to generate models representing arbitrary human body sizes. GEBOD produces geometric and inertia properties of human beings [33]. Joint resistance models for an adult male GEBOD model are described by Ma et al. [26]. GEBOD generates a model consisting of 15 segments: head, neck, upper arms, lower arms, thorax, abdomen, pelvis, upper legs, lower legs and feet. Computations for the geometrical parameters and mass distribution are based on a set of 32 body measurements. From these 32 parameters body segment sizes and joint locations are derived. Segments are described by ellipsoids except for the thorax and feet where more complex approximations (so-called elliptical solids) are used. Inertial properties are estimated by calculating the inertial properties of each segment ellipsoid or elliptical solid, assuming homogeneous body density. The 32 body parameters can be measured at a subject or can be generated by GEBOD using regression equations on the basis of body height and/or weight for both adult males and females. For children, regression equations are available on the basis of height, weight, age and combinations of these parameters. A major limitation of GEBOD is the approximation of body segments by simple geometrical volumes.

More recently the RAMSIS model [34] has been used anthropometry source for human body models [35]. RAMSIS has primarily been developed for ergonomic analyses and allows the generation of models with a wide range of anthropometry parameters. The RAMSIS model describes the human body as a set of rigid bodies connected by kinematic joints and the skin is described as a triangulated surface. RAMSIS provides a detailed geometric description of the body segments based on extensive anthropometric measurements on various civilian populations including automotive seated postures. The skin of the entire body is described as one "continuous" surface. Segment mass and centres of gravity are derived in RAMSIS using this realistic geometric description. RAMSIS provides a mathematical prediction for the increase of the average body height of the entire population during a given time period ("secular growth").

Anthropometric studies have shown that the body dimensions of each individual can be classified according to three dominant and independent features. These features are body height, the amount of body fat, and body proportion, i.e. the ratio of the length of the limbs to the length of the trunk. Using this classification scheme RAMSIS describes the entire population in a realistic way. This method takes into account the correlation between body dimensions which are disregarded in GEBOD. (For instance tall persons typically have long legs combined with a comparably short trunk.).

A translator has been developed to convert RAMSIS models into MADYMO models. The resulting model contains joint locations, joint ranges of motion, segment masses and centres of gravity and a triangulated skin connected to various body segments. Inertia properties are derived by integration over segment volume assuming a homogeneous density. The conversion can be performed for any anthropometry specified in RAMSIS and examples of such models are shown in Fig. 8.22.

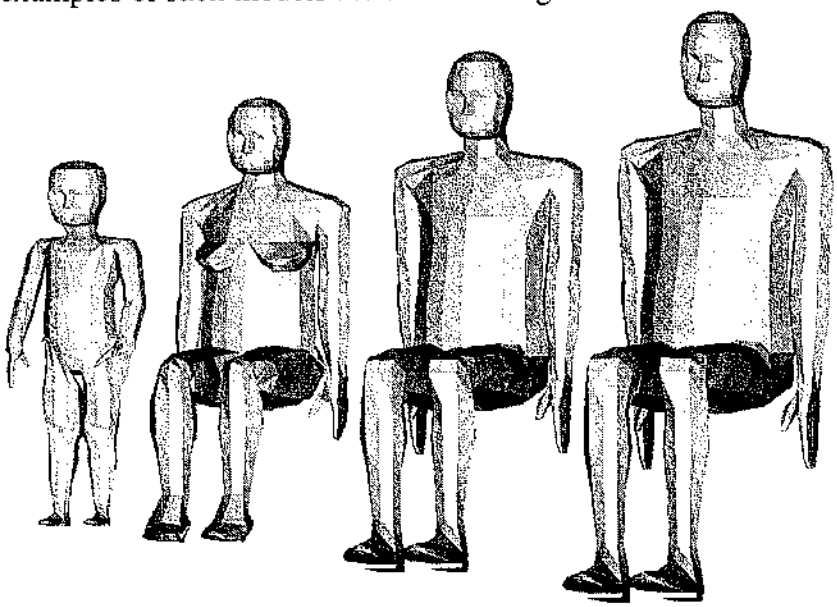

Fig. 8.22 MADYMO human models of various body sizes generated from the RAMSIS model, from left to right: 3 year old child, extremely small female, 50th percentile male, extremely large male

8.4.3 Examples of a human body model

Two examples will be shown here, the first one being a multi-body model and the second a full finite element model.

The multi-body model is the 50th percentile male model from Fig. 8.22. This model has been validated in a number of crash conditions including frontal, rearward and lateral volunteer tests and several types of cadaver tests [35]. The simulation shown in Fig. 8.23 is a 15 g frontal sled tests with human volunteers conducted by the Naval Biodynamics Laboratory in New Orleans. For the neck in this model a global 7-segment model is available with lumped properties as well as detailed neck model with separate representations for the facet joints, intervertebral discs, ligaments and (active) muscle response. Fig. 8.24 shows the response of this neck model in comparison with human volunteer response. In the model active muscle response was taken into account. The performance of this neck model appeared to be much more realistic than the neck behaviour of the current Hybrid III crash dummy [36]. Also for some of the other body parts, like for the ankle/foot and the head/brain, detailed multi-body and/or finite elements representations are available in this 50th percentile male model. Fig. 8.25 illustrates a finite element model of the brains developed at the Eindhoven Technical University.

The second example is shown in Fig. 8.26. It is a finite element model representing a 50th percentile male developed by Lizee et. al. in the RADIOSS programme package [37]. Detailed representations of the neck, shoulder, thorax and pelvis have been developed and the resulting model has been validated in more than 30 test configurations. The model has more than 10.000 elements. Head and arms and legs (not shown) were represented as rigid bodies.

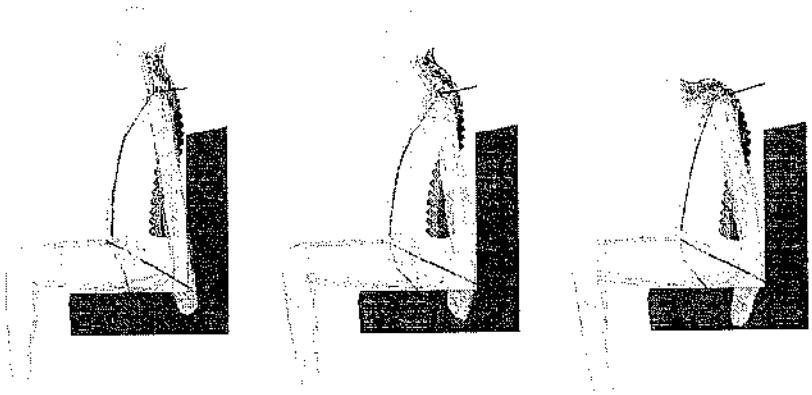

Fig. 8.23 Simulation of 50th male human body model in 15g volunteer test [35]

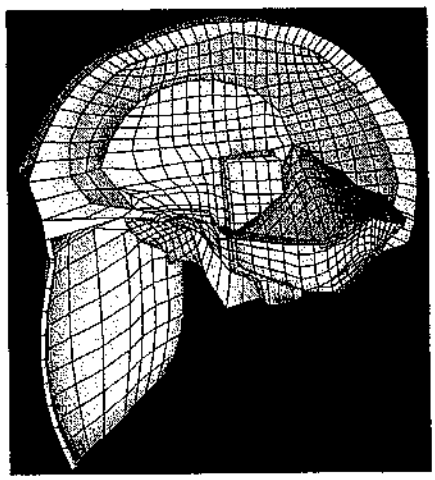

Fig. 8.24 MADYMO finite element brain model developed at the Eindhoven Technical University, The Netherlands

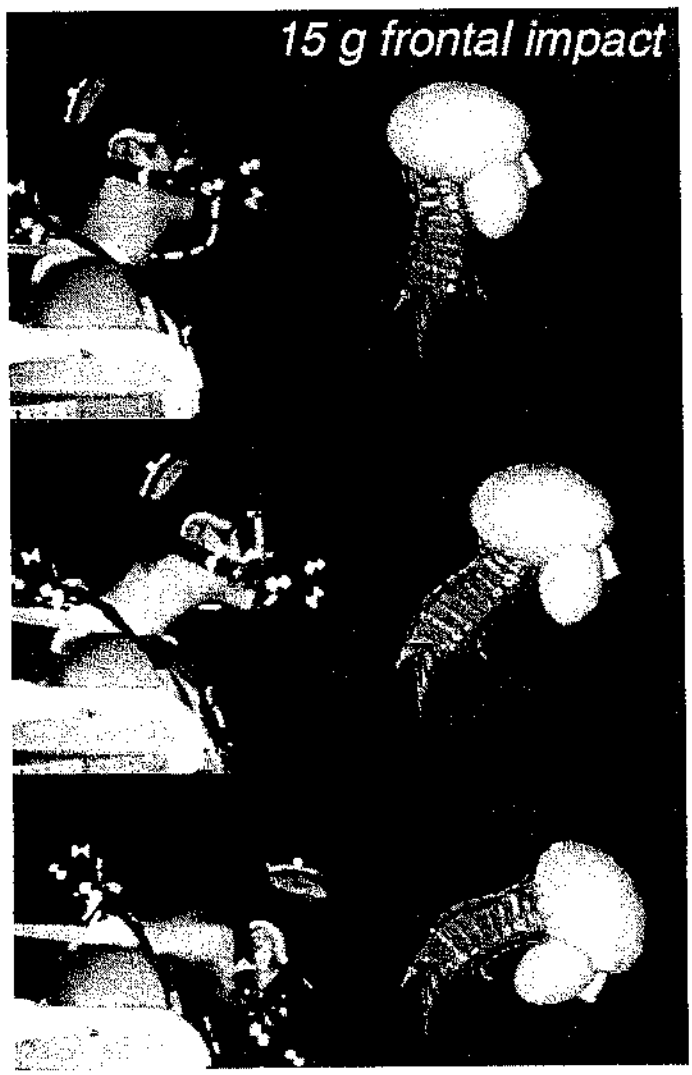

Fig. 8.24 Comparison of human neck model response and volunteer response [36]

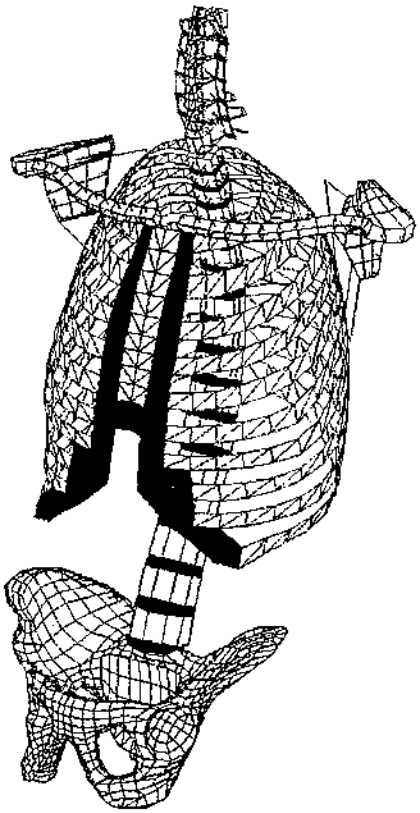

Fig. 8.26 Finite element human body model developed by Lizee et. al.[37]

8.5 Concluding remarks

The earliest numerical models of the full human body have been based on multibody techniques. More recently also finite element techniques have been used for this purpose. A mayor advantage of the multibody approach is its capability of simulating, in an efficient way, spatial motions of mechanical systems with complex kinematical connections like they are present in the human body and in parts of the vehicle structure. The advantage of the finite element method is the capability of describing (local) structural deformations and stresses in a realistic way. But the creation of a finite element model is a time consuming job and the availability of realistic material data is limited, particular in case of biological tissue response. Furthermore relatively large computer times are required to perform a finite element crash simulation, making the method less attractive for complex optimisation studies involving many design parameters.

A general advantage of computer crash simulations over crash tests with mechanical human substitutes (crash dummies) is that the safety performance of design concepts and the effect of changes in the design can be studied efficiently, sometimes even without a prototype to be build (virtual testing). An important condition for the usage of such models is that well-

validated databases of the human body are available. Continuous efforts are needed to further improve the quality of existing human body models in order to allow their usage in even a wider range of applications. Standards for validation procedures and performance criteria are needed in order to further enhance and extent the applicability of crash simulations. In the past some attempts have taken place to develop such standards. Table 8.1 shows a model Validation Index developed in the early eighties by the "Analytical Human Simulation Task Force" of the SAE Human Biomechanics and Simulation Subcommittee (HBSS) [38]. The index with levels from 0-8 was agreed upon by the Committee but a number if issues were not resolved like the number and type of tests to be conducted.

Table 8.1 Validation Index proposed by SAE sub committee [38]

Class	Characteristics
Level 0	No agreement between predicitions of model and "reference event"
Level 1	Qualitative agreement: a) Trends of predicted parameters same b) Kinematics correspond qualitatively c) Contacts between the occupant and vehicle interior are the same in general
Level 2	HIC and similar indicators predicted by simulation are within 20% of those obtained in reference event
Level 3	Peak values of important occupant responses limited to a relative error of 20% (20% on vector magnitude, 11.31 deg on vector direction)
Level 4	Same as level 3 except 5%
Level 5	Timing of peaks of important vector responses limited to 5% relative difference
Level 6	All peaks and valleys in the duration of time-dependent predictions must match the reference event within 10%
Level 7	Same as level 6 except 5%
Level 8	1% relative error, point-by-point, over the durations of the reference and predicted events

Models of the human body can be subdivided into models of crash dummies and models of the real human body. Many models of crash dummies have been developed in the eighties/nineties and extensive series of validation studies have been conducted with rather impressive results. Also in the field of real human body models in the nineties rather promising results have been achieved. An important advantage of real human body models is that they allow the study of the effect of body size, posture influence as well as muscular activity. A major step forward will have been made once mathematical models reach a stage where they offer a more realistic representation of the human body than current crash test dummies do. Some recent achievements in this field indicate that this stage has been reached closely now.

A unique advantage of a design strategy based on real human body crash models over a design strategy based on crash tests with dummies is the possibility to benefit without delay, in principle, from new scientific knowledge on injury mechanisms and injury criteria obtained through biomechanical research. In case of a crash test dummy based design strategy usually a long period elapses before new findings actually can be implemented in crash dummy hardware. For example the current most frequently used crash dummy, the Hybrid III dummy, is based to a large extent on biomechanical knowledge of more than twenty years old. New scientific findings have so far seldom resulted in improvements in the dummy design particularly since safety regulations which specify this dummy as a regulatory test device tend to freeze the specifications in the regulation for a long period.

Apart from design studies and the analysis of biomechanical tests, an increased usage of computer models also can be observed in the area of accident reconstruction and litigation. Application of computer models in this field should be handled with much care, due to the limited level of development of real human body models for different body sizes, the usually large number of unknown accident parameters and the lack of experimental data available for validation for the case under consideration. Development of a code of practice with guidelines for usage of models in this field is highly recommended.

Several areas can be identified in the field of human body crash simulations where further developments should take place. As far as crash dummies is concerned, in particular realistic models for the foam type structures (skin and damping material) are required. Area's of future developments in the field of real human body models include further improvements in the description of the non-linear dynamic behaviour of muscles (incl. neuro-muscular control), the modelling of complex human joints and the study of constitutive equations and parameters for biological materials (e.g. brain, skin).

This Chapter has concentrated in particular on the usage of multi-body technology for human body modelling. Further refinements of the models using finite element techniques constitutes an increase in model complexity, however, with the advantage that detailed stress and strain analysis can be performed. Particular for detailed studies of injury mechanisms in specific body part this is a necessary and feasible approach. Boundary conditions for such segment models may be obtained from experiments or from results obtained through more global models. The usage of finite element techniques coupled with multi-body techniques will allow the user to benefit from the capabilities of both approaches and will offer him the flexibility of merging more global multi-body models with, whenever needed, detailed representations for certain parts in his model.

REFERENCES

1. Lobdell T.E.: "Impact response of the human thorax", In: Human impact response: Measurement and simulation, pp 201-245, Plenum Press, New York, 1973.

2. McHenry, R.R., "Analysis of the dynamics of automobile passenger restraint systems", Proc. 7th Stapp Car Crash Conference, pp.207-249, 1963.

3. Final report for publication "EU compatibility project", European Commission, Brussel, (in press), 2000.

4. Shugar, T.A.: "A finite element head injury model", Final report Vol 1 Contract DOT HS 289-3-550-IA, NHTSA , Washington DC, july 1977.

5. Bruijs, W.E.M., Subcycling in Transient Finite Element Analysis. Thesis, Department of Mechanical Engineering, Eindhoven University of Technology, Eindhoven, The Netherlands. ISBN 90-9003684-9, 1990.

6. Robbins, D.H., Bowman, B.M. and Bennett, R.O., "The MVMA two-dimensional crash victim simulation", Proc. 18th Stapp Car Crash Conference, pp. 657-678, 1974.

7. Robbins, D.H., Bennett, R.O. and Bowman, B.M., "User-oriented mathematical crash victim simulator", Proc. 16th Stapp Car Crash Conference, pp. 128-148, 1972.

8.. Huston, R.L., Hessel, R. and Passerello, C., " A three-dimensional vehicle-man model of collision and high acceleration studies", Paper No. 740725, Society of Automotive Engineers Inc., (1974).

9. Fleck, J.T., Butler, F.E. and Vogel, S.L., "An improved three-dimensional computer simulation of motor vehicle crash victims". Final Technical Report No. ZQ-5180-L-1, Calspan Corp,. (4 Vols.), 1974.

10. King, A.I. and Chou, C.C., "Mathematical modelling, simulation and experimental testing of biomechanical system crash response", J. Biomechanics, 9, 301-317, 1976.

11. Wismans, J. and L. Obergefell: "Data Bases and Analytical Modelling", Chapter 8 in AGARD Advisary Report 330 Anthropomorphic Dummies for Crash and Escape system testing, AGARD/AMP/WG21, 1996.

12. MADYMO Theory Manual, Version 5.4, TNO Automotive, Delft, The Netherlands, May, 1999.

13. Prasad, P., "An overview of major occupant simulation models", Mathematical simulation of occupant and vehicle kinematics, SAE Publication P-146, SAE paper no. 840855, 1984.

14. Prasad, P., "Comparative evaluation of the MVMA2D and the MADYMO2D occupant simulation models with MADYMO-test comparisons", 10th international technical conference on Experimental Safety Vehicles, Oxford, 1985.

15. Prasad, P. and Chou, C.C., "A review of mathematical occupant simulation models, Crashworthiness and occupant protection in transportation systems", Proceedings AMD-Vol. 106, BED-Vol. 13 of the Winter Annual Meeting of ASME, Dec. 1989.

16. Wittenburg, J., "Dynamics of Systems of Rigid Bodies", B.G. Teubner, Stuttgart, 1977.

17. Prasad, P. and Padgaonkar, A.J., "Static-to-dynamic amplification factors for use in lumped mass vehicle crash models", SAE paper no. 810475, 1981.

18. Kaleps, I., J. Whitestone, "Hybrid III Geometrical and Inertial Properties"; SAE 880638, International Congress and Exposition, Detroit, 1988.

19. Prasad P.: "Comparative evaluation of the dynamic response of the Hybrid II and Hybrid III dummies", SAE paper No. 902318, Proc. of the 34th Stapp Conference, 1990.

20. Obergefell, L., Kaleps, I. And S. Steele: "Part 572 and Hybrid III dummy comparisons in sled test simulations, SAE paper No. 880639, SAE PT-44, SAE Int. Congress and Exposition, Detroit, Society of Automotive Engineers Inc.,1988.

21. J. Wismans and J.H.A. Hermans: "MADYMO 3D Simulations of Hybrid III Dummy Sled Tests". SAE paper No. 880645, SAE PT-44, SAE Int. Congress and Exposition, Detroit, Society of Automotive Engineers Inc.,1988.

22. Khatua, T., L. Chang and Pizialli: "ATB simulation of the Hybrid III dummy in sled tests", SAE paper No. 880646, SAE PT-44, SAE Int. Congress and Exposition, Detroit, Society of Automotive Engineers Inc.,1988.

23. Huang Y., A.I. King, J.M. Cavanaugh. "A MADYMO Model of Near-Side Human Occupants in Side Impacts". Journal of Biomechanical Engineering, vol. 116, may 1994, p.228-235, 1994.

24. Huang Y., A.I. King, J.M. Cavanaugh. "Finite Element Modelling of Gross Motion of Human Cadavers in Side Impact". STAPP 1994, SAE 942207, 1994.

25. Irwin A.L. (1994). Analysis and CAL3D Model of the Shoulder and Thorax Response of Seven Cadavers Subjected to Lateral Impacts. Ph.D. Thesis Wayne State University, 1994.

26. Ma D., Obergefell A., Rizer A. "Development of human articulating joint model parameters for crash dynamics simulations" STAPP Conference 1995, SAE 952726, 1995.

27. Jakobsson L., Norin H., Jernstrom C., et al. "Analysis of different head and neck responses in rear-end car collisions using a new humanlike mathematical model", IRCOBI conference 1994 proc., pp. 109-125, 1994.

28. Kroonenberg A. van den, Thunnissen J., Wismans J.: "A human model for low severity rear-impacts". IRCOBI conference, 1997.

29. Prasad P., King A.I.: "An experimentally validated dynamic model of the spine". J Appl Mech, 1974, pp. 546-550, 1974.

30. Ishakawa H., Kajzer J., Schroeder G.: "Computer simulation of impact response of the human body in car-pedestrian accidents", Proceedings of the 37th STAPP Car Crash Conference, SAE-933129, 1993.

31. Yang J.K, Lovsund P: " Development and validation of a human body mathematical model for simulation of car-pedestrian impacts", IRCOBI Conference 1997.

32. Wismans, J., Maltha, J.W., Melvin, J.W. and Stalnaker, R.L., "Child Restraint Evaluation by Experimental and Mathematical Simulation", 23rd Stapp Car Crash Conference, Paper No. 791017, San Diego, USA, 1979.

33. Baughman, L.D., "Development of an Interactive Computer Program to Produce Body Description Data". University of Dayton Research Institute, Ohio, USA, Report nr. AFAMRL-TR-83-058, NTIS doc. no. AD-A 133 720, 1983.

34. Geuß H. Entwicklung eines anthropometrischen Mebsystems für das CAD-Menschmodel Ramsis. PhD thesis, München University, 1994.

35. R. Happee, M. Hoofman, A.J. van den Kroonenberg, P. Morsink and J. Wismans: "A mathematical human body model for frontal and rearward seated automotive impact loading", in: Proceedings of the 42nd Stapp Car Crash Conference, Tempe, USA, November 2-4, 1998.

36. J. Wismans, A.J. van den Kroonenberg, M.L.C. Hoofman and M.J. van der Horst: "Neck performance of human subjects in frontal impact direction", RTO Specialist' Meeting "Models for aircrew safety assessment: uses, limitations and requirements", Dayton, USA, 26-28 October 1998.

37. E. Lizee, S. Robin, N. Bertholon, J.Y. Le Coz, B. Besnault and F. Lavaste: " Development of a 3D Finite Element Model of the Human Body", in: Proceedings of the 42nd Stapp Car Crash Conference, Tempe, USA, November 2-4, 1998.

38. P. Prasad: "Occupant simulation models: experiment and practice", Crashworthiness of Transportation Systems: structural impact and occupant protection, J.A.C. Ambrosio et. al. (eds), 209-219, Kluwer Academic Publishers, 1997.

CHAPTER 9

LOWER EXTREMITY INJURY BIOMECHANICS

9.1 Introduction

Injuries to the lower extremities frequently occur in accidents involving car occupants, pedestrians, cyclists, motorcyclists; in sports; in domestic accidents, and due to military actions (e.g. mines). This chapter deals with leg injuries resulting from road accidents where for practical reasons this chapter is limited to car and pedestrian injuries. A typical accident scenario for car occupants is shown in Fig. 1. Typical scenarios for pedestrian and cyclist impact are illustrated in Fig. 2 where it is noted that injury scenarios for cyclists are similar to those for pedestrians. Injury scenarios for motorcycles are beyond the scope of this chapter.

Although leg injuries alone are rarely life threatening, they do impose large costs on society. Leg injuries often require a long rehabilitation process and in many cases permanent disabilities result. Luchter (1995) estimated that lower extremity injuries result in 41% of all life years lost to injury (LLI) in police reported towaway motor vehicle crashes. Table 6 in Chapter 3 also indicates considerable social costs for several types of leg injury. Due to their risk of long term impairment leg injuries have lately received substantial attention.

This chapter reviews current biomechanical knowledge on leg injuries and on applicable injury reduction methods. For recent literature surveys it is referred to Crandall et al. (1996), Philippens et al. (1997) and relevant publications can also be found in Backaitis (1996).

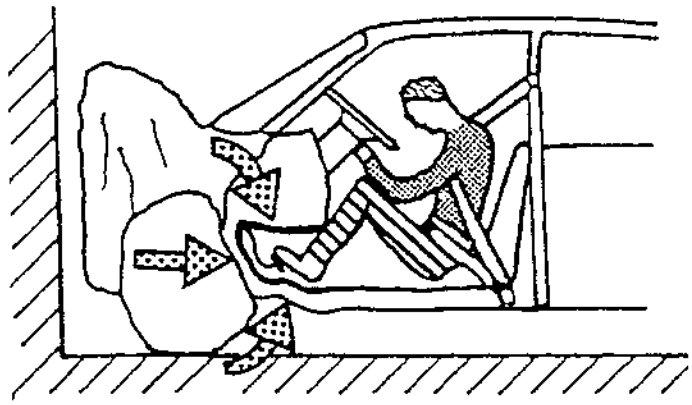

Fig. 9.1 *Typical lower extremity loading of a car occupant resulting from inertial loading and from footwell and dashboard deformation in frontal impact, from Otte (1996).*

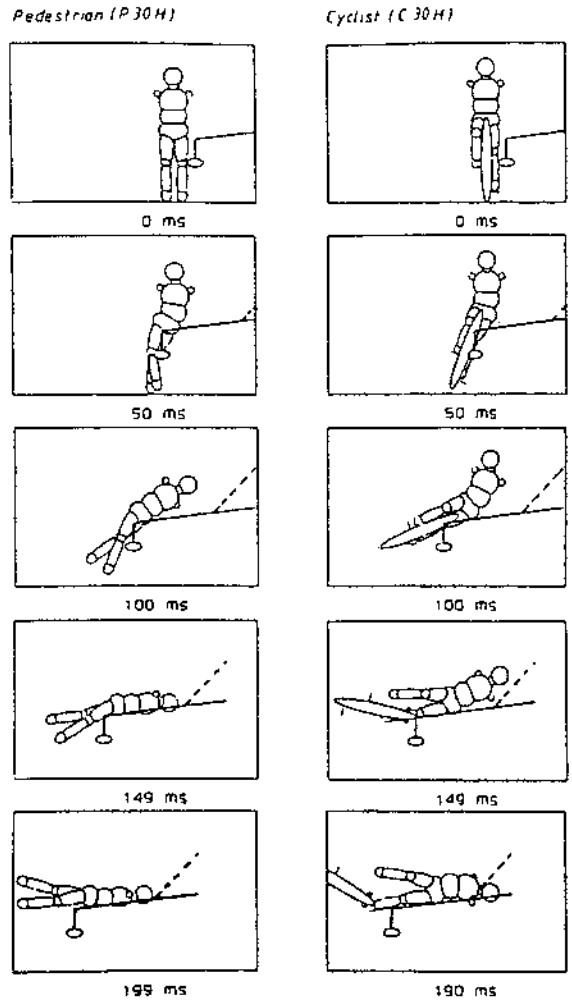

Fig.9.2 *Typical pedestrian (left) and cyclist (right) impact by a passenger car, from Janssen and Wismans (1985).*

9.2 Anatomy

The human lower extremity is composed of six morphologically distinct regions: the hip, thigh, knee, lower leg, ankle, and foot (Figs. 3-5). The hip joint connects the leg to the pelvis and can well be regarded as a ball and socket joint allowing three rotational degrees of freedom. The thigh or upper leg contains one bone; the femur. The knee joint contains three articulations: one between each condyle of the femur and the tibia, and one between the patella and the femur. The patella is a small bone anterior to the knee joint connecting tendons and ligaments (see also Figs 7 and 8). The knee contains a complicated structure of internal and external ligaments and menisces. The internal (cruciate) ligaments are always stressed and stabilise the joint. Flexion-extension is the main degree of freedom of the knee. In full stretch the knee is transversally stable and allows hardly any axial rotation due to the combined action of the ligaments. The lower leg contains the tibia (medial) and fibula (lateral) bones that are attached at marginally moveable joints both inferiorly and superiorly. The posterior muscles of the calf play a large role in determining the response of foot, leg and ankle (Crandall et al., 1996a). The bones and joints of the ankle and foot are illustrated in Fig. 3 and the 3D motions of the ankle are defined in Fig. 4. The ankle joint mainly allows dorsiflexion and plantarflexion whereas both ankle and subtalar joint contribute to inversion and eversion (Parenteau et al., 1995). A further description of the anatomy of the human lower extremity is given by Huelke (1986).

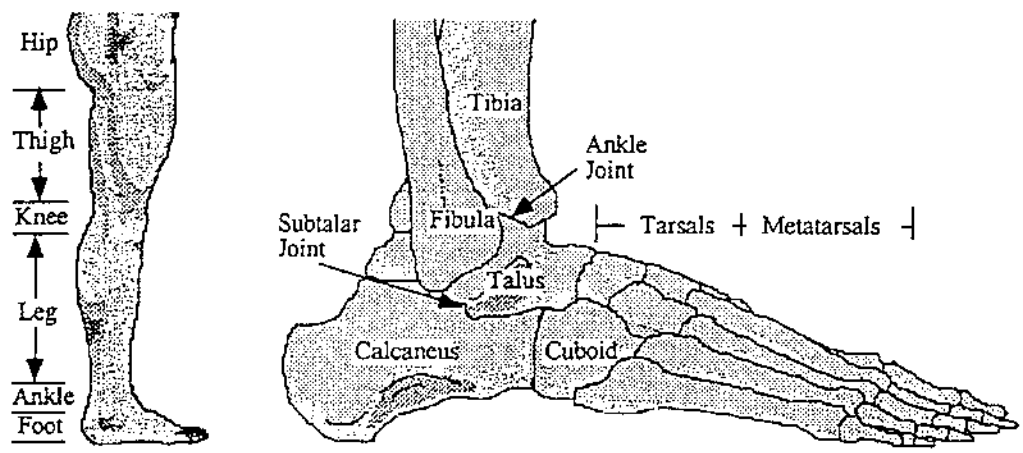

Fig. 9.3. Anatomy of the lower extremities (from Crandall et al., 1996a)

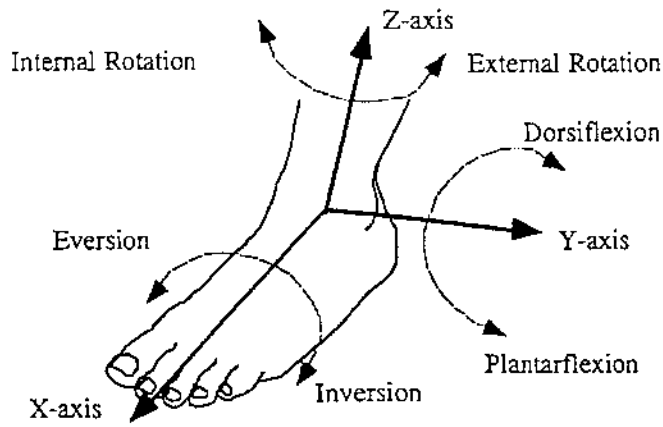

Fig. 9.4 Anatomical motions and co-ordinate axes of hindfoot joints (from Crandall et al., 1996a)

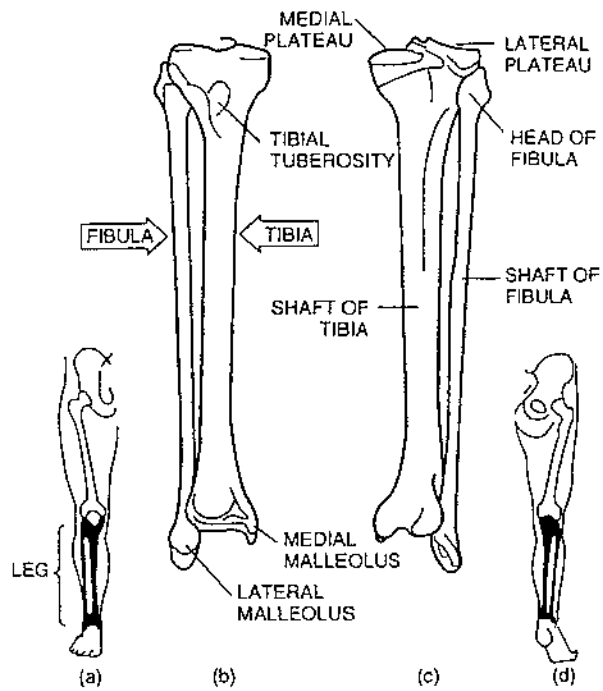

Fig. 9.5 Bones of the lower leg (Huelke, 1982)

9.3 Injuries and injury mechanisms

9.3.1 Car occupant injuries

A wide range of leg injuries has been reported for car occupants. As much as 83% of leg injuries occur to the skin and only 15% to the skeletal system in towed passenger car occupant injuries (see Table 1, left columns). A breakdown of skeletal injuries to different areas is given in the right columns of Table 1. Apparently injuries occur through the complete skeletal system of the lower extremity.

Table 9.1 *Pelvis and leg injuries in towed passenger car occupants, all injuries by type of structure (left) and skeletal injuries by location (right), from Franklin (1995) describing NASS CDS 1993-1994 data, where NASS stands for the US National Accident Sampling System and CDS stands for Crashworthiness Data System..*

Type of anatomic structure	**Incidence [%]**
Skin	83.12
Skeletal	15.08
Muscles/Nerves	1.66
Nerves	0.11
Vessels	0.00
Whole area	0.02

Skeletal injury by specific anatomic structure [%]		
Bones	Toe	2.65
	Tibia	10.02
	Talus	0.95
	Symphysis Pubis	0.89
	Sacroilum	0.75
	Pelvis	16.70
	Patella	3.35
	Toe Fx	2.19
	Foot Fx	5.09
	Femur	11.50
	Fibula	11.34
	Calcaneus	1.56
Joints	Toe joint	0.76
	Knee joint	12.59
	Hip joint	3.36
	Foot joint	1.13
	Ankle joint	14.91

Leg injuries occur much more frequently in frontal impact as compared to in side impact, where slightly more pelvis injuries result from side impact (Dischinger 1995). Leg injury is frequently found in "pole impact" (Otte, 1996) which is an impact mode typically leading to large intrusions. This counts for all impact directions but in particular for side impact. (Pole impact means impact of a vehicle with a narrow object like a tree).

It should be expected that belts and airbags by their restraining effect on the torso, limit the forces acting on the legs. As compared to belted drivers, for unbelted drivers a significantly higher risk of femur fracture was found by Dishinger (1995). In this study the incidence of leg injuries other than femur fracture was not affected significantly by belt use (see Fig. 6). However, a significantly higher incidence of *lower leg* injury for unbelted drivers and passengers was found by Partyka and Backaitis (1995).

Contradictive results have been found with respect to the relation between airbag use and leg injury. Dishinger et al. (1996) found a significantly *larger* incidence of leg injuries for drivers with airbags as compared to drivers without airbags. It was suggested that this results from a statistical correlate like a higher velocity in the airbag cases. Contrary to

these findings Siegel et al. (1995) found that the incidence of lower leg fracture was *reduced* significantly with airbag use.

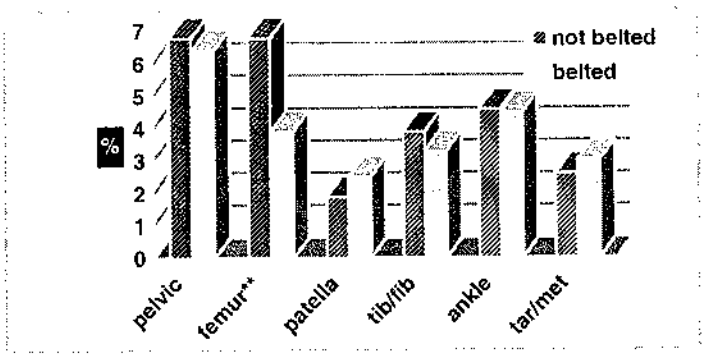

Fig. 9.6. *Lower extremity fracture probability as function of reported belt use, from Dishinger (1995), ** statistically significant $p < 0.05$.*

The driver risk of AIS2+ injuries to the legs was found to be 52% greater than the passenger risk in UK CCIS data (Thomas et al., 1995) where CCIS stands for Co-operative Crash Injury Study. This is most probably a consequence of the increased exposure to intrusion and the presence of structures such as the pedals and the steering column.
A positive correlation between intrusion and the occurrence of fracture has been reported in several studies. The suggested relation has however been criticised as these studies did not separate the injury causation effect of the intrusion from that of collision severity. Intrusion is expected to increase with increasing delta-V and it has been suggested that intrusion is merely a correlate. However, Thomas et al. (1995) separated effects of intrusion and delta-V on a statistical basis. The range of intrusion levels seen was typically between 0 and 0.5 m. Facia intrusion (dash) was found to increase the risk of knee, femur and pelvis injury. Footwell intrusion was found to increase the risk of lower leg, ankle and foot injury. Nevertheless 30% of all leg and pelvis injuries occurred in the absence of intrusion.

9.3.2 Pedestrian injuries

Accident studies show that in most pedestrian accidents, the pedestrian is impacted by the front of the vehicle. Head and leg injuries are the predominant pedestrian injuries. The age distribution for pedestrian injuries shows two peaks, one for children and one for the elderly where elderly are more frequently killed and children are more frequently injured. Elderly pedestrians were found to sustain relatively more fractures of lower limb, pelvis and upper thigh. Children reveal a high incidence of head, torso and upper thigh injuries due to their limited height. Lower extremity injuries accounted for 38% of recent pedestrian injuries in the United States (Isenberg et al., 1996).

9.3.3 Injury mechanisms for car occupants and pedestrians

Below some observations on injury mechanisms will be given per region of the lower extremity. These observations are mainly based on cadaver testing, where obvious injuries like fracture and ligament tear well can be assessed. One of the limitations of cadaver testing is that so-called "occult" injuries may remain unnoticed. A common complication associated with lower extremity trauma is acute pain followed by chronic disease. This disease abbreviated as OA (osteoarthrosis or osteoarthritis) affects the cartilage and subchondral bone of articulating joints. Changes include an early softening and fibrillation of the articular cartilage followed by a complete loss of cartilage. Haut and Atkinson (1995) showed occult microcracks after cadaver knee loading. Mechanical testing on rat cartilage indicated significant softening 12 months post-impact (Newberry and Haut, 1996).

Upper leg injury

Femur fracture in frontal impact mostly results from axial femur loads induced by knee loading. Due to the shape of the femur, axial loading induces local bending loads which may cause fracture. Femur bending fracture may sometimes result from femur entrapment below the knee bolster. Bending may also cause femur fracture in side impact, especially in conditions with large intrusions like pole impact to the side of the vehicle (Otte, 1996).
Bending of the femur is also an important injury mechanism in pedestrian impact due to contact of the upper leg with the vehicle bonnet leading edge (see Figs 2 and 12).

Knee injury

Knee injury in frontal impact mainly results from contact with the dashboard area of the vehicle. This area is often referred to as the knee bolster. The type of injury depends on the force distribution on the leg. Generally most load is applied on the patella and the condyles and is well distributed by padding (see Fig. 7). The load is limited by crushing of the structures supporting this padding.
Patellar fracture has been observed in cadaver tests with rigid impactors, but not for impactors with sufficient padding (Haut and Atkinson, 1995; Hayashi et al., 1996). Thus it is stated that patellar fracture can be prevented by the application of padding on the knee bolster. A reduced risk of *split condylar fracture* by padding was also reported by Hayashi et al. (1996) (see Fig. 7).
When a load is applied below the knee, shear loading of the knee results (Fig 8 middle). This may well result in ligament injury, in particular of the posterior cruciate ligament (see Fig. 9).
Ligament tear is also an important source of injury in pedestrian impact. However, the injury mechanism is quite different as pedestrians are mostly loaded laterally. Lateral knee

bending easily induces ligament tear. Lateral shear can also result in ligament damage and is also considered to be an important injury mechanism in pedestrians.

Lower leg injury

Fractures of the tibia in frontal impact are mostly the result of axial forces transmitted through the foot to the tibia (Yoganandan et al., 1996). It has been hypothesised that foot/ankle injuries were produced by the entrapment of the knee in the lower dash and by upward motion of the toepan (States, 1986; Crandall et al., 1996b).

In pedestrian impact, soft tissues are generally injured at the contact areas and violent impact can result in local tibia fracture.

Foot and ankle injury

Axial forces transmitted through the foot to the tibia may also cause injury to the bones and joints of foot and ankle. Additional causes of trauma are forced rotations of the foot. Forced dorsiflexion caused malleolar fractures, torn ligaments and malleolar avulsion fractures in a cadaver study (Begeman and Prasad, 1990). Contrary to this study and to other studies, Lestina et al. (1992) found that eversion/inversion cause more injuries than dorsiflexion. Injuries are also reported in metatarsus, calcaneum and toes (Otte, 1996).

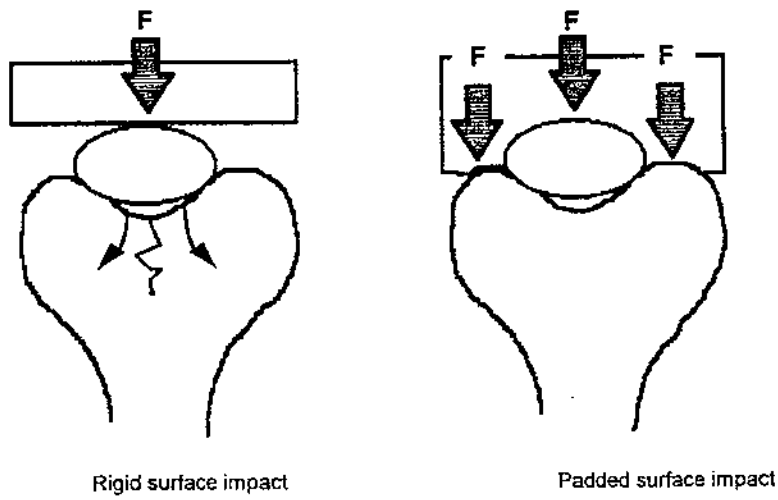

Fig. 9.7 The effect of padding in frontal knee loading; split condylar fracture (left) and load sharing between patella and condyles (right) from Hayashi et al. (1996).

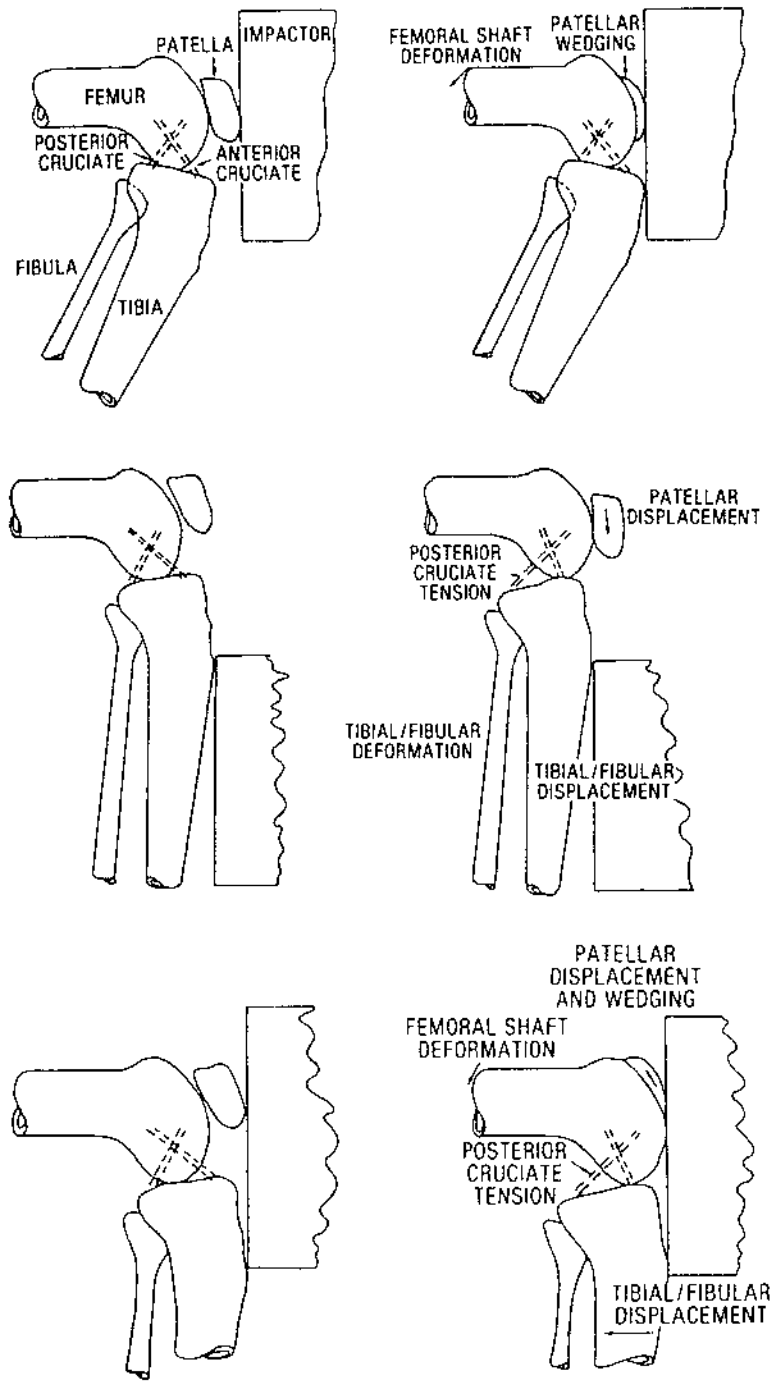

Fig. 9.8 Frontal loading of knee and lower leg, from Viano et al. (1978).

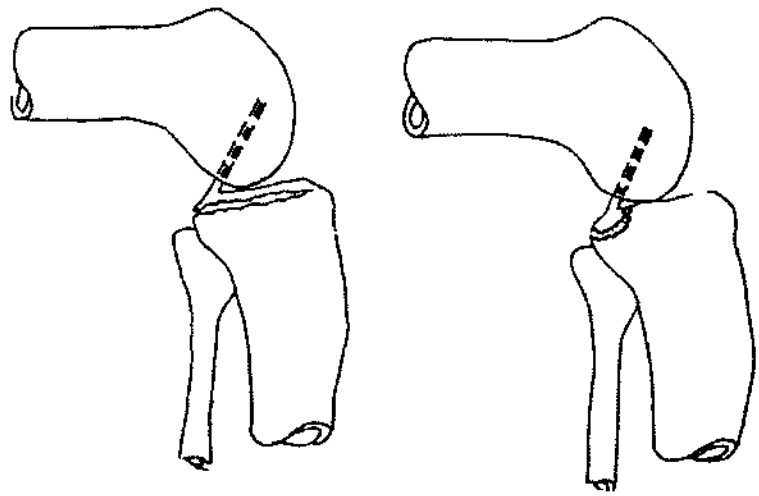

Fig. 9.9 Avulsion fracture (left) of the posterior cruciate ligament PCL and plateau fracture through extension of the PCL (right), from Viano et al. (1978)

9.4 Biomechanical response

The current knowledge on the biomechanical impact response of the leg mainly comes from cadaver testing on complete subjects or body segments. Only rarely volunteer tests have been performed.

In order to quantify the biomechanical response of the bones of the lower extremity, several quasi-static and some dynamic tests have been performed. Such tests aimed at a description of stiffness and of fracture phenomena. Some stiffness values have been reviewed by Tarriere et al. (1995). Fracture load thresholds will be treated in the next paragraph.
Studies of the knee focused on rearward shear displacement. Furthermore a contact response requirement for frontal impact to a flexed knee was defined. This requirement describes compression of soft tissues and patella and axial compression of the femur. For pedestrian impact evaluation requirements were formulated for lateral knee bending and lateral knee shear (EEVC, 1994).

Studies on the foot-ankle complex focused on impact to the sole of the foot, and on forced dorsiflexion and inversion/eversion. Force-deflection characteristics based on static and dynamic loading of volunteer and cadaver feet can be found in Crandall et al. (1996a). An example of an experimental set-up for ankle dorsiflexion is shown in Fig 10. Results for quasi-static forced dorsiflexion are shown in Fig. 11 including volunteers, cadavers and several dummy ankle designs. The effect of knee flexion in volunteers is explained by the role of gastrocnemius which is a bi-articular muscle spanning both ankle and knee joint. When the knee is bent, slack is introduced in the gastrocnemius and the resistance to ankle dorsiflexion is reduced. Apparently the dorsiflexion resistance of the dummy ankles is much

lower than indicated by the volunteer experiments up to about 45 degrees flexion. In dynamic forced dorsiflexion an increased resistance was found both for cadavers and for dummy ankles. However, just like in the static experiments, the resistance of the different dummy ankles tested is too low for small bending angles.

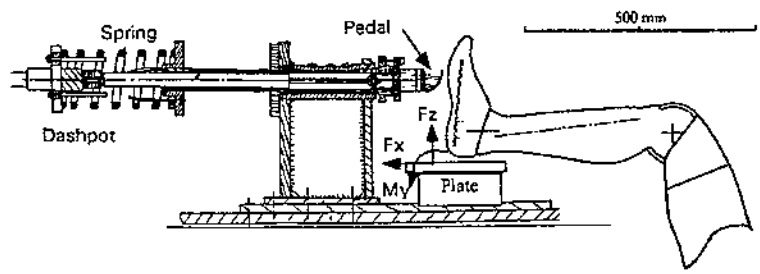

Fig. 9.10 Apparatus used to determine dynamic ankle dorsiflexion properties (Parenteau et al. 1995)

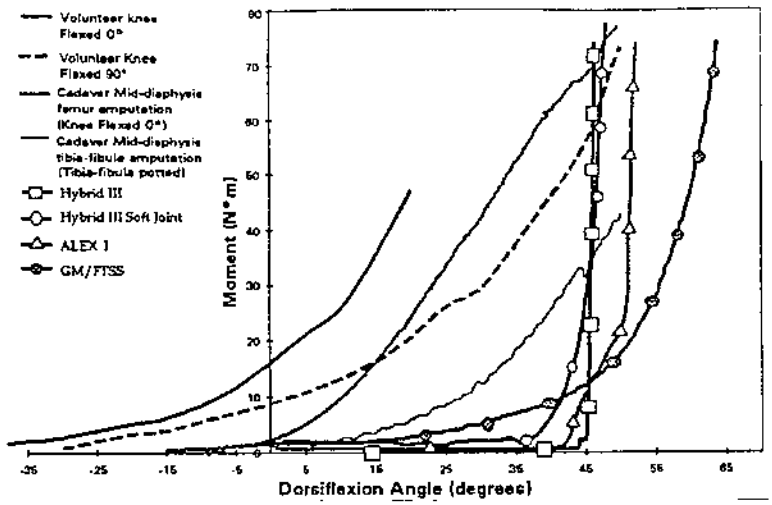

Fig. 9.11 Quasi-static ankle dorsiflexion resistance, from Crandall et al. (1996a)

9.5 Injury tolerance and criteria

Injury reduction strategies for car occupants are mainly based on optimisation of restraint systems like belts and airbags and on limitation of intrusion.

For *frontal* impact, effective restraints of the lower torso are needed to limit leg loading. This is mainly achieved by an effective lap belt. A well designed knee bolster may also contribute as a restraint system. This can be achieved by a padded surface supported by a structure which deforms at a non-injurious load. Frontal loading below the knee joint should be limited to avoid knee shear loading. Finally, intrusion should be limited in the knee-bolster area and in the footwell area.

For *side* impact, intrusion in the leg area should be limited and door padding can be applied.
Injury reduction strategies for *pedestrians* have been proposed by minimisation of the aggressiveness of vehicle fronts. In particular by a strong reduction of the contact stiffness in the applicable areas, but also by modification of the vehicle shape.

9.5.1 Available dummies/subsystems and injury criteria

Proposed injury criteria for the leg are summarised in Table 2 together with available mechanical test devices (crash dummies or dummy subsystems).
Dummies for frontal and side impact are described in Chapter 8. The use of Hybrid III for estimating femur axial loads is generally accepted and a reasonable correlation with cadaver tests has been found (Daniel, 1995). As described above the Hybrid III foot and ankle are considered not biofidelic (see Fig. 11). Therefore the Hybrid III is considered not suitable for the assessment of many foot-ankle injury risks (Tarriere and Viano, 1995). A slightly improved foot and ankle design is now available for the Hybrid III. This so called "soft stop foot" has a more biofidelic ankle rotation centre, and the heel has a biofidelic compression behaviour. However, the ankle rotation stiffness is still not biofidelic (see Fig. 11) and mechanical failure has been observed (Crandall et al., 1996a). More advanced designs like the GM/FTSS foot and the ALEX lower leg have been reviewed by Crandall et al. (1996a). Recently the Thor-Lx leg has been presented, retrofitting Hybrid III and THOR, matching biofidelity requirements for axial loading at the heel and for ankle bending (Shams et al., 1999).
Application of leg injury criteria for side impact has hardly been considered. However femur loads can be recorded in the Eurosid-1 dummy. Such loads are particularly relevant for tests leading to large door intrusions like lateral pole tests.
Pedestrian injuries have been evaluated using complete dummies like the standing versions of the Hybrid II and III or with special modified versions of these dummies (Wismans and Janssen, 1994). A special pedestrian dummy has been developed for Honda (Huang et al., 1999), but this dummy is not commercially available.
Evaluation of pedestrian safety with complete dummies has several drawbacks. Such tests are very sensitivity towards the initial position, in particular of the limbs. This sensitivity leads to limited reproducibility, and furthermore many different initial postures could be relevant. Another drawback is that it has proven to be difficult to develop a durable pedestrian dummy. For these reasons, the EEVC (1994) has proposed a test method using 4 subsystems (Fig. 12) representing human body parts. A complete legform with a deformable knee joint is used to test the bumper area. An "upper legform" is used to test the bonnet leading edge and headforms for adult and child are used to test the bonnet top (Janssen, 1996).

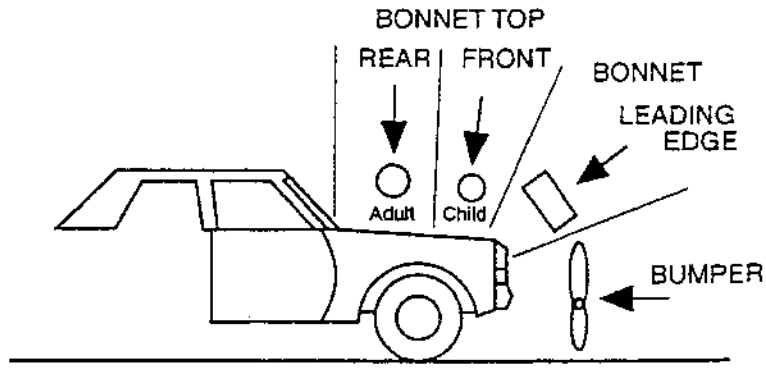

Fig. 9.12 Proposed pedestrian protection vehicle sub-system tests, from Wismans and Janssen (1994).

Table 9.2 Proposed leg injury criteria

Measurement	Threshold	test device	Source and comments
Car occupants in frontal impact			
femur axial force	10 kN	Hybrid III & Thor-Lx leg	• static and dynamic cadaver tests, see Haut and Atkinson (1995) • supported by Hayashi et al. (1996) for padded dynamic cadaver knee loading • accepted injury criterion since 1976
femur bending torque	366 Nm		
knee slider displacement	15 mm	Hybrid III & Thor-Lx leg	Cadaver tests (Viano et al, 1978)
knee shear force (clevis load)	5 kN		
tibia axial force Fz	see Fig. 13		• age dependent risk function based on cadavers (Yoganandan, 1996) • see also Tarriere and Viano (1995) • see also Klopp et al (1995) who indicate a poor prediction and suggest including power, and suggest that force should be recorded at sole instead of tibia • see also Schueler et al. (1995) who found better correlation for force and acceleration at the sole.
tibia shear force Fx	?		see also Tarriere and Viano (1995)
tibia resultant torque Mr (x,y)	244 Nm		see also Tarriere and Viano (1995)
Tibia Index TI = Mr/225 [Nm] + Fz/35.9	1		• Combined criterion: axial force+bending • TI did not correlate with injury in static and dynamic cadaver tests (Tarriere and Viano, 1995) • Currently used for design
ankle dorsiflexion	45 deg		Begeman and Prasad (1990)
ankle inversion/eversion	60 deg		Begeman et al. (1993)
Pedestrians			
knee lateral bending angle	15 deg	EEVC complete legform	EEVC (1998)
knee lateral shear displacement	6 mm		
tibia acceleration	150 G		
femur bending torque	300 Nm	EEVC upper legform	
femur load force	5 KN		

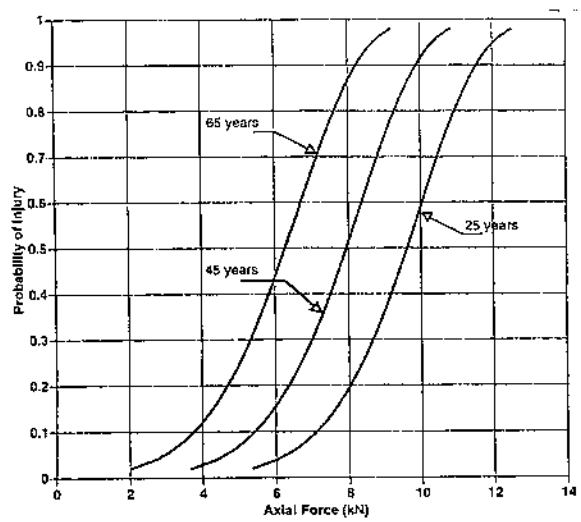

Fig. 9.13 . Probability distribution for foot-ankle injury as a function of the dynamical axial tibia force for three discrete ages, from Yoganandan (1996).

9.6 Discussion

Injury statistics have shown that lower extremity injury for car occupants and for pedestrians impose large costs on society. Currently, in vehicle design the only established leg injury criterion is the axial femur load in frontal impact. The tibia index is used to predict tibia fractured but this criterion has been found not to correlate with injury in static and dynamic cadaver tests (Tarriere et al., 1995). Injuries to the knee joint, tibia and foot require further attention. Injury criteria should be established and a more biofidelic dummy legs should be applied.

Side impact is also a cause of leg injury, but no established injury criteria are available for this type of loading.

Leg injury reduction for pedestrians can be achieved by reduction of the agressiveness of vehicle fronts. Test methods and injury criteria have been developed (EEVC, 1994). In spite of substantial efforts spent on review and discussion (EEVC, 1998) the methods were still not accepted in January 2000.

References

1. Backaitis S.H. (1996). Biomechanics of impact injury and injury tolerances of the extremities. SAE PT-56, ISBN 1-56091-749-0.
2. Begeman P.C., Prasad P. (1990). Human ankle impact response in dorsiflexion. STAPP 1990, SAE 902308.
3. Begeman P.C., Balakrishnan P., Levine R., King A., (1993). Dynamic Human ankle response to inversion eversion. STAPP 1993. SAE 933115.
4. Crandall J.R., Portier L., Petit P., Hall G.W., Bass C.R., Klopp G.S., Hurwitz S., Pilkey W.D., Trosseille X., Tarriere C., Lassau J.P., (1996a). Biomechanical response and physical properties of the leg, foot and ankle. STAPP 1996, SAE 962424.
5. Crandall J.R., Bass C.R., Klopp G.S., Pilkey W.D. (1996b). Sled tests with toepan intrusion using post-mortem human surrogates and the Hybrid III dummy. IRCOBI 1996.
6. Cesari D., Bonnoit J., Cavallero C., Lhen J. (1995). Pedestrian knee injuries: Mechanisms, Tolerance and methods of projection. PLEI 1995.
7. Daniel R.P. (1995). The use of the Hybrid III legs in developing Ford's knee bolster parameters. PLEI 1995.
8. Dischinger P. C. (1995). The epidemiology of pelvic and lower extremity fractures among hospitalized drivers. PLEI 1995.
9. Dischinger P. C., Ho S.M, Kerns T.J., Kerns J., Brennan P. (1996). Patterns of injury in frontal collisions with and without airbags. IRCOBI 1996.
10. EC (1996). Draft Directive III/5021/96 EN "European Parliament and Council Directive relating to the protection of pedestrians and other road users in the event of a collision with a motor vehicle", Brussels, DG3, February 1996.
11. EEVC (1994). EEVC Working Group 10 Report. Proposals for methods to evaluate pedestrian protection for passenger cars. November 1994.
12. EEVC (1998). EEVC Working Group 17 Report. Improved test methods to evaluate pedestrian protection afforded by passenger cars, December 1998.
13. Franklin L.N. (1995). Pelvic and lower extremity injury related data in the National Accident Sampling System Crashworthiness data system. PLEI 1995.
14. Happee, et al. (1999). Passenger car pedestrian friendliness. Evaluation of proposed EEVC subsystem test procedures by mathematical simulation. Study performed by TNO for VDA, TNO Report 98.OR.BV.033.1/RHA, final version February 10, 1999.
15. Haut R.C., Atkinson P.J. (1995). Insult to the human patellofemoral joint: Effects of age on fracture tolerance and occult injury. STAPP 1995, SAE 952729.
16. Hayashi S., Choi H.Y., Levine S., Yang K.H., King A. (1996). Experimental an analytical study of knee fracture mechanisms in a frontal knee impact. STAPP 1996, SAE 962423.
17. Huang T.J., McDonald J., Artis M., Rangarajan N., Shams T., White R.P. Jr, Beach D, Campbel R. Jr, Akiyama A., Yoshida S., Ishikawa H., Konosu A., (1999). Development of a biofidelic dummyfor car-pedestrian accident studies. IRCOBI Conference 1999.
18. Huelke D. (1986). Anatomy of the lower extremity - An overview. STAPP, 1986, SAE 861921.
19. Isenberg R.A., Walz M., Chidester C., Kaufman R. (1996). Pedestrian crash data study - An interim evaluation. ESV 1996, 96-S9-O-06.
20. Janssen E.G., Wismans J.S.H.M. (1985), Experimental and mathematical simulation of pedestrian-vehicle and cyclist-vehicle accidents. ESV conference 1985.
21. Janssen E.G. (1996). EEVC test methods to evaluate pedestrian protection afforded by passenger cars. ESV-1996, 96-S7-W-17.
22. Klopp G.S., Crandall J.R., Hurwitz S.R., Pilkey W.D., Morgan R,M., Eppinger R.H., Kuppa S.M. (1995). Risk of injury to the human ankle for longitudinal impacts to the foot. PLEI 1995.
23. Lestina D.C., Kuhlmann T.P., Keats T.E., Alley R.M. (1992). Mechanisms of fracture in ankle and foot injuries to drivers in motor vehicle crashes. STAPP-1992.
24. Luchter S. (1995). Long term consequences of lower extremity injuries. PLEI 1995.

25. Newberry W.N., Haut R. (1996). The effects of substructure impact loading on the patellofemoral joint in a rabbit model. STAPP-1996, SAE 962422.
26. Otte D. (1996). Biomechanics of lower limb injuries of belted car drivers and the influence of intrusion and accident severity. STAPP 1996, SAE 962425.
27. Philippens M., Twisk. D, Thunnissen J. (1997). Literature review on lower leg-footwell intrusion, low severity facial injuries and side impact children; An Inmagic database. TNO report 97.OR.BV.008.1/MP.
28. Parenteau C.S., Viano D.C, Lovsund P. (1995). Foot-ankle injury, Epimiological and biomechanical studies. PLEI 1995.
29. Partyka S.C. and Backaitis S.H. (1995). Comparison of driver/passenger and left/right lower leg injuries in NASS frontal crashes. PLEI 1995.
30. Ramet M., Bouquet R., Bermond F., Caire Y. (1995). Shearing and bending human knee joint tests in quasistatic lateral load. IRCOBI 1995.
31. Schueler F., Mattern R., Zeidler F., Scheunert D. (1995). Injuries of the lower legs-foot, ankle joint, tibia; Mechanisms, Tolerance limits, Injury criteria. Evaluation of a recent biomechanic experiment series. IRCOBI 1995.
32. Shams T., Beach D., White R.P., Rangarajan, Haffner M., Eppinger R., Pritz H, Kuppa S., Beebe M. (1999). Development and design of Thor-Lx: The Thor lower extremity. STAPP 1999 Conference, paper 99SC09.
33. Siegel et al. (1995). Patterns of associated injuries in lower extremity and pelvic MVC injury: The effect of safety restraints. ???
34. States J.D. (1986). Adult occupant injuries of the lower limb. In: Symposium on biomechanics and medical aspects of lower limb injuries. 1986. San Diego, CA. Society of Automotive Engineers Inc./STAPP 1986.
35. Viano et al. (1978). Bolster impacts to the knee and tibia of human cadavers and an anthropomorphic dummy. STAPP 1978, SAE 780896.
36. Tarriere C., Viano D. (1995). Biomechanical synthesis of new data on human lower leg responses and tolerances in parallel with dummy design and injury criteria. PLEI 1995.
37. Thomas P., Bradford M., Charles J., Fay P. (1995). Lower extremity injuries and their causation in frontal car crashes: Real world accident data collection. PLEI 1995.
38. Wismans J.S.H.M., Janssen E.G. (1994). Improved safety of pedestrians and cyclists. FISITA conference 1994, paper 945169.
39. Yoganandan N., Pintar F.A., Boynton M., Begeman P., Prasad P., Kuppa S.M., Morgan R., Eppinger R.H. (1996). Dynamic axial tolerance of the human foot-ankle complex. STAPP 1996, SAE 962426.

APPENDIX A

ANATOMY AND INJURY TERMINOLOGY

In this Appendix some frequently used anatomy and injury terminology as used in the field of injury biomechanics and traffic safety is summarized. Most of these terms are based on definitions given in Refs. [5,16] of Chapter 3. A division in three different categories is made: Anatomical structures, anatomical directions and motions and injury terminology.

Name	Description
Anatomical structures	
Articular	Pertaining to a joint
Cancellous Bone	The spongy or lattice-like structure of a bone occurring towards its inner core.
Cartilage	Fibrous connective tissue.
Cervical	Pertaining to the neck.
Compact Bone	The dense structure of the bone which constitutes its outer portion.
Condyle	A rounded projection on a bone usually associated with a joint.
Femur	Thigh bone.
Fibula	The outer and smaller of the two bones of the lower leg.
Frontal bone	The bone constituting the forehead and upper forward portion of the skull.
Intervertebral Disc	Circular pads of fibrous cartilage situated between adjacent vertebrae in the backbone.
Larynx	The muscle/cartilage structure at the front of the neck.
Ligament	A band of tissue that connects bone or supports viscera.
Mandible	The bone of the lower jaw.
Maxilla	The bone which forms the central portion of the upper jaw.
Occipital Condyles	Rounded prominences on each side of the base of the skull with articulate with the uppermost vertebra of the neck.
Occiput	The bone forming the rear and lower rear portion of the skull.
Patella	Knee cap.
Process	A prominence or projection on a bone.
Spinous Process	A projection of the rear on a vertebra.
Sternum	Breastbone.

Subclavian Arteries	Two of the four major blood vessels arising from the top of the heart; the subclavian arteries pass under the clavicles and supply blood to the upper body.
Suture	A joint in which the opposed bone surfaces are closely united.
Symphysis	A line of union; a type of joint in which the opposing bones are firmly united by cartilage.
Temporal Bones	Two bones which make up the lower sides of the skull.
Temporo-Parietal	Side of the skull.
Tendon	A fibrous cord by which a muscle is attached to a bone.
Thyroid Cartilage	A wishbone shaped stiff tissue located in the upper portion of the neck.
Tibia	The larger of the two long bones of the lower leg.
Trachea	The windpipe.
Vertebra	One of the thirty-three bones of the spinal column.

Anatomical directions and locations

Abduction	Moving away from a centerline (See Fig. A.2 for arm abduction).
Adduction	Opposite to abduction.
Anterior	Front.
Anterior-Posterior (a-p)	Front to back (- x direction in Fig. 3.7 of Chapter 3).
Distal	Remote; further away from the point of reference (usually the point of attachment of the limb to the torso).
Dorsal	Towards the back (posterior).
Extension	Rearward bending when applied to the neck (see Fig. A.1 for knee joint).
External rotation	Opposite to internal rotation (see Fig. A3 for ankle).
Flexion	Bending; forward bending when applied to the neck (see Fig. A.1 for knee joint).
Hyperextension	Extreme or excessive extension of a limb or a badge part; backward overbending when applied to the neck.
Hyperflexion	Extreme or excessive flexion of a limb or part; forward overbending when applied to the neck.
Inferior	Below.
Inferior-Superior(i-s)	Below to above or lower to upper + z direction in Fig. 3.7 of Chapter 3.
Internal rotation	Inward rotation (twist) around the longitudinal axes of a body segment (see Fig. A3 for Ankle).
Lateral	Away from the mid-sagittal plane; a lateral direction is a + or - y-direction (see Fig. 3.7 of Chapter 3).
Medial	Toward the mid-sagittal plane.

Posterior	Rear.
Proximal	Opposite to distal, e.g.: the knee is proximal to the ankle.
Sagittal	A plane or Section dividing the body into right and left portions. The mid-sagittal plane contains the centre of the body.
Superior	Above.
Ventral	Toward the front (anterior).

Injury terms

Abrasion	Scrape (Dutch: schaafwond).
Avulsion	Tearing away of a part.
Bruise	Surface injury without outside damage but causing discoloration (Dutch: kneuzing).
Comminuted	Broken into small pieces.
Contusion	Bruising from a direct impact.
Haemorrhage	Bleeding.
Haemothorax	A collection of blood in the sac surrounding the lungs.
Laceration	A wound made by cutting or tearing.
Lesion	Any bodily disfunction or damage.
Paralysis	Loss of motion.
Paresis	Decreased motion
Pneumothorax	An accumulation of air or gas in the sac surrounding the lungs.
Sprain	(Dutch: verstuiking, verrekking).
Subdural Haematoma	Bleeding between the two layers surrounding the brain.

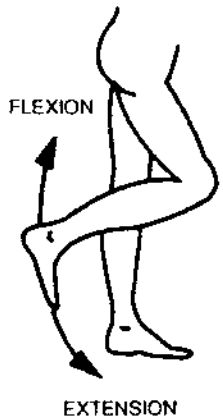

Fig. A1 *Flexion-extension of the knee joint.*

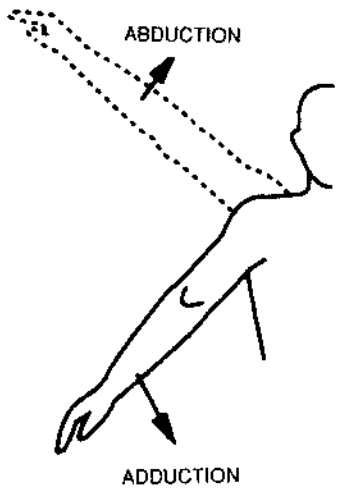

Fig. A2 *Abduction-adduction of the shoulder.*

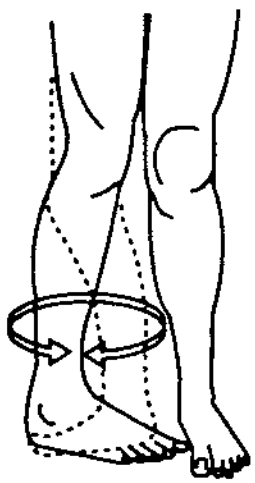

Fig. A3 *Internal-external rotation of the ankle.*
——— : Internal, -----: External

APPENDIX B

COUPLED FINITE ELEMENT/MULTIBODY SIMULATIONS

The behaviour of the human body under crash loads is can be studied by multibody codes (see Chapter 8). For these simulations usually the deceleration history of the vehicle and the deformations of the structure surrounding the crash victim must be known. Such data can be are taken from experimental or simulation results. But it is not possible to take the interaction between the occupant and deformable vehicle structures or restraint systems into account unless the a finite element and a multibody program are coupled. This is especially of interest when highly deformable structures, like airbags, are included. In MADYMO for this purpose beside the multibody module also a finite element module is available. A description of the interaction between the MADYMO multibody and finite element module is provided in [7]*. Moreover an interface has been developed between the MADYMO multibody module and the finite element codes PAMCRASH, MSC/DYTRAN and DYNA 3D. In this Annex a brief description of this interface is presented.

For the interaction between rigid bodies and finite element structures, two types can be considered. The first one is contact between finite element nodes and the bodies. The second one is the fixing of a node to a body. The necessity of these two types of interaction can be illustrated using the example of an occupant simulation which includes an airbag. The airbag is modelled using the finite element method, and the occupant with multibody techniques. The necessity of the first type of interaction, i.e. contact, is clear. During the crash, the occupant will contact the airbag. The necessity of the second type of interaction is due to the fact that during a frontal crash the steering column, which can be represented as a rigid body system, moves with respect to the vehicle. Since the airbag inflator is connected to the steering wheel, the part of the airbag connected to the inflator must move with the rigid body system representing the steering column.

Contact with Nodes

The outer surface of the bodies in MADYMO is described by ellipsoids and planes. Here only contact with ellipsoids is discussed, but contact with planes can be treated in a similar way. Suppose that the position of the nodes and the bodies are known up to $(n-1)\Delta t$. Then first the positions of the MADYMO bodies are updated. The information of the positions and the velocity of the ellipsoids describing the outer surface of the bodies are transferred to the finite element program. The finite element program first updates the positions of the nodes as if no contact with the ellipsoids occurs. Afterwards, the nodes are checked upon penetration with the ellipsoids. If penetration occurs, the nodes are placed back to the outer surface of the ellipsoid, and the position and the velocity of the node is updated. Suppose

---

* For reference list see Chapter 8.

that the change in velocity of the node is $\Delta\mathbf{v}$. The momentum change $\mathbf{p}$ of the node due to the interaction with the ellipsoid is:

$$\mathbf{p} = m\,\Delta\mathbf{v} \tag{B.1}$$

The momentum change of the node is caused by the ellipsoid, so in the contact point a force $\mathbf{F}$ will act on the ellipsoid, that can be calculated by:

$$\mathbf{F} = -\,m\,\Delta\mathbf{v} / \Delta t \tag{B.2}$$

where Δt is the time step. In general, the centre of mass of the body will not be situated on the line of action of the force, so also a moment $\mathbf{M}$ is applied on the ellipsoid:

$$\mathbf{M} = \mathbf{r} \times \mathbf{F} \tag{B.3}$$

with $\mathbf{r}$ the vector pointing from the centre of mass of the body to the contact point. All nodes that possibly make contact with the ellipsoid are treated in the same way. The forces and moments due to the interactions are summed and the total force and moment on the body are known. Actually this force and moment are acting on the body during this time increment. If this is taken into account, the positions of the ellipsoids have to be calculated again, the nodes have to be checked again etc. This will result in an iteration process which will highly disturb the computational efficiency of the central difference method. For that reason the assumption is made that the forces and moments act on the body during the next cycle. This means that the interaction term is applied on the bodies one time step later than they are applied on the nodes. Due to the small time steps in crash simulation, the error made by this assumption will be small.

Fixing of Nodes

Again first the position of the MADYMO bodies are updated. Then the new positions of the bodies to which the nodes are fixed are transferred to the finite element program. The finite element program updates the position of the nodes as if all nodes were free. But the position of the nodes that are fixed to the MADYMO bodies are prescribed by the position of the MADYMO body. The fixed finite element nodes are forced in the position prescribed by MADYMO. Due to this change, the node undergoes a velocity change $\Delta\mathbf{v}$. With this $\Delta\mathbf{v}$, again a momentum change of the node, a force on the MADYMO body and a moment on the MADYMO body can be calculated with the equations (B.1), (B.2) and (B.3) respectively.

Subcycling

The typical time step for multibody simulations is larger than the typical time step of finite element simulations. The methods of taking into account the interactions that are discussed above, presume equal time steps for the multibody and the finite element simulations. Here an adaptation of the algorithm is treated in which the time step for the finite element simulation is smaller than the multibody time step, so the finite element simulation will be subcycled. Suppose that the multibody time step is $\alpha\Delta t$ and the FEM time step is Δt. The parameter α must be an integer, equal to or larger than one. First the position of the MADYMO bodies is updated with $\alpha\Delta t$ and calculated at $(n+\alpha)\Delta t$. The positions of the contact ellipsoids and the bodies to which nodes are fixed are transferred to the FEM program. Now the positions of the FEM nodes are updated with Δt. The positions of the bodies and the ellipsoids are calculated at $(n+1)\Delta t$ by linear interpolation between $n\Delta t$ and $(n+\alpha)\Delta t$. Now the forces and moments on the bodies can be calculated as described in the two foregoing paragraphs. These forces are stored. The nodes are again updated and calculated at $(n+2)\Delta t$. Again the forces and moments are calculated after interpolation of the positions of the ellipsoids and the bodies. The forces and moments are added to the forces and moments on the MADYMO bodies calculated during the last finite element cycle. This is repeated until also the node positions are known at $(n+\alpha)\Delta t$. Every finite element cycle, the forces and moments on the MADYMO bodies are added to the forces and moments calculated on previous cycles. Now again another MADYMO cycle is performed and the summed forces and moments on the ellipsoids are applied.

Algorithm

The algorithm of the coupling is given in Fig. C1.

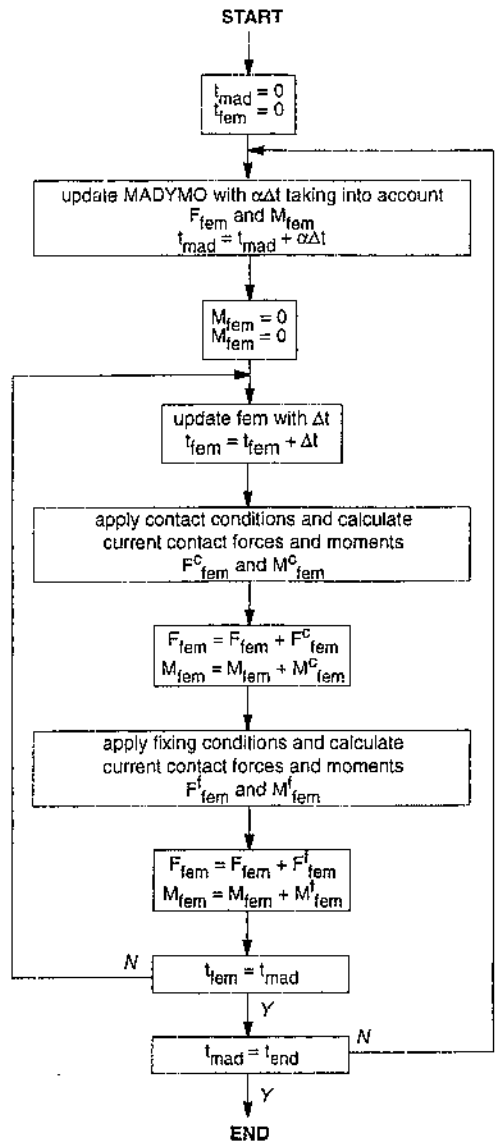

Fig. C.1 *The coupling algorithm*